frontiers | Research Topics

Go with the vet-flow! The current uses and new frontiers of flow cytometry in veterinary sciences

Edited by
Fulvio Riondato, Francesco Grandoni and Alberto Alvarez-Barrientos

Published in
Frontiers in Veterinary Science

ISSN 1664-8714
ISBN 978-2-8325-6230-7
DOI 10.3389/978-2-8325-6230-7

About Frontiers

Frontiers is more than just an open access publisher of scholarly articles: it is a pioneering approach to the world of academia, radically improving the way scholarly research is managed. The grand vision of Frontiers is a world where all people have an equal opportunity to seek, share and generate knowledge. Frontiers provides immediate and permanent online open access to all its publications, but this alone is not enough to realize our grand goals.

Frontiers journal series

The Frontiers journal series is a multi-tier and interdisciplinary set of open-access, online journals, promising a paradigm shift from the current review, selection and dissemination processes in academic publishing. All Frontiers journals are driven by researchers for researchers; therefore, they constitute a service to the scholarly community. At the same time, the *Frontiers journal series* operates on a revolutionary invention, the tiered publishing system, initially addressing specific communities of scholars, and gradually climbing up to broader public understanding, thus serving the interests of the lay society, too.

Dedication to quality

Each Frontiers article is a landmark of the highest quality, thanks to genuinely collaborative interactions between authors and review editors, who include some of the world's best academicians. Research must be certified by peers before entering a stream of knowledge that may eventually reach the public - and shape society; therefore, Frontiers only applies the most rigorous and unbiased reviews. Frontiers revolutionizes research publishing by freely delivering the most outstanding research, evaluated with no bias from both the academic and social point of view. By applying the most advanced information technologies, Frontiers is catapulting scholarly publishing into a new generation.

What are Frontiers Research Topics?

Frontiers Research Topics are very popular trademarks of the *Frontiers journals series*: they are collections of at least ten articles, all centered on a particular subject. With their unique mix of varied contributions from Original Research to Review Articles, Frontiers Research Topics unify the most influential researchers, the latest key findings and historical advances in a hot research area.

Find out more on how to host your own Frontiers Research Topic or contribute to one as an author by contacting the Frontiers editorial office: frontiersin.org/about/contact

Go with the vet-flow! The current uses and new frontiers of flow cytometry in veterinary sciences

Topic editors

Fulvio Riondato — University of Torino, Italy

Francesco Grandoni — Council for Agricultural Research and Agricultural Economy Analysis | CREA, Italy

Alberto Alvarez-Barrientos — Universidad de Extremadura, Spain

Citation

Riondato, F., Grandoni, F., Alvarez-Barrientos, A., eds. (2025). *Go with the vet-flow! The current uses and new frontiers of flow cytometry in veterinary sciences*. Lausanne: Frontiers Media SA. doi: 10.3389/978-2-8325-6230-7

Table of contents

frontiers | Frontiers in Veterinary Science

TYPE Editorial
PUBLISHED 05 December 2024
DOI 10.3389/fvets.2024.1532735

OPEN ACCESS

EDITED AND REVIEWED BY
Francisco Javier Salguero,
UK Health Security Agency (UKHSA),
United Kingdom

*CORRESPONDENCE
Fulvio Riondato
✉ fulvio.riondato@unito.it

RECEIVED 22 November 2024
ACCEPTED 25 November 2024
PUBLISHED 05 December 2024

CITATION
Riondato F, Alvarez-Barrientos A and Grandoni F (2024) Editorial: Go with the vet-flow! The current uses and new frontiers of flow cytometry in veterinary sciences. *Front. Vet. Sci.* 11:1532735. doi: 10.3389/fvets.2024.1532735

Editorial: Go with the vet-flow! The current uses and new frontiers of flow cytometry in veterinary sciences

Fulvio Riondato[1]*, Alberto Alvarez-Barrientos[2] and Francesco Grandoni[3]

[1]Department of Veterinary Sciences, School of Agriculture and Veterinary Medicine, University of Turin, Grugliasco, Italy, [2]Bioscience Applied Techniques Facility (STAB), Universidad de Extremadura, Badajoz, Spain, [3]Research Centre for Animal Production and Aquaculture, Consiglio per la Ricerca in Agricoltura e l'Analisi dell'Economia Agraria (CREA), Monterotondo, Italy

KEYWORDS

flow cytometry, veterinary, dog, cat, marine mammals, camel, chicken, pig

Editorial on the Research Topic
Go with the vet-flow! The current uses and new frontiers of flow cytometry in veterinary sciences

Flow cytometry has captured the interest of veterinary scientists since the late 1970s. Despite advancements, the gap between veterinary and biomedical flow cytometry remains significant. The present Research Topic was primarily developed to address two questions. The first question, posed by the scientist, is: *"Veterinary sciences and flow cytometry—what are the connections between these two fields?"* A search for "flow cytometry" (in the title, abstract, or keywords) within the Scopus database yields 6,797 publications in journals classified under the subject area "Veterinary" (at November 19, 2024). These publications are predominantly co-classified in medical and biological subject areas ("Immunology and Microbiology", "Agricultural and Biological Sciences", "Medicine", "Biochemistry, Genetics and Molecular Biology"), although other fields are also represented ("Pharmacology, Toxicology and Pharmaceutics", "Environmental Science", "Health Professions", "Nursing", and "Social Sciences"). The earliest paper included in this search was published in 1980 (1). Although some earlier studies exist (2, 3), they are published in journals not classified within the "Veterinary" subject area. Since then, the number of publications has shown steady growth, reaching 469 in 2024, with a significant increase starting in 2020. Against this background, this Research Topic aims to "take the pulse" of flow cytometry in the veterinary field today and to present findings from recent studies in relevant areas.

The second question, posed by the cytometrist, is: *"Where should I publish the results of my work?"* The search in the Scopus database reveals that the 6,797 papers have been published in over 150 different journals. This diversity reflects the lack of journals or journal sections specifically dedicated to flow cytometry within the veterinary sciences. Nonetheless, a minority of papers have been published in journals specifically focused on flow cytometry. Specifically, a Scopus search for the word "cytometry" in the journal title, combined with "Veter*" or an animal species in the "Article Title, Abstract, Keywords" field, resulted in over 150 papers in 6 different journals, most of which are published in *Cytometry*. However, none of these journals are classified under the "Veterinary" subject

area. As a result, authors are compelled to publish in journals focused on specific disciplines or, if they choose to publish in flow cytometry journals, they must forego making a direct contribution to the "official" veterinary field. This situation limits the development of a "vet-flow community" and hinders the growth of interest, expertise, collaboration, and thus, the achievement of meaningful results.

The Research Topic was open to studies from various disciplines to address these two aims. The 11 included articles provide a broad, albeit partial, overview depicting a highly diverse and dynamic field. They demonstrate that flow cytometry is currently used for studies on various animal species, applied to different biological samples, and serving multiple purposes. Studies encompass a range of species, including dogs, cats, pigs, dromedary camels, chickens, and marine mammals, with flow cytometric analyses performed on neoplastic masses, lymph nodes, peripheral blood, and cavity effusions, reporting results of cross-cutting interest. Sini et al. demonstrate that flow cytometry is a reliable alternative to immunohistochemistry for detecting cytokeratin, vimentin, and desmin in canine effusions, paving the way for including these markers in flow cytometric panels as a diagnostic tool to differentiate mesothelial, epithelial, and mesenchymal cells. The article by Ubiali et al. highlights the role of PD-L1 in the pathogenesis of canine lymphomas, revealing differences among B-cell, aggressive T-cell, and T-zone lymphomas. The study examines the surface membrane protein expression and relative mRNA levels in neoplastic cells, and the soluble protein concentration in plasma. Stokol et al. describe CD80 expression in leukocytes from canine peripheral blood and bone marrow, recommending its inclusion in flow cytometric immunophenotyping panels as a lineage marker for diagnosing acute myeloid leukemia. A method for evaluating Ki67 expression by flow cytometry in canine mast cell tumors is presented by Wu et al., offering oncologists a potential tool for prognostication. Rütgen et al. provide a significant case series of gastrointestinal lymphomas in cats, correlating multicolor flow cytometric analysis results with histopathologic classification and PCR clonality testing (PARR), and identifying unique immunophenotypes within B-cell and T-cell gastrointestinal neoplasms. An interesting study by Zwicklbauer et al. introduces a method for stabilizing whole blood from cats to enable long-term flow cytometric analyses, proving the reliability of quantifying T-helper cells, cytotoxic T-cells, B-cells, monocytes, and neutrophils up to 2 years post-sampling. Hussen et al. describe the application of a flow cytometric panel to analyze immune cell composition in the lymph node population compared to peripheral blood in dromedary camels, highlighting differences in lymphoid subset prevalence and specific marker expression. A multicolor approach for characterizing T $CD4^+$ and $CD8^+$ subsets in pigs aimed at studying activation-induced markers is reported by Moorton et al.. Härtle et al. provide an extensive overview of flow cytometry's potential to characterize different leukocyte populations in chickens, summarizing available reagents and guidelines for multicolor approaches. Finally, Felipo-Benavent, Mart-Romero et al. and Felipo-Benavent, Valls et al. focus on marine mammals in two separate articles, detailing flow cytometric methods for assessing phagocytic capacity and platelet function. They provide the first physiological values for various species, offering new tools for evaluating marine mammal health with potential clinical application in aquariums and other settings.

In addition to providing a snapshot of current flow cytometry applications in veterinary medicine and presenting recent findings across disciplines, this Research Topic could represent an important agora for all veterinary cytometrists regardless of their specific field. Considering the number and scientific quality of the manuscripts selected, we believe that the first issue has successfully achieved its objectives and laid the groundwork for a second volume. We hope this work will encourage interest and attract resources to support the continued growth of the "vet-flow" field in the future and help establish flow cytometry as an independent discipline within veterinary sciences too.

Author contributions

FR: Writing – original draft, Writing – review & editing. AA-B: Writing – original draft, Writing – review & editing. FG: Writing – original draft, Writing – review & editing.

Conflict of interest

The authors declare that the research was conducted in the absence of any commercial or financial relationships that could be construed as a potential conflict of interest.

The author(s) declared that they were an editorial board member of Frontiers, at the time of submission. This had no impact on the peer review process and the final decision.

Publisher's note

References

1. Cram LS, Forslund JC, Jarnagin JL, Thoen CO. Flow cytometry: an aid in monitoring lymphocyte transformation in whole blood cultures. *Comp Immunol Microbiol Infect Dis*. (1980) 3:373–80. doi: 10.1016/0147-9571(80)90014-4

2. Hoshino T, Wheeler KT, Nomura K. Differences in brain cell nuclear dna as determined by flow cytometry. *Neurol Med Chir*. (1977) 17:87–93. doi: 10.2176/nmc.17pt1.87

3. Pinkel D, Dean P, Lake S, Peters D, Mendelsohn M, Gray J, et al. Flow cytometry of mammalian sperm progress in DNA and morphology measurement. *J Histochem Cytochem*. (1979) 27:353–8. doi: 10.1177/27.1.86565

frontiers | Frontiers in Veterinary Science

TYPE Brief Research Report
PUBLISHED 21 November 2023
DOI 10.3389/fvets.2023.1279881

OPEN ACCESS

EDITED BY
Marta Vascellari,
Experimental Zooprophylactic Institute of the Venezie (IZSVe), Italy

REVIEWED BY
Valeria Martini,
University of Milan, Italy
Joy Archer,
University of Cambridge, United Kingdom

*CORRESPONDENCE
BinXi Wu
bwu@midwestern.edu

RECEIVED 18 August 2023
ACCEPTED 06 November 2023
PUBLISHED 21 November 2023

CITATION
Wu B, Lejeune A, Affolter VK, Iamone G, Riondato F and Kol A (2023) Development of a flow cytometric panel to assess prognostic biomarkers in fine needle aspirates of canine cutaneous or subcutaneous mast cell tumors. *Front. Vet. Sci.* 10:1279881. doi: 10.3389/fvets.2023.1279881

Development of a flow cytometric panel to assess prognostic biomarkers in fine needle aspirates of canine cutaneous or subcutaneous mast cell tumors

BinXi Wu[1]*, Amandine Lejeune[2], Verena K. Affolter[1], Giulia Iamone[3], Fulvio Riondato[3] and Amir Kol[1]

[1]Department of Pathology, Microbiology and Immunology, University of California Davis School of Veterinary Medicine, Davis, CA, United States, [2]Department of Surgical and Radiological Sciences, University of California Davis School of Veterinary Medicine, Davis, CA, United States, [3]Department of Veterinary Sciences, School of Agriculture and Veterinary Medicine, University of Turin, Turin, Italy

Mast cell tumor (MCT) is a common skin cancer in dogs that has a wide range of clinical behaviors. The purpose of this study was to develop a novel multicolor flow cytometry (FC) panel that will enable the quantification of candidate prognostic markers (Ki-67 and pKIT) in fine needle aspirate (FNA) samples prior to surgical removal of the tumors. FNA of canine MCTs and the NI-1 cell line were utilized to develop a FC panel that includes a viability dye (FVS620, BD Biosciences; 7-AAD, Invitrogen) and the following primary conjugated antibodies: CD117-PE (ACK45, BD Biosciences), pKIT-A647 (polyclonal bs-3242R, BIOSS) and Ki-67-FITC (20Raj1, eBioscience; MIB-1, DAKO). A total of nine FNA samples of canine MCTs were collected, seven out which produced sufficient cells for FC analysis. The Ki-67 antibody clone 20Raj1 produced a positive signal when applied to blood leukocytes but failed to provide robust labeling of neoplastic mast cells. The Ki-67 antibody clone MIB-1 delivered a superior staining quality in both the NI-1 cells and primary MCT cells. CD117-PE signal was adequate post fixation and permeabilization and in the combination of 7-AAD. pKIT produced non-specific staining and was not suitable for this multicolor FC panel. In conclusion, FNA samples of canine MCTs can often yield adequate cell numbers for FC analysis, and a multicolor FC panel was developed that can detect Ki-67 in canine mast cells. This would permit further studies into the potential use of this panel for canine cutaneous and subcutaneous MCT prognostication purposes.

KEYWORDS

flow cytometry, fine needle aspirate, canine cutaneous mast cell tumor, biomarkers, Ki-67, CD117

Introduction

Canine mast cell tumor (MCT) is a common tumor may occur within the dermis (i.e., cutaneous MCT) or within the subcutaneous fat tissue (i.e., sub-cutaneous MCT) (1, 2), and it accounts for 7–21% of all cutaneous neoplasms (2–4). These tumors have a highly variable biologic behavior ranging from benign to highly metastatic and aggressive (3, 5, 6). An extensive staging diagnostic workup is indicated for cutaneous MCTs if negative prognostic factors are

present, such as high tumor grade, but may be unnecessary in low-risk tumors (7, 8). Furthermore, a standardized approach for determining the appropriate extent of lateral surgical margins needed to achieve clear histologic margins remains unavailable, and a tumor of lower grade may not require as extensive a margin to accomplish complete excision (1, 9). While subcutaneous MCTs are considered to have a mostly benign biological behavior (10), a recent study reports a 18% local recurrence rate, a 27% rate of lymph node metastasis and a 13% MCT-related mortality in a cohort of 45 dogs (11). In this context, prognostication assays that can be performed prior to tumor removal are urgently needed.

Ancillary tools have been investigated to help clinicians decide when to be more aggressive in staging and therapy of canine cutaneous MCT. For instance, tumor grade (3, 12) and adjunctive immunohistochemical (IHC) markers such as Ki-67 and phosphorylated c-kit (pKIT) are valuable in predicting the behavior of canine cutaneous MCT. Specifically, the IHC expression level of the nuclear proliferation marker Ki-67 is associated with tumor grade (13) and tumor-related mortality (14). Quantification of pKIT via IHC has been associated with CD117 protein localization, mitotic rate, survival time, tumor grade, and *KIT* mutation at exon 8 and 11 (15). Similarly, Ki-67 may further serve as a useful prognostic indicator in subcutaneous MCTs as well (16). In other words, histologic tumor grading, and biomarker expressions help predict the biological behavior of canine cutaneous and subcutaneous MCTs, providing valuable information on staging and treatment planning, including surgical options and the inclusion of chemotherapy and/or radiotherapy. Unfortunately, histopathology and IHC are most often done following definitive surgery rather than as a preoperative incisional tissue biopsy, thereby limiting their utilities to guide staging and surgical recommendations. Moreover, with the recent commercialization of the intratumoral anti-cancer agent tigilanol tiglate (17), some patients may never get a biopsy or histopathologic analysis of their tumor, further highlighting the need for an accurate, pre-biopsy, prediction of canine MCT biologic behavior.

Fine needle aspirate (FNA) cytology is the primary diagnostic method for canine MCT. Unlike incisional biopsy, FNA cytology is a minimally invasive, affordable, and rapid diagnostic modality with high accuracy in diagnosing MCT (18). It is also a common modality to obtain samples for lymphocyte immunophenotyping via flow cytometry (FC), and has also been used to detect the presence of mast cells in the lymph nodes of dogs with cutaneous MCTs (19). Moreover, FC has been used to quantify Ki-67 expression in canine lymphoma (20). When compared to IHC, additional benefits of using FC to analyze these markers include the potential for more objective, precise, and robust results. For example, a wide range of Ki-67 IHC indices (from 0.01 to 0.135) has been reported as cutoffs for increased risk of mortality and histologic grade in dogs with cutaneous MCTs (13, 21–23), and FC may be better equipped to standardize the cutoff due to a larger number of cells analyzed. Potential limitations of FC include lack of spatial context within the tumor and uneven distribution of biomarker expression within the tumor (24). Finally, FC panels using FNA samples from canine MCTs to quantify Ki-67 and pKIT in canine MCT have not been reported yet. The objectives of this study were to determine if FNA samples of canine cutaneous or subcutaneous MCT can yield sufficient cells for flow cytometric analysis in the clinical setting and to develop a FC panel that includes CD117 (c-kit, a mast cell identity marker) (19), Ki-67, pKIT, and a viability dye.

Materials and methods

Cell culture

To optimize the flow cytometric protocol for the quantification of Ki-67 and pKIT in canine neoplastic mast cells, the NI-1 (25) canine mast cell line (abm) was used. This cell line was established from a 3.5-years old mixed breed dog with mast cell leukemia. These cells express both CD117 and pKIT (25). The cells were cultured in an incubator with PriGlow II culture media (abm) or RMPI 1640 (Gibco) with 10% FBS (R&D Systems) and 1% penicillin/streptomycin (Gibco) at 37°C and 5% CO_2 and passaged every 3–4 days.

Clinical samples

The study protocol was approved by the University of California, Davis Institutional Animal Care and Use Committee (IACUC protocol #21854). To be included, patients had to be diagnosed with cutaneous or subcutaneous MCT based on FNA cytology. FNA samples from dogs were obtained after an informed consent form was signed by the dog owners. The samples were obtained using a 22ga needle attached to a 3 mL syringe and coated with potassium EDTA. Negative suction was applied after penetrating the tumor followed by redirection of the syringe at least 3 times. Two to four syringes were typically obtained from each tumor. The samples were immediately emptied into a sterile tube containing 1 mL of RMPI 1640 with 10% FBS and 1% penicillin/streptomycin with gentle flushing. Discarded canine whole blood from the hematology diagnostic laboratory at the UC Davis, Veterinary Medical Teaching Hospital was used for individual marker staining optimization. Cell counts and viability on all clinical FNA samples were performed by a Muse Cell Analyzer (Millipore) or a hemocytometer.

Flow cytometry

Four antibodies and two viability dyes were evaluated individually (see Table 1). Initial optimization of these antibodies was performed using the NI-1 mast cells, with or without the addition of canine peripheral blood leukocytes as an internal negative control. Titration studies were completed to determine the optimal antibody concentration for each antibody. Clinical samples were processed within 2 h of FNA sample collection. Single color controls (AbC total antibody compensation kit, Invitrogen), viability control (1:1 mixture

TABLE 1 List of the antibodies and viability dyes used for flow cytometry analysis of mast cells in this study.

Marker	Clone/ reference	Fluorophore	Manufacturer
Viability	N/A	FVS620	BD Horizon
Viability	N/A	7-AAD	Invitrogen
CD117	ACK45 (19)	PE	BD Pharmingen
pKIT	Polyclonal 5401R (15)	A647	BIOSS
Ki-67	20Raj1 (26)	FITC	eBioscience
Ki-67	MIB-1 (13, 20, 22, 23)	FITC	DAKO

of freshly cultured NI-1 cells and heat-killed NI-1 cells), and fluorescent minus one (FMO) controls were included for every multicolor panel. Flow cytometry data were acquired between 24 and 48 h post staining and fixing for 8/9 of the samples, using a FACScalibur (BD Biosciences). Data for one sample was collected 1 week after staining due to analyzer malfunction. A minimum of 10,000 events (20) in the intact cell gate were acquired. Flow cytometric data were analyzed using a commercially available software (Flowjo).

Staining protocol

The samples were incubated, in 100 uL culture media, with anti-CD117 (ACK45-PE) antibody and 7-AAD, at 4°C for 15 min. After incubation, 2 mL of an ammonium chloride-based RBC lysis buffer was used to lyse the RBC and as a wash. This was followed immediately by fixation and permeabilization of the cells (FoxP3 transcription factor fix/perm set, eBioscience) with 30 min of fixation time at 4°C and a single wash using the permeabilization agent. The samples were then incubated at 4°C with anti-Ki-67 (20Raj1-FITC or MIB-1-FITC) antibody and anti-pKIT (Polyclonal 5401R-A647) antibody in 100 uL of permeabilization buffer (with added 2% bovine serum albumin) for 30 min and then followed by a single wash in the permeabilization buffer. 200–300 uL of 1% paraformaldehyde (PFA) in Dulbecco's phosphate-buffered saline (DPBS) was used to resuspend the samples prior to FC data acquisition. For each run of our final FC panel, 7 tubes were ran as follows: unstained cells, complete panel, FMO-Ki67, FMO-CD117, Viability-only (NI-1 cells), PE single color control (beads), and FITC single color control (beads).

Modifications of the staining protocol were made in an attempt to detect Ki-67 using the 20Raj1 clone. Two different fix/perm reagent kits (FoxP3 transcription factor fix/perm set, eBioscience; True-Nuclear transcription factor fix/perm set, BioLegend) were tested. Modifications of the permeabilization reagent with additional 0.1% Tween, 0.1% Triton, and 0.1% saponin were tested. Different fixation times (30 min vs. 60 min), fixation temperatures (4°C vs. room temperature), antibody incubation times (30 min vs. 60 min), and antibody incubation temperatures (4°C vs. room temperature) were also evaluated.

Statistics

Commercially available statistical software (GraphPad Prism and Excel) was used for statistical analysis. Descriptive statistics were calculated where appropriate.

Results

FNA samples can yield adequate cell number and quality for FC analysis in the clinical setting

Nine FNA samples from dogs with cytologically confirmed MCTs were analyzed for cell yield. Patient demographics, tumor size, location, grade and stage as well as sample collection method and cell yield are detailed in Supplementary Table S1. Six samples were obtained during pre-surgical visits, and three samples were obtained right after surgical excision using the same FNA technique. Tumor size (longest axis) ranged from 0.5 cm to 5 cm. 2–4 syringes were collected from all cases except one where only 1 syringe was collected. Sample cellularity ranged from only 200 to over 16,000,000 total viable cells (200–4,000,000 per syringe) with a median total viable cell yield of 800,000 cells (Supplementary Figure S1). Using 150,000 cells (estimated minimal cells needed for the multicolor panel) as a cutoff, 7/9 (78%) of the samples were adequate for FC analysis. Two out of nine samples (22%) did not yield sufficient cells. Both samples were from tumors that occurred on the limbs/extremities. One of these tumors measured 1.2 cm with only one syringe collected and the other one had measured 0.5 cm. Mild, local adverse events (tumor appeared mildly erythematous or oozing) were noted for two cases and were treated accordingly. Six out of nine samples were used for cell yield analysis and panel development, and 3/9 cases had the full panel performed.

The anti-CD117-PE antibody (clone ACK45) retains its ability to label canine neoplastic mast cells with subsequent cell fixation and permeabilization

The anti-CD117 antibody that was used in this study (ACK45) has been extensively studied in the past and its capacity to label canine mast cells has been reported (19). Nonetheless, cell surface receptor staining protocols (which have been previously reported) (19) do not require cell fixation and permeabilization, which can impact cell staining properties. As the goal is to label CD117 and Ki-67 (intra-nuclear transcription factor) concurrently, fixation and permeabilization steps had to be incorporated into the protocol. The anti-CD117 antibody produced a strong signal when applied to the NI-1 cells without fixation, as expected (Figure 1A). When NI-1 cells were spiked with canine whole blood followed by subsequent fixation and permeabilization, the high CD117 expression of NI-1 cells formed a discrete population that could be readily separated from the peripheral blood leukocytes (Figure 1B). A fixed and permeabilized peripheral blood sample from a dog with mastocytemia (10% mast cells on a 100-cell differential count) showed adequate separation of mast cells from other leukocytes (Figure 1C). This anti-CD117 antibody was further effective in differentiating mast cells from non-mast cells in an FNA sample that was fixed and permeabilized from a dog with MCT (Figure 1D).

pKIT staining yields a non-specific staining pattern

The polyclonal 5401R anti-pKIT antibody showed significant non-specific staining of NI-1 cells and peripheral blood leukocytes (data not shown). Consequently, pKIT was excluded from the final FC panel.

The MIB-1 anti-Ki-67 antibody provides a superior staining quality of canine neoplastic mast cells

The MIB-1 clone of the anti-Ki-67 antibody produced a clearly identifiable and distinct signal in NI-1 cells using the FoxP3 transcription factor fix/perm buffer set (Figure 2). On the other hand,

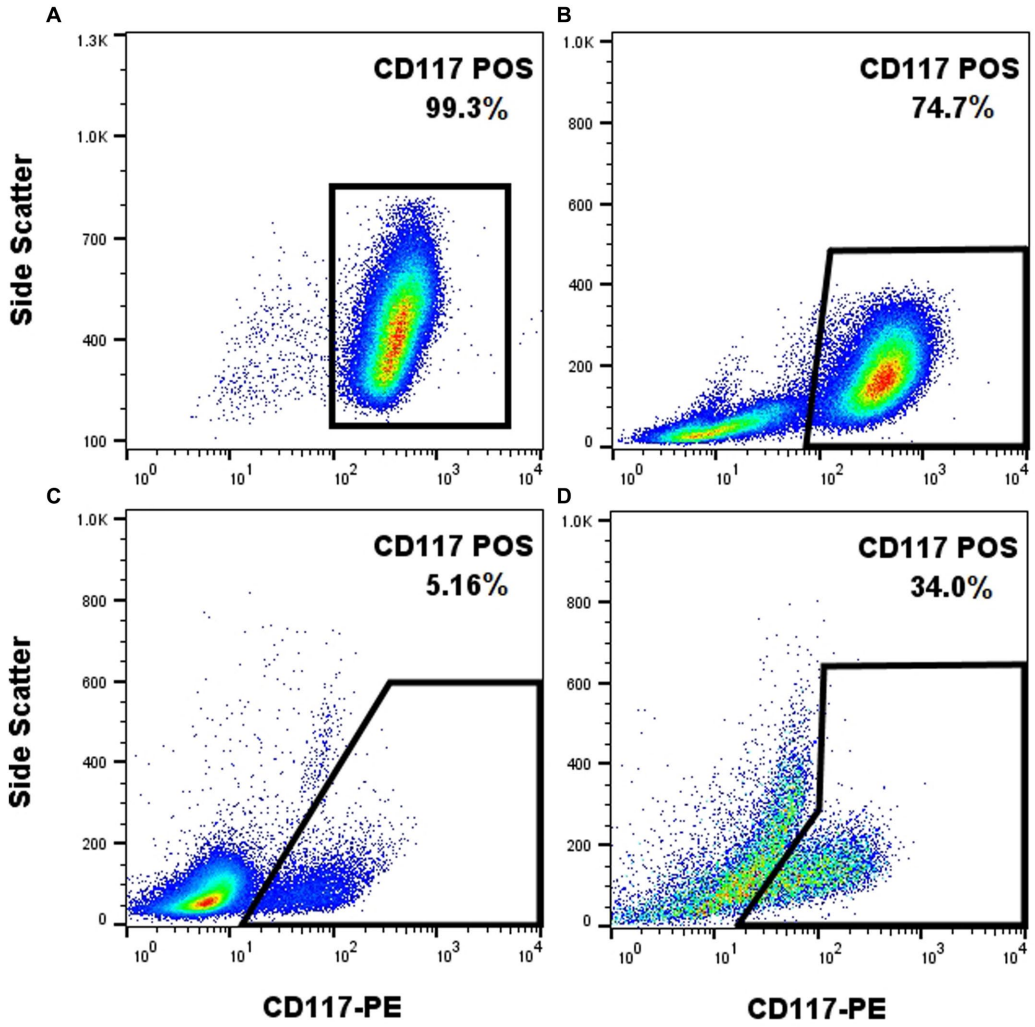

FIGURE 1
The anti-CD117-PE antibody (clone ACK45, BD Pharmingen) enables effective labeling of canine mast cells with post-labeling fixation and permeabilization. CD117-PE (x-axis) fluorescence plotted against side scatter (y-axis) of different samples containing mast cells. Unfixed NI-1 mast cells showed uniform positivity **(A)**. Fixed and permeabilized NI-1 mast cells spiked with peripheral blood leukocytes showed a discrete population of the mast cells **(B)**. Fixed and permeabilized whole blood from a dog with mastocytemia showed effective separation of mast cells from non-mast cells **(C)**. Fixed and permeabilized FNA sample of a MCT showed effective separation of mast cells from non-mast cells **(D)**.

the 20Raj-1 clone of the anti-Ki-67 antibody did not produce credible staining in NI-1 cells, despite the many protocol modifications to the fix/perm reagents, concentration, incubation time, and incubation temperature (Figure 2). It also did not produce credible staining of clinical MCT FNA samples (data not shown). However, it did produce positive staining on peripheral blood lymphocytes and one case of suspected acute leukemia (Supplementary Figure S2).

Proof of concept application of our FC panel

Once the staining protocol for each individual marker was optimized, they were combined to determine if appropriate staining patterns could be identified in FNA samples of clinical MCTs. Appropriate single-color and FMO controls were used. Application of the FC panel to a histologic grade 1/low grade tumor and to a biologically aggressive tumor (confirmed metastasis to the lymph node on cytology) produced a distinct Ki-67 signal that was low (5.2%) in the low-grade tumor sample and was markedly higher (28.8%) in the biologically aggressive tumor (Figure 3). The biologically aggressive tumor had a low number of mast cells on cytology, consistent with the FC results. A 500-cell differential was performed on a Wright Giemsa stained slide consisting mostly of neutrophils with fewer macrophages, lymphocytes, and eosinophils and 1.6% well-granulated mast cells.

Discussion

Canine cutaneous MCTs have a highly variable biological behavior and the subcutaneous tumors could be aggressive as well. Limited pre-surgical options are available to assess their prognosis and guide further staging and treatment. The current

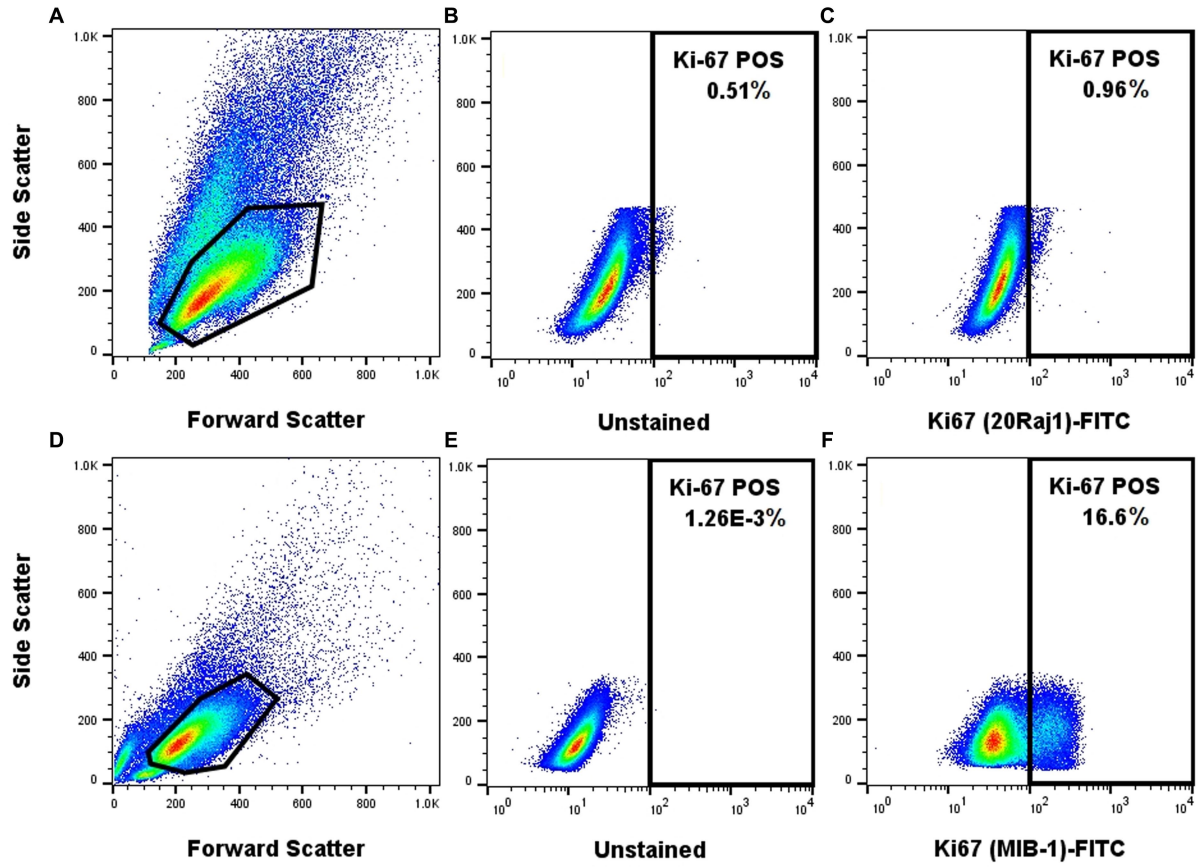

FIGURE 2
The MIB-1 anti-Ki67 antibody provides a superior staining quality of NI-1 canine neoplastic mast cells. NI-1 cells were either stained with the 20Raj1 clone **(A–C)** or MIB-1 clone **(D–F)**.

study developed a FC panel that enables the quantification of Ki-67 expression, a validated IHC prognostic marker, in viable neoplastic mast cells using FNA samples that can be applied pre-surgically. Future studies will be required to determine its clinical efficacy for canine MCT prognostication.

Cell yield experiments showed that sufficient cells can be readily obtained from mast cell tumors via FNA, with 78% of the cases having a total cell yield well above the estimated 150,000 cells needed for this panel (Supplementary Figure S1). This reflects the results of a previous report, where 34/38 (89%) FNA samples of MCT yielded sufficient cells (19). Unlike this previous report, the majority (6/9) of our samples were obtained during the pre-surgical visit as opposed to post-surgical excision. Moreover, all of our samples were obtained by the FNA technique and none were supplemented with tumor scraping. Two out of our nine cases (22%) did not yield sufficient cells. Both of these samples came from small tumors (longest axis 1.2 cm and 0.5 cm) and were located on the limbs. One FNA was obtained prior to surgery and the other was obtained immediately post-surgery. Unfortunately, the low number of samples with insufficient cell numbers ($n = 2$) did not allow us to determine if there were any statistical associations. Lastly, different operators collecting the FNA samples may have further contributed to variation in cell yield. Further studies are needed to confirm these observations and offer more guidance on FNA sampling for FC.

To ensure only live cells were assessed for biomarker expression, the DNA-binding dye 7-amino-actinomycin D (7-AAD) was applied. In the current protocol, 7-AAD showed a bright and effective signal that differentiated viable cells from non-viable cells. Although typically used for cell-surface-only staining protocols, 7-AAD previously has been reported for intracellular staining with subsequent cell fixation and permeabilization (27). The alternate intracellular amine-reactive dye (FVS620) produced poor CD117 staining index in clinical mast cell tumor samples and was not included in our final panel (data not shown).

Two different anti-Ki-67 antibody clones (20Raj1 and MIB-1) were tested, including different fixation/permeabilization protocols. The MIB-1 clone showed superior staining of mast cells using the FoxP3 transcription factor fix/perm set (Figure 2). The NI-1 cells (Figure 2) and clinical mast cell tumor samples (data not shown) were not reactive to the 20Raj1 antibody, despite different fixation/permeabilization reagents, incubation time, and incubation temperatures applied. This is in contrast to a study reporting the successful use of the 20Raj1 antibody in flow cytometric analysis of canine lymphocytes (26). Moreover, the immunoreactivity of this antibody was detected in a blood sample from a dog with acute leukemia (Supplementary Figure S2), demonstrating that the antibody can detect the Ki-67 antigen in canine cells. The different results with these two antibodies may be due to specificity to different epitopes or

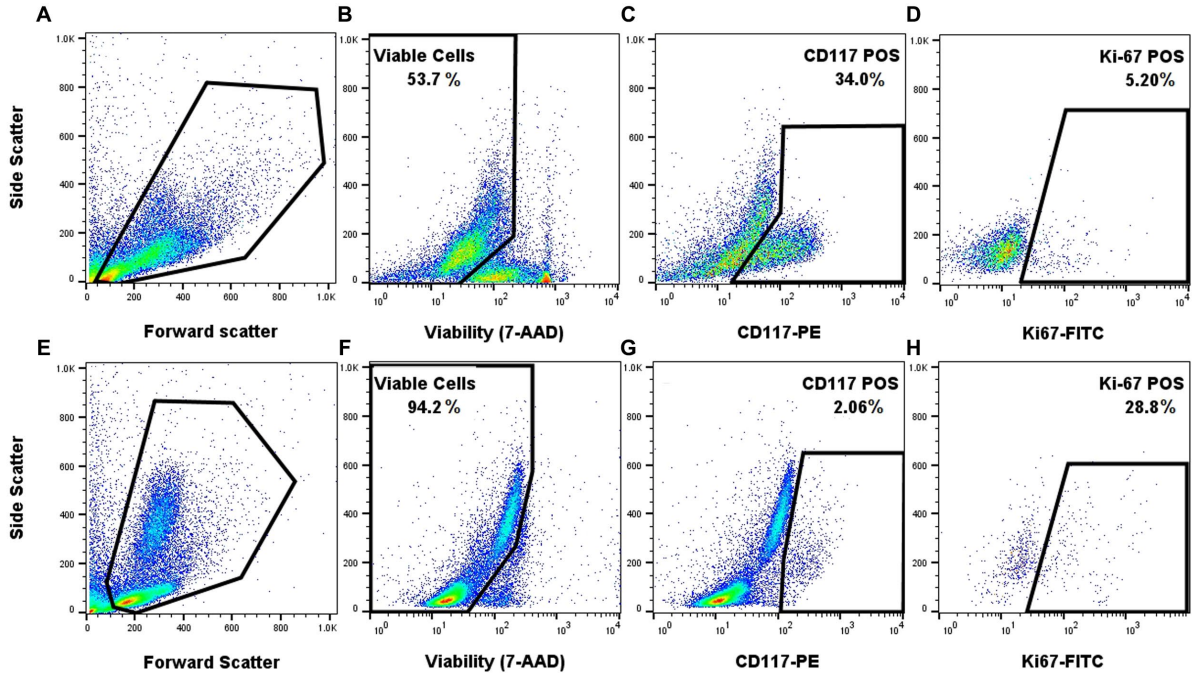

FIGURE 3
Proof of concept application of the FC panel using samples from a low-grade canine cutaneous MCT **(A–D)** and a biologically aggressive MCT **(E–H)**. Forward and side scatter for the two different samples **(A,E)**. Gating on the viable cells using 7-AAD **(B,F)**. Gating on CD117 positive cells within the viable cells **(C,G)**. Gating on viable and CD117 positive cells that express Ki-67 **(D,H)**. Appropriate single-color and FMO controls were used.

that 20Raj1 antibody may require a different type of cell permeabilization. The cause of this discrepancy was not further investigated as it is outside the scope of this project.

A polyclonal pKIT antibody (5401R, BIOSS) showed broad non-specific and uniform binding to peripheral blood leukocytes (data not shown), which should not express CD117 nor its phosphorylated form. Potential causes for this significant non-specific staining include this being a polyclonal antibody, and also targeting a phosphorylated target, which may require a different type of permeabilization (such as methanol-based) that may not be compatible with the rest of our panel markers. As such, this marker was not included in the final multicolor panel.

Finally, and most importantly, the application of the combined multicolor panel showed that a biologically aggressive mast cell tumor, with cytologic evidence of metastasis to the draining lymph node, had a much higher Ki-67 expression compared to a low-grade tumor (Figure 3). Moreover, this case also demonstrated the robustness of the panel and the biomarkers, where the FC was able to delineate the low percentage of mast cells from the predominating leukocytes. Indeed, the primary tumor was markedly inflamed with only a few mast cells identified on cytologic evaluation (1.6% mast cells in a 500-cell differential count), which is consistent with the low percentage of mast cells on FC (2.06% CD117+ cells). More samples will be needed to determine if there is a significant difference in Ki-67 expression level between low-grade and high-grade tumors and if it can be used for disease prognostication.

There are several limitations to this panel development. First, the low number of FNA samples prevents meaningful assessment if the tumor size and tumor location affects FNA cell yield. Second, multiple operators obtaining the FNA samples can lead to variation in cell yield. Third, the NI-1 cell line is from a dog with mast cell leukemia, not a cutaneous mast cell tumor, and may not have the same pattern of biomarker expression. Lastly, spiked peripheral blood leukocytes were used as a negative control population with the NI-1 cells, but they do not represent the typical leukocyte population (mostly eosinophils) in mast cell tumors.

Nevertheless, we provide proof-of-concept data using clinical FNA samples demonstrating the robustness of our FC panel, its ability to separate neoplastic mast cells from non-mast cells, and effectively label Ki-67 within this neoplastic cell population. The development of a multicolor FC panel on canine cutaneous MCT that includes Ki-67 gives us a powerful tool to assess tumor behavior prior to surgery. The immediate next step would be to examine if there is a correlation between Ki-67 expression in neoplastic mast cells via FC and histologic grade, tumor stage and survival.

Data availability statement

The raw data supporting the conclusions of this article will be made available by the authors, without undue reservation.

Ethics statement

The animal studies were approved by Institutional Animal Care and Use Committee University of California, Davis. The studies were

conducted in accordance with the local legislation and institutional requirements. Written informed consent was obtained from the owners for the participation of their animals in this study.

Author contributions

BW: Conceptualization, Data curation, Formal Analysis, Investigation, Methodology, Validation, Visualization, Writing – original draft, Writing – review & editing, Funding acquisition. AL: Conceptualization, Funding acquisition, Methodology, Writing – review & editing. VA: Conceptualization, Funding acquisition, Writing – review & editing. GI: Methodology, Writing – review & editing. FR: Formal Analysis, Methodology, Visualization, Writing – review & editing. AK: Conceptualization, Formal Analysis, Funding acquisition, Investigation, Methodology, Project administration, Resources, Software, Supervision, Validation, Visualization, Writing – review & editing.

Funding

The author(s) declare financial support was received for the research, authorship, and/or publication of this article. This project is funded by the University of California Davis, Center for Companion Animal Health, grant number 2021-49-R.

Acknowledgments

The authors would like to thank the Center for Companion Animal Health for funding this project, and to thank Dr. Emir Hadzijusufovic for his help with the NI-1 cells and optimization of the anti-Ki-67 antibodies.

Conflict of interest

The authors declare that the research was conducted in the absence of any commercial or financial relationships that could be construed as a potential conflict of interest.

The author(s) declared that they were an editorial board member of Frontiers, at the time of submission. This had no impact on the peer review process and the final decision.

Publisher's note

Supplementary material

The Supplementary material for this article can be found online at: https://www.frontiersin.org/articles/10.3389/fvets.2023.1279881/full#supplementary-material

SUPPLEMENTARY FIGURE S1
Cell yield from FNA of nine cases of canine MCT. The black dots represent the six cases in which FNA samples were obtained before surgery. The blue dots represent the three cases in which FNA samples were obtained immediately after surgery. The solid black line represents the median total viable cell yield. The dotted black line represents the estimated minimum cell yield required to perform this FC panel.

SUPPLEMENTARY FIGURE S2
20Raj1 anti-Ki67 antibody labeling of peripheral blood cells of a dog with acute leukemia. Forward and side scatter **(A)**. Unstained control **(B)**. 20Raj1 stained sample **(C)**. Appropriate single-color and FMO controls were used.

SUPPLEMENTARY TABLE 1
Data collected for all nine cases of canine mast cell tumors.

References

1. Selmic LE, Ruple A. A systematic review of surgical margins utilized for removal of cutaneous mast cell tumors in dogs. *BMC Vet Res*. (2020) 16:5. doi: 10.1186/s12917-019-2227-8

2. Villamil JA, Henry CJ, Bryan JN, Ellersieck M, Schultz L, Tyler JW, et al. Identification of the most common cutaneous neoplasms in dogs and evaluation of breed and age distributions for selected neoplasms. *J Am Vet Med Assoc*. (2011) 239:960–5. doi: 10.2460/javma.239.7.960

3. Kiupel M, Webster JD, Bailey KL, Best S, DeLay J, Detrisac CJ, et al. Proposal of a 2-tier histologic grading system for canine cutaneous mast cell tumors to more accurately predict biological behavior. *Vet Pathol*. (2011) 48:147–55. doi: 10.1177/0300985810386469

4. Kiupel M. Mast cell tumors In: *Tumors in domestic animals*. Hoboken, New Jersey: John Wiley & Sons, Ltd (2016). 176–202.

5. Donnelly L, Mullin C, Balko J, Goldschmidt M, Krick E, Hume C, et al. Evaluation of histological grade and histologically tumour-free margins as predictors of local recurrence in completely excised canine mast cell tumours. *Vet Comp Oncol*. (2015) 13:70–6. doi: 10.1111/vco.12021

6. Marconato L, Polton G, Stefanello D, Morello E, Ferrari R, Henriques J, et al. Therapeutic impact of regional lymphadenectomy in canine stage II cutaneous mast cell tumours. *Vet Comp Oncol*. (2018) 16:580–9. doi: 10.1111/vco.12425

7. Fejös C, Troedson K, Ignatenko N, Zablotski Y, Hirschberger J. Extensive staging has no prognostic value in dogs with low-risk mast cell tumours. *Vet Comp Oncol*. (2021) 20:265–75. doi: 10.1111/vco.12773

8. Pecceu E, Serra Varela JC, Handel I, Piccinelli C, Milne E, Lawrence J. Ultrasound is a poor predictor of early or overt liver or spleen metastasis in dogs with high-risk mast cell tumours. *Vet Comp Oncol*. (2020) 18:389–401. doi: 10.1111/vco.12563

9. Simpson AM, Ludwig LL, Newman SJ, Bergman PJ, Hottinger HA, Patnaik AK. Evaluation of surgical margins required for complete excision of cutaneous mast cell tumors in dogs. *J Am Vet Med Assoc*. (2004) 224:236–40. doi: 10.2460/javma.2004.224.236

10. Thompson JJ, Pearl DL, Yager JA, Best SJ, Coomber BL, Foster RA. Canine subcutaneous mast cell tumor: characterization and prognostic indices. *Vet Pathol*. (2011) 48:156–68. doi: 10.1177/0300985810387446

11. Cherzan NL, Fryer K, Burke B, Farrelly J. Factors affecting prognosis in canine subcutaneous mast cell tumors: 45 cases. *Vet Surg*. (2023) 52:531–7. doi: 10.1111/vsu.13944

12. Patnaik AK, Ehler WJ, MacEwen EG. Canine cutaneous mast cell tumor: morphologic grading and survival time in 83 dogs. *Vet Pathol*. (1984) 21:469–74. doi: 10.1177/030098588402100503

13. Vascellari M, Giantin M, Capello K, Carminato A, Morello EM, Vercelli A, et al. Expression of Ki67, BCL-2, and COX-2 in canine cutaneous mast cell tumors: association with grading and prognosis. *Vet Pathol*. (2013) 50:110–21. doi: 10.1177/0300985812447829

14. Webster JD, Yuzbasiyan-Gurkan V, Miller RA, Kaneene JB, Kiupel M. Cellular proliferation in canine cutaneous mast cell tumors: associations with c-KIT and its role in prognostication. *Vet Pathol*. (2007) 44:298–308. doi: 10.1354/vp.44-3-298

15. Halsey CHC, Thamm DH, Weishaar KM, Burton JH, Charles JB, Gustafson DL, et al. Expression of phosphorylated KIT in canine mast cell tumor. *Vet Pathol*. (2017) 54:387–94. doi: 10.1177/0300985816688943

16. Thompson JJ, Yager JA, Best SJ, Pearl DL, Coomber BL, Torres RN, et al. Canine subcutaneous mast cell tumors: cellular proliferation and KIT expression as prognostic indices. *Vet Pathol*. (2011) 48:169–81. doi: 10.1177/0300985810390716

17. De Ridder TR, Campbell JE, Burke-Schwarz C, Clegg D, Elliot EL, Geller S, et al. Randomized controlled clinical study evaluating the efficacy and safety of intratumoral treatment of canine mast cell tumors with tigilanol tiglate (EBC-46). *J Vet Intern Med*. (2021) 35:415–29. doi: 10.1111/jvim.15806

18. Ghisleni G, Roccabianca P, Ceruti R, Stefanello D, Bertazzolo W, Bonfanti U, et al. Correlation between fine-needle aspiration cytology and histopathology in the evaluation of cutaneous and subcutaneous masses from dogs and cats. *Vet Clin Pathol*. (2006) 35:24–30. doi: 10.1111/j.1939-165X.2006.tb00084.x

19. Sulce M, Marconato L, Martano M, Iussich S, Dentini A, Melega M, et al. Utility of flow cytometry in canine primary cutaneous and matched nodal mast cell tumor. *Vet J*. (2018) 242:15–23. doi: 10.1016/j.tvjl.2018.10.004

20. Poggi A, Miniscalco B, Morello E, Comazzi S, Gelain ME, Aresu L, et al. Flow cytometric evaluation of ki67 for the determination of malignancy grade in canine lymphoma. *Vet Comp Oncol*. (2015) 13:475–80. doi: 10.1111/vco.12078

21. Berlato D, Murphy S, Monti P, Stewart J, Newton JR, Flindall A, et al. Comparison of mitotic index and Ki67 index in the prognostication of canine cutaneous mast cell tumours. *Vet Comp Oncol*. (2015) 13:143–50. doi: 10.1111/vco.12029

22. Horta RS, Lavalle GE, Monteiro LN, Souza MCC, Cassali GD, Araújo RB. Assessment of canine mast cell tumor mortality risk based on clinical, histologic, Immunohistochemical, and molecular features. *Vet Pathol*. (2018) 55:212–23. doi: 10.1177/0300985817747325

23. Scase TJ, Edwards D, Miller J, Henley W, Smith K, Blunden A, et al. Canine mast cell tumors: correlation of apoptosis and proliferation markers with prognosis. *J Vet Intern Med*. (2006) 20:151–8. doi: 10.1892/0891-6640(2006)20[151:cmctco]2.0.co;2

24. Aubreville M, Bertram CA, Marzahl C, Gurtner C, Dettwiler M, Schmidt A, et al. Deep learning algorithms out-perform veterinary pathologists in detecting the mitotically most active tumor region. *Sci Rep*. (2020) 10:16447. doi: 10.1038/s41598-020-73246-2

25. Hadzijusufovic E, Peter B, Herrmann H, Rülicke T, Cerny-Reiterer S, Schuch K, et al. NI-1: a novel canine mastocytoma model for studying drug resistance and IgER-dependent mast cell activation. *Allergy*. (2012) 67:858–68. doi: 10.1111/j.1398-9995.2012.02833.x

26. Sparger EE, Chang H, Chin N, Rebhun RB, Withers SS, Kieu H, et al. T cell immune profiles of blood and tumor in dogs diagnosed with malignant melanoma. *Front Vet Sci*. (2021) 8:772932. doi: 10.3389/fvets.2021.772932

27. Schmid I, Ferbas J, Uittenbogaart CH, Giorgi JV. Flow cytometric analysis of live cell proliferation and phenotype in populations with low viability. *Cytometry*. (1999) 35:64–74. doi: 10.1002/(SICI)1097-0320(19990101)35:1<64::AID-CYTO9>3.0.CO;2-Y

frontiers | Frontiers in Veterinary Science

TYPE Original Research
PUBLISHED 30 April 2024
DOI 10.3389/fvets.2024.1365319

OPEN ACCESS

EDITED BY
Fulvio Riondato,
University of Torino, Italy

REVIEWED BY
Wilhelm Gerner,
The Pirbright Institute, United Kingdom
Martin Faldyna,
Veterinary Research Institute (VRI), Czechia

*CORRESPONDENCE
Jamal Hussen
✉ jhussen@kfu.edu.sa

RECEIVED 04 January 2024
ACCEPTED 15 April 2024
PUBLISHED 30 April 2024

CITATION
Hussen J, Althagafi H, Al-Sukruwah MA, Falemban B and Abdul Manap AS (2024) Flow cytometric analysis of immune cell populations in the bronchial and mesenteric lymph nodes of the dromedary camel. *Front. Vet. Sci.* 11:1365319. doi: 10.3389/fvets.2024.1365319

Flow cytometric analysis of immune cell populations in the bronchial and mesenteric lymph nodes of the dromedary camel

Jamal Hussen[1]*, Hind Althagafi[2], Mohammed Ali Al-Sukruwah[1], Baraa Falemban[1] and Aimi Syamima Abdul Manap[3]

[1]Department of Microbiology and Parasitology, College of Veterinary Medicine, King Faisal University, Al-Ahsa, Saudi Arabia, [2]Department of Biology, College of Science, Princess Nourah bint Abdulrahman University, Riyadh, Saudi Arabia, [3]Department of Biomedical Sciences, College of Veterinary Medicine, King Faisal University, Al-Ahsa, Saudi Arabia

Dromedary camel is an important livestock species with special economic value in arid and semi-arid regions of the world. Given the limited data on detailed immune cell composition and cell marker expression in the dromedary camel lymph node tissue, the present study was undertaken to investigate the immune cell composition of bronchial and mesenteric lymph nodes from healthy dromedary camels using flow cytometry. In this study, we applied flow cytometry and multicolor immuno-fluorescence to phenotype the main populations of immune cells in the bronchial and mesenteric camel lymph nodes and compared them with separated peripheral blood mononuclear cells and granulocytes. We used antibodies to detect several cell surface molecules associated with camel T cells (CD4, WC1), B cells (MHCII, BAQ44A), monocytes/macrophages (CD172a, CD14, CD163), in addition to the pan-leukocyte marker CD45 and the cell adhesion molecules CD44 and CD18. Compared to blood mononuclear cells, camel lymph node cells contained a higher percentage of lymphoid cells with only a minor fraction of myeloid cells. In addition, the lower expression of CD44 and CD18 on lymph node lymphocytes compared to lymphocytes from peripheral blood indicates higher frequency of naïve lymphocytes in the lymph nodes. The frequency of $CD4^+$ T cells, B cells and γδ T cells within camel lymph node lymphocytes compared to blood indicates a similar tissue distribution pattern of lymphocyte subsets in camel and bovine and supports previous reports on the similarity between the camel immune system and the immune system of other ruminants. Lymph node neutrophils were identified as $CD45^{++}$ $CD172a^{++}$, $CD14^+$, $MHCII^{low}$, $BAQ44A^+$, $CD44^{++}$, $CD18^{++}$ cells. In conclusion, the present study is describing the employment of flow cytometric single-cell analysis and immunostaining for the analysis of the immune cell composition in the camel lymph node.

KEYWORDS

camel, immune system, lymph node, B cells, T cells, flow cytometry

1 Introduction

The classification of lymphoid organs encompasses primary organs, including the bone marrow and thymus, where immune cells are generated and undergo differentiation into functional cells. Additionally, secondary organs such as the spleen, lymph nodes, and the mucosa-associated lymphoid organs (MALT) serve as the sites where immune

responses occur (1). Lymph nodes are specialized structures dispersed throughout the body and are responsible for the filtration of the lymph (2). They lymph node is traditionally classified into three distinct histological regions, namely the cortex, paracortex, and medulla, with a capsule that surround the node. The lymphatic tissue within the node is characterized by clusters of immune cells, predominantly consisting of lymphoid cells alongside some myeloid cells, such as macrophages and dendritic cells. Within the node tissue compartments, B and T cells home to distinct areas, where they interact with antigen presenting cells and undergo clonal expansion.

The local immune cell composition within a lymphoid organ is indicative of the balance between cellular migration towards the organ and the rates at which immune cells become trapped and released within it during an immune response (3). The analysis of changes in immune cell distribution in different primary and secondary immune organs has been proven a valuable tool to investigate the immune response to infection or vaccination (4, 5). Different techniques were employed for the analysis of immune cell composition of lymph nodes. Techniques like immunohistochemistry are the best choice when analyzing the area-specific cellular composition of the different compartments of the nodes. Flow cytometry in combination with monoclonal antibody (mAb) staining enables single cell analysis that has proven a useful tool to detect and characterize immune cells in cell suspension. It has the advantage of higher sensitivity for the identification in minor changes in cellular composition, which is pivotal in the early diagnosis of pathologies. The applicability of this method has been addressed in areas of immunopathology and tumor research and diagnosis by the identification of the pattern of distribution of a cell population within tissue homogenates (6). In addition, the comparison between flow cytometry and image cytometry revealed that measurements of lymph node cell populations obtained with the two methods are comparable (6).

Flow cytometric analysis of the cellular composition of bovine lymph nodes revealed the dominance of lymphocytes with minor proportions of CD172a-positive cells, including macrophages and neutrophils (7). Although they are mainly recognized as circulatory short-lived innate immune cells with the ability to infiltrate tissues upon infection or inflammation, neutrophils are now discussed as bridging cells at the interface of innate and adaptive immune systems (8). Recent studies reported the presence of tissue-resident neutrophils in the lymph node under steady-state conditions before the onset of inflammation (9). They enter uninfected lymph nodes via high endothelial venules and patrol the lymph nodes of the skin and mucosal systems under homeostatic conditions (10).

Although some immunohistochemical studies described the structure of the camel lymph nodes and identified some immune cells with a distribution that seems similar to the bovine lymph node (11, 12), flow cytometric analysis of the immune cell composition of the camel lymph node has not been investigated so far. Therefore, the present study was undertaken to test the reactivity of camel lymph node cells with monoclonal antibodies to selected cell surface antigens using flow cytometry. Uncovering the immune cell composition of lymph nodes in healthy animals will help in the establishment of normal values that could be used as reference values for the diagnosis of immunopathology and the analysis of local immune response in lymphoid organs to infection and vaccination.

2 Materials and methods

2.1 Animals and collection of blood and lymph nodes samples

Ten healthy male one-humped camels (*Camelus dromedarius*) were included in the present study for the collection of blood (only sex animals) and lymph node samples (ten animals). The animals (aged between 8 and 11 years; mean age 8.9 ± 1.1 years) were selected from the camels admitted for normal slaughtering for human consumption at Al-Omran Slaughterhouse in Al-Ahsa Region in Saudi Arabia. All the camels were from Al-Majaheem breed. Each animal was clinically examined for clinical signs like injuries, reproductive, gastrointestinal, or respiratory disease. Venous blood was collected from the jugular vein into vacutainer tubes containing EDTA (Becton Dickinson, Heidelberg, Germany). Directly after euthanasia of animals via bleeding, all viscera were examined to exclude animals with signs of abdominal, thoracic, or reproductive disorders. After collection, bronchial and mesenteric lymph nodes were immediately placed on ice in cold PBS containing 1 mM EDTA and transported to the laboratory within one hour.

2.2 Separation of blood mononuclear cells and neutrophilic granulocytes

Peripheral blood mononuclear cells (MNC) were separated as previously described (13). Briefly, 10 mL camel blood was diluted 1:2 in PBS and overlaid on 15 mL Lymphoprep™ (STEMCELL Technologies Inc. Vancouver, BC, Canada). After centrifugation for 30 min at 1000 × g and 10°C without brake, the MNC were collected from the interphase into new 15 mL tubes containing 2 mL cold PBS. The collected cells were washed three times with PBS (500, 250, and 100 × g, each for 10 min). Finally, the cell pellet was resuspended in PBS and adjusted to 1×10^7 cells/mL. Cell viability (always more than 95%) was evaluated by flow cytometry after adding propidium iodide (2 µg/mL) to the cells. The immunophenotype of blood neutrophils was analyzed by staining whole blood leukocytes. For this, red blood cells were removed by hypotonic lysis and the remaining cell pellet were suspended in PBS (5×10^6 cells/mL).

2.3 Cell separation from lymph node samples

Bronchial and mesenteric lymph node cell suspension was prepared as previously described (14) with some modifications. Firstly, fat and connective tissue were removed from the capsule and the lymph nodes were placed in sterile Petri dishes containing cold PBS-EDTA. The nodes were then cut into small pieces and minced using sterile scissors and forceps. The minced lymph nodes were suspended in PBS-EDTA and the cell supernatants were passed through a cell strainer. After that, the cell suspensions prepared from different regional pieces were merged to homogenize the content making it representative for the whole lymph node. After a washing step in PBS-EDTA for 10 min at 4°C and 300 × g, the cell pellet was resuspended in PBS-EDTA and contaminating red blood cells were removed by hypotonic lysis. Finally, the cell pellet was resuspended in PBS-EDTA at 1.0×10^7 cells/mL. Cell viability (always more than 95%)

was evaluated by flow cytometry after adding propidium iodide (2 μg/mL) to the cells.

2.4 Antibodies used in the study

The specificity, clone, species of origin, and commercial provider for all primary and secondary antibodies used in the current study are described in Table 1. The antibody combinations used for the multi-color staining are described in Table 2.

2.5 Membrane immunofluorescence and flow cytometry

Lymph node cells, blood MNC, or total leukocytes were labeled with monoclonal antibodies (mAbs) to camel leukocyte antigens and analyzed by flow cytometry (13). Separated cells (1×10^6 cells/well) were incubated in the wells of a 96-well plate with mAbs cross-reactive with the homologous camel molecules: CD45, CD44, BAQ44A, WC1, CD4, CD18, CD172a, CD14, CD163, and MHCII (15, 16). After incubation (15 min; 4°C), cells were washed twice and were incubated with mouse secondary antibodies (IgM, IgG1, IgG2a; Invitrogen) labelled with different fluorochromes or with mouse isotype control antibodies (Becton Dickinson Biosciences). After washing, cells were analyzed on a Becton Dickinson Accuri C6 flow cytometer (Becton Dickinson Biosciences, San Jose, California, United States). Data of at least 100,000 cells were collected and analyzed with the flow cytometric software C-Flow (Becton Dickinson Biosciences, San Jose, California, United States). For multi-color staining tubes, correction of fluorescence spillover was done after calculation of compensation matrix using the Accuri C6 compensation calculator Excel sheet. For this, a set of single-stained control samples was used to determine the extent of fluorescence spillover from each fluorochrome.

2.6 Statistical analyses

Data analysis was performed using the flow cytometric software C-Flow (BD). Means and standard error of mean (SEM) were calculated using the column statistic function of the Prism software (GraphPad). Differences between means were tested with *t*-test with *p*-value of less than 0.05 being considered significant.

3 Results

3.1 Lymph node and peripheral blood mononuclear cells show different fractions of lymphocytes and monocytes

The majority of both lymph node cells and blood MNC stained positively with mAbs to the pan-leukocyte marker CD45 (Figure 1A). A higher ($p < 0.05$) fraction of lymphocytes (CD172a− CD45+) was found within bronchial (97.9 ± 0.2; mean ± SEM) and mesenteric (96.6 ± 0.5) lymph node than blood MNC (83.1 ± 2.6) (Figures 1B,D). Staining with mAbs to CD14 revealed a lower percentage of monocytes within bronchial (2.3 ± 0.2) and mesenteric (5.2 ± 0.2) lymph node cells compared to blood (17.2 ± 2.4) MNC (Figures 1C,E). The complete gating strategy is described in the Supplementary Figure S1.

TABLE 1 List of antibodies.

Antigen	Antibody clone	Labeling	Source	Isotype
CD45	LT12A	–	Kingfisher	Mouse IgG2a
CD44	LT41A	–	Kingfisher	Mouse IgG2a
CD14	CAM36A	–	Kingfisher	Mouse IgG1
MHCII	TH81A5	–	Kingfisher	Mouse IgG2a
CD172a	DH59b		Kingfisher	Mouse IgG1
CD163	LND68A	–	Kingfisher	Mouse IgG1
CD4	GC50A1	–	VMRD	Mouse IgM
WC1	BAQ128A	–	VMRD	Mouse IgG1
B cells	BAQ44A	–	Kingfisher	Mouse IgM
CD18	6.7	FITC	BD	Mouse IgG2a
Mouse IgM	poly	APC	Thermofisher	Goat IgG
Mouse IgG1	poly	FITC	Thermofisher	Goat IgG
Mouse IgG2a	poly	PE	Thermofisher	Goat IgG

MHC, major histocompatibility complex; WC1, workshopcluster 1; APC, allophycocyanin; FITC, fluorescein isothiocyanate; PE, phycoerythrin; poly, polyclonal.

TABLE 2 Staining combinations.

Combination	Primary antibody cocktail	Secondary antibody cocktail
1	CD45/CD172a	Mouse IgG1-FITC/Mouse IgG2a-PE
2	CD4/WC1	Mouse IgG1-FITC/Mouse IgM-APC
3	CD14/MHCII/ BAQ44A	Mouse IgG1-FITC/Mouse IgG2a-PE/ Mouse IgM-APC
4	CD163/CD44	Mouse IgG1-FITC/Mouse IgG2a-PE
5	CD18-FITC	
6	CD4/MHCII	Mouse IgG2a-PE/Mouse IgM-APC
7	–	Mouse IgG1-FITC/Mouse IgG2a-PE/ Mouse IgM-APC

MHC, major histocompatibility complex; WC1, workshop cluster 1; APC, allophycocyanin; FITC, fluorescein isothiocyanate; PE, phycoerythrin.

3.2 Different cellular composition of lymph node and blood lymphocytes

Staining of blood and lymph node cells with monoclonal antibodies to camel CD4, WC1 (Figure 2A), and MHCII (Figure 2B), revealed higher ($p < 0.05$) percentage of CD4+ lymphocytes (Figure 2C) in bronchial (49.2 ± 3.3) and mesenteric (43.7 ± 0.9) lymph nodes than in blood (27.8 ± 3.8), while the percentage of WC1+ lymphocytes (Figure 2D) was significantly higher ($p < 0.05$) in blood (5.0 ± 0.2) than bronchial (1.6 ± 0.9) and mesenteric lymph nodes (0.8 ± 0.9). Bronchial lymph node lymphocytes (17.4 ± 0.6) contained the highest ($p < 0.05$) percentage of B cells compared to mesenteric lymph nodes (10 ± 0.3) and blood lymphocytes (13.8 ± 0.9) cells (Figure 2E). The complete gating strategy is described in the Supplementary Figure S2.

10.3389/fvets.2024.1365319

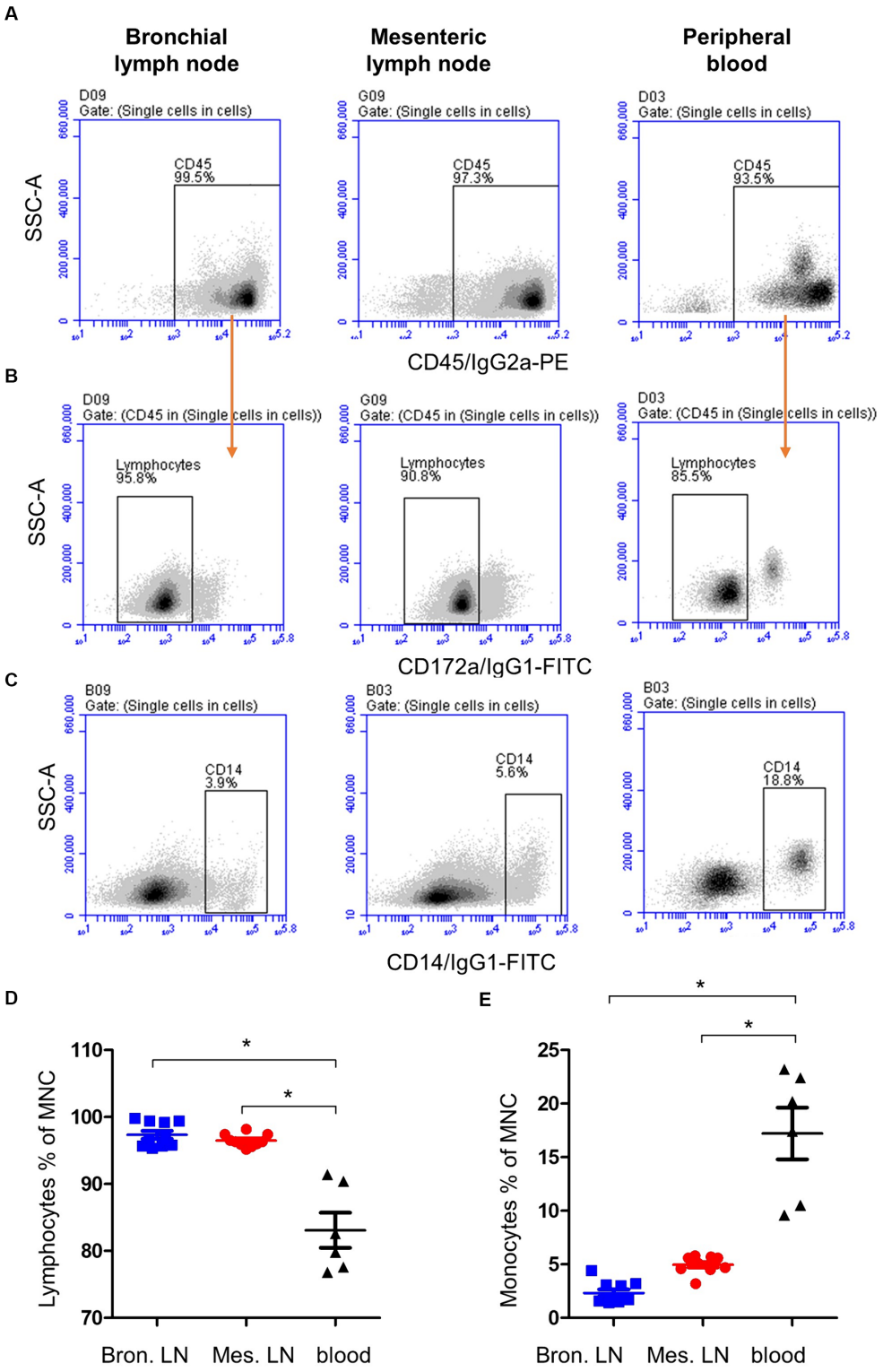

FIGURE 1
Gating strategy for the flow cytometric analysis of blood and lymph node (bronchial and mesenteric) mononuclear cells. Cells were stained with mAbs to CD45, CD172a, and CD14 and analyzed on the flow cytometer. **(A)** The percentage of cells stained positive with CD45 mAb was identified within single cells after excluding the cell doublets. **(B)** Staining of lymph node cells and blood MNC with mAbs to CD172a within CD45-positive cells. **(C)** Staining pattern of lymph node cells and blood MNC with mAbs to CD14. The percentage of lymphocytes **(D)** and monocytes **(E)** of total bronchial (blue color), mesenteric (red color) lymph node, or blood MNC (black color) were calculated and presented. * indicates significant differences ($n = 10$ animals for lymph node samples and six animals for blood samples; $p < 0.05$).

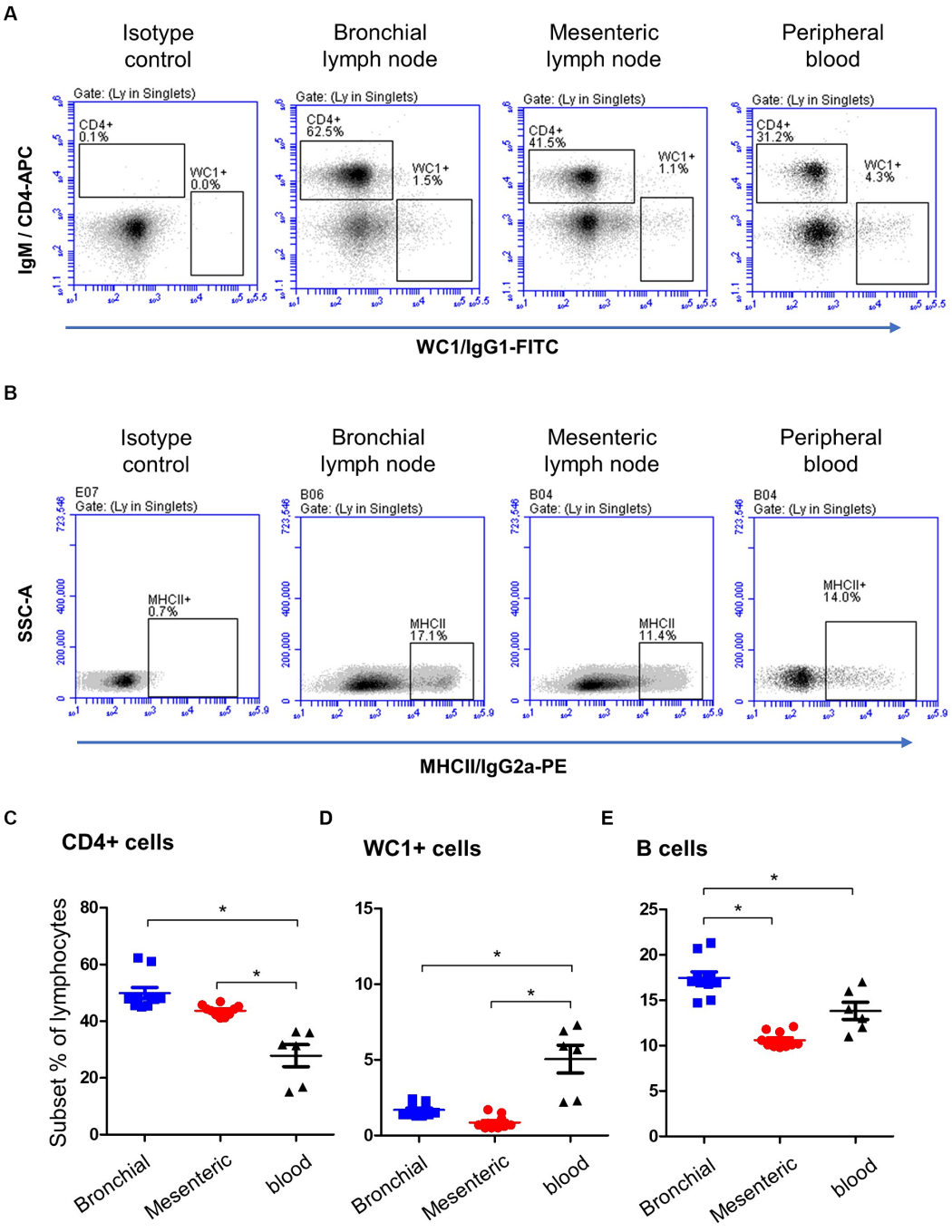

FIGURE 2
Lymphocyte subsets in bronchial and mesenteric lymph node and blood of camels. **(A)** After gating on lymphocytes within MNC, CD4+ and WC1+ cells were identified based on their staining with corresponding monoclonal antibody compared to isotype control staining. **(B)** Camel B cells were identified as MHCII-positive cells within the lymphocyte population (CD14-negative MNC). The percentages of CD4+ **(C)**, WC1+ **(D)**, and B cells **(E)** within lymphocytes were calculated and presented comparatively for bronchial (blue color), mesenteric (red color) lymph node, or blood MNC (black color).

3.3 The camel B cell marker BAQ44A is differently expressed on lymph node and blood lymphocytes

A combined staining with antibodies to CD14, MHCII, and BAQ44A (Figures 3A,B) revealed different expression of BAQ44A on lymph node and blood cells. The percentage of BAQ44A+ cells within total lymphocytes was ten-time higher ($p < 0.05$) in blood (17.9 ± 1.8) than bronchial (1.9 ± 0.2) lymph nodes. The lowest ($p < 0.05$) frequency of BAQ44A+ cells was, however, found in mesenteric lymph nodes (0.4 ± 0.1). Similarly, blood MHCII+ lymphocytes contained a higher ($p < 0.05$) fraction of BAQ44A+ cells than bronchial and mesenteric lymph nodes cells (Figure 3C).

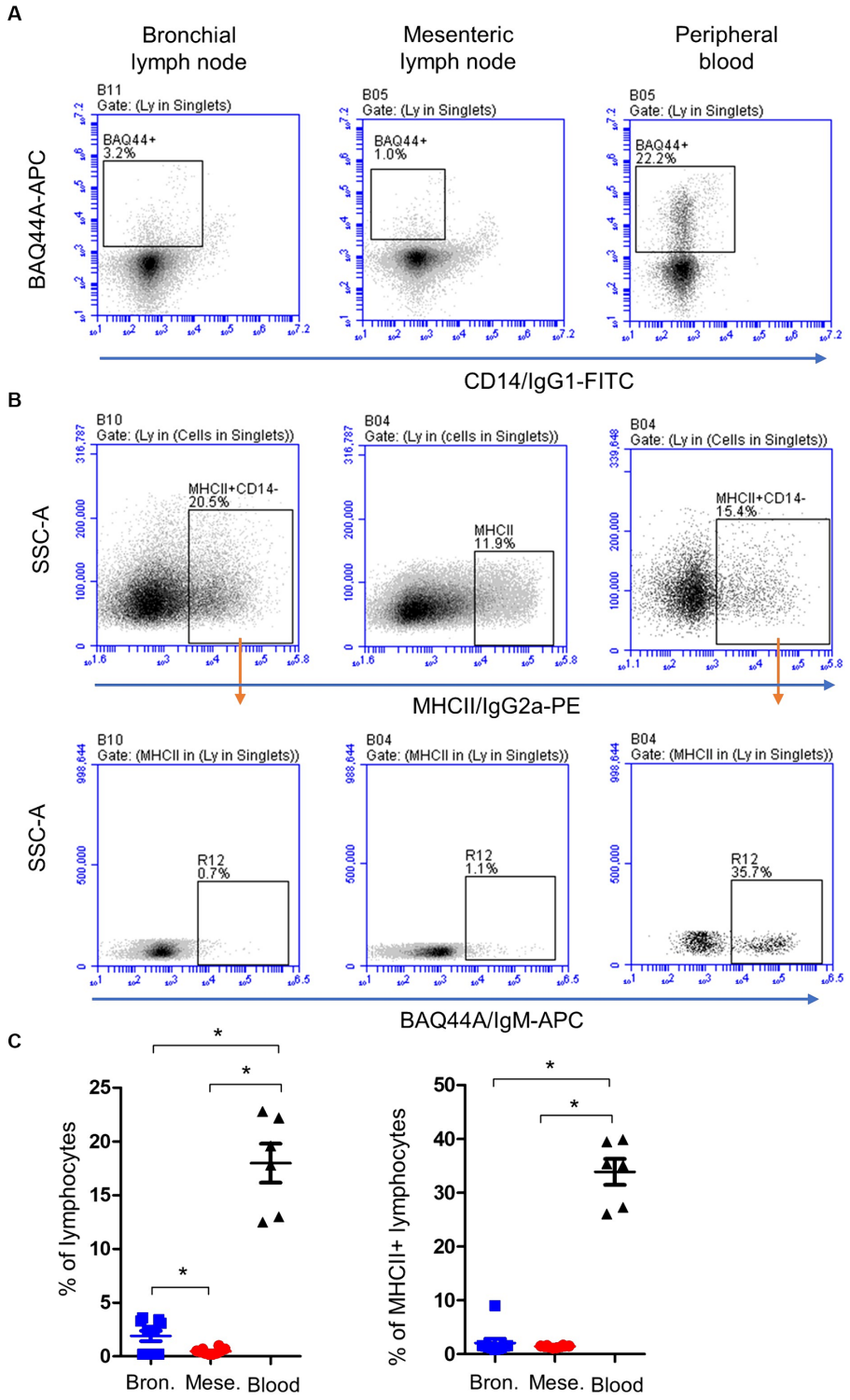

FIGURE 3
Expression of the B cell marker BAQ44A on bronchial and mesenteric lymph node and blood lymphocytes. Lymph node cells or blood MNC were labeled with antibodies to CD14, MHCII, and BAQ44A. **(A)** The fraction of BAQ44A+ cells within lymphocytes was identified as CD14-BAQ44A+ cells. **(B)** After gating on lymphocytes (CD14- MNC), a gate was placed on MHCII+ cells and the percentage of BAQ44A+ cells within MHCII+ cells was identified in a separate dot plot. **(C)** The BAQ44A+ cells within total lymphocytes or within B cells (MHCII+ lymphocytes) were calculated and presented for bronchial (blue color), mesenteric (red color) lymph node, or blood MNC (black color).

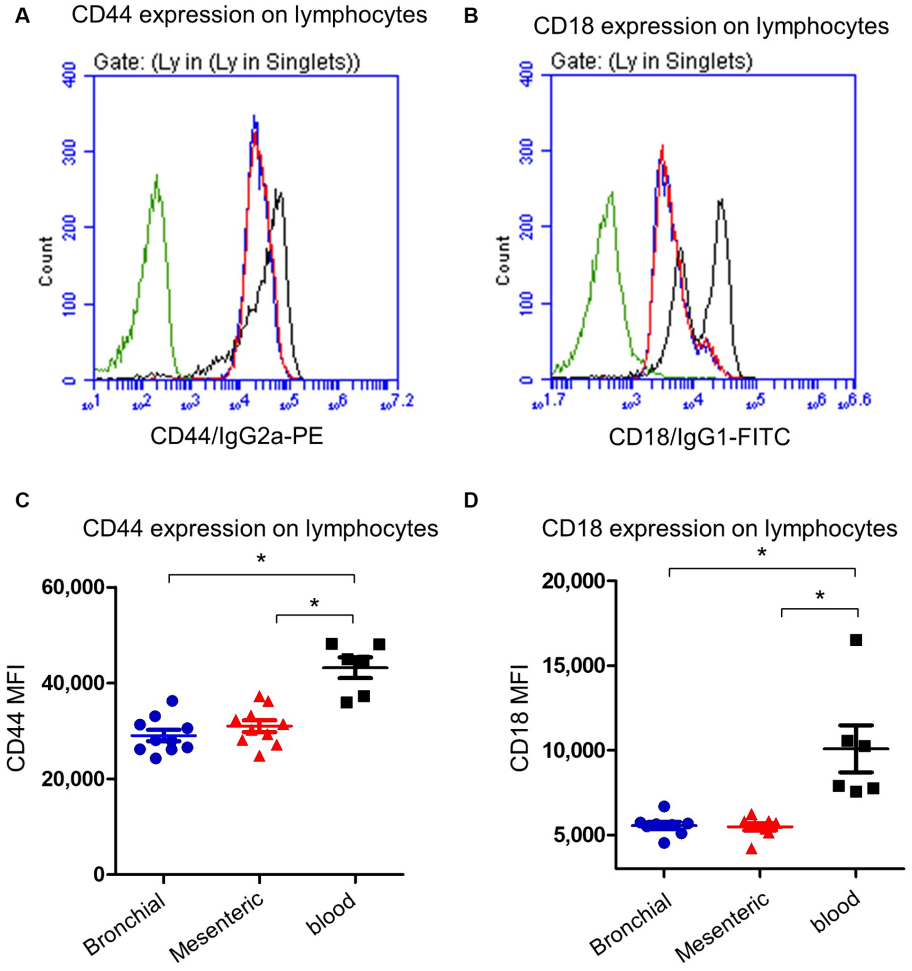

FIGURE 4
Expression of the cell adhesion molecules CD44 and CD18 on camel lymph node and blood lymphocytes. Camel lymph node cells and blood MNC were stained with antibodies to camel CD44 or CD18 and analyzed by flow cytometry. Histogram presentation of CD44+ **(A)** or CD18+ **(B)** lymphocytes within bronchial lymph node (blue line), mesenteric lymph node (red line), and blood cells (black line) in comparison to isotype control (green line). Mean fluorescence intensity (MFI) of CD44+ cells **(C)** or CD18+ cells **(D)** were calculated and presented in scattered plot graphs for bronchial (blue color), mesenteric (red color) lymph node, or blood MNC (black color).

3.4 Expression of the cell adhesion molecules CD44 and CD18 on lymph node and blood lymphocytes

Bronchial and mesenteric lymph node lymphocytes showed lower expression ($p<0.05$) of the cell surface molecule CD44 (Figures 4A,C) compared to lymphocytes from peripheral blood with a mean fluorescence intensity (MFI) value cells of 29,472 ± 1,676 on mesenteric lymph node compared to bronchial lymph node (29,047 ± 1,135) and blood cells (43,180 ± 2,174). Similarly, the expression of CD18 was significantly ($p<0.05$) lower on bronchial (5,563 ± 214) and mesenteric lymph nodes (5,675 ± 102) lymphocytes than blood (10,091 ± 1,393) lymphocytes (Figures 4B,D).

3.5 Lymph node and peripheral blood neutrophils showed different immunophenotype

Neutrophils were identified within lymph nodes and blood cells based on their light scatter properties (Figures 5A,B). With a mean of 4.7 (±0.4; standard error of the mean; SEM) for bronchial lymph nodes and 6.2 ± 0.8 for mesenteric lymph nodes, neutrophils were only a minor fraction within lymph nodes cells (Figure 5C), which is significantly ($p<0.05$) lower than their percentage in peripheral blood (72 ± 2.4).

The immunophenotype of neutrophils was identified based on their staining with mAbs against CD45, CD172a, CD14, MHCII, CD163, CD44, and CD18 (Figure 6A). Staining with marker-specific mAbs were compared with isotype control background staining. Additionally, the expression of the BAQ44A marker antigen was compared between lymph node (Figure 6A) and blood neutrophils (Figure 6B).

Similar to blood neutrophils, lymph node neutrophils stained positive for the pan-leukocyte marker CD45, the myeloid marker CD172a, and the LPS-receptor CD14, the cell adhesion molecules CD44 and CD18 with different surface molecules abundance in comparison to blood neutrophils. Compared to their counterparts in blood, lymph node neutrophils showed comparable level of the pan-leukocyte marker CD45 (Figure 7A). The abundance of the monocyte markers CD14 and MHCII (Figures 7C,D) was significantly higher on lymph node cells, while the myeloid marker CD172a was significantly lower expressed on lymph

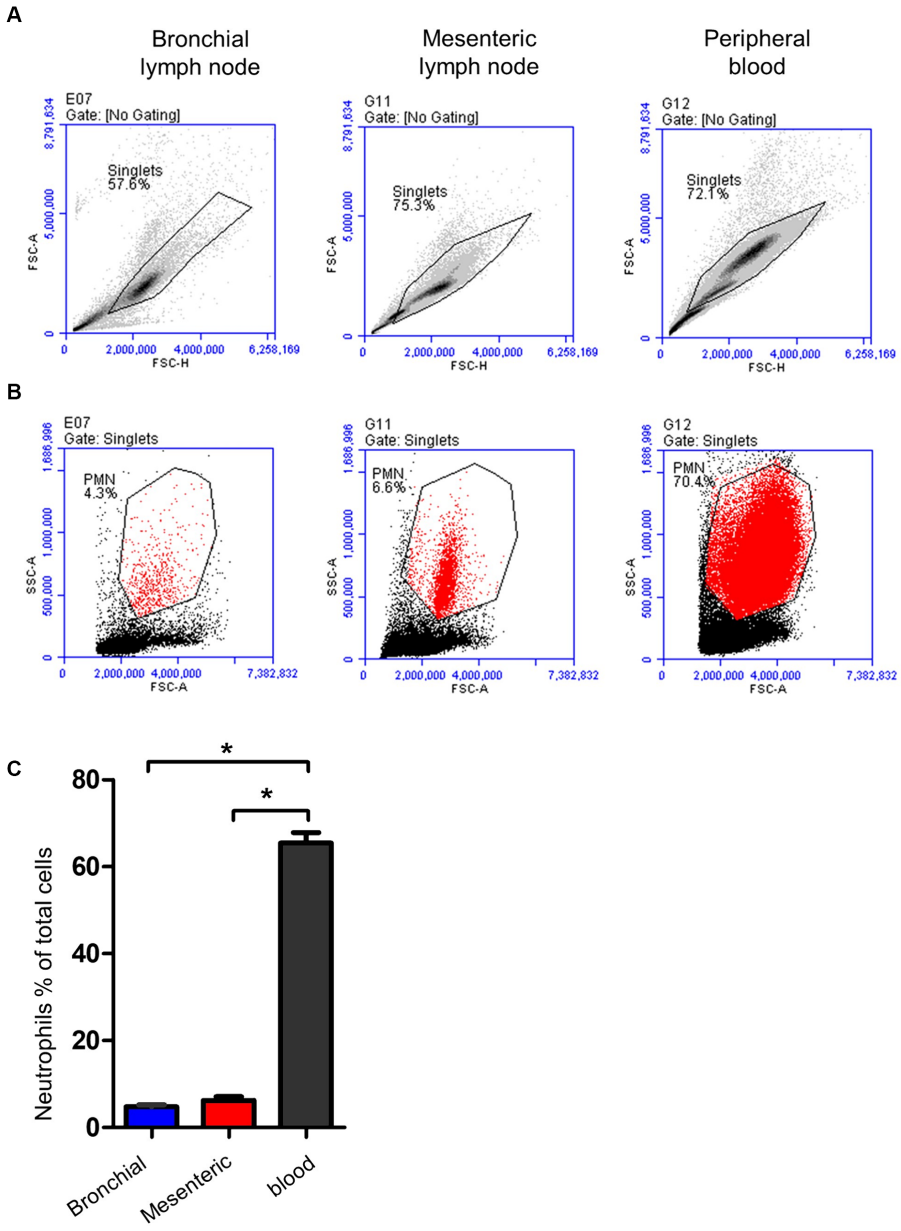

FIGURE 5
Gating strategy for lymph node and blood neutrophils (PMN). **(A)** Camel leukocytes or lymph node cells were analyzed by flow cytometry. **(B)** Neutrophils were identified based on their forward and side scatter properties and their percentages within bronchial (blue color), mesenteric (red color) lymph node, or blood leukocytes (black color) were presented **(C)**.

node neutrophils compared to blood neutrophils (Figure 7B). The cell adhesion molecules CD44 and CD18 were also higher expressed on lymph node neutrophils compared to blood neutrophils (Figures 7E,F). Interestingly, lymph node neutrophils showed a positive staining with the B cell marker BAQ44A, which was in contrast to neutrophils from peripheral blood (Figure 7G). For all surface markers, no significant differences could be identified between values for mesenteric and bronchial lymph nodes neutrophils ($p > 0.05$).

4 Discussion

Lymphocytes are migratory cells that circulate through the different lymphoid and non-lymphoid organs of the body (17). Although their numbers in the peripheral blood represent only a minor fraction (about 2% in adult human) of the total numbers of lymphocytes pool in the body, the frequency of lymphocyte subsets in the peripheral blood is beneficial in daily clinical routine for the evaluation of the immune status of diseased individuals and to design and monitor treatment plans (18, 19). As changes in composition and phenotype of blood lymphocyte does not always reflect changes in the body lymphocyte compartment, the analysis of the tissue-specific distribution of lymphocyte subsets is of primary importance. Given the limited data on detailed immune cell composition and cell marker expression in the dromedary camel lymph node tissue, the present study was undertaken to investigate the immune cell composition of bronchial and mesenteric lymph nodes from healthy dromedary camels using flow cytometry.

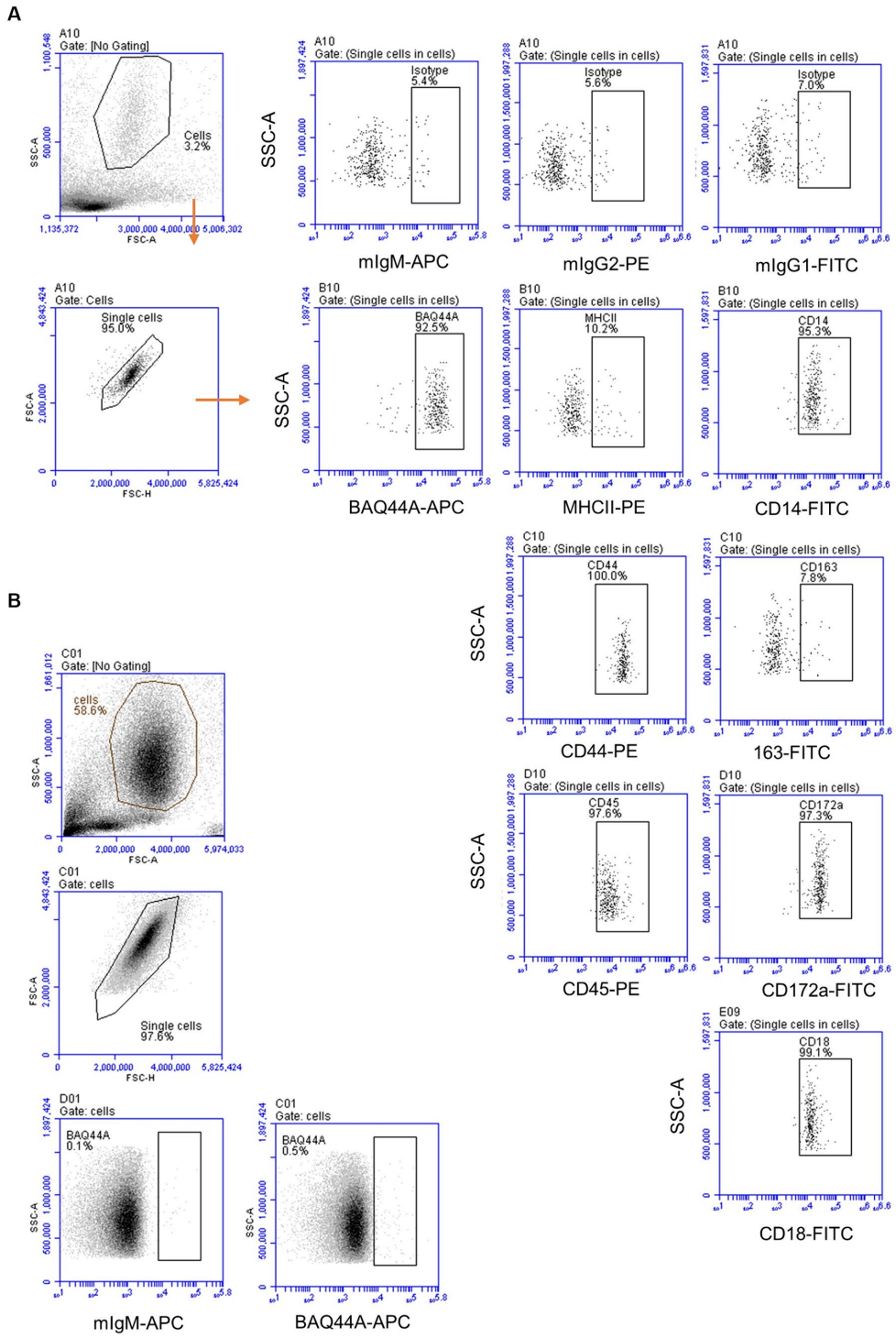

FIGURE 6
The immunophenotype of lymph node and blood neutrophils. **(A)** Lymph node neutrophils were stained with mAbs to different cell markers and analyzed on the Accuri flow cytometer. **(B)** Blood-derived neutrophils were stained with mAbs to BAQ44A and analyzed by flow cytometry.

Combined staining with mAbs to the pan-leukocyte marker CD45 and the myeloid markers CD172a and CD14 enabled the differentiation between myeloid and lymphoid cells within camel lymph node cells with a comparable composition to bovine (7) and ovine (20) lymph nodes. In addition, the dominance of CD4+ T cells within camel lymph node lymphocytes seems in line with reports in other ruminants (7, 21, 22). Using the same mAbs clones used in the present study, Navarro et al. found similar percentage of CD4+ T cells in bovine blood and lymph nodes (21). Gamma delta (γδ_) T cells represent a major component of the lymphocyte system in ruminants including camels (23). The workshop cluster (WC) 1 antigen, which is a transmembrane glycoprotein related to the scavenger receptor

10.3389/fvets.2024.1365319

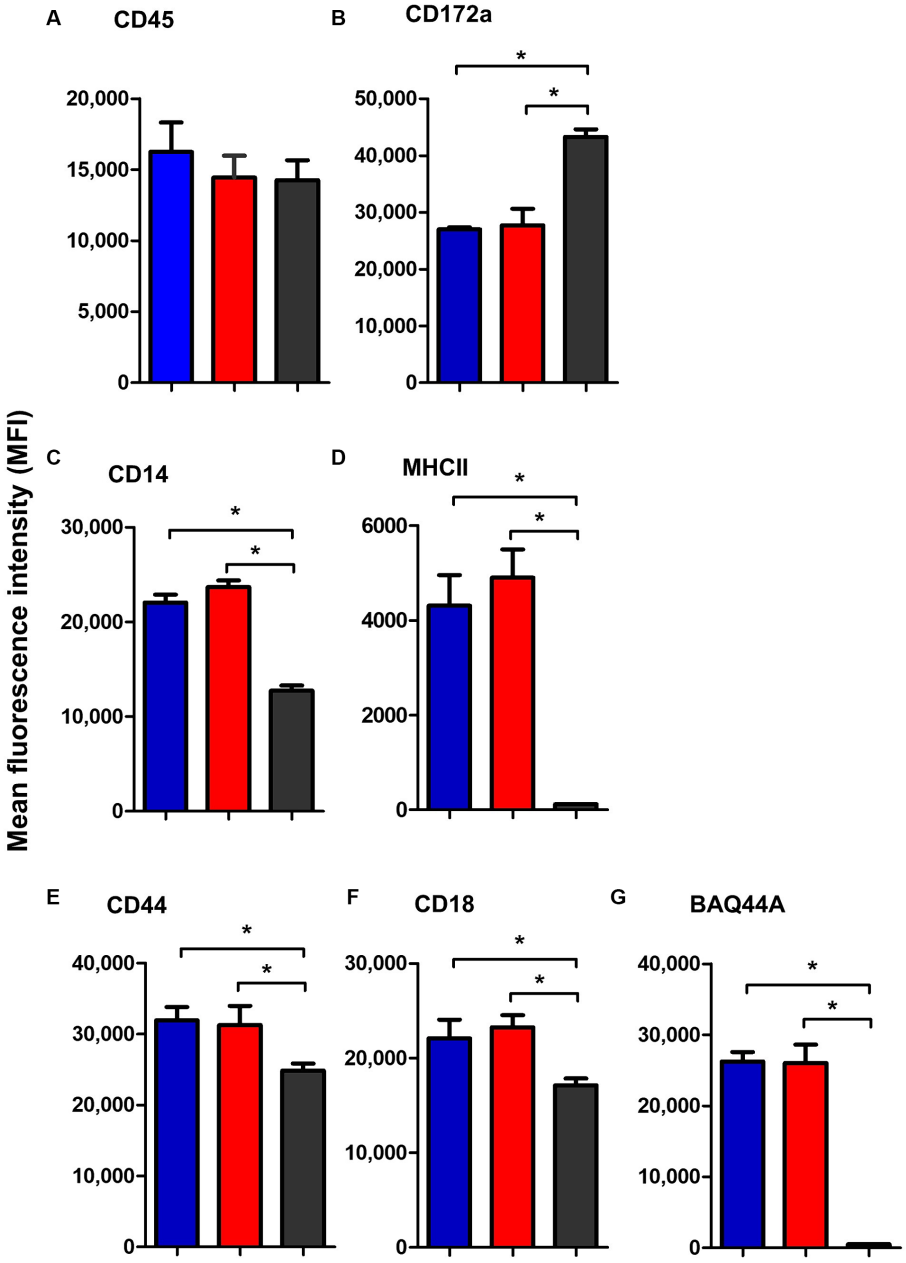

FIGURE 7
The abundance of CD45 **(A)**, CD172a **(B)**, CD14 **(C)**, MHCII **(D)**, CD44 **(E)**, CD18 **(F)**, and BAQ44A **(G)** on neutrophils from camel bronchial (blue color), mesenteric (red color) lymph node, or blood neutrophils (black color). Molecule expression level was presented as mean fluorescence intensity (MFI) of the corresponding antibody staining.

CD163 (24), was used in the present study to identify camel γδ T cells. Although it is expressed on a large proportion of ruminant γδ T cells, using WC1 mAbs will probably miss WC1-negative γδ T cells (25). Therefore, the development of antibodies to camel γδ TCR is essential for complete identification of all γδ T cell subsets. In the present work, the frequency of MHCII+ and WC1+ lymphocytes in lymph nodes compared to blood indicates a similar tissue distribution pattern of B cells and γδ T cells in camel and bovine (21). All these results support previous reports on the similarity between the camel immune system and the immune system of other ruminants (26). Although mesenteric and bronchial lymph nodes showed similar frequency of lymphoid and monocytic cells as well as of helper and γδ T cell subsets, the lower fraction of B cells in the mesenteric lymph nodes indicates a tissue-specific distribution of these cells in the camel.

The BAQ44A mAb recognizes a non-immunoglobulin 60,000 MW B cell-lineage-specific molecule that has been characterized in ruminants and does not correspond to the human CD nomenclature (27–29). In goats, BAQ44A mAb marked both surface immunoglobulin (sIg)+ and sIg− B cells in the B cell areas in the germinative center dark zone, but did not label plasma cells (30). In the present study, a significant proportion (25 to 40%) of camel peripheral blood B cells (MHCII+CD14− lymphocytes) stained positive with BAQ44A, which is similar to the expression pattern for blood B cells from bovine and small ruminants (21). In contrast, the

lower fraction of BAQ44A+ cells within total lymphocytes and MHCII+ lymphocytes in camel lymph nodes cells compared to blood MNC indicates different expression pattern of BAQ44A in camel and other ruminants (30). The functional relevance of this species-specific expression of BAQ44A requires functional characterization of the BAQ44A molecule. Using MHCII staining for the identification of camel B cells represents a limitation of the present study. This is because MHCII molecules could also be detected on a minor subsets of activated T cells in bovine (31) and human (32). In the healthy dromedary camel, although we could not identify any MHCII expression on CD4+ T cells (Supplementary Figure S3), we cannot exclude the induction of such subset within stimulated T cells in diseased animals. Although we tested several antibodies to human and bovine CD19, CD20, CD21 for their reactivity with camel homologous antigens without any potential cross-reactivity, further studies are required to screen antibodies to other specific B cell markers like CD79a and Pax5 for their reactivity with camel B cells.

CD44 is a cell adhesion receptor (also known as P-glycoprotein 1) involved in cell adhesion and migration (33, 34). In immunophenotyping studies involving human and mice, CD44 abundance is usually used as a marker for the differentiation between memory or effector and naïve lymphocytes (4), with low CD44 expression being indicative of the naïve cell phenotype (4, 35). In the present study, lymph node lymphocytes showed lower CD44 expression compared to lymphocytes from peripheral blood, indicating a higher frequency of naïve lymphocytes in the lymph nodes. This was also supported by the lower expression of the cell adhesion molecule CD18 on lymph node compared to blood lymphocytes (36). The presence of naïve T cells in lymphoid and mucosal tissues has been described previously with the evidence that these cells are blood-derived cells that supply the draining lymph nodes with cells that can be rapidly sampled by local antigen-presenting cells (4, 37).

Lymph nodes serve as sites for the immune response against infections, carrying out the crucial role of filtering tissues and tissue fluids. Their immune cell composition and phenotype may reflect pathologies in tissues they drain. Although bronchial and mediastinal lymph nodes are responsible for trapping and immune response to respiratory and intestinal antigens, respectively, recent studies reported the existence of gut-lung axis with a bidirectional migration and cross-talk between immune cells in the two localizations (38, 39). In subsequent *in vivo* investigations, it is plausible to employ the mAbs elucidated in the current study in combination with cell tracking dyes, to examine the homing and migratory behaviors of immune cells within the two compartments in both healthy and diseased states of camels.

For the human and murine systems, recent studies reported tissue-specific phenotype for lymph node circulating neutrophils (10). In the present study, immunostaining of lymph node neutrophils revealed a $CD45^{++}$ $CD172a^{++}$, $CD14^{+}$, $MHCII^{low}$, $BAQ44A^{+}$, $CD44^{++}$, $CD18^{++}$ phenotype with some differences to their phenotype in blood. The expression of low levels of CD14 on lymph node neutrophils seems in line with the expression pattern of this LPS receptor on camel (40) and bovine (41) blood neutrophils. In addition, the lack of BAQ44A expression on lymph node monocytes (Supplementary Figure S4) argues against a general expression of this marker on all lymph node myeloid cells. Uncovering the function of BAQ44A in future studies would help in understanding the relevance of its expression on lymph node neutrophils. In addition, the elevated abundance of the MHCII molecules suggests a role for these tissue cells in antigen presentation and activation of CD4-positive T helper cells in the camel lymph nodes. This finding seems in line with recent reports revealing high MHCII expression on human lymph nodes neutrophils (42, 43). In addition, murine neutrophils gained the ability to activate T helper cells through the up-regulation of MHCII molecules and costimulatory molecules upon stimulation with immune complexes (42, 44). Together, all these findings suggest a new role for neutrophils in antigen presentation and indicate their involvement in the adaptive immune response. In fact, these findings related to the immunophenotype of lymph node neutrophils are still limited by the lack of antibodies to specific neutrophils marker in camel like the CD15 in human, Ly-6G in mice, or CH138A in cattle. As a result, the cell population identified as granulocytes based on their FSC and SSC properties may contain other large cells including stromal cell types with high SSC signals. Therefore, future studies may focus on the isolation of these cells using cell sorting and confirming their phenotype under microscope.

Based on their reactivity with blood and lymph node immune cells, the mAbs used in the current work represent a tool for the analysis of the immune cell composition in camel lymphoid tissues. The expansion of the mAbs toolbox with reactivity to new camel antigens, especially CD8 and NKP46, would help in the identification of other lymphocyte subsets, including camel cytotoxic T cells and NK cells. After the establishment of reference values for the lymphocyte composition in blood and secondary lymphoid organs in healthy animals, subsequent studies may investigate the impact of different physiological (such as age, gender, nutritional status), environmental (stress), and pathological (infectious and noninfectious diseases) factors on the tissue-specific distribution of lymphocyte subsets in camels. The efficacy of the lymph node cell preparation process employed in the current investigation may not uniformly release all node cell populations, thereby accounting for the observed reduced occurrence of CD14+ cells. Nevertheless, the benefit of circumventing the potential impact of digestive enzymes on the cell immunophenotype, as previously documented for the often employed digestive enzymes, Collagenase and Dispase, is noteworthy (45). Another limitation of the present work is the low number of animals used for collection of blood and lymph node samples, which may not be representative of the diversity and variability of the camel population. In addition, the study does not investigate the potential effects of physiological factors, such as age, breed, and gender or environmental factors, such as diet, climate, or living conditions, on the makeup of immune cells, which is another limitation of the present work.

5 Conclusion

In conclusion, the present study employed flow cytometric single-cell analysis and monoclonal antibody staining for immunophenotyping the main populations of immune cells in the bronchial and mesenteric camel lymph nodes. A distinct expression pattern was found for the B cell marker BAQ44A in camel lymph node, with only a low fraction of BAQ44A+ cells in camel lymph nodes cells compared to blood MNC. In addition, the lower expression of CD44 and CD18 on lymph node lymphocytes compared to lymphocytes from peripheral blood indicates higher frequency of naïve lymphocytes in the lymph nodes. The identification of key

immune cells in the camel lymph node provides a valuable tool to investigate the structure of the camel lymphoid system in health and disease. Further studies are, therefore required to investigate the clinical relevance of the observed results on specific camel respiratory diseases.

Data availability statement

The raw data supporting the conclusions of this article will be made available by the authors, without undue reservation.

Ethics statement

The animal studies were approved by Ethics Committee of King Faisal University, Saudi Arabia (KFU-REC-2021-DEC-EA000326). The studies were conducted in accordance with the local legislation and institutional requirements. Written informed consent was obtained from the owners for the participation of their animals in this study.

Author contributions

JH: Conceptualization, Methodology, Writing – original draft, Writing – review & editing. HA: Conceptualization, Funding acquisition, Methodology, Writing – review & editing. MA-S: Methodology, Writing – review & editing. BF: Methodology, Writing – review & editing. AA: Methodology, Writing – review & editing.

Funding

The author(s) declare that financial support was received for the research, authorship, and/or publication of this article. This work was supported through Princess Nourah bint Abdulrahman University Researchers Supporting Project number (PNURSP2024R460), Princess Nourah bint Abdulrahman University, Riyadh, Saudi Arabia.

Conflict of interest

The authors declare that the research was conducted in the absence of any commercial or financial relationships that could be construed as a potential conflict of interest.

Publisher's note

Supplementary material

The Supplementary material for this article can be found online at: https://www.frontiersin.org/articles/10.3389/fvets.2024.1365319/full#supplementary-material

References

1. Rehfeld A, Nylander M, Karnov K. *The immune system and the lymphatic organs*. Compendium of Histology Springer Cham, (2017). 379–409

2. Yang JHM, Khatri L, Mickunas M, Williams E, Tatovic D, Alhadj Ali M, et al. Phenotypic analysis of human lymph nodes in subjects with new-onset type 1 diabetes and healthy individuals by flow cytometry. *Front Immunol*. (2019) 10:2547. doi: 10.3389/fimmu.2019.02547

3. Lun S, Astrom G, Magnusson U, Ostensson K. Total and differential leucocyte counts and lymphocyte subpopulations in lymph, afferent and efferent to the supramammary lymph node, during endotoxin-induced bovine mastitis. *Reprod Domest Anim*. (2007) 42:126–34. doi: 10.1111/j.1439-0531.2006.00741.x

4. Caucheteux SM, Torabi-Parizi P, Paul WE. Analysis of naive lung CD4 T cells provides evidence of functional lung to lymph node migration. *Proc Natl Acad Sci USA*. (2013) 110:1821–6. doi: 10.1073/pnas.1221306110

5. Koets A, Rutten V, Hoek A, van Mil F, Muller K, Bakker D, et al. Progressive bovine paratuberculosis is associated with local loss of CD4(+) T cells, increased frequency of gamma delta T cells, and related changes in T-cell function. *Infect Immun*. (2002) 70:3856–64. doi: 10.1128/IAI.70.7.3856-3864.2002

6. Gunnes G, Valheim M, Press CM, Tverdal A, Storset A. Comparison of flow cytometry and image morphometry in the quantitative analysis of cell population markers in the lymph node of sheep. *Vet Immunol Immunopathol*. (2003) 94:177–83. doi: 10.1016/s0165-2427(03)00080-1

7. Aylward BA, Clark ML, Galileo DS, Baernard AM, Wilson JR, Brannick E, et al. Immune cell populations residing in mesenteric adipose depots and mesenteric lymph nodes of lean dairy cows. *J Dairy Sci*. (2019) 102:3452–68. doi: 10.3168/jds.2018-15156

8. Jakovija A, Chtanova T. Neutrophil interactions with the lymphatic system. *Cells*. (2021) 10:82106. doi: 10.3390/cells10082106

9. Bogoslowski A, Butcher EC, Kubes P. Neutrophils recruited through high endothelial venules of the lymph nodes via PNAd intercept disseminating Staphylococcus aureus. *Proc Natl Acad Sci USA*. (2018) 115:2449–54. doi: 10.1073/pnas.1715756115

10. Lok LSC, Dennison TW, Mahbubani KM, Saeb-Parsy K, Chilvers ER, Clatworthy MR. Phenotypically distinct neutrophils patrol uninfected human and mouse lymph nodes. *Proc Natl Acad Sci USA*. (2019) 116:19083–9. doi: 10.1073/pnas.1905054116

11. Zidan M, Pabst R. Histological, histochemical and immunohistochemical study of the lymph nodes of the one humped camel (Camelus dromedarius). *Vet Immunol Immunopathol*. (2012) 145:191–8. doi: 10.1016/j.vetimm.2011.11.004

12. Zidan M, Pabst R. Lymphocyte proliferation in lymphoid organs of the dromedary camel using the monoclonal antibody MIB-5 against the proliferation-associated nuclear epitope Ki-67. *Anat Histol Embryol*. (2002) 31:286–9. doi: 10.1046/j.1439-0264.2002.00392.x

13. Eger M, Hussen J, Drong C, Meyer U, von Soosten D, Frahm J, et al. Impacts of parturition and body condition score on glucose uptake capacity of bovine monocyte subsets. *Vet Immunol Immunopathol*. (2015) 166:33–42. doi: 10.1016/j.vetimm.2015.04.007

14. Barut GT, Kreuzer M, Bruggmann R, Summerfield A, Talker SC. Single-cell transcriptomics reveals striking heterogeneity and functional organization of dendritic and monocytic cells in the bovine mesenteric lymph node. *Front Immunol*. (2022) 13:1099357. doi: 10.3389/fimmu.2022.1099357

15. Hussen J. Changes in cell vitality, phenotype, and function of dromedary camel leukocytes after whole blood exposure to heat stress in vitro. *Front Vet Sci*. (2021) 8:647609. doi: 10.3389/fvets.2021.647609

16. Hussen J, Alkuwayti MA, Falemban B, Alhojaily SM, Adwani SA, Hassan EAE, et al. Impact of selected bacterial and viral toll-like receptor agonists on the phenotype and function of camel blood neutrophils. *Vet Sci*. (2023) 10:20154. doi: 10.3390/vetsci10020154

17. McDaniel MM, Ganusov VV. Estimating residence times of lymphocytes in ovine lymph nodes. *Front Immunol*. (2019) 10:1492. doi: 10.3389/fimmu.2019.01492

18. Westermann J, Pabst R. Distribution of lymphocyte subsets and natural killer cells in the human body. *Clin Investig*. (1992) 70:539–44. doi: 10.1007/BF00184787

19. Blum KS, Pabst R. Lymphocyte numbers and subsets in the human blood. Do they mirror the situation in all organs? *Immunol Lett*. (2007) 108:45. doi: 10.1016/j.imlet.2006.10.009

20. Lund H, Boysen P, Akesson CP, Lewandowska-Sabat AM, Storset AK. Transient migration of large numbers of CD14(++) CD16(+) monocytes to the draining lymph node after onset of inflammation. *Front Immunol*. (2016) 7:322. doi: 10.3389/fimmu.2016.00322

21. Navarro JA, Caro MR, Seva J, Rosillo MC, Gomez MA, Gallego MC. Study of lymphocyte subpopulations in peripheral blood and secondary lymphoid organs in the goat using monoclonal antibodies to surface markers of bovine lymphocytes. *Vet Immunol Immunopathol*. (1996) 51:147–56. doi: 10.1016/0165-2427(95)05497-9

22. Suraud V, Jacques I, Olivier M, Guilloteau LA. Acute infection by conjunctival route with Brucella melitensis induces IgG+ cells and IFN-gamma producing cells in peripheral and mucosal lymph nodes in sheep. *Microbes Infect*. (2008) 10:1370–8. doi: 10.1016/j.micinf.2008.08.003

23. Hussen J, Shawaf T, Al-herz AI, Alturaifi HR, Alluwaimi AM. Expression patterns of cell adhesion molecules on CD4+ T cells and WC1+ T cells in the peripheral blood of dromedary camels. *Pak Vet J*. (2018) 38:231–6. doi: 10.29261/pakvetj/2018.055

24. Holm D, Fink DR, Gronlund J, Hansen S, Holmskov U. Cloning and characterization of SCART1, a novel scavenger receptor cysteine-rich type I transmembrane molecule. *Mol Immunol*. (2009) 46:1663–72. doi: 10.1016/j.molimm.2009.02.016

25. Guzman E, Hope J, Taylor G, Smith AL, Cubillos-Zapata C, Charleston B. Bovine gammadelta T cells are a major regulatory T cell subset. *J Immunol*. (2014) 193:208–22. doi: 10.4049/jimmunol.1303398

26. Elhussieny O, Zidan M. Temporospatial characterization of the bronchus associated lymphoid tissue (BALT) of the one humped camel (Camelus dromedarius). *Trop Anim Health Prod*. (2021) 53:265. doi: 10.1007/s11250-021-02694-3

27. Davis WC, Hamilton MJ. Use of flow cytometry to develop and characterize a set of monoclonal antibodies specific for rabbit leukocyte differentiation molecules. *J Vet Sci*. (2008) 9:51–66. doi: 10.4142/jvs.2008.9.1.51

28. Soder KJ, Holden LA. Lymphocyte proliferation response of lactating dairy cows fed varying concentrations of rumen-protected methionine. *J Dairy Sci*. (1999) 82:1935–42. doi: 10.3168/jds.S0022-0302(99)75429-9

29. Stabel JR, Bannantine JP, Humphrey S. B cell phenotypes and maturation states in cows naturally infected with Mycobacterium avium subsp. *Paratuberculosis PLoS One*. (2022) 17:e0278313. doi: 10.1371/journal.pone.0278313

30. Pallares FJ, Seva J, Bernabe A, Gomez MA, Navarro JA. Characterization and distribution of B cells in the lymphoid organs of goats. *Anat Histol Embryol*. (1999) 28:171–6. doi: 10.1046/j.1439-0264.1999.00192.x

31. Isaacson JA, Flaming KP, Roth JA. Increased MHC class II and CD25 expression on lymphocytes in the absence of persistent lymphocytosis in cattle experimentally infected with bovine leukemia virus. *Vet Immunol Immunopathol*. (1998) 64:235–48. doi: 10.1016/s0165-2427(98)00139-1

32. Holling TM, van der Stoep N, Quinten E, van den Elsen PJ. Activated human T cells accomplish MHC class II expression through T cell-specific occupation of class II transactivator promoter III. *J Immunol*. (2002) 168:763–70. doi: 10.4049/jimmunol.168.2.763

33. Senbanjo LT, Chellaiah MA. CD44: A multifunctional cell surface adhesion receptor is a regulator of progression and metastasis of cancer cells. *Front Cell Dev Biol*. (2017) 5:18. doi: 10.3389/fcell.2017.00018

34. Underhill C. CD44: the hyaluronan receptor. *J Cell Sci*. (1992) 103:293–8. doi: 10.1242/jcs.103.2.293

35. Sckisel GD, Mirsoian A, Minnar CM, Crittenden M, Curti B, Chen JQ, et al. Differential phenotypes of memory CD4 and CD8 T cells in the spleen and peripheral tissues following immunostimulatory therapy. *J Immunother Cancer*. (2017) 5:33. doi: 10.1186/s40425-017-0235-4

36. Bondarenko AV, Boyarchuk OR, Sakovich IS, Polyakova EA, Migas AA, Kupchinskaya AN, et al. Variable CD18 expression in a 22-year-old female with leukocyte adhesion deficiency I: clinical case and literature review. *Clin Case Rep*. (2023) 11:e7791. doi: 10.1002/ccr3.7791

37. Cose S, Brammer C, Khanna KM, Masopust D, Lefrancois L. Evidence that a significant number of naive T cells enter non-lymphoid organs as part of a normal migratory pathway. *Eur J Immunol*. (2006) 36:1423–33. doi: 10.1002/eji.200535539

38. Elmore SA. Histopathology of the lymph nodes. *Toxicol Pathol*. (2006) 34:425–54. doi: 10.1080/01926230600964722

39. Ma Y, Yang X, Chatterjee V, Wu MH, Yuan SY. The gut-lung Axis in systemic inflammation. Role of mesenteric lymph as a conduit. *Am J Respir Cell Mol Biol*. (2021) 64:19–28. doi: 10.1165/rcmb.2020-0196TR

40. Hussen J. Flow cytometric analysis of phenotype and composition of peripheral blood leukocytes in young and old dromedary camels (Camelus dromedarius). *J Camel Pract Res*. (2018) 25:29–8. doi: 10.5958/2277-8934.2018.00004.8

41. Sohn EJ, Paape MJ, Bannerman DD, Connor EE, Fetterer RH, Peters RR. Shedding of sCD14 by bovine neutrophils following activation with bacterial lipopolysaccharide results in down-regulation of IL-8. *Vet Res*. (2007) 38:95–108. doi: 10.1051/vetres:2006052

42. Culshaw S, Millington OR, Brewer JM, McInnes IB. Murine neutrophils present class II restricted antigen. *Immunol Lett*. (2008) 118:49–54. doi: 10.1016/j.imlet.2008.02.008

43. Castell SD, Harman MF, Moron G, Maletto BA, Pistoresi-Palencia MC. Neutrophils which migrate to lymph nodes modulate CD4(+) T cell response by a PD-L1 dependent mechanism. *Front Immunol*. (2019) 10:105. doi: 10.3389/fimmu.2019.00105

44. Vono M, Lin A, Norrby-Teglund A, Koup RA, Liang F, Lore K. Neutrophils acquire the capacity for antigen presentation to memory CD4(+) T cells in vitro and ex vivo. *Blood*. (2017) 129:1991–2001. doi: 10.1182/blood-2016-10-744441

45. Abuzakouk M, Feighery C, O'Farrelly C. Collagenase and Dispase enzymes disrupt lymphocyte surface molecules. *J Immunol Methods*. (1996) 194:211–6. doi: 10.1016/0022-1759(96)00038-5

frontiers | Frontiers in Veterinary Science

TYPE Original Research
PUBLISHED 02 May 2024
DOI 10.3389/fvets.2024.1389977

OPEN ACCESS

EDITED BY
Alberto Alvarez-Barrientos,
Universidad de Extremadura, Spain

REVIEWED BY
Jordi Petriz,
Germans Trias i Pujol Health Science Research Institute (IGTP), Spain
Andre Mozes,
Champalimaud Foundation, Portugal

*CORRESPONDENCE
José-Enrique
✉ O'Connorjose.e.oconnor@uv.es
Consuelo Rubio-Guerri
✉ consuelo.rubio@uchceu.es

RECEIVED 22 February 2024
ACCEPTED 27 March 2024
PUBLISHED 02 May 2024

CITATION
Felipo-Benavent M, Martínez-Romero A, Valls M, Rojo-Solís C, Álvaro T, García-Párraga D, Rubio-Guerri C and O'Connor J-E (2024) Physiological values of phagocytic capacity in marine mammals and alterations during pathological situations. *Front. Vet. Sci.* 11:1389977. doi: 10.3389/fvets.2024.1389977

Physiological values of phagocytic capacity in marine mammals and alterations during pathological situations

Mar Felipo-Benavent[1,2], Alicia Martínez-Romero[3], Mónica Valls[4], Carlos Rojo-Solís[4], Teresa Álvaro[4], Daniel García-Párraga[4,5], Consuelo Rubio-Guerri[5,6]* and José-Enrique O'Connor[1,7]*

[1]Laboratory of Cytomics, Joint Research Unit CIPF-UVEG, Department of Biochemistry and Molecular Biology, University of Valencia, Valencia, Spain, [2]Department of Biomedical Sciences, Faculty of Health Sciences, Universidad CEU Cardenal Herrera, CEU Universities, Valencia, Spain, [3]Cytomics Technological Service, Príncipe Felipe Research Center, Valencia, Spain, [4]Veterinary Services, Avanqua Oceanográfic SL, Oceanogràfic, Ciudad de las Artes y las Ciencias, Valencia, Spain, [5]Research Department, Fundación Oceanogràfic de la Comunitat Valenciana, Oceanogràfic, Ciudad de las Artes y las Ciencias, Valencia, Spain, [6]Department of Pharmacy, Faculty of Health Sciences, Universidad CEU Cardenal Herrera, CEU Universities, Valencia, Spain, [7]Laboratory of Cytomics, Department of Biochemistry and Molecular Biology, Faculty of Medicine, Valencia University, Valencia, Spain

The study of the immune function in marine mammals is essential to understand their physiology and can help to improve their welfare in the aquariums. Dedicating efforts to studying marine mammal physiology, pathophysiology, and implementing new diagnostic and therapeutic tools promote progress towards preventive medicine in aquariums by facilitating early detection and treatment of diseases. However, biological and clinical research on marine mammals is currently very limited due to difficult access to these species and their biological samples. With this objective, our group has adapted to marine mammals a commercially available assay routinely used to evaluate the phagocytic capacity of monocytes and granulocytes in human whole blood samples. We adapted IngoflowEx kit to bottlenose dolphins (*Tursiops truncatus*), beluga whales (*Delphinapterus leucas*), walruses (*Odobenus rosmarus*), Patagonian sea lions (*Otaria flavescens*), and harbor (*Phoca vitulina*). In this paper, we report the modifications carried out on the original protocol for their correct functioning in marine mammals. We obtained physiological values of phagocytic capacity in each species after repeated sampling for 4 years in various individuals of each species. Specific results revealed that the % phagocytic cells that ingested E.coli in bottlenose dolphins were 59.6 $\pm$ 1.27, in walruses 62.6 $\pm$ 2.17, in sea lions 57.5 $\pm$ 4.3, and in beluga whales 61.7 $\pm$ 1.4. In the case of the % phagocytic cells producing respiratory burst in bottlenose dolphins were 34.2 $\pm$ 3.6, in walruses 36.3 $\pm$ 4.3, in sea lions 40.8 $\pm$ 10.2, and in beluga whales 26.3 $\pm$ 3.7. These preliminary results can be used as a reference to detect alterations in phagocytic capacity either by immunosuppression or by exacerbation of the response in infectious inflammatory processes. Clinical applicability of the assay was verified in two clinical cases in which Ingoflow was useful to detect immune alterations in two diseased individuals, before and after the onset of clinical signs.

KEYWORDS

phagocytosis, marine mammals, respiratory burst, dolphins, beluga, walrus, sea lion, seal

1 Introduction

Marine mammals, positioned at the apex of the aquatic food chain, are characterized by their long-life spans, and serve as the ultimate recipients of impacts within marine ecosystems (1, 2). These impacts can arise from various threats, including pollution, pathogens, and accidental fishing.

Presently, the discharge of pollutants into the ocean stands as a prominent global environmental challenge. Urban, agricultural, and industrial waste, totaling nearly 400 million tons annually, introduces a variety of heavy metals, solvents, and xenobiotics into marine ecosystems. Alarmingly, approximately 80% of the wastewater released into the sea remains untreated (3). These pollutants settle in the water and sediment on the ocean floor, where smaller organisms ingest them. Larger species then bioaccumulate contaminants through their diet (2). The biomagnification process leads predators to accumulate higher concentrations than their prey, given their extended exposure and longevity (4). Consequently, marine mammals serve as bioindicators in aquatic ecosystems, playing a crucial role in pathophysiological and toxicological studies (2). Various pollutants, such as heavy metals, insect repellents, pesticides, per- and polyfluoroalkyls (PFAs), polychlorinated biphenyls (PCBs), organochlorine pesticides (OCPs) or tributyltins, have been identified in tissues of different marine mammal species. Specifically, striped dolphins (*Stenella coeruleoalba*) (5, 6), Fraser's dolphins (*Lagenodelphis hosei*) (7), common dolphins (*Delphinus delphis*) (8), killer whales (*Orcinus orca*), polar bears (*Ursus maritimus*) (9) or harbour seal (*Phoca vitulina*) (10) presented one or more of these compounds. In addition, by 2014, the worldwide production of plastics had exceeded 300 million metric tons annually. Plastic waste has been identified across all major marine environments globally, ranging in size from microns to meters (11). This pervasive presence of plastics is a growing concern, particularly as marine mammals are also known to suffer from the impacts of plastic pollution. In fact other studies confirmed the presence of phthalates in the urine of bottlenose dolphins (*Tursiops truncatus*), demonstrating their dietary exposure to microplastics or plastic derivates (12).

The exposure to certain contaminants, such as PCBs, pesticides, or heavy metals, can lead to diseases in animals. Specifically, the direct relationship between exposure to certain xenobiotics and alterations in immune functionality has been demonstrated in several *in vitro* studies conducted in different marine mammal species. On one hand, certain PCBs have been shown to decrease the function of granulocytes and lymphocytes in killer whales and polar bears (9). PCBs have also been associated with a reduction in NK cell activity in Californian sea lions (*Zalophus californianus*) (13). On the other hand, OCPs have been found to reduce the phagocytic capacity in killer whales (9). Heavy metals such as Hg and Cd can alter the viability and function of lymphocytes and granulocytes in bottlenose dolphins (14). Also, tributyltin and some of its metabolites, especially dibutyltin, have the potential to alter leukocyte function in seals, leading to a reduction in the activity of phagocytes, B lymphocytes, and NK cells (10). Additionally, silver nanoparticles from textile and cosmetic industries have been observed to generate a decreased proliferative capacity of lymphocytes and induce apoptosis in dolphins (15).

Nevertheless, the human impact on the marine ecosystem is not limited to the leakage of pollutants. Overfishing has resulted in competition for fish between humans and cetaceans (16), leading to increased accidental net captures (17). Furthermore, maritime traffic, military maneuvers, and oil or gas extraction generate high levels of sound in the ocean (18), often overlapping or surpassing the sounds emitted by marine mammals for communication, reproduction, or hunting (19). All these situations can trigger an acute stress response in the animals, accompanied by alterations in behavior and the release of cortisol and catecholamines into the bloodstream (18). Catecholamines, such as epinephrine and norepinephrine, increase respiratory and heart rates and the arrival of blood to the muscles, facilitating the fight or flight response (20). This occurs at the expense of the function of other structures, such as the digestive, reproductive, or immune systems. Both catecholamines and glucocorticoids affect the functionality of immune cells by binding to specific leukocyte receptors, triggering alterations in cytokine production and inhibition of cell maturation and mobilization. The primary stress molecule in mammals is cortisol, which binds to glucocorticoid type II receptors in the cytoplasm of immune cells. Subsequently, this receptor is translocated to the cell nucleus, where it alters the production of numerous cytokines such as interferon-gamma (IFNγ), interleukins IL-1, IL-2, and IL-6, or tumor necrosis factor (TNFα) (20). Therefore, stress can also impair immune function in marine mammals.

Additionally, marine mammals are exposed to numerous pathogens in the ocean. Some of them can enter through untreated human wastewater that is discharged into the sea (3), while others are natural environmental organisms. As is well known, bacterial or fungal infections (21, 22), may exacerbate immune function, while others, typically of viral origin, may induce immunosuppression in animals.

Finally, as is widely recognized, stress can induce significant physiological alterations in living organisms, one of which, in the animal kingdom, is immunosuppression (23). It is well known that animals under human care can suffer stress in specific conditions and this result in a decrease of the functionality of the immune system (24).

In summary, the immune function of marine mammals can be altered through various mechanisms and serves as a biomarker not only of the health status of the animal but also of the environment in which it resides. Establishing standardizable methods to monitor immune function in these species is necessary to determine, firstly, the physiological immune functionality in healthy animals, and secondly, immune alterations due to pathologies, stress, or exposure to xenobiotics. This is particularly relevant in aquarium veterinary clinics, as these species may not exhibit signs of weakness until the disease has advanced, to avoid appearing vulnerable to larger predators in the wild. Routinely measuring immune function could be a valuable tool in the early diagnosis and monitoring of certain pathologies in marine mammals.

In this study, our group concentrates on adapting a human commercial assay for measuring the phagocytic capacity of granulocytes and monocytes to marine mammals. The objective was to establish a fast, simple, and cell-respectful methodology that can be employed to assess the phagocytosis of animals, either to evaluate their health status or to conduct immunity studies. The use of commercial solutions ensures a high level of standardization in experiments, facilitating the comparison of results across studies conducted by different research groups or aquariums. Specifically, our focus has been on adapting the IngoFlow assay for use in bottlenose dolphins (*Tursiops truncatus*), beluga whales (*Delphinapterus leucas*), walruses (*Odobenus rosmarus*), seals (*Phoca vitulina)* and sea lions

(*Otaria flavescens*). The assay measures pathogen ingestion and our group simultaneously analyzed respiratory burst in granulocytes and monocytes from whole blood samples. Subsequently, we have defined a range of physiological values for each parameter in each species, considering the limited sample size and the living conditions of the individuals. We have observed alterations in the phagocytic capacity of animals with various infections, demonstrating the diagnostic and clinical effectiveness of the method.

2 Materials and methods

2.1 Blood sampling

Heparinized whole blood was obtained from healthy animals under human care at Oceanogràfic Aquarium (Valencia, Spain). One mL of venous blood was drawn from the ventral face of the caudal fin in cetaceans and from interdigital veins on the caudal flippers in pinnipeds. For that, 21G gauge size Butterfly needle (Venofix® by Fa. Braun) and 10 mL single-use syringes (Covetrus) were used. All the animals had been previously trained for blood collection. Samples were analyzed in the Cytomics Laboratory at the Príncipe Felipe Research Center (CIPF, Valencia, Spain) within 2 h after being obtained. We obtained 44 samples from 15 bottlenose dolphins (*Tursiops truncatus*), 20 samples from 3 beluga whales (*Delphinapterus leucas*), 18 samples from 3 walruses (*Odobenus Rosmarus*), 4 samples from 4 sea lions (*Otaria flavescens*) and 2 samples from 1 seal (*Phoca vitulina*). All the experiments were approved by the Animal Care Committee of the Oceanogràfic Aquarium (Reference: OCE-6-17).

2.2 Reactive and solutions

2.2.1 Fluorochromes

Hydroethidine (HE) is an indicator of intracellular superoxide. It was prepared at 1 mg/mL in dimethyl sulphoxide (DMSO) and used at a final concentration of 0.3 µg/mL. Hoechst 33342 (HO) is a vital nuclear marker. It was prepared at 1 mg/mL in distilled H_2O and used at a final concentration of 3 µg/mL. Propidium iodide (PI) is a cell viability indicator that stains cells with damaged membrane. It was prepared at 1 mg/mL in distilled H_2O, and used at a final concentration of 5 µg/mL. All fluorochromes were obtained from Merck (Darmstadt, Germany).

2.2.2 IngoFlowEx Kit for quantification of phagocytic activity

IngoFlowEx (phagocytic assay) (Exbio, Prague, Czech Republic, Cat. ED7040) was adapted to evaluate the phagocytic capacity of monocytes and granulocytes in marine mammals. This kit includes: suspension of fluorescein-labelled *E. coli* bacteria (*E. coli*-FITC), quenching solution (trypan blue), solution for erythrocyte lysis and leukocyte fixation, washing buffer and DNA staining solution (PI). Trypan blue (TB) is introduced to freely diffuse into the cell, ensuring uniform distribution throughout the cytoplasm and nucleus. TB can swiftly diffuse through cellular and nuclear membranes. At suitable concentrations, this indiscriminate dispersion of dye molecules positions them effectively in proximity and orientation to autofluorescent or nonspecifically bound fluorescent molecules, enabling quenching to take place (25).

2.2.3 Reactive

Cytochalasin A (ENZO, Farmingdale, NY, United States) is a phagocytosis inhibitor. It was prepared at 10 mM in DMSO and aliquoted and stored at −20°C. It was used at a final concentration of 400 µM.

2.2.4 Buffers, solutions and mediums

Versalyse Lysing Solution (Beckman Coulter, Brea, CA, United States) was used as a non-fixative erythrocyte lysant. RPMI 1640 medium (GIBCO, 21875034) was used to reconstitute the samples. PBS phosphate buffer saline pH 7.4 (Gibco-Thermo Fisher, Waltham, MA, United States) was used as a general buffer.

2.3 Quantification of phagocytic activity

To assess phagocytic cells function, we studied two essential phases in the phagocytosis process: pathogen ingestion and pathogen destruction by the respiratory burst. The phagocytic assay measures the pathogen ingestion capacity of monocytes and granulocytes in humans. Our group, which was routinely using this kit at that time to measure immune function in humans, introduced several modifications of the original experimental design to optimize its application to marine mammals and added the simultaneous measurement of respiratory burst using HE. The green fluorescent *E. coli* bacteria provided by the phagocytic assay were used as stimulus, since, like in humans, it is also capable of infecting cetaceans and pinnipeds (21, 22).

2.3.1 Phagocytic assay principle

This assay is based on measuring the fluorescence of phagocytic cells after ingesting green, fluorescent *E. coli*-FITC. Bacteria is added to the blood and incubated at 37°C (physiological temperature of marine mammals) for 30 min. In parallel, the negative control, not exposed to the pathogen, is incubated too and used to establish in the flow cytometer (FC) the limit between the cells that have phagocytosed the bacteria and those that have not. At the end of the incubation, the sample may contain: (a) autofluorescent phagocytic cells that have not ingested *E. coli*-FITC. (b) Green-fluorescent phagocytic cells with *E. coli*-FITC attached to the plasma membrane but not yet ingested. (c) Green-fluorescent phagocytic cells that have actually ingested *E. coli*-FITC. (d) Green-fluorescent free bacteria.(e) The rest of the blood components (erythrocytes, platelets, debris…).

Erythrocytes are lysed and cell debris and uningested bacteria are removed by washing with PBS. In addition, leukocytes are fixed and stained with PI for being identified as nucleated cells in the flow cytometer. The fluorescence of bacteria attached to the cell surface but not yet ingested is quenched by trypan blue.

2.3.2 Modifications of the assay for its application to marine mammals

We have improved the biological relevance of the original assay by incorporating additional reagents and discarding others provided by the kit. First, HE, an indicator of superoxide radical generated during the oxidative burst is incorporated to the assay. After oxidation during the

respiratory burst, HE yields ethidium that intercalates into DNA and emits orange-red fluorescence. So, the phagocytic capacity (estimated by the green fluorescence of the bacteria) and the respiratory burst production (estimated by the red fluorescence of the HE) can be simultaneously evaluated. Since the fluorescence properties of HE-generated ethidium overlap those of PI, we replaced this dye by HO to discriminate nucleated cells.

On the other hand, we have introduced several modifications of the original experimental design to optimize its application to marine mammals, as listed below:

a) Including an additional negative biological control:

The negative control proposed by the manufacturer reports the cell autofluorescence. An additional biological negative control was included by using cytochalasin A as phagocytosis inhibitor. This control is more comparable to the test tube, since it contains the same components (*E. coli*-FITC and HE), but avoiding the phagocytosis process.

b) Increased incubation period:

We have extended the incubation period from 30 min (according to the manufacturer) to 1 h at 37°C, observing better results in the discrimination between the population of phagocytic cells that had ingested the bacteria and those that had not. The temperature was set to 37°C because the physiological temperature of marine mammals is around 37°C, as it is in humans. Thus, we are recreating the same physiological conditions that would be encountered *in vivo*.

c) Changing to a non-fixing erythrocyte lysis solution:

The erythrocyte lysis solution provided by phagocytic assay is also fixative. To keep the cells alive, we replaced it with VersaLyse Lysing Solution (Beckman Coulter, California, United States), a non-fixing solution. VersaLyse Lysing Solution is a reagent used to lyse red blood cells from any biological fluid and, in particular, to lyse erythrocytes from whole blood. It is a highly specific and very gentle lysing solution that ruptures erythrocytes but, as it does not fix all cells, does not affect the viability of the remaining immune cells. In the cetacean samples, the manufacturer's instructions were followed observing good results, however pinniped samples required twice the volume of VersaLyse or the incubation time with the lysis solution to achieve similar results. The variation in the impact of the lysis solution is attributed to the elevated blood lipid content present in pinnipeds. This may hinder, to some extent, the interaction between the reagent and erythrocytes, thereby impeding its effectiveness. This heightened blood lipid content has been documented in previous studies (26).

d) Using RPMI medium to preserve cells until cytometric analysis:

The original assay uses PBS to preserve cells until the analysis. To be more respectful with cell viability, PBS was replaced with warm RPMI medium.

e) Trypan blue addition time:

In the original assay trypan blue is added after the incubation with *E. coli*-FITC. We observed better results quenching the fluorescence of non-ingested bacteria by adding it just before the reading in the cytometer, avoiding washing after its addition and ensuring its permanence in the sample to quench the fluorescence of free or membrane attached bacteria.

2.3.3 Protocol for the simultaneous measurement of the ingestion capacity and respiratory burst production of monocytes and granulocytes in marine mammals

Five tubes were prepared per analysis: (1) *Negative control*: to evaluate the autofluorescence of the sample. Without *E. coli*-FITC and HE. (2) *Control of cellular basal oxidative state*: adding HE but not *E. coli*-FITC. This tube allows also for fluorescence compensation of HE into FITC. (3) *Biological negative control*: inhibiting phagocytosis with cytochalasin A. Adding *E. coli*-FITC and HE. (4) *Control of phagocytosis*: adding *E. coli*-FITC but not HE. This tube allows also for fluorescence compensation of FITC into HE. (5) *Test tube*: adding *E. coli*-FITC and HE for the simultaneous measurement of pathogen ingestion and respiratory burst production capacities.

The protocol steps are shown in Figure 1. First, 50 µL of heparinized blood are added to each tube. The tubes are kept on ice for 10 min. After this time, the biological negative control is preincubated with cytochalasin A at a final concentration of 400 µM for 30 min at 37°C CO_2 in an incubator. Subsequently, 10 µL of *E. coli*-FITC are added to the biological and ingestion controls and to the experimental tube. All tubes were incubated for 1 h at 37°C in the CO_2 incubator. After incubation, the tubes were placed on ice and in dark for 5 min to stop the phagocytosis process. Then, Versalyse Lysing Solution is added to each tube in cetacean samples (500 µL) or 1 mL in the pinniped samples (1 mL). The lysis solution is allowed to act for 10 min at room temperature and in the dark. Once lysed, the samples are centrifuged for 5 min at 200 g and 4°C. The supernatant is removed, and samples washed twice with 3 mL of cold filtered PBS. After removing the supernatant, the samples are resuspended in 300 µL of tempered RPMI. Finally, HO and HE are added to the corresponding tubes at a final concentration of 3 µg/mL and 0.3 µg/mL, respectively, and incubated for 15 min at 37°C in a CO_2 incubator. Before the analysis in the flow cytometer, 10 µL of trypan blue solution is added to each tube. Samples are analyzed on the cytometer immediately.

2.3.4 Flow cytometer settings

The CytoFlex S flow cytometer with blue (488 nm) and violet (405 nm) lasers (Beckman Coulter, Brea, CA, United States) was configured to collect forward scatter (FSC) and side scatter (SSC) signals as well as the fluorescence emitted by the bacteria *E. coli*-FITC (exc 488 nm/em 525 nm, FITC channel), HO (exc 405 nm/em 450 nm, BP450 channel) and HE (exc 561 nm/em 585 nm, PE channel).

The population identification and gating strategy is detailed in Figure 2. Leukocytes were identified as HO fluorescence positive events (Figure 2A). From leukocytes, phagocytic cells (monocytes and granulocytes) were selected by morphology, according to their relative size (FSC) and internal complexity (SSC). Dead cells were also discarded morphologically in this step (Figure 2B). Subsequently, cell aggregates were electronically removed using the area (FSC-A) and peak (FSC-H) signals of the FSC (Figure 2C). To ensure the same number of events in all the experiments carried out, a limit of 10,000 events was established in the single cell population in all the analyzes

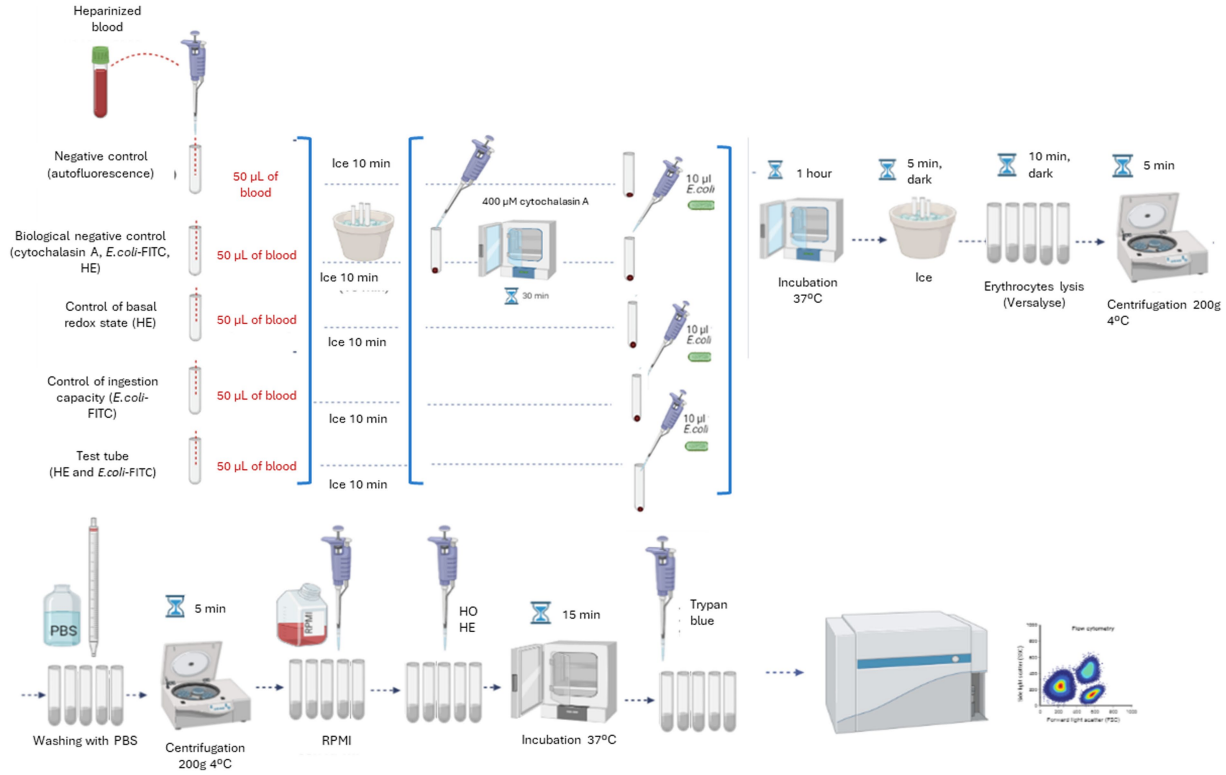

FIGURE 1
Diagram of the definitive protocol steps for the simultaneous measurement of the ingestion capacity and the respiratory burst production of monocytes and granulocytes in marine mammals.

carried out. In live and individual monocytes and granulocytes, the phagocytosis capacity and respiratory burst production were quantified simultaneously. For this, a dot-plot comparing the *E. coli*-FITC and HE-PE signals was used in the different tubes: (1) *Negative control*: in this tube phagocytic cells were not exposed to either *E. coli*-FITC or HE, so all events are negative to both fluorescence, giving the cells autofluorescence (Figure 2D). (2) *Control of the basal oxidative state*: provides an estimation of the cells basal redox state, since HE is added but not *E. coli*-FITC (Figure 2E). (3) *Biological negative control*: in this tube the phagocytosis is inhibited with cytochalasin A, so few events present FITC and HE fluorescence (Figure 2F). (4) *Control of ingestion capacity*: in this tube *E. coli*-FITC is added but not HE, observing the percentage of phagocytic cells emitting bacteria-dependent fluorescence (Figure 2G). (5) *Test tube:* this tube shows the percentage of phagocytic cells that: have not ingested and destroyed the bacteria (*E. coli*$^{-}$ HE^{-}); contain bacteria inside but have not yet destroyed them (*E. coli*$^{+}$ HE^{-}); have ingested bacteria and are producing the respiratory burst (*E. coli*$^{+}$ HE^{+}) (Figure 2H).

2.3.5 Numerical analysis of phagocytic capacity

Two parameters were assessed using Flowjo software: (a) *The percentage of cells that ingested the pathogen:* calculated by subtracting the percentage of FITC positive events of the biological control from that of the experimental tube. (b) *The percentage of cells generating the respiratory burst after ingesting the bacteria:* calculated by subtracting the percentage of *E. coli*$^{+}$/HE^{+} cells of biological control from that of the experimental tube.

2.4 Statistical analysis

The mean, median and standard error of the median (SEM) were calculated for each parameter in all the species. To evaluate differences between animals per sex and age we performed *t*-test in GraphPad Prism 5. The results were considered statistically significant when p-value <0.05. To evaluate differences between species, the distribution of the data for each parameter was tested using Shapiro–Wilk test. In all cases the data distribution was normal one-way ANOVA test was utilized.

3 Results

3.1 Adapting a standardized assay to measure phagocytic capacity in marine mammals

It is the first time that a commercial kit intended for human medicine has been adapted to measure phagocytic capacity in dolphins, beluga whales, walruses, sea lions and seals. It represents a novelty in the field of marine mammal immunology and a new study tool that allows the standardization of the results in different investigations. Since IngoFlow Kit is originally intended for diagnosis in human medicine, it undergoes numerous and exhaustive quality controls before being commercialized to hospitals or research centers. So, the use of this adapted kit with added solutions and modified protocol implies the

10.3389/fvets.2024.1389977

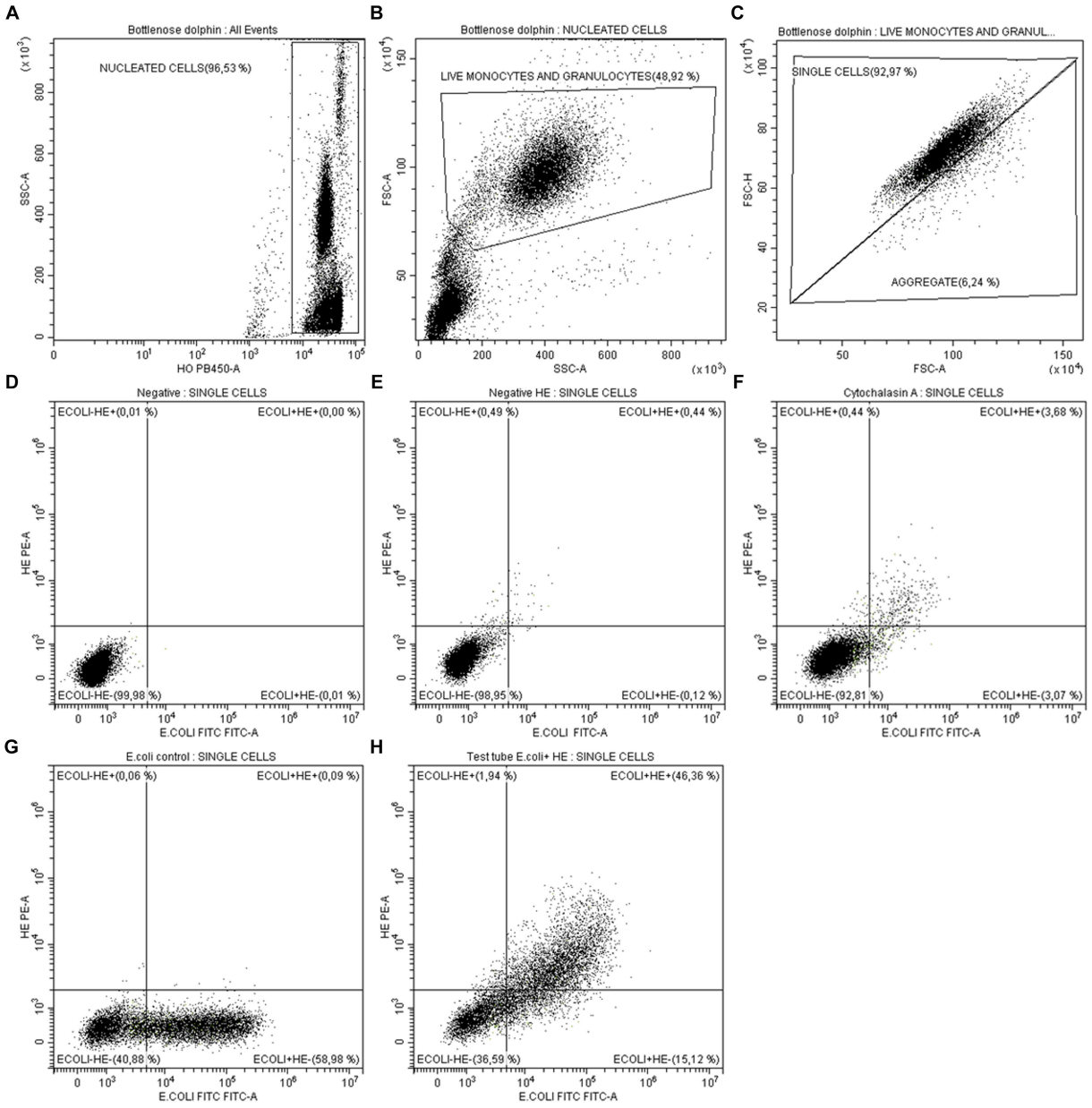

FIGURE 2
Analysis by flow cytometry of monocytes and granulocytes phagocytic capacity in marine mammals. **(A)** Identification and gating of nucleated cells as HO^+ events (leukocytes). **(B)** From leukocytes, gating of live monocytes and granulocytes by morphology (FSC-SSC). **(C)** Aggregates exclusion by analysis of FSC-height vs. FSC-area of live monocytes and granulocytes. To ensure the same number of events in all the experiments carried out, a limit of 10,000 events was established in the single cell population. From single events: **(D)** Negative tube: since *E. coli*-FITC and HE-PE were not added, all events are negative for both fluorescences. **(E)** Control of cells basal redox state: since only was added HE. **(F)** Biological negative control: few events present *E. coli*-FITC and HE-PE fluorescence after inhibiting phagocytosis with cytochalasin A. **(G)** Control of ingestion capacity: percentage of cells present *E. coli*-FITC fluorescence after having ingested it. HE was not added. **(H)** Test tube: shows the percentage of cells that have not ingested *E. coli*-FITC and produced respiratory burst (*E. coli*$^-$ HE$^-$), the percentage of cells that ingested *E. coli*-FITC but have not yet produced respiratory burst (*E. coli*$^+$ HE$^-$) and the percentage of cells that ingested *E. coli*-FITC and produced respiratory burst (*E. coli*$^+$ HE$^+$).

standardization of the results between individuals, samples from the same individual at different times or even between studies. Adapting this assay to marine mammals allows the results obtained between different research groups to be very reliably comparable.

On the other hand, the use of HE to study the respiratory burst production is also an innovation in immunological studies in marine mammals, demonstrating its usefulness as superoxide marker in these species.

3.2 Obtaining physiological values of phagocytic capacity in healthy marine mammals

In order to detect eventual alterations in phagocytic capacity, first it was necessary a previous descriptive study of phagocytes normal function for each specie. With this purpose, periodically samples of individuals of different species were analyzed over

4 years. Specifically, 44 total samples were obtained from 15 dolphins, 20 samples from 3 belugas, 18 samples from three walruses, and to a lesser extent, 4 samples from 4 sea lions and 2 samples from a seal. In the last two species the data must be taken with caution due to the small number of samples, but it can be indicative for future studies. The median for each animal was obtained, discarding the data obtained when the animal was sick. Then, the mean and standard error (SEM) of the specie was calculated obtaining a range of physiological values for each parameter in healthy animals of the different species.

The most robust data were obtained in dolphins, since the population size and the number of samples per individual were greater. This methodology was useful for the internal control of the animals under study, but to extrapolate the results to other animals it would be convenient to carry out routine analysis in animals housed in different aquariums.

3.2.1 Ranges of phagocytic capacity of monocytes and granulocytes in marine mammals

The ranges of the physiological values for ingestion capacity and respiratory burst production in each species, and the effects of sex and age are detailed below (Tables 1–4). The physiological values were calculated for all species except seals, since in that case we only had samples from one animal. In this case, the main objective was to set up the methodology for its use in future studies. On the other hand, the results obtained in sea lions should be taken with caution due to the small sample size.

TABLE 1 Physiological phagocytic capacity values in dolphins after 1 h of incubation with the pathogen.

	% phagocytic cells that ingested *E. coli* (mean ± SEM)	% phagocytic cells producing respiratory burst (mean ± SEM)
Bottlenose dolphins $n = 15$, 44 samples	59.6 ± 1.27 (min: 53; max: 69)	34.2 ± 3.6 (min: 9; max: 48.6)
Adults $n = 12$, 36 samples	59.1 ± 1.3	32 ± 3.8
Calves $n = 3$, 8 samples	61.9 ± 3.5	48.3 ± 0.3
Males $n = 5$, 17 samples	60.3 ± 2.7	42.4 ± 2.15
Females $n = 10$, 27 samples	59.3 ± 1.5	31 ± 4.7

Forty-four samples from 15 dolphins were analyzed. The table shows the % of monocytes and granulocytes capable of ingest the pathogen and produce respiratory burst in the global population and by sex and age. The minimum and maximum values are also detailed. No significant differences were observed by sex or age (NSD: $p \geq 0.05$).

TABLE 2 Physiological phagocytic capacity values in beluga whales after 1 h of incubation with the pathogen.

	% phagocytic cells that ingested *E. coli* (mean ± SEM)	% phagocytic cells producing respiratory burst (mean ± SEM)
Walruses $n = 3$, 18 samples (6 per animal)	62.6 ± 2.17 (min: 50; max: 79)	36.3 ± 4.3 (min: 13; max: 64)

Eighteen samples from 3 walruses were analyzed. The table shows the % of monocytes and granulocytes capable of ingest the pathogen and produce respiratory burst in the global population. All animals were adult females so differences by sex or age could not be evaluated. No significant differences were observed between the animals (NSD: $p \geq 0.05$). The minimum and maximum values are also detailed in the table.

TABLE 3 Physiological phagocytic capacity values in walruses after 1 h of incubation with the pathogen.

	% phagocytic cells that ingested *E. coli* (mean ± SEM)	% phagocytic cells producing respiratory burst (mean ± SEM)
Beluga whales $n = 3$, 20 samples	61.7 ± 1.4 (min: 52; max: 74)	26.3 ± 3.7 (min: 5.8; max: 57.2)
Adults $n = 2$, 14 samples	63.3 ± 1.8	29.7 ± 4.4
Calf $n = 1$, 6 samples	58 ± 0.9	18.6 ± 6.2
Males $n = 2$, 12 samples	58.7 ± 0.75	22.6 ± 4.5
Female $n = 1$, 8 samples	65 ± 2.4	32 ± 6.3

Twenty samples from 3 beluga whales were analyzed. The table shows the % of monocytes and granulocytes capable of ingest the pathogen and produce respiratory burst in the global population and by sex and age. The minimum and maximum values are also detailed. No significant differences were observed by age (NSD: $p \geq 0.05$). Phagocytic cells from female presented a significant higher ingestion capacity than males ($p = 0.0175$*).

TABLE 4 Physiological phagocytic capacity values in sea lions after 1 h of incubation with the pathogen.

	% phagocytic cells that ingested *E. coli* (mean ± SEM)	% phagocytic cells producing respiratory burst (mean ± SEM)
Sea lions $n = 4$, 4 samples	57.5 ± 4.3 (min: 51; max: 70)	40.8 ± 10.2 (min: 21; max: 68)
Males $n = 2$, 2 samples	54.6 ± 2.5	32.15 ± 11.25
Females $n = 2$, 2 samples	60.5 ± 9.5	49.5 ± 18.5

Four samples from 4 sea lions were analyzed. The table shows the % of monocytes and granulocytes capable of ingest the pathogen and produce respiratory burst in the global population and by sex. All the animals were adults so differences by age could not be evaluated. The minimum and maximum values are also detailed. No significant differences were observed by sex (NSD: $p \geq 0.05$). These results should be taken with caution due to the small sample size.

3.2.1.1 Bottlenose dolphins

The physiological values of phagocytic function obtained from more than 40 samples from 15 dolphins are detailed in Table 1. No significant differences were observed between animals of different ages or sexes.

3.2.1.2 Beluga whales

The physiological values of phagocytic function obtained from 20 samples from 3 beluga whales are detailed in Table 2. No significant differences were observed between animals of different ages, however, the female presented a significantly higher percentage of phagocytic cells capable of ingesting the pathogen than males ($p = 0.0175^{*}$). Since we only provided samples from one female, this finding could be due to intrinsic characteristics of the individual. To confirm the dependence on the gender of this effect, it is necessary to increase the population size.

3.2.1.3 Walruses

The physiological values of phagocytic function obtained from 18 samples from 3 walruses are detailed in Table 3. As all the walruses were females and of the same age, no sex or age differences could be investigated in this species.

3.2.1.4 Sea lions

For the study, 4 samples from 4 healthy adult sea lions were obtained. Although the sample size is insufficient to obtain physiological values of the population, Table 4 shows the results obtained in this group, which can be indicative of the species. It would be necessary to expand the sample size in future studies. No statistically significant differences were observed between sexes.

3.2.2 Differences in phagocytic capacity among marine mammal species

Shapiro Wilks test determined the normal distribution of the data for both parameters studied: pathogen ingestion capacity and respiratory burst production, presenting the p-values $p = 0.23$ and $p = 0.09$, respectively, ($p > 0.05$). No statistically significant differences were observed between the different species in pathogen ingestion capacity ($p = 0.2$) and respiratory burst production ($p = 0.87$) using one way ANOVA.

3.3 Application of phagocytic capacity measurement to health monitoring in clinical cases

After establishing the physiological phagocytic capacity values per species, it was possible to detect alterations in several clinical cases of animals with different disorders.

3.3.1 Clinical case 1: bottlenose dolphin with fungal infection

One dolphin in the aquarium suffered chronic intermittent respiratory infections due to the fungus *Rhizopus microsporus*. This fungus belongs to the class Zygomycetes, which are widely distributed in the environment. The most common mode of infection is by inhalation of spores traveling in the air. The first defensive barriers against zygomycetes are the mucous membranes and the endothelium, although some spores can invade it. Phagocytic cells act against the fungus, preventing its germination and the proliferation of hyphae (27). Normally, the spores are easily fought by the host's phagocytic cells, however, if the spore load is very high or the animal is immunodeppressed, hyphae are developed producing lesions in the area (27).

The phagocytic capacity values of the dolphin during three different episodes of *Rhizopus microsporus* infection are detailed next. In all three cases, the animal showed a percentage of phagocytic cells ingesting the pathogen significantly higher than the population average. Specifically, the percentages were the following: episode 1: 79%; episode 2: 76.6%; episode 3: 76%. The mean ± SEM of the three episodes was 77.2 ± 0.9%, which is significantly higher ($p < 0.0001^{***}$) than the mean presented by the population of healthy dolphins (59.6 ± 1.27%) (Figure 3A). Furthermore, during one of the episodes it also showed an increase in the percentage of cells that produced the respiratory burst (61%) compared to the healthy population (34.2 ± 3.6%) (Figure 3B).

These findings not only demonstrate the higher activation of the animal's phagocytic cells during infection trying to combat the fungus. It also validates the usefulness of the assay to detect alterations in the immune function of animals during certain pathologies, supposing a new diagnostic tool in clinical veterinary medicine in the aquariums.

3.3.2 Clinical case 2: bottlenose dolphin with low phagocytic capacity and subsequent yeast infection

During one of the routinary samplings of the animals, it was observed that a dolphin presented a percentage of phagocytic cells ingesting the pathogen (30%) and producing the respiratory burst (7.2%) lower than the average of the healthy population (59 0.6 ± 1.27% and 34.2 ± 3.6% respectively) (Figures 3C,D). The animal was apparently healthy and did not show any signs of illness. Three days later the dolphin showed digestive symptoms, mainly diarrhea. The veterinary staff diagnosed a yeast infection.

Some types of yeast are part of the natural intestinal flora of dolphins. Immunodepression has been described as one of the key factors in the imbalance of the intestinal flora, which can trigger, among other things, an overgrowth of yeast that is accompanied by digestive sickness (28).

This clinical case is of special relevance, since the finding of the diminished phagocytic capacity in the animal preceded the appearance of the symptoms, demonstrating the usefulness of this assay to early detect disorders related to alterations in immune function, contributing to the improvement of preventative aquarium medicine.

4 Discussion

Although phagocytosis has been previously studied in marine mammals, the assay adapted by our group in this work represents a significant advancement in the methodology. The main advantage lies in the standardization of the method that ensures its reliable and comparable use in different research groups or aquariums worldwide. In most prior studies, the methodologies used to measure phagocytosis and respiratory burst in marine mammals

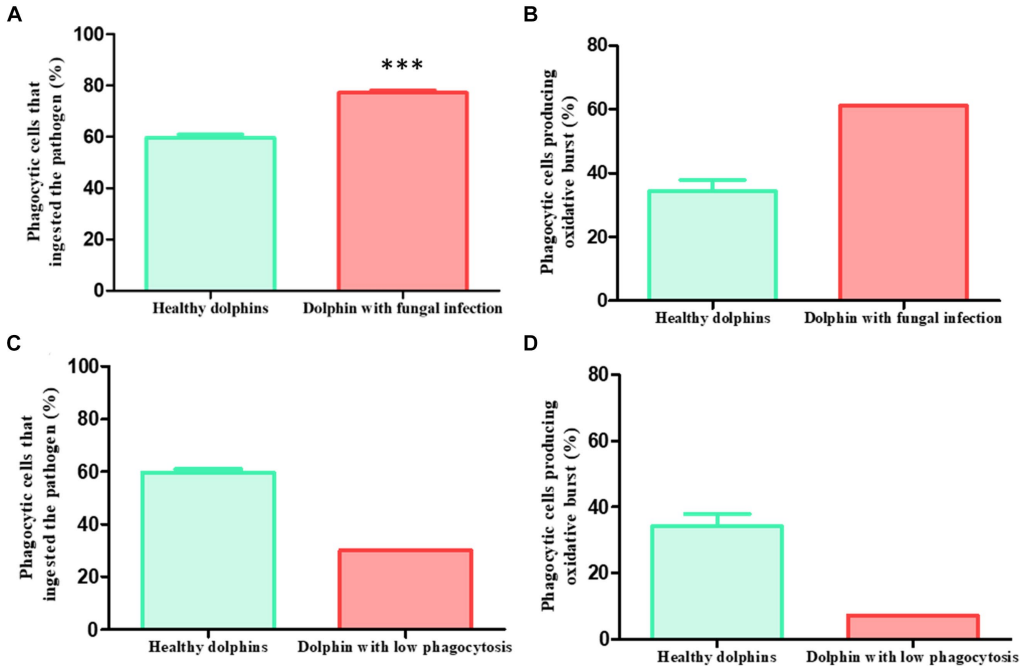

FIGURE 3
Clinical cases. Phagocytic capacity values in two sick dolphins. Clinical case 1: **(A)** dolphin with recurrent fungal infection presented pathogen ingestion capacity values significantly higher than healthy average in three different episodes ($p<0.0001$***) (sick: 79, 76.6 and 76%, mean±SEM: 77.2±0.9%; healthy: 59.6±1.27%). **(B)** During one episode, it also presented a higher capacity to generate respiratory burst than the healthy average (sick: 61%; healthy: 34.2±3.6%). Clinical case 2: 3days before showing digestive symptoms due to yeast, a dolphin presented a lower phagocytic capacity than healthy average in a routine control. **(C)** This effect was observed both in the ingestion capacity (sick: 30%; healthy: 59.6±1.27%) **(D)** and in the production of the respiratory burst (sick: 7.2%; healthy: 34.2±3.6%).

relied either on the use of *Staphylococcus aureus* with prelabelled PI (1, 15, 29) or of fluorescent polystyrene beads (10, 14, 30–32) as a stimulus. In the first case, the staining of the pathogen is homemade, making it challenging to compare results between studies. In the second case, the stimulus used is not biological, deviating from the natural response of phagocytes. In our assay, we employed green, fluorescent *E. coli*, a natural pathogen of marine mammals (21, 22), as a biological stimulus. Additionally, the bacteria were prepared by the commercial company Exbio, following rigorous quality and standardization controls to ensure identical and comparable use in all the kits sold. This assay is also more respectful to the cells compared to those conducted in previous studies, where leukocytes were isolated, followed by cell counts before incubation with the pathogen, erythrocyte lysis, and cell fixation with 1% paraformaldehyde (1, 15, 29, 32). The excessive manipulation of leukocytes can alter their functionality. In our case, whole blood was used to closely mimic the *in vivo* physiological immune response, keeping the sample as unaltered as possible during incubation with bacteria. Erythrocyte lysis and washes are performed in the final steps, ensuring optimal function of the cells during the phagocytosis process. Respiratory burst has been measured previously in different species of marine mammals, either simultaneously with phagocytosis (1, 15) or separately (29). For this purpose, the reagent dichlorofluorescein diacetate (DCFH-DA) has been used (1, 15, 32). Our choice of HE was based on preventing fluorescence overlap of the bacterium and the oxidative burst indicator. Thus, our assay with the IngoFlow Kit is a new and useful tool to compare results between studies, while also being more respectful of cell viability and functionality. The adaptation of the IngoFlowEx assay to marine mammals enables its use as a diagnostic assay in the daily veterinary clinic of aquariums or as a new tool in future immune studies.

Phagocytosis and respiratory burst have been previously studied in dolphins (1, 9, 14, 15, 29, 31), belugas (32), sea lions (9, 31), seals (9, 10, 31), killer whales (9, 31), polar bears (9), and sea otters (31). The study of these parameters in walruses is a new contribution of this work. Our group previously adapted another human kit for measuring phagocytosis in dolphins, namely the pHrodo Red *E. coli* BioParticles Kit (Thermo Fisher, Massachusetts, United States) (33). However, in most of these studies, the focus was on a methodological approach to the study of phagocytosis in these species and the detection of alterations in phagocyte function after *in vitro* exposure to environmental pollutants such as PCBs (31), heavy metals (14), tributylins (10), or silver nanoparticles (15). Only one of the previous studies aimed to generate a range of physiological values for phagocytic capacity and respiratory burst production in dolphins (29). Reif et al. (29) analyzed 40 wild dolphin blood samples and established a range of values for ingestion capacity and production of respiratory burst. On the one hand, they obtained the percentages of granulocytes and monocytes capable of ingesting the pathogen, in their case, a pre-labeled *Staphylococcus aureus*, with values of 19.9 ± 10.5% and 19.1 ± 10.1%, respectively. These percentages differ significantly from those described in this work (59.6 ± 1.27%). It's important to note that Reif et al. (29) broke down the percentages by cell populations, while in this study, we present a general score of monocytes and granulocytes. Additionally, the protocols are not

comparable. In their case, cells were incubated for 75 min with *Staphylococcus aureus*, while in our assay, they were incubated for 1 hour with *E. coli*. They used N-ethylmaleimide to block phagocytosis, while we used ice. The lysis of erythrocytes differs in both protocols, and they fixed the cells with 1% paraformaldehyde, a step omitted in our assay. Due to these differences in protocols, the results are not directly comparable. Hence, the standardization of the method provided by the adaptation of the phagocytic assay to marine mammals represents a significant advancement in this context. It's also noteworthy that Reif's et al. study (29) was conducted with a population of wild dolphins, while our group studied dolphins under human care. In their case, 89 wild dolphins were sampled, but only 40 samples were used for phagocytosis analysis. In our case, 15 dolphins have been sampled, but they have been tested periodically until reaching a total of 44 samples. While the number of samples is similar, our study takes a step further in elucidating the physiological values of dolphins' phagocytic function. We obtained serial samples for 4 years from the same individuals, always ensuring they were in good health and excluding samples from sick animals. This rigorous approach has been consistently applied across all studied species. Although Reif's et al. study (29) represents a significant advancement in understanding the immune function of wild dolphins, the challenging access to these animals limits them to one result per individual, making it difficult to ascertain whether the animals suffered from diseases during sampling. So obviously, the results are different between wild dolphins and dolphins under human care, but it is true that it is a very useful tool since most animals that arrive stranded on beaches are usually sick due to some infectious disease such as cetacean morbillivirus or *Brucella ceti*, both of which have been associated with immunosuppression (34). Indeed, co-infections of these microorganisms are common (34). However, the problem is that most animals that arrive stranded on our beaches are found dead, and in this case, there is no possibility of obtaining samples of fresh blood to conduct the study of immune function. This is what has happened in our study period; we have not been able to access fresh samples from stranded animals. However, we hope in the future to obtain samples and relate them to the study of possible infections in these animals. For beluga whales, walruses, sea lions, and seals, our study marks the first continuous examination of the same individuals in phagocytic function, establishing physiological values for each species. Interestingly, we have not observed significant differences in phagocytic function values between different species, suggesting a consistent action of phagocytes in marine mammals. While our study serves as an initial exploration in this field, it is crucial to expand the sample size, study more animals from different aquariums, and establish more robust results. Despite these considerations, the utility of our study is evident. Its successful application in various clinical cases of sick animals in aquariums, as demonstrated in the results section, highlights its value. This work presents two cases where the assay proved useful in detecting alterations in phagocyte function in animals suffering from infections, even before presenting symptoms. This underscores its effectiveness in enhancing preventive medicine in aquariums and better monitoring the health status of animals. Notably, the measurement of phagocytosis has never been used for diagnostic purposes in marine mammals before. In conclusion, the adaptation of the IngoFlow assay to these species emerges as a new diagnostic tool in aquariums. Furthermore, it holds potential for research studies, enabling result comparisons between different works conducted globally.

Data availability statement

The original contributions presented in the study are included in the article/supplementary material, further inquiries can be directed to the corresponding authors.

Ethics statement

The animal study was approved by Animal Care and Welfare Committee of the Oceanogràfic Aquarium (Reference: OCE-6-17). The study was conducted in accordance with the local legislation and institutional requirements.

Author contributions

MF-B: Conceptualization, Formal analysis, Methodology, Writing – original draft, Writing – review & editing. AM-R: Conceptualization, Formal analysis, Visualization, Writing – review & editing. MV: Data curation, Writing – review & editing. CR-S: Data curation, Writing – review & editing. TÁ: Data curation, Writing – review & editing. DG-P: Conceptualization, Supervision, Validation, Writing – original draft, Writing – review & editing. CR-G: Conceptualization, Supervision, Writing – original draft, Writing – review & editing. J-EO'C: Conceptualization, Formal analysis, Investigation, Methodology, Supervision, Validation, Writing – original draft, Writing – review & editing.

Funding

The author(s) declare that financial support was received for the research, authorship, and/or publication of this article. This work was supported by the Fundacion Oceanografic in Valencia, Spain, funding the project.

Acknowledgments

The authors acknowledge at Oceanografic Aquarium staff, especially to veterinarians and trainers for participating in this project and the authors acknowledge to Consellería d'Educació, Investigació, Cultura i Esport de la Generalitat Valenciana (Fondo Social Europeo), for awarding the fellowship to MF-B to carry out her PhD.

Conflict of interest

The authors declare that the research was conducted in the absence of any commercial or financial relationships that could be construed as a potential conflict of interest.

The author(s) declared that they were an editorial board member of Frontiers, at the time of submission. This had no impact on the peer review process and the final decision.

Publisher's note

References

1. Keogh MJ, Spoon T, Ridgway SH, Jensen E, Van Bonn W, Romano TA. Simultaneous measurement of phagocytosis and respiratory burst of leukocytes in whole blood from bottlenose dolphins (*Tursiops truncatus*) utilizing flow cytometry. *Vet Immunol Immunopathol*. (2011) 144:468–75. doi: 10.1016/j.vetimm.2011.08.017

2. Wells RS, Rhinehart HL, Hansen LJ, Sweeney JC, Townsend FI, Stone R, et al. Bottlenose dolphins as marine ecosystem sentinels: developing a health monitoring system. *EcoHealth*. (2004) 1:246–54. doi: 10.1007/s10393-004-0094-6

3. Díaz S, Settele J, Brondízio ES, Ngo HT, Guèze M, Agard J, et al. Summary for policymakers of the global assessment report on biodiversity and ecosystem services of the intergovernmental science-policy platform on biodiversity and ecosystem services In: *Report of the plenary of the intergovernmental science-policy platform on biodiversity and ecosystem services on the work of its seventh session*. Bonn, Germany: IPBES secretariat (2019).

4. Newman MC. *Fundamentals of ecotoxicology: the science of pollution*. *4th* ed. New York: CRC Press (2014). 633 p.

5. Martínez-López E, Peñalver J, Escriña A, Lara L, Gens MJ, María Dolores E, et al. Trace metals in striped dolphins (*Stenella coeruleoalba*) stranded along the Murcia coastline, Mediterranean Sea, during the period 2009–2015. *Chemosphere*. (2019) 229:580–8. doi: 10.1016/j.chemosphere.2019.04.214

6. Shoham-Frider E, Goffman O, Harlavan Y, Kress N, Morick D, Roditi-Elasar M, et al. Trace elements in striped dolphins (*Stenella coeruleoalba*) from the eastern Mediterranean: a 10-years perspective. *Mar Pollut Bull*. (2016) 109:624–32. doi: 10.1016/j.marpolbul.2016.05.021

7. Durante CA, Moura Reis BM, Azevedo A, Crespo EA, Lailson-Brito J. Trace elements in trophic webs from South Atlantic: the use of cetaceans as sentinels. *Mar Pollut Bull*. (2019) 150:110674. doi: 10.1016/j.marpolbul.2019.110674

8. Lahvis GP, Wells RS, Kuehl DW, Stewart JL, Rhinehart HL, Via CS. Decreased lymphocyte responses in free-ranging bottlenose dolphins (*Tursiops truncatus*) are associated with increased concentrations of PCBs and DDT in peripheral blood. *Environ Health Perspect*. (1995) 103 Suppl 4:67–72. doi: 10.1289/ehp.95103s467

9. Desforges JP, Levin M, Jasperse L, de Guise S, Eulaers I, Letcher RJ, et al. Effects of polar bear and killer whale derived contaminant cocktails on marine mammal immunity. *Environ Sci Technol*. (2017) 51:11431–9. doi: 10.1021/acs.est.7b03532

10. Frouin H, Lebeuf M, Saint-Louis R, Hammill M, Pelletier E, Fournier M. Toxic effects of tributyltin and its metabolites on harbour seal (*Phoca vitulina*) immune cells *in vitro*. *Aquat Toxicol*. (2008) 90:243–51. doi: 10.1016/j.aquatox.2008.09.005

11. Lavender-Law K. Plastics in the marine environment. *Annu Rev Mar Sci*. (2017) 9:205–29. doi: 10.1146/annurev-marine-010816-060409

12. Hart LB, Beckingham B, Wells RS, Alten Flagg M, Wischusen K, Moors A, et al. Urinary phthalate metabolites in common bottlenose dolphins (*Tursiops truncatus*) from Sarasota Bay, FL, USA. *GeoHealth*. (2018) 2:313–26. doi: 10.1029/2018GH000146

13. Peñín I, Levin M, Acevedo-Whitehouse K, Jasperse L, Gebhard E, Gulland FMD, et al. Effects of polychlorinated biphenyls (PCB) on California Sea lion (*Zalophus californianus*) lymphocyte functions upon *in vitro* exposure. *Environ Res*. (2018) 167:708–17. doi: 10.1016/j.envres.2018.08.028

14. Cámara Pellissó S, Muñoz MJ, Carballo M, Sánchez-Vizcaíno JM. Determination of the immunotoxic potential of heavy metals on the functional activity of bottlenose dolphin leukocytes *in vitro*. *Vet Immunol Immunopathol*. (2008) 121:189–98. doi: 10.1016/j.vetimm.2007.09.009

15. Li WT, Chang HW, Yang WC, Lo C, Wang LY, Pang VF, et al. Immunotoxicity of silver nanoparticles (AgNPs) on the leukocytes of common bottlenose dolphins (*Tursiops truncatus*). *Sci Rep*. (2018) 8:5593. doi: 10.1038/s41598-018-23737-0

16. Demaster DP, Fowler CW, Perry SL, Richlen MF. Predation and competition: the impact of fisheries on marine-mammal populations over the next one hundred years. *J Mammal*. (2001) 82:641–51. doi: 10.1644/1545-1542(2001)082<0641:PACTIO>2.0.CO;2

17. Read AJ, Drinker P, Northridge S. Bycatch of marine mammals in U.S. and global fisheries. *Conserv Biol*. (2006) 20:163–9. doi: 10.1111/j.1523-1739.2006.00338.x

18. Wright AJ, Aguilar Soto N, Baldwin AL, Bateson M, Beale C, Clark C, et al. Anthropogenic noise as a stressor in animals: a multidisciplinary perspective. *Int J Comp Psychol*. (2007) 20:250–73. doi: 10.46867/IJCP.2007.20.02.02

19. O'Brien JM, Beck S, Berrow SD, André M, van der Schaar M, O'Connor I, et al. Chapter 95 the use of deep water berths and the effect of noise on bottlenose dolphins in the Shannon Estuary cSAC In: *The effects of noise on aquatic life II, advances in experimental medicine and biology*. New York: Springer Science + Business Media (2016). 775–84.

20. Moscoso MS. De la mente a la célula: impacto del estrés en psiconeuroinmunoendocrinologia. *Liberabit*. (2009) 15:143–52. Available at: http://www.scielo.org.pe/scielo.php?script=sci_arttext&pid=S1729-48272009000200008&lng=es&tlng=es

21. Schaefer AM, Bossart GD, Mazzoil M, Fair PA, Reif J. Risk factors for colonization of *E. coli* in Atlantic bottlenose dolphins (*Tursiops truncatus*) in the Indian River Lagoon, Florida. *J Environ Public Health*. (2011) 2011:597073. doi: 10.1155/2011/597073

22. Delport TC, Harcourt RG, Beaumont LJ, Webster KN, Power ML. Molecular detection of antibiotic-resistance determinants in *Escherichia coli* isolated from the endangered Australian sea lion (*Neophoca cinerea*). *J Wildl Dis*. (2015) 51:555–63. doi: 10.7589/2014-08-200

23. Glaser R, Kiecolt-Glaser JK. Stress-induced immune dysfunction: implications for health. *Nat Rev Immunol*. (2005) 5:243–51. doi: 10.1038/nri1571

24. Kurogi J, Lida T. Social stress suppresses defence activities of neutrophils in tilapia. *Fish Pathol*. (1999) 34:15–8. doi: 10.3147/jsfp.34.15

25. Mosiman VL, Patterson BK, Canterero L, Goolsby CL. Reducing cellular autofluorescence in flow cytometry: an *in situ* method. *Cytometry*. (1997) 30:151–6. doi: 10.1002/(SICI)1097-0320(19970615)30:3<151::AID-CYTO6>3.0.CO;2-O

26. Daniel E, Crocker CD. Champagne, pinniped physiology In: B Würsig, JGM Thewissen and KM Kovacs, editors. *Encyclopedia of marine mammals*. *3rd* ed. Amsterdam, Netherlands: Academic Press (2018). 726–33.

27. Arias G, Garzón J. Zygomycosis. *Infection*. (2010) 14:S181–92. doi: 10.1016/S0123-9392(10)70135-1

28. Park G, Munley JA, Kelly LS, Kannan KB, Mankowski RT, Sharma A, et al. Gut mycobiome dysbiosis after sepsis and trauma. *Crit Care*. (2024) 28:18. doi: 10.1186/s13054-023-04780-4

29. Reif JS, Peden-Adams MM, Romano TA, Rice CD, Fair PA, Bossart GD. Immune dysfunction in Atlantic bottlenose dolphins (*Tursiops truncatus*) with lobomycosis. *Med Mycol*. (2009) 47:125–35. doi: 10.1080/13693780802178493

30. Noda K, Aoki M, Akiyoshi H, Asaki H, Shimada T, Ohashi F. Evaluation of the polymorphonuclear cell functions of bottlenose dolphins. *J Vet Med Sci*. (2003) 65:727–9. doi: 10.1292/jvms.65.727

31. Levin M, Morsey B, Mori C, Nambiar PR, De Guise S. PCBs and TCDD, alone and in mixtures, modulate marine mammal but not B6C3F1 mouse leukocyte phagocytosis. *J Toxicol Environ Health A*. (2005) 68:635–56. doi: 10.1080/15287390590921766

32. De Guise S, Flipo D, Boehm JR, Martineau D, Béland P, Fournier M. Immune functions in beluga whales (*Delphinapterus leucas*): evaluation of phagocytosis and respiratory burst with peripheral blood leukocytes using flow cytometry. *Vet Immunol Immunopathol*. (1995) 47:351–62. doi: 10.1016/0165-2427(94)05399-D

33. Cossarizza A, Chang HD, Radbruch A, Acs A, Adam D, Adam-Klages S, et al. Guidelines for the use of flow cytometry and cell sorting in immunological studies. *Eur J Immunol*. (2019) 49:1457–973. doi: 10.1002/eji.201970107

34. Cuvertoret-Sanz M, López-Figueroa C, O'Byrne A, Canturri A, Martí-Garcia B, Pintado E, et al. Causes of cetacean stranding and death on the Catalonian coast (western Mediterranean Sea), 2012–2019. *Dis Aquat Org*. (2020) 142:239–53. doi: 10.3354/dao03550

frontiers | Frontiers in Veterinary Science

TYPE Original Research
PUBLISHED 10 May 2024
DOI 10.3389/fvets.2024.1393977

OPEN ACCESS

EDITED BY
Alberto Alvarez-Barrientos,
STAB, Universidad de Extremadura, Spain

REVIEWED BY
Jordi Petriz,
Germans Trias i Pujol Health Science Research Institute (IGTP), Spain
Roberto Pozner,
CONICET Rosario, Argentina

*CORRESPONDENCE
Consuelo Rubio-Guerri
✉ consuelo.rubio@uchceu.es
Alicia Martínez-Romero
✉ amartinez@cipf.es
José-Enrique O'Connor
✉ jose.e.oconnor@uv.es

RECEIVED 29 February 2024
ACCEPTED 25 April 2024
PUBLISHED 10 May 2024

CITATION
Felipo-Benavent M, Valls M, Monteiro MC, Jávega B, García-Párraga D, Rubio-Guerri C, Martínez-Romero A and O'Connor J-E (2024) Platelet phosphatidylserine exposure and microparticle production as health bioindicators in marine mammals. *Front. Vet. Sci.* 11:1393977. doi: 10.3389/fvets.2024.1393977

Platelet phosphatidylserine exposure and microparticle production as health bioindicators in marine mammals

Mar Felipo-Benavent[1,2], Mónica Valls[3], Maria Céu Monteiro[4], Beatriz Jávega[1], Daniel García-Párraga[3,5], Consuelo Rubio-Guerri[5,6]*, Alicia Martínez-Romero[7]* and José-Enrique O'Connor[1]*

[1]Laboratory of Cytomics, Joint Research Unit CIPF-UVEG, Department of Biochemistry and Molecular Biology, University of Valencia, Valencia, Spain, [2]Department of Biomedical Sciences, Faculty of Health Sciences, Universidad CEU Cardenal Herrera, CEU Universities, Valencia, Spain, [3]Veterinary Services, Oceanogràfic, Ciudad de las Artes y las Ciencias, Valencia, Spain, [4]1H-TOXRUN—One Health Toxicology Research Unit, University Institute of Health Sciences (IUCS), CESPU, CRL, Gandra, Portugal, [5]Research Department, Fundación Oceanogràfic de la Comunitat Valenciana, Valencia, Spain, [6]Department of Pharmacy, Faculty of Health Sciences, Universidad CEU Cardenal Herrera, CEU Universities, Valencia, Spain, [7]Cytomics Technological Service, Príncipe Felipe Research Center, Valencia, Spain

In human medicine, various pathologies, including decompression sickness, thrombocytopenia, and rheumatoid arthritis, have been linked to changes in cellular microparticles (MP) formation, particularly platelet microparticles (PMP). Similar disorders in marine mammals might be attributed to anthropogenic threats or illnesses, potentially impacting blood PMP levels. Thus, detecting platelet phosphatidylserine (PS) exposure and PMP formation could serve as a crucial diagnostic and monitoring approach for these conditions in marine mammals. Our group has developed a methodology to assess real-time PS exposure and PMP formation specifically tailored for marine mammals. This method, pioneered in species such as bottlenose dolphins, beluga whales, walruses, and California sea lions, represents a novel approach with significant implications for both clinical assessment and further research into platelet function in these animals. The adapted methodology for evaluating PS exposure and PMP formation in marine mammals has yielded promising results. By applying this approach, we have observed significant correlations between alterations in PMP levels and specific pathologies or environmental factors. These findings underscore the potential of platelet function assessment as a diagnostic and monitoring tool in marine mammal health. The successful adaptation and application of this methodology in marine mammals highlight its utility for understanding and managing health concerns in these animals.

KEYWORDS

hemostasis, calcium ionophore, Annexin V, bottlenose dolphin, sea lion, beluga whale, walrus, CD41

1 Introduction

Microparticles (MP) are vesicles derived from cell membranes with diameters ranging between 0.1 μm and 1 μm, having important functions in cell communication (1). Among MP, platelet microparticles (PMP) are the most abundant in the bloodstream of healthy animals

(1–3), constituting 70–90% of MP and presenting a wide variety of preanalytic variables and analytic variables, resulting in a wide range of PMP values in platelet-free plasma (PFP) of healthy subjects (100–4,000 PMPs μL^{-1}). These data indicate that standardization of PMP enumeration by flow cytometry is feasible but is dependent on intrinsic characteristics of the flow cytometer and the calibration strategy (4). PMP, which contain CD41, are physiologically produced during the final phase of platelet activation. Following intraplatelet Ca^{2+} mobilization, shape alteration, aggregation, and granule secretion, platelets manifest procoagulant activity by exposing phosphatidylserine (PS) from the inner to the outer face of the platelet membrane (5). Subsequently, small membrane fragments are released as PMP (5), playing crucial roles in cell communication, transporting bioactive molecules, and signaling various processes associated with hemostasis and thrombosis.

Moreover, various pathologies are linked to alterations in PMP production, such as decompression sickness (1), thrombocytopenia, rheumatoid arthritis (6), cancer (3, 7, 8), arterial thrombosis (9) atherosclerosis (10), immune thrombocytopenic purpura, or even malaria infection (3). Alterations in blood PMP levels can be associated with different risks. On the one hand, elevated PMP levels can lead to platelet deposition and thrombus formation (3). On the contrary, reduced levels are associated with a propensity for bleeding, as occurs in Castaman's defect or Scott's syndrome (11).

For this reason, monitoring blood PMP production serves as a valuable diagnostic and monitoring tool for several disorders, including cancer (12). Despite some of these diseases are not necessarily documented in marine mammals, this is likely due to limited information available compared to other mammals, stemming from the challenges of accessing these creatures in the sea rather than a lack of interest.

An interesting approach to PMP comprehension in marine mammals could be to determine whether, as in humans, diving perturbances can affect the production of PMPs. A similar study has previously been carried out measuring MP in the blood of Steller sea lions, needing more research to elucidate whether decompression has effects on its production (13).

In human divers, a fast ascent from the depth to the surface causes decompression sickness. At high pressures nitrogen is more soluble and accumulates dissolved in blood and tissues. During ascent nitrogen dissolved in the blood and tissues becomes less soluble forming bubbles as ambient pressure decreases swiftly (1). Studies have shown that even asymptomatic divers exhibit elevated levels of cellular microparticles in the blood, primarily carrying specific membrane proteins: CD41, CD31, CD66b, CD142, and CD235 (1). Blood levels of cellular MP have been demonstrated to be 2.4 to 11.7 times higher in symptomatic divers with decompression sickness compared to asymptomatic individuals (1). Therefore, levels of MP serve as reliable indicators for diagnosing and monitoring the progression of decompression sickness in humans (1). In fact, the decrease in MP levels correlates proportionally with the remission of the disease when treating decompression sickness (14). While decompression sickness in marine mammals is unclear, compatible lesions have been detected in some individuals (15, 16). The myoglobin content exhibited a positive and significant correlation with maximum dive duration in odontocetes, indicating its role in facilitating prolonged dives. Additionally, the syndrome of decompression sickness is intricately linked to the diving behavior of cetaceans, with variations in diving types influencing the likelihood of experiencing this condition (17). The rise in human life expectancy has led to an unprecedented increase in the population, consequently driving up the demand for food products such as fish. As a result, fishing practices have become industrialized and expanded into new areas, covering more than 55% of the ocean and causing overexploitation of certain fish populations (18, 19). This expansion has heightened interactions between fishermen and marine mammals, leading to competition for the same resources (20). Occasionally, marine mammals directly encounter fishing nets and become entangled, a process known as bycatch, where they are subsequently released back into the sea (21, 22). Bycatch may inflict severe injuries or mortality on the animals, potentially impacting their demographics and overall survival (23, 24). While marine mammals are anatomically and physiologically adapted to withstand normal diving conditions without experiencing decompression sickness, it has been hypothesized their adaptive mechanisms could fail in highly stressful situations like interaction with fisheries interaction or exposure to high intensity noise exposure (25, 26). There is an hypothesis that provides avenues for new areas of research, offers an explanation for how sonar exposure may alter physiology causing gas embolism, and provides a new mechanism for how air-breathing marine vertebrates usually avoid the diving-related problems observed in human divers (26). Severe gas embolism has been proposed to cause the death of the animals and eventual stranding on the coast (15, 16, 27). In such cases, the absence of bacteria or autolytic changes serves as histological indicators of pre-mortem gas bubble formation (27).

Additionally, a specific acoustic phenomenon termed "rectified diffusion" has the potential to directly cause gas embolism (15). Indeed, instances of mass strandings of marine mammals in regions characterized by high levels of noise pollution have been documented (28, 29). Notably, the significant stranding events involving beaked whales occurring mere hours or days following the use of military sonars in the same maritime zones stand out as crucial examples of the consequences of high intensity underwater noise on certain marine mammals, with gas embolism identified as the primary cause of death in some species (15, 30). Beaked whales typically engage in deep dives (31), so an acute stress response triggered by sonar signals has been proposed can result in gas embolism.

To study the role of the pathologies or anthropogenic threats in PMP production alterations the first step is to set up an assay for PMP detection. In the realm of marine mammals, the requisite methodology for analyzing PS exposure, MP formation, and detecting MP levels had not been fully developed. There is only one study on Steller sea lions that examines the measurement of blood microparticles to understand their correlation with decompression stress (13). However, our study specifically targets PMP since they constitute the predominant type in the bloodstream. Our group employed a flow cytometric technique utilizing an anti-human CD41 antibody, previously established and described in our prior research involving bottlenose dolphins, beluga whales, walruses, sea lions, and seals (32), the binding of the antibody to platelets is demonstrated not only by the morphological characteristics of the CD41+ events but also by their physiological response to the platelet agonist, showing the changes in annexin V exposure and production of PMP (32).

PMP hold promise as potential indicators of several diseases such as rheumatoid arthritis, thrombocytopenia or arterial thrombosis among others. It may also help to elucidate the pathophysiology of the alterations that occur during decompression processes in marine mammals, especially in captured or stranded animals. The primary challenge with these wild animals is accessing their blood when they

are stranded, as they are often dehydrated or appear dead. This poses a significant problem as it is difficult to obtain a sufficient quantity of blood, or none at all in the case of dead animals. Additionally, another challenge is the necessity to process the blood samples within a narrow timeframe of 3–4 h, complicating the organization of the experiment. On the other hand, it provides a novel avenue for investigating platelet function in these species. Assessing real-time PS exposure and PMP production could potentially benefit veterinary practices in aquariums and research of marine mammals. In this work we present a pilot study on the effects of aspirin on the PMP production of dolphins, demonstrating the usefulness of the assay in the research on physiology and toxicological approaches in these species.

2 Materials and methods

2.1 Animals and samples

To carry out the study, 11 samples were obtained from 11 bottlenose dolphins (*Tursiops truncatus*; 1 sample per animal), 11 samples from 3 beluga whales (*Delphinapterus leucas*), 12 samples from 3 pacific walruses (*Odobenus rosmarus divergens*) and 4 samples from 4 Patagonian sea lions (*Otaria flavescens*; 1 per animal). All the animals inhabit Oceanogràfic Aquarium of the City of Arts and Sciences (Valencia, Spain) except two sea lions from Mundomar Aquarium (Benidorm, Spain). The samples were analyzed to evaluate PMP blood levels and real time PS exposure and release of PMP after activating the platelets with an agonist. All the experiments were approved by the Animal Care and Welfare Committee of the Oceanogràfic and Mundomar Aquariums (Reference: OCE-6-17).

2.2 Blood sampling

We collected 1 mL citrated whole blood from healthy animals that had been all previously trained to cooperate voluntarily with trainers and veterinarians for blood collection. In cetaceans, blood samples were drawn from a vein on the ventral surface of the caudal fin, while in pinnipeds, blood was obtained from interdigital veins on the caudal flippers. Specific equipment was utilized for blood sampling in both pinnipeds and cetaceans. This included a 21G gauge size Butterfly needle known as Venofix®, manufactured by Fa. Braun, which is commonly employed. Furthermore, single-use syringes with 10 mL capacity from Covetrus were used for blood collection in both pinnipeds and cetaceans. These syringes are designed for one-time use, ensuring sterility and minimizing the risk of contamination during the blood sampling process.

Samples were analyzed in the Cytomics Laboratory at the Príncipe Felipe Research Center (CIPF, Valencia, Spain) within 2 h after being obtained.

2.3 Reagents and solutions

Antibody CD41 PE, clone P2 was from Beckman Coulter (Cat. No: A07781). Annexin V was from the Annexin V-FITC / PI Kit, Miltenyi Biotec, (Order no. 130–092-052). Calcium ionophore A23187 (Merck, Cat No: C7522-1MG) was prepared at 10 mg/mL in DMSO, aliquoted and stored at −20°C. Modified Tyrode's Buffer was home prepared using 137 mM NaCl, 2.8 mM KCl, 1 mM $MgCl_2$, 12 mM $NaHCO_3$, 0.4 mM Na_2HPO_4 and 10 mM HEPES, adjusted to pH 7.4 and stored at 4°C. Before starting each experiment, 0.35% Bovine Serum Albumin (BSA) and 5.5 mM glucose were added to the buffer and kept at room temperature until use. Annexin binding buffer was a modified Tyrode's Buffer enriched with 0.22 mg/mL $CaCl_2$.

2.4 Sample staining

Citrated whole blood was diluted 1:10 in Modified Tyrode's Buffer. Then, 100 µL of the dilution was incubated for 10 min with 20 µL of the CD41-PE anti-human antibody, 2 µL of Annexin V-FITC and 150 µL of Annexin binding buffer at 37°C and 5% CO_2. After that, 2 mL of Annexin binding buffer was added to each tube. Finally, 500 µL of the suspension was dispensed into an Eppendorf microtube for its acquisition on the flow cytometer.

2.5 Flow cytometry setup

The experiments were performed on a CytoFLEX S Flow Cytometer (Beckman Coulter, United States) using the cytometer-interfaced CytExpert software (Beckman Coulter, Californa, United States).

The flow cytometer was set up to measure Forward Scatter signal (FSC), Violet Side Scatter signal (VSSC), Annexin-V-FITC fluorescence (FL1, exc 488 nm/em 525 nm), CD41-PE fluorescence (FL10, exc 561 nm/em 585 nm) and time. To optimize the detection of PMP, we used the SSC signal from the violet laser (405 nm, VSSC), since this signal facilitates the amplification of the differences in the refractive indices between the particles and their surrounding medium. The trigger used for PMP assessment was VSSC-Height, with a threshold in 40,000. All the signals were acquired in logarithmic amplification. Data analysis was performed using CytExpert Software (Beckman Coulter) and FlowJo™ v10.5.3 Software (BD Life Sciences).

2.5.1 Real time PS exposure and PMP production evaluation stimulating platelets with calcium ionophore A23187

A protocol previously described in humans (32) was adapted and modified to marine mammals. Figure 1A shows the count of cells and time course representative of the kinetic evaluated in the study. "Baseline" region corresponds to the time before adding the stimulus until 50 s of acquisition. At this time the calcium ionophore A23187 is added to the sample while the cytometer continues aspirating the sample. "Activated" region spans from the addition of the agonist to the end point and includes the platelets that have been stimulated.

Platelets and PMP can be identified using the CD41-PE fluorescence combined either with FSC or VSSC signals, using size or internal complexity, respectively, as morphological indicators (Figures 1B–E). Figure 1B shows the resting platelet population identified as positive CD41 events with the smallest relative size (region R1). Erythrocytes and leukocytes are also distinguished as the larger CD41 negative events (region R2). On the other hand, R3 include platelets bound to with erythrocytes or leukocytes or coincident with them when crossing the cytometer laser. When platelets are activated with calcium ionophore 0.02 µg/mL A23187

10.3389/fvets.2024.1393977

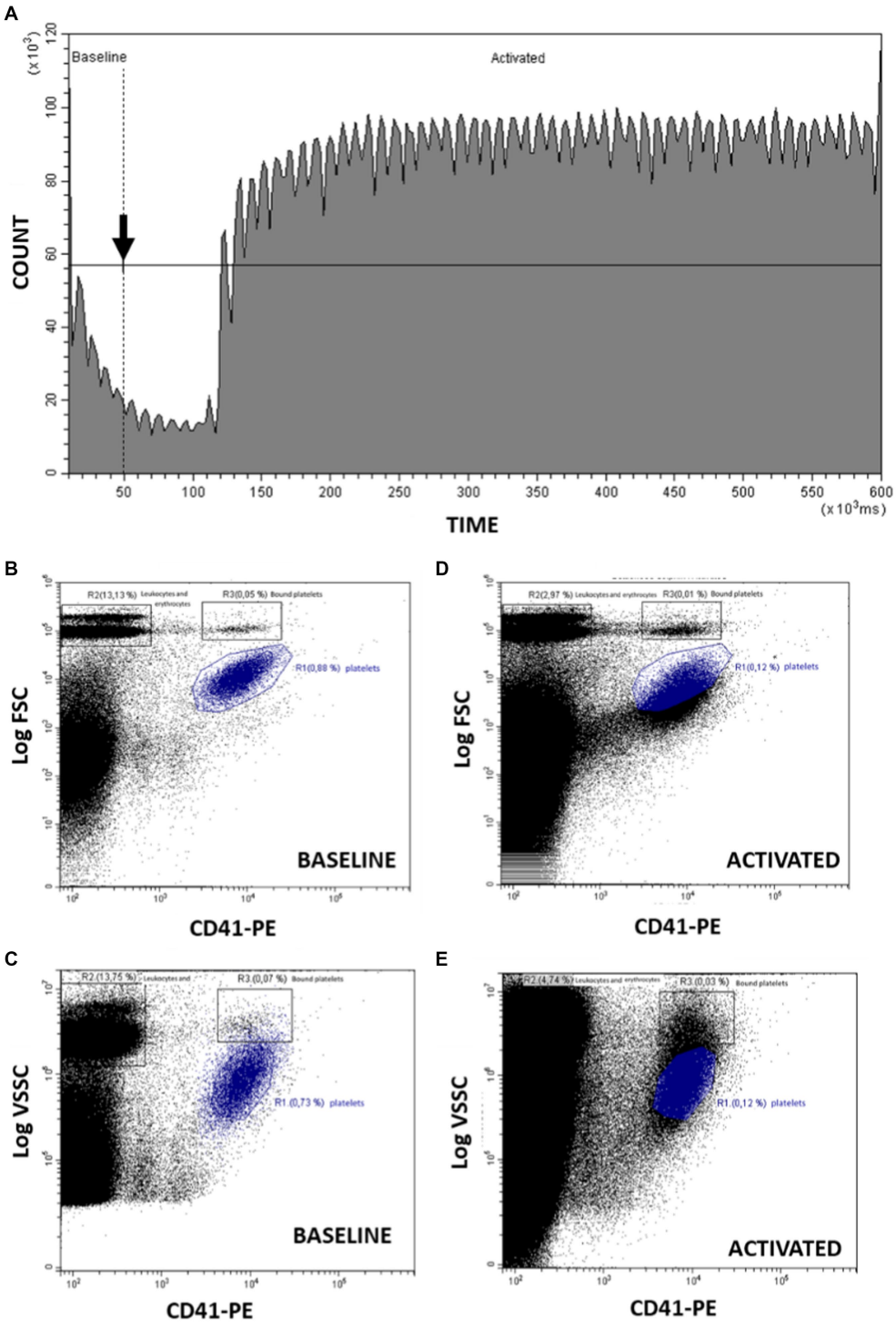

FIGURE 1
Analysis by flow cytometry of PMP formation stimulating platelets with Ca^{2+} ionophore A23187. **(A)** Count of cells and time course representative of the kinetics before (baseline) and after (activated) adding the stimulus (arrow). The observed periodic oscillations in the Count vs. Time graph reflect the minor variations in sampling rate provided by the peristaltic pump of this flow cytometer model. **(B)** From "baseline," dot-plot CD41-PE/FSC for identification of platelets (R1), erythrocytes and leukocytes (R2) and coincident platelets erythrocytes and leukocytes (R3). **(C)** From "activated," dot-plot CD41-PE/FSC changes after platelet activation with A23187. **(D)** From "baseline," dot-plot CD41-PE/VSSC for identification of platelets (R1), erythrocytes and leukocytes (R2) and coincident platelets erythrocytes and leukocytes (R3). **(E)** From "activated," dot-plot CD41-PE/VSSC changes after platelet activation with A23187. R1: region including platelets; R2: region including erythrocytes and leukocytes; R3: region including platelets bound to or coincident in flow with erythrocytes and leukocytes.

starts the PS exposure and PMP production decreasing the FSC and CD41 signal as seen in Figure 1C. These changes can also be observed using VSSC instead of FSC as detailed in Figures 1D,E.

Kinetics of PS exposure and PMP formation after activating the platelets with A23187 were assessed following the Annexin V-FITC and FSC signals over time (Figure 2). These changes can also

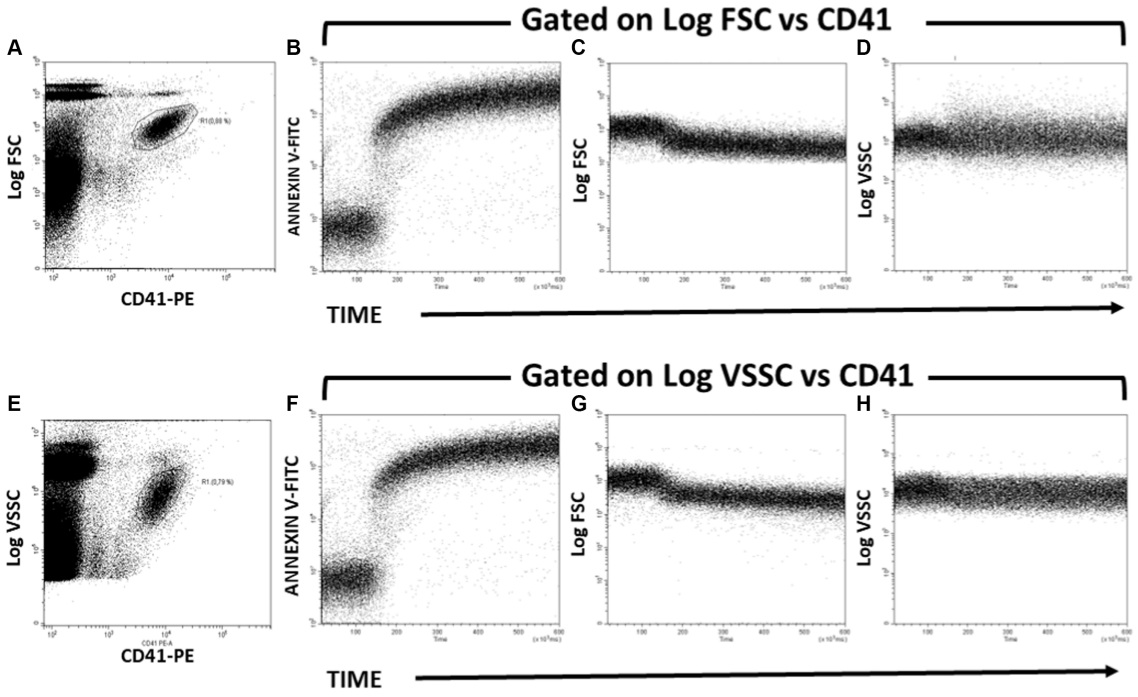

FIGURE 2
Kinetics of PS exposure and PMP formation after activating Bottlenose dolphin platelets in a whole blood sample with calcium ionophore A23187. **(A,E)** Gating of the main platelet population on CD41-PE/Log FSC **(A)** and CD41-PE/Log VSSC **(E)** dot plots for further kinetic representation of changes over time in Annexin-V-FITC fluorescence **(B,F)**, Log FSC **(C,G)**, and Log VSSC **(D,H)** after addition of calcium ionophore A23187 50 s after the start of the run. The kinetic plots in panels **B–D** are gated in the platelet region defined in the dot plot of panel **A**. The kinetic plots in panels **B–D** are gated in the platelet region defined in the dot plot of panel **B**.

be assessed by identifying platelets from CD41/FSC (Figures 2A–D) or CD41/VSSC (Figures 2E–H) dot plots. Briefly, the baseline Annexin V-FITC and FSC signals were registered for 20–50 s. At this time, calcium ionophore was added to the sample in acquisition and mixed with a Pasteur pipette, while the cytometer continued aspiring the sample. Changes over time on Annexin V-FITC fluorescence intensity and FSC and VSSC signals were recorded up to 10 min.

2.5.2 Obtaining numerical values of platelet PS exposure and PMP formation

The analysis was carried out with the Flowjo software using the same strategy for region selection as in the sample acquisition. Changes in Annexin V and FSC signals over time were represented in dot plots. To obtain numerical parameters, analytical regions were defined throughout the length of the plot, dividing them in five parts to evaluate the mean fluorescence intensity (MFI) of Annexin V and FSC (A to E regions) variations over time (Figure 3). In the Annexin V/Time dot plot, region A corresponds to the baseline fluorescence intensity of Annexin V-FITC in resting platelets. After stimulating with calcium ionophore, the Annexin V-FITC MIF increases, due to the externalization of PS in activated platelets. Annexin V binds to PS increasing its fluorescence. The peak of fluorescence is framed in region B. Regions C to E record the changes in PS exposure over time until 10 min of acquisition (Figure 3A). In FSC/time dot plot, region A establish the baseline platelets relative size. After stimulating with calcium ionophore, the platelets break down into PMP, so FSC signal progressively decreases over time (regions B to E; Figure 3B).

From these regions we propose different parameters to evaluate PS exposure and PMP production:

Focusing on Annexin-V/time dot plot, we obtained the mean of the time and Annexin V-FITC MIF (fluorescence arbitrary units, FAU) for each region (A–E). These values can be represented in a graphic (Figure 3C). From these, we calculate: Ratio between peak and baseline Annexin-V fluorescence intensity (RPB): the fold that platelet PS exposure increases after A23187 addition; differential between peak and baseline Annexin-V fluorescence intensity (ΔPB): the absolute difference in platelet PS exposure between activated and resting platelets; ratio between end-point and baseline Annexin-V fluorescence intensity (REB): the fold that platelet PS exposure remains elevated above the PS exposure in resting platelets; differential between end-point and baseline Annexin-V fluorescence intensity (ΔEB): the absolute difference between the remaining platelet PS exposure at 10 min post-activation and in resting platelets; and slope of the Annexin-V fluorescence curve from the peak to the end point (SPE): the rate of PS exposure after platelet stimulation.

In the FSC/time kinetics plot, for each region (A to E), we obtained the mean FSC and time. These values can be graphed (Figure 3D) and the slope of the line could be calculated to quantify the decrease speed of the relative size after PMP formation (SFSC).

2.6 Obtaining normal values of PS exposure and PMP formation for the different species

To obtain the values of PS exposure and PMP production in healthy individuals of the different species, we analyzed RPB, ΔPB, REB, ΔEB, SPE and SFSC in 11 dolphins (1 sample per animal), 11

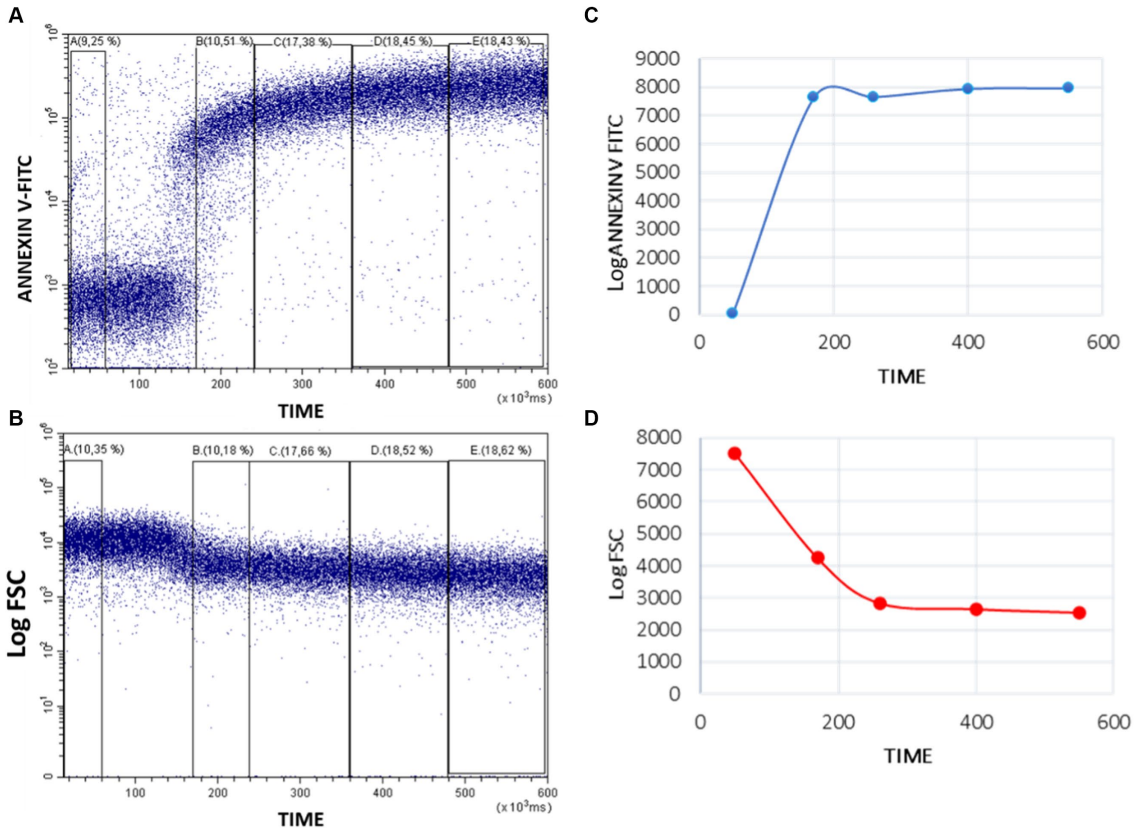

FIGURE 3
Quantitative analysis of Annexin-V-FITC binding and FSC decrease in whole blood platelets after activating Bottlenose dolphin platelets in a whole blood sample with calcium ionophore A23187. Five regions **(A–E)** were defined over the Time axis in Annexin V-FITC/Time **(A)** and FSC/Time kinetic plots **(B)** and the mean intensity values obtained with the CytExpert software. The resulting values were represented in standard kinetic graphs displaying in arbitrary units (Y-axes) the mean fluorescence intensity (Annexin-V-FITC) **(C)** and the mean scatter intensity (Log FSC) variations along time **(D)**.

samples from 3 beluga whales, 12 samples from 3 walruses and 4 samples from 4 sea lions. Calculating the mean, median, standard error (SEM), minimum and maximum for each parameter in all the species.

2.7 Application of PS exposure and PMP formation assessment in *in vitro* toxicological studies in marine mammals

Blood from three healthy dolphins was used for this proof of concept of the effects of aspirin on PMP production in dolphins.

2.7.1 Preparation of aspirin stock and culture medium

The final aspirin concentrations used in the assay were 0.02 µM, 2 µM, and 200 µM. Aspirin stocks were prepared each day solubilizing it as ethanol solutions at concentrations 200 times higher than those used in the assay. For each experiment, the aspirin stocks were diluted in modified culture medium obtaining the double the required final concentration (2X) per well.

Culture medium was RPMI 1640 + GlutaMAX-I (GIBCO, 61870–010) supplemented with 10 mM HEPES (GIBCO, 15630–056), 0.1 mM non-essential amino acids (GIBCO, 11140), 50 U/mL penicillin/50 µg/mL streptomycin (GIBCO, 15140–122), 50 µM 2-mercaptoethanol (GIBCO, 21985–023) and 10% bovine serum (GIBCO, 26010–074).

2.7.2 Blood treatment with aspirin

For the *in vitro* studies, 96-well plates were used for acute and sustained (24 h) blood treatment with different concentrations of aspirin. To do this, 50 µL of citrated whole blood, 50 µL of modified RPMI medium and 100 µL of 2X aspirin were mixed in each well and incubated up to 24 h. PMP production was evaluated at different concentrations of aspirin comparing with the non-exposed control.

On the other hand, the acute response to aspirin was also studied by exposing the blood to the compound and measuring its immediate effects, without previous incubation.

2.8 Statistical analysis

The statistical significance of the differences in PS exposure and PMP formation parameters between animals per sex, age or species, were evaluated by a t-test in Graphpad Prism 5. In the toxicological study with aspirin, the effect of the drug in the PS exposure and PMP formation was statistically assessed using t-test and ANOVA in Graphpad Prism 5.

3 Results

The use for the first time of Annexin-V as a PS marker in platelets of marine mammals was successful. The combined measurement of Annexin-V-FITC, CD41-PE, FSC and VSSC signals was useful to discriminate PMP in marine mammals, as previously described for humans (33). Platelets response to stimulation with the agonist was similar to that observed in humans too, increasing the MFI of Annexin-V by PS exposure and reducing FSC signal by PMP formation (33) (Figure 2).

3.1 Measurement of PS exposure and PMP production in stimulated platelets

The human-reacting monoclonal antibody CD41 (clone P2) was found to identify the platelets in different species of marine mammals (32), but also PMP. PMP are platelet membrane fragments that can be distinguished by their expression of CD41, PS and their low relative size. Our group has been exploring a technique utilizing flow cytometry that shows promise in distinguishing PMP in marine mammals (32).

Figure 1A shows a time course representative of the kinetic experiments performed in this work. As described in point 2.5.1 of Material and Methods, fluorescence and light scatter signals are recorded continuously up to 600 s. In our experimental setup, the Ca^{2+}-ionophore A23187, a strong platelet agonist, is added to the sample vial 50 s after the start (arrow Figure 1A), while the cytometer continues aspirating the sample. The cytometer software allows to define two consecutive regions in the count-versus-time graph that include the events registered before (Baseline) or after (Activated) the addition of the stimulus. Such regions can be used to gate in separate plots the basal cytometric features of the unstimulated sample (panels Figures 1B,D) and the changes induced by the Ca^{2+}-ionophore (panels 1C and 1E). With this approach, real-time monitoring of the platelet activation process is feasible.

Platelets in whole blood samples can be identified clearly by their expression of CD41, a constitutive marker of platelet membrane, and their morphological features estimated by their light scatter signature. Prior to ionophore addition, bivariate plots of CD41-PE vs. blue-laser forward scatter (Log FS, panel Figure 1B) or of CD41-PE vs. violet-laser side scatter (Log VSC, panel 1D) clearly show the cluster of individual platelets, as well as the cluster that represents the platelets that are bound-to or coincident-with other blood elements (mostly erythrocytes). More relevant to our experimental objective, the presence of circulating platelet-derived microparticles (PMP) is supported by a cohort of events characterized by decreased intensity of CD41-PE fluorescence and of either Log FSC or Log VSC, and that gradually merge into the background noise.

The bivariate plots gated in the time region post-ionophore addition allow to visualize the A23187-stimulated release of microparticles by activated platelets. Panel Figure 1D shows an average decrease of FSC intensity in the gated platelet population upon ionophore addition, accompanied of an increase in the continuum of lower CD41-PE/lower FSC events. The changes in VSSC and CD41-PE intensity (panel Figure 1E) upon ionophore addition are less straightforward. As seen in the plot, the gated platelet population maintains the average VSSC, while a continuum of CD41-PE+/higher VSSC events reaches and overpopulates the plot area where platelets bound or coincident with blood elements are expected. This observation suggests that this new population reflects the swarm effect (34) due to simultaneous laser illumination of platelets and released PMPs, amplified by the higher sensitivity of VSSC for assessing particle complexity by flow analysis (35). On the other hand, consistent with the changes depicted in panel Figure 1D, an increase in the continuum of lower CD41-PE/lower VSSC events is also observed, confirming that VSSC is also suitable for detecting PMP shedding.

Finally, it is worth to mention that the shedding of PMP induced by the ionophore explains the fast and noticeable increase in event count rate happening in the ungated kinetic plot (panel Figure 1A). As clearly seen, there is a sharp increase (approx. seven-fold) in the count rate that reflects the rapid appearance of PMP in the sample followed by stabilization of the count rate until the end of the run. This is consistent with the immediate effect of the strong platelet agonist used and shows that this assay may provide a very fast endpoint for assessing platelet functional responses associated to experimental or clinical studies of hemostasis.

Activated platelets expose PS, thus providing the procoagulant surface to which thrombin-generating enzyme complexes bind and assemble. The exposure of PS on platelets can be assessed in flow by the binding of fluorochrome-labeled Annexin V to platelets (36), while the subsequent release of PMP upon platelet activation can be monitored by the emerging of Annexin V-positive events with lower FSC or VSSC signals than the main platelet population. Since the generation of PMP by whole blood platelets induced by exposure to Ca^{2+}-ionophore is a very fast process (Figure 1) we attempted to monitor in real time the generation of platelet procoagulant surface. To this extent, whole blood samples were stained with both CD41-PE (for platelet and PMP identification) and Annexin V-FITC (for detecting PS exposure in platelets and PMP), and then challenged with Ca^{2+}-ionophore A23187 in the same experimental conditions as indicated for Figure 1. Again, the main platelet population was identified and gated in CD41-PE vs. Log FSC (panel Figure 2A) or CD41-PE vs. Log VSSC (panel Figure 2E) bivariate plots and the variations in Annexin V-FITC (panels Figures 2B,F), Log FSC (panels Figures 2C,G) and Log VSSC (panels Figures 2D,H) monitored by means of kinetic graphs gated-in by the indicated criteria.

As seen in Figure 2, addition of Ca^{2+}-ionophore A23187 induced a very fast binding of Annexin to platelets, as evidenced by the time course of the kinetic plots of Annexin V-FITC versus Time (panel Figures 2B,F), which were quite similar to the time course of the Count versus Time graph in Figure 1, thus supporting that Ca^{2+}-ionophore stimulation of platelets results in an almost simultaneous generation of procoagulant surface and PMP shedding, as expected (36). In consistence, the increase in Annexin V binding overlaps essentially in the time interval with a clear decrease of FSC signal (panels Figures 2C,G) and a less pronounced decrease of VSSC (panels Figures 2D,H). No apparent difference was observed in these kinetics regarding whether the platelet population was gated by its Log FSC (panel Figure 2A) or Log VSSC (panel Figure 2E) signatures.

In order to complete the above observations with a more accurate description of PMP generation (Figure 4), we defined two additional gating criteria, based on CD41-PE vs. Log FSC (panel Figure 4A) or CD41-PE vs. Log VSSC (panel Figure 4E) enlarged regions that could allow to track events described by their CD41-PE and Annexin

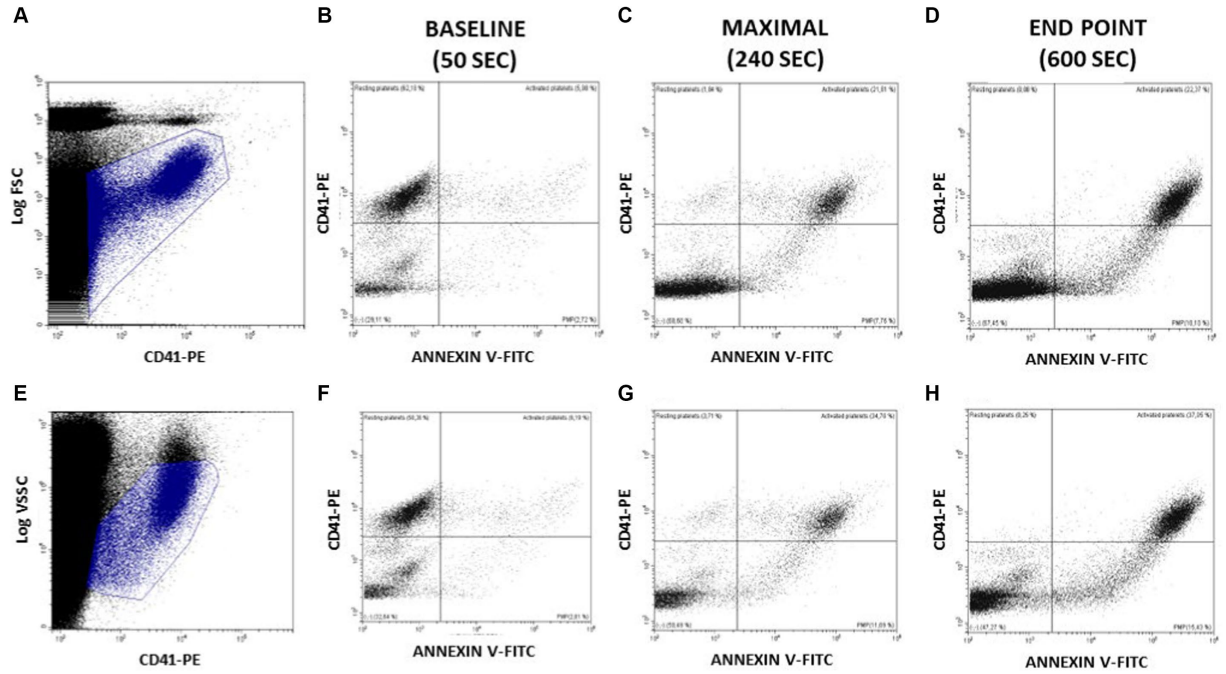

FIGURE 4
Assessment of PS exposure on platelet surface and PMP generation at relevant times after activating Bottlenose dolphin platelets in a whole blood sample with calcium ionophore A23187. The main platelet population and the continuous cohort of PMPs were gated for further analysis in the displayed regions amply drawn on CD41-PE/Log FSC **(A)** or CD41-PE/Log VSSC dot plots **(E)**. At the indicated time intervals a series of CD41-PE/Annexin V-FITC dot plots were used to display the relative proportions of platelets at rest (CD41+/Annexin V- events); platelets exposing PS (CD41+/Annexin V+ events); PMP of varying size and PS (CD41 variable/Annexin V variable events) and PMP merging with background noise (CD41−/Annexin V- events) **(B–D** and **F–H)**.

V-FITC expression in a more extended range. This strategy displays better the populations of non-activated (CD41+/Annexin V-) and activated (CD41+/Annexin V+) platelets, and the cohort of generated PMP with different sizes, as estimated by their variable expression of both CD41-PE and Annexin-V (CD41var/Annexin Vvar). The CD41neg/Annexin Vneg region includes the background noise and the undetectable PMP beyond the limit of sensitivity of the flow cytometer. Although we have not made still any attempt to calibrate the size of PMP nor to quantify their abundance, we show in Figures 4B–D,F–H, the distribution of the above populations in three distinct relevant stages of the ionophore-activation experiment, namely prior to ionophore addition (baseline: 0–50 s); at the time of maximal Annexin V-FITC binding (maximal: 120–240 s) and at the final time of the run (end point: 460–600 s). As seen, at baseline most platelets are non-activated, but the presence of some activated platelets and PMP is observed. At maximal, most platelets are activated and PMP are increased, but some platelets are unstimulated or still express lower levels of Annexin V-FITC. At the end point, no resting or partially activated platelets are evident and the cohort of PMP is more abundant. As in the previous experiments, quite similar distributions were observed, independently of whether Log FSC or Log VSSC were used as gating criteria.

Our kinetic approach based on Annexin V binding and FSC variations can be made quantitative by establishing appropriate intervals in the Annexin V-FITC versus Time (Figure 3A) and the Log FSC versus Time (Figure 3C) plots and calculating the mean intensity of fluorescence and FSC signals, that can be then plotted in conventional graphs (Figures 3B,D). Such graphs allow to compare better different processes of platelet activation or to show differences among different individuals or among zoological groups. In this context, we have extended our kinetic assay, that has been set up using blood samples from bottlenose dolphins to individuals of other species of marine mammals, namely beluga whales, walruses and sea lions. As seen in Figure 5, the kinetic assay here described can be applied without any modification of the experimental conditions and cytometer settings to other marine mammals and shows quite similar qualitative behavior of platelets when challenged with the Ca^{2+}-ionophore A23187 used for activation of bottlenose dolphin platelets.

3.2 Normal values of PS exposure and PMP formation in the different species and differences by age, sex or specie

The median, standard error (SEM), minimum and maximum values for each parameter studied of PS exposure and PMP formation in bottlenose dolphins, beluga whales, walruses and sea lions are detailed in Tables 1–4.

Within the same species, differences in platelet PS exposure and PMP production were only found between cetaceans of different ages. To confirm these results, the population size should be increased.

Regarding differences by species, our findings are shown in Table 5. The fast and sustained increased in Annexin V-FITC binding

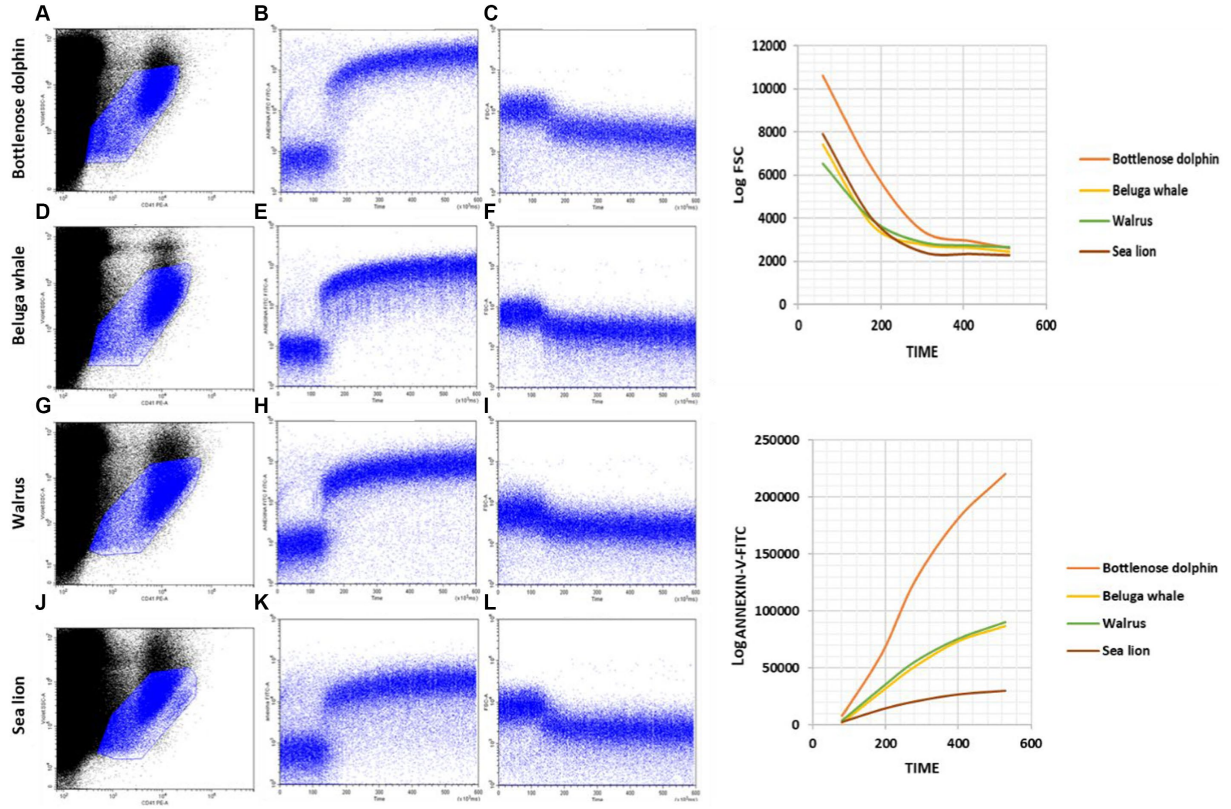

FIGURE 5
Kinetics of PS exposure and FSC decrease after activating marine mammal platelets in whole blood samples with calcium ionophore A23187. **(A,D,G,J)** Gating of the main platelet population on CD41-PE/Log VSSC dot plots for further kinetic representation of changes over time in Annexin-V-FITC fluorescence **(B,E,H,K)** and Log FSC **(C,F,I,L)** after addition of calcium ionophore A23187 50 s after the start of the run. Plots are representative examples of the results obtained with Bottlenose dolphins **(A–C)**; Beluga whales **(D–F)**; Walruses **(G–I)** and Sea lions **(J–L)**.

TABLE 1 **Range of values for each PS exposure and PMP formation parameters in dolphins under human care.**

	SFSC	RPB	REB	ΔPB	ΔED	SPE
Bottlenose dolphins $n = 11$, 11 samples	−18.5 ± 1.5 (min: −27; max: −12)	41.7 ± 15.6 (min: 1.5; max: 182)	19.5 ± 5 (min: 1.6; max: 51)	23.932 ± 2.876 (min: 11271; max: 41804)	16.809 ± 1.326 (min: 8601; max: 23384)	13 ± 5.6 (min: −38; max: 33)
Calves $n = 3$	−15 ± 1.8	77 ± 35	35 ± 15	25.890 ± 4.885	19.316 ± 1.170	25 ± 8
Adults $n = 11$	−19 ± 1.3	23.7 ± 5.6	23.5 ± 5	20.835 ± 2.124	19.322 ± 1.666	22.5 ± 3
Calves vs. Adults	NSD	p = 0.02*	NSD	NSD	NSD	NSD
Males $n = 5$	−17.8 ± 1.5	57 ± 23	28 ± 9	24.378 ± 2.808	19.116 ± 814	23 ± 4.6
Females $n = 9$	−16.7 ± 1.4	23 ± 7	25 ± 6	20.552 ± 2.622	19.434 ± 2042	23 ± 4
Males vs. Females	NSD	NSD	NSD	NSD	NSD	NSD

Significant differences were observed between calves and adults in the PS exposure after stimulation with calcium ionophore A23187 ($p \leq 0.05$*) (NSD: $p \geq 0.05$).

is observed in dolphins' samples (Figure 5). However, when such individual cytometric plots are transformed into quantitative standard kinetic graphs, a better comparison among the rate and intensity of the parameters reporting platelet activation is possible. Thus, the strongest expression of procoagulant surface is observed in bottlenose dolphin, while sea lion shows the lowest velocity and intensity of expression. Beluga whale and walrus have a similar behavior among them, with velocity and intensity values intermediate between bottlenose dolphin and sea lion. As for the decrease in FSC the intensity of the change is highest in bottlenose dolphin (Table 5), but sea lion and beluga whale, which have similarly smaller platelet FSC signals than dolphins, show similar rates of FSC decrease among them and compared to dolphins. Finally, walrus shows both slightly lower FSC baseline values and rate of FSC decrease. However, walruses exhibited a significantly higher end-point PS concentration than dolphins (REB).

TABLE 2 Range of values for each PS exposure and PMP formation parameters in beluga whales under human care.

	SFSC	RPB	REB	ΔPB	ΔEB	SPE
Beluga whales $n = 3$, 11 samples	-12 ± 0.5 (min: −14; max: −9)	63 ± 14 (min: 3.3; max: 163)	29.5 ± 4 (min: 15; max: 60)	24.055 ± 3.335 (min: 1142; max: 42076)	12.248 ± 1.190 (min: 5289; max: 17256)	-2 ± 5 (min: −25; max: 26)
Adults $n = 2$, 8 samples	-13.00 ± 0.3	74.16 ± 17.7	32.93 ± 5	27.367 ± 3.241	13.343 ± 1.317	-4.3 ± 5.6
Calf $n = 1$, 3 samples	-9.667 ± 0.3	33.44 ± 15	20.64 ± 3.7	15.224 ± 7.083	9.329 ± 1915	4.333 ± 11
Calf vs. Adults	$p = 0.0003$***	NSD	NSD	NSD	NSD	NSD
Males $n = 2$, 6 samples	-11.50 ± 0.8	47.41 ± 13.5	28.72 ± 4.7	20.608 ± 5.456	12.380 ± 1.696	4.5 ± 6.2
Female $n = 1$, 5 samples	-12.80 ± 0.5	81.83 ± 26.3	30.61 ± 7.6	28.191 ± 2.840	12.090 ± 1841	-9.8 ± 7
Males vs. female	NSD	NSD	NSD	NSD	NSD	NSD

Significant differences were observed between the calf and adults in the rate of decrease in the FSC signal after stimulation with A23187 ($p = 0.0003$***) (NSD: $p \geq 0.05$).

TABLE 3 Range of values for each PS exposure and PMP formation parameters in walruses under human care.

	SFSC	RPB	REB	ΔPB	ΔEB	SPE
Walruses $n = 3$, 12 samples	-11.6 ± 0.7 (min: −15; max: −7)	71.7 ± 17.5 (min: 13; max: 226)	39.7 ± 4 (min: 13; max: 67)	26.019 ± 3.171 (min: 11247; max: 41778)	$18{,}320.5 \pm 2.622$ (min: 9021; max: 37630)	14.6 ± 7.8 (min: −25; max: 51)

All the animals were adult females.

TABLE 4 Range of values for each PS exposure and PMP formation parameters in sea lions under human care.

	SFSC	RPB	REB	ΔPB	ΔEB	SPE
Sea lions $n = 4$, 4 samples	-18.7 ± 3 (min: −27; max: −14)	22 ± 8 (min: 5; max: 43)	30 ± 9 (min: 7; max: 46)	14.005 ± 1976(min:9664; max: 17883)	20.344 ± 3.980 (min: 15431; max: 32149)	31.75 ± 10 (min: 18; max: 62)

All the animals were adult males.

TABLE 5 Differences in PS exposure and PMP formation between species with ANOVA (NSD: $p \geq 0.05$).

	SFSC	RPB	REB	ΔPB	ΔEB	SPE
Dolphins vs. beluga whales	D > BW $p \leq 0.01$**	NSD	NSD	NSD	NSD	NSD
Dolphins vs. Walruses	D > W $p \leq 0.01$**	NSD	W > D $p \leq 0.01$**	NSD	NSD	NSD
Beluga whales vs. Walruses	NSD	NSD	NSD	NSD	NSD	NSD

** SFSC was significant different in dolphins than in beluga whales and walruses (**$p \leq 0.01$) and REB was significantly higher in walruses than in dolphins (**$p \leq 0.01$) (NSD: $p \geq 0.05$).

3.3 Application of PS exposure and PMP formation assessment to *in vitro* toxicology assays

The assay adapted in this work to measure platelet PS exposure and PMP formation has been successfully applied to *in vitro* toxicology studies. Specifically, aspirin had effects on both processes in dolphin platelets.

3.3.1 Acute exposure to aspirin

PMP formation rate after the stimulation with A23187 was significantly lower in the samples treated with aspirin than in controls. This is evident by measuring the speed at which the FSC signal decreases when passing from platelets to PMP. Specifically, the production of PMP was $50\% \pm 18.5$ slower in samples exposed to 0.02 µM than in controls ($p = 0.036$*) and $38\% \pm 0.06$ slower in samples exposed to 2 µM ($p = 0.0006$***) than in controls. At 200 µM, the speed was reduced by 40%, although not significantly, due to the high variability of the data.

PS exposure, given by changes in Annexin-V fluorescence, was not affected by acute aspirin exposure at any concentration, with no significant differences comparing to the control.

3.3.2 24 H exposure to aspirin

After 24 h of incubation, PS exposure rate after stimulation with A23187 decreased in the samples treated with the highest aspirin concentrations. Specifically, it decreased by $19.2 \pm 4.6\%$ at 2 µM ($p = 0.04$) and $34.5 \pm 8.5\%$ at 200 µM ($p = 0.02$). No significant

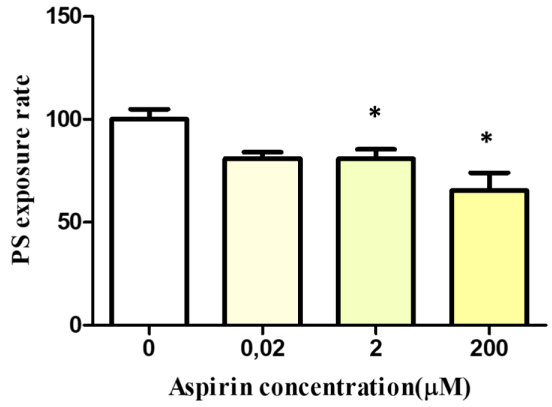

FIGURE 6
In vitro effect of aspirin on platelet PS exposure and PMP formation in whole blood platelets of Bottlenose dolphins after activation with calcium ionophore A23187. Dose–response of PS exposure rate in whole blood platelets after 24 h of incubation with aspirin.

differences were observed between the control and the sample treated with 0.02 μM (Figure 6).

However, PMP formation (given by FSC signal changes), was not affected by 24 h aspirin exposure at any concentration, with no significant differences comparing to the control.

4 Discussion

Platelet-derived microparticles (PMP) constitute a predominant type of microparticles in healthy animals, released during platelet activation, stress, or apoptosis (1–3). Physiologically, these particles are typically present in the range of 100–4,000 PMPs $\mu L^{-1}$of blood in humans depending intrinsic characteristics of the flow cytometer and the calibration strategy that has been used (4). Changes in PMP levels have been associated with various health conditions, including decompression sickness, thrombocytopenia, rheumatoid arthritis, cancer, arterial thrombosis, atherosclerosis, immune thrombocytopenic purpura, and malaria infection (1, 3, 6–10). On the one hand, elevated PMP levels are implicated in thrombus formation, while reduced levels are connected to bleeding tendencies observed in conditions like Castaman's defect or Scott's syndrome (3, 11).

Hence, monitoring blood PMP levels proves to be a valuable diagnostic and monitoring tool for various disorders. While some of these conditions are not extensively documented in marine mammals, this is likely due to limited available information rather than a lack of affliction. The challenges of accessing sea creatures may contribute to this data gap. Establishing a method for detecting PMP in the blood of dolphins, beluga whales, walruses, and sea lions can enhance the diagnostic tool for clinical assessments across multiple pathologies. In this work we have developed the methodology to measure in real time the exposure of PS in platelets and the formation of PMP by stimulating platelets with an agonist. Furthermore, we have carried out a pilot study to obtain normal values in these parameters in each species and enable the early detection of alterations in this process, related to different disorders, stress, pollution.

Although it is still an incipient field of study, PMP not only have been described as biomarkers of certain pathologies, but as triggers of others too (3), transporting growth factors, mRNA, microRNAs or surface receptors from platelets to other cells (37). PMP fuse with the target cell membrane and deposit the content (37), modulating multiple cell behaviors related to inflammation, immunomodulation, adaptative immunity, hemostasis, or tumor cell growth or metastasis (3). On this last case, PMP can be implicated in metastasis, but in the growth suppression of solid tumors too in mice and humans (38). They also play an important role in the course of diseases with endothelial injuries, such as some diabetic nephropaties (39) or atrial fibrillation (40), adhering to the subendothelium and stimulating the adhesion of other cells like platelets or leukocytes, leading to the formation of an atheroma and finally a local thrombus (3). In this context, PMP have been proposed as a possible therapeutic tool for the endothelium tissue repair (3). Despite this idea is already under investigation, the local application of these microparticles could be a new tool in the treatment of some vascular or brain injuries (40).

The study of PMP is expanding, revealing associations with various pathologies, and serving as enhancers, valuable biomarkers for diagnosis, and potentially even part of therapy. While much of the progress in understanding PMP is derived from research in humans and mice, this knowledge can be extrapolated to other mammalian species, including marine mammals. The initial step involves detecting PMP in their blood, utilizing established methodologies from human and mouse studies across all relevant species. In our work, we adapted this method for bottlenose dolphins, beluga whales, walruses, and sea lions. The selection of these species was intentional, given that marine mammals serve as sentinel species in marine ecosystem studies. Their considerable longevity and position at the apex of the food chain make them the ultimate recipients of numerous threats in the sea (13, 41). Using this assay in conservation studies we can also approach how different anthropogenic threats such as pollution, bycatch or maritime noise can affect the function of platelets and specifically the exposure of PS and formation of PMP.

Although the number of samples has not been too large, in this pilot study we show normal values of PS exposure and PMP formation in the different species under study, which can serve as a reference to detect alterations related to different pathologies or human impacts. From this information, we have also been able to observe that there are some differences in the behavior of platelets against A23187 between species, mainly the greater PS exposure of dolphin's platelets comparing to the rest of the species.

The application of this methodology and establishing normal values for each species is an important novelty in the study of the physiology of these species. There is only a prior study in MP detection on Steller sea lions, specifically in connection with decompression stress (13). In this study, total blood MP levels were evaluated, using beads of known size as reference. However, no previous study in marine mammals has evaluated cell type-specific MP levels, such as PMP, or their real time formation. On the other hand, Fahlman et al. did not elucidate a way to use PMP levels as a biomarker of decompression alterations.

The relevance of decompression sickness in wild marine mammals remains under discussion. Intense stress responses at depth may compromise their adaptive diving mechanisms,

potentially leading to gas embolism (26, 28). Developing a simple, non-invasive technique to assess PMP levels in marine mammals, similar to approaches used in humans (1), could significantly advance the diagnosis and understanding of decompression sickness in this taxonomic group. This advancement is crucial, especially since stranded animals often reach the coast in poor condition or deceased, and PMP detection could provide insights into their physiological status and the potential cause of stranding. Additionally, regularly assessing PMP levels in the blood during rehabilitation could offer a non-invasive means to gauge disease progression following a decompressive event. In humans, as the disease subsides, there is a concurrent decrease in PMP levels (1).

Definitely, this assay could be a diagnostic tool in processes with altered platelet function, using A23187, ADP or others as agonists. Our results show as have been explain in Results an average decrease of FSC intensity in the gated platelet population upon ionophore addition, accompanied of an increase in the continuum of lower CD41-PE/lower FSC events. These changes are compatible with a decrease in platelet size resulting from ionophore-triggered shedding of PMP from the platelet body (36). Platelets, upon activation, release components of their plasma membranes into the extracellular space, forming microparticles (MPs). It has been demonstrated that platelets release MP following activation with agonists such as collagen and/or thrombin, the Ca^{2+} ionophore A23187, or the complement protein C5b-9, which induces PMP formation. Therefore, our findings are consistent with previous findings regarding ionophore-induced platelet microparticle release, reinforcing the interpretation of our data in the context of research on microparticle release by activated platelets (36). The use of A23187 aids in technique development, producing abundant platelet-derived microparticles (PMP) for clearer observation. Moreover, our efforts extended beyond PMP detection, we have also adapted the methodology to study real-time platelet PS exposure and PMP formation. With this approach, functional studies across various realms, including diseases, functional toxicology, and other aspects related to the physiology and conservation of these species, can be pursued. This opens avenues to further investigate the involvement of these microparticles in different pathologies experienced by animals in their natural habitats or in aquarium settings, aiming to enhance their health, well-being and conservation. In fact, in this work we have demonstrated the usefulness of this assay in research studies, beyond its clinical application. The technique was applied to the evaluation of the effects of aspirin on PS exposure and PMP formation during platelet activation. Specifically, the effect of aspirin on PMP formation has been poorly studied previously. There are previous studies in which the inhibitory effect of aspirin on this process in humans has been documented, however in other studies no effects have been observed (42). Since aspirin blocks the binding of arachidonic acid to COX-1, inhibit its transformation into endoperoxides, which are subsequently transformed into prostaglandins and thromboxane (42). Thromboxane A2 promotes the release of calcium into the cytosol of platelets, with consequent change in shape, platelet aggregation, secretion of granules and release of PMP. So PMP formation is inhibited by aspirin.

As can be seen, the application of this assay can not only help us to diagnose and monitor pathologies in marine mammals but also opens a new field of study around the physiology of the PS exposure and PMP formation process and its alterations induced by contaminants, stress, anthropogenic threats, or diseases.

5 Conclusion

Our study on platelet functionality in marine mammals, represents a significant advancement in analytical techniques for this taxonomic group. The development and application for the first time of this novel diagnostic method, exploring PMP levels, phosphatidylserine exposure, and PMP formation in marine mammals, provide a valuable tool for diagnosing platelet disorders in these species. Our study introduces a non-invasive and gentle handling method, preserving optimal platelet function during analysis. This innovative investigation not only enhances diagnostic capabilities but also opens avenues for diverse research applications, benefiting both wild and aquarium-based marine mammals. The adaptation of these assays offers a versatile tool for various studies related to marine mammal health and well-being, addressing limitations in clinical capacities for this taxonomic group. Overall, our work lays the foundation for new diagnostic and therapeutic possibilities in marine mammal health, where clinical capabilities are often constrained.

Data availability statement

The original contributions presented in the study are included in the article/supplementary material, further inquiries can be directed to the corresponding authors.

Ethics statement

The animal study was approved by Animal Care and Welfare Committee of the Oceanogràfic. The study was conducted in accordance with the local legislation and institutional requirements.

Author contributions

MF-B: Writing – original draft, Writing – review & editing, Data curation, Formal analysis, Investigation, Methodology. MV: Writing – review & editing, Data curation. MM: Writing – review & editing, Conceptualization. BJ: Writing – review & editing, Methodology. DG-P: Conceptualization, Writing – review & editing, Data curation, Resources, Writing – original draft. CR-G: Writing – review & editing, Funding acquisition, Supervision, Validation, Writing – original draft. AM-R: Methodology, Writing – review & editing, Conceptualization, Formal analysis, Supervision, Validation. J-EO'C: Conceptualization, Writing – original draft, Writing – review & editing, Investigation, Methodology, Supervision.

Funding

The author(s) declare that financial support was received for the research, authorship, and/or publication of this article. This work was

supported by the Fundacion Oceanografic in Valencia, Spain, funding the project.

Acknowledgments

We acknowledge at Oceanográfic and Mundomar Aquarium staff, especially to veterinarians and marine mammal trainers for participating in this project and we acknowledge to Consellería d'Educació, Investigació, Cultura i Esport de la Generalitat Valenciana (Fondo Social Europeo), for awarding the fellowship to MF-B to carry out her PhD. J-EO'C is a member of the Spanish Network of Inflammatory Diseases (REI-RICORS: RD21/0002/0032), Institute of Health Carlos III, Madrid, Spain.

Conflict of interest

The authors declare that the research was conducted in the absence of any commercial or financial relationships that could be construed as a potential conflict of interest.

Publisher's note

References

1. Thom SR, Bennett M, Banham ND, Chin W, Blake DF, Rosen A, et al. Association of microparticles and neutrophil activation with decompression sickness. *J Appl Physiol*. (2015) 119:427–34. doi: 10.1152/japplphysiol.00380.2015

2. Zhang Y, Ma KL, Gong YX, Wang GH, Hu ZB, Liu L, et al. Platelet microparticles mediate glomerular endothelial injury in Early diabetic nephropathy. *J Am Soc Nephrol*. (2018) 29:2671–95. doi: 10.1681/ASN.2018040368

3. Burnouf T, Goubran HA, Chou ML, Devos D, Radosevic M. Platelet microparticles: detection and assessment of their paradoxical functional roles in disease and regenerative medicine. *Blood Rev*. (2014) 28:155–66. doi: 10.1016/j.blre.2014.04.002

4. Lacroix R, Robert S, Poncelet P, Kasthuri RS, Key NS, Dignat-George F. Standardization of platelet-derived microparticle enumeration by flow cytometry with calibrated beads: results of the international society on thrombosis and Haemostasis SSC collaborative workshop. *J Thromb Haemost*. (2010) 8:2571–4. doi: 10.1111/j.1538-7836.2010.04047.x

5. do Céu Monteiro M, Sansonetty F, Gonçalves MJ, O'Connor JE. Flow cytometric kinetic assay of calcium mobilization in whole blood platelets using Fluo-3 and CD41. *Cytometry*. (1999) 35:302–10. doi: 10.1002/(SICI)1097-0320(19990401)35:4<302::AID-CYTO2>3.3.CO;2-A

6. Rodríguez-Carrio J, Alperi-López M, López P, Alonso-Castro S, Carro-Esteban SR, Ballina-García FJ, et al. Altered profile of circulating microparticles in rheumatoid arthritis patients. *Clin Sci (Lond)*. (2015) 128:437–48. doi: 10.1042/CS20140675

7. Simak J, Gelderman MP. Cell membrane microparticles in blood and blood products: potentially pathogenic agents and diagnostic markers. *Transfus Med Rev*. (2006) 20:1–26. doi: 10.1016/j.tmrv.2005.08.001

8. Mezouar S, Mege D, Darbousset R, Farge D, Debourdeau P, Dignat-George F, et al. Involvement of platelet-derived microparticles in tumor progression and thrombosis. *Semin Oncol*. (2014) 41:346–58. doi: 10.1053/j.seminoncol.2014.04.010

9. Suades R, Padró T, Vilahur G, Badimon L. Circulating and platelet-derived microparticles in human blood enhance thrombosis on atherosclerotic plaques. *Thromb Haemost*. (2012) 108:1208–19. doi: 10.1160/TH12-07-0486

10. Tan KT, Lip GY. The potential role of platelet microparticles in atherosclerosis. *Thromb Haemost*. (2005) 94:488–92. doi: 10.1160/TH05-03-0201

11. Italiano JE Jr, Mairuhu AT, Flaumenhaft R. Clinical relevance of microparticles from platelets and megakaryocytes. *Curr Opin Hematol*. (2010) 17:578–84. doi: 10.1097/MOH.0b013e32833e77ee

12. Chen M, Hou L, Hu L, Tan C, Wang X, Bao P, et al. Platelet detection as a new liquid biopsy tool for human cancers. *Front Oncol*. (2022) 12:983724. doi: 10.3389/fonc.2022.983724

13. Fahlman A, Moore MJ, Trites AW, Rosen DA, Haulena M, Waller N, et al. Dive, food, and exercise effects on blood microparticles in Steller Sea lions (Eumetopias jubatus): exploring a biomarker for decompression sickness. *Am J Phys Regul Integr Comp Phys*. (2016) 310:R596–601. doi: 10.1152/ajpregu.00512.2015

14. Madden D, Thom SR, Milovanova TN, Yang M, Bhopale VM, Ljubkovic M, et al. Exercise before SCUBA diving ameliorates decompression-induced neutrophil activation. *Med Sci Sports Exerc*. (2014) 46:1928–35. doi: 10.1249/MSS.0000000000000319

15. Fernández A, Edwards JF, Rodríguez F, de los Monteros AE, Herráez P, Castro P, et al. "gas and fat embolic syndrome" involving a mass stranding of beaked whales (family Ziphiidae) exposed to anthropogenic sonar signals. *Vet Pathol*. (2005) 42:446–57. doi: 10.1354/vp.42-4-446

16. Fernández A, Sierra E, Díaz-Delgado J, Sacchini S, Sánchez-Paz Y, Suárez-Santana C, et al. Deadly acute decompression sickness in Risso's dolphins. *Sci Rep*. (2017) 7:13621. doi: 10.1038/s41598-017-14038-z

17. Noren SR, Williams TM. Body size and skeletal muscle myoglobin of cetaceans: adaptations for maximizing dive duration. *Comp Biochem Physiol A Mol Integr Physiol*. (2000) 126:181–91. doi: 10.1016/S1095-6433(00)00182-3

18. Demaster DP, Fowler CW, Perry SL, Richlen MF. Predation and competition: the impact of fisheries onmarine-mammal populations over the next one hundred years. *J Mammal*. (2001) 82:641–51. doi: 10.1644/1545-1542(2001)082<0641:PACTIO>2.0.CO;2

19. Díaz S, Settele J, Brondízio E, Ngo HT, Guèze M, Agard J, et al. Summary for policymakers of the global assessment report on biodiversity and ecosystem services of the intergovernmental science-policy platform on biodiversity and ecosystem services In: *Report of the plenary of the intergovernmental science-policy platform on biodiversity and ecosystem services on the work of its seventh session*. IPBES secretariat, Bonn, Germany (2019).

20. Read AJ, Drinker P, Northridge S. Bycatch of marine mammals in U.S. and global fisheries. *Conserv Biol*. (2005) 20:163–9. doi: 10.1111/j.1523-1739.2006.00338.x

21. Beverton RJH. Analysis of marine mammal–fisheries interactions In: JR Beddington, RJH Beverton and DM Lavigne, editors. *Marine mammals and fisheries*. London, United Kingdom: George Allen & Unwin (1985). 3–33.

22. Alverson DL, Freeburg MH, Murawski SA, Pope JG. A global assessment of fisheries bycatch and discards In: *Fisheries technical paper 339*. Rome: Food and Agriculture Organization (1994).

23. Reeves RR, Smith BD, Crespo E. Notarbartolo di Sciara D, cetacean specialist group. Dolphins, whales, and porpoises: 2003–2010 conservation action plan for the world's cetaceans In: *IUCN species survival commission*. Switzerland: Gland (2003).

24. Reeves RR, Berggren P, Crespo EA, Gales N, Northridge SP, Notarbartolo di Sciara D, et al. *Global priorities for reduction of cetacean bycatch*. WWF (World Wide Fund) (2020).

25. Dolman SJ, Brakes P. Sustainable fisheries management and the welfare of bycaught and entangled cetaceans. *Front Vet Sci*. (2018) 5:287. doi: 10.3389/fvets.2018.00287

26. Garcia Párraga D, Moore M, Fahlman A. Pulmonary ventilation-perfusion mismatch: a novel hypothesis for how diving vertebrates may avoid the bends. *Proc Biol Sci*. (2018) 285:20180482. doi: 10.1098/rspb.2018.0482

27. Moore MJ, Bogomolni AL, Dennison SE, Early G, Garner MM, Hayward BA, et al. Gas bubbles in seals, dolphins, and porpoises entangled and drowned at depth in gillnets. *Vet Pathol*. (2009) 46:536–47. doi: 10.1354/vp.08-VP-0065-M-FL

28. Wright AJ, Aguilar Soto N, Baldwin AL, Bateson M, Beale C, Clark C, et al. Anthropogenic noise as a stressor in animals: a multidisciplinary perspective. *Int J Comp Psychol*. (2007) 20:250–73. doi: 10.46867/IJCP.2007.20.02.02

29. Weilgart LS. A brief review of known effects of noise on marine mammals. *Int J Comp Psychol*. (2007) 20:159–68. doi: 10.46867/IJCP.2007.20.02.09

30. Jepson PD, Arbelo M, Deaville R, Patterson IAP, Castro P, Baker JR, et al. Gas-bubble lesions in stranded cetaceans. *Nature*. (2003) 425:575–6. doi: 10.1038/425575a

31. Tyack PL, Johnson M, Aguilar-Soto N, Sturlese A, Madsen PT. Extreme diving of beaked whales. *J Exp Biol*. (2006) 209:4238–53. doi: 10.1242/jeb.02505

32. Felipo-Benavent M, O'Connor JE, Álvaro-Álvarez T, Valls-Torres M, Rojo C, García-Párraga D, et al. Monitoring platelet function in marine mammals: intracellular Ca^{2+} mobilization as a biomarker of platelet activation. *Dev Comp Immunol*. (2024) 150:105080. doi: 10.1016/j.dci.2023.105080

33. Ponomareva AA, Nevzorova T, Mordakhanova ER, Andrianova IA, Rauova L, Litvinov RI, et al. Intracellular origin and ultrastructure of platelet-derived microparticles. *J Thromb Haemost*. (2017) 15:1655–67. doi: 10.1111/jth.13745

34. Wisgrill L, Lamm C, Hartmann J, Preißing F, Dragosits K, Bee A, et al. Peripheral blood microvesicles secretion is influenced by storage time, temperature, and anticoagulants. *Cytometry A*. (2016) 89:663–72. doi: 10.1002/cyto.a.22892

35. Brittain GC 4th, Chen YQ, Martinez E, Tang VA, Renner TM, Langlois MA, et al. A novel semiconductor-based flow cytometer with enhanced light-scatter sensitivity for the analysis of biological nanoparticles. *Sci Rep*. (2019) 9:16039. doi: 10.1038/s41598-019-52366-4

36. Barry OP, Fitz Gerald GA. Mechanisms of cellular activation by platelet microparticles. *Thromb Haemost*. (1999) 82:794–800. doi: 10.1055/s-0037-1615913

37. Freyssinet JM. Cellular microparticles: what are they bad or good for? *J Thromb Haemost*. (2003) 1:1655–62. doi: 10.1046/j.1538-7836.2003.00309.x

38. Michael JV, Wurtzel JGT, Mao GF, Rao AK, Kolpakov MA, Sabri A, et al. Platelet microparticles infiltrating solid tumors transfer mi RNAs that suppress tumor growth. *Blood*. (2017) 130:567–80. doi: 10.1182/blood-2016-11-751099

39. Wang GH, Ma KL, Zhang Y, Hu ZB, Liu L, Lu J, et al. Platelet microparticles contribute to aortic vascular endothelial injury in diabetes via the mTORC1 pathway. *Acta Pharmacol Sin*. (2019) 40:468–76. doi: 10.1038/s41401-018-0186-4

40. Lenart-Migdalska A, Drabik L, Kaźnica-Wiatr M, Tomkiewicz-Pająk L, Podolec P, Olszowska M. Flow cytometric assessment of endothelial and platelet microparticles in patients with atrial fibrillation treated with dabigatran. *Clin Appl Thromb Hemost*. (2020) 26:107602962097246. doi: 10.1177/1076029620972467

41. Martínez-López E, Peñalver J, Escriña A, Lara L, Gens MJ, María Dolores E, et al. Trace metals in striped dolphins (Stenella coeruleoalba) stranded along the Murcia coastline, Mediterranean Sea, during the period 2009-2015. *Chemosphere*. (2019) 229:580–8. doi: 10.1016/j.chemosphere.2019.04.214

42. Driver B, Marks DC, van der Wal DE. Not all (N) SAID and done: effects of nonsteroidal anti-inflammatory drugs and paracetamol intake on platelets. *Res Pract Thromb Haemost*. (2019) 4:36–45. doi: 10.1002/rth2.12283

frontiers | Frontiers in Veterinary Science

TYPE Review
PUBLISHED 23 May 2024
DOI 10.3389/fvets.2024.1385400

OPEN ACCESS

EDITED BY
Francisco Javier Salguero,
UK Health Security Agency (UKHSA),
United Kingdom

REVIEWED BY
Roberta Salaroli,
University of Bologna, Italy
Maria Carmela Scata',
Council for Agricultural and Economics Research (CREA), Italy

*CORRESPONDENCE
Sonja Härtle
✉ Sonja.Haertle@lmu.de
Lonneke Vervelde
✉ lonneke.vervelde@roslin.ed.ac.uk

†PRESENT ADDRESS
Lonneke Vervelde,
Royal GD Animal Health, Deventer, Netherlands

‡These authors have contributed equally to this work

RECEIVED 12 February 2024
ACCEPTED 02 May 2024
PUBLISHED 23 May 2024

CITATION
Härtle S, Sutton K, Vervelde L and Dalgaard TS (2024) Delineation of chicken immune markers in the era of omics and multicolor flow cytometry.
Front. Vet. Sci. 11:1385400.
doi: 10.3389/fvets.2024.1385400

Delineation of chicken immune markers in the era of omics and multicolor flow cytometry

Sonja Härtle[1]*, Kate Sutton[2], Lonneke Vervelde[2]*†‡ and Tina S. Dalgaard[3‡]

[1]Department of Veterinary Sciences, LMU Munich, Munich, Germany, [2]Division of Immunology, The Roslin Institute, Royal (Dick) School of Veterinary Studies, University of Edinburgh, Edinburgh, United Kingdom, [3]Department of Animal and Veterinary Sciences, Aarhus University, Tjele, Denmark

Multiparameter flow cytometry is a routine method in immunological studies incorporated in biomedical, veterinary, agricultural, and wildlife research and routinely used in veterinary clinical laboratories. Its use in the diagnostics of poultry diseases is still limited, but due to the continuous expansion of reagents and cost reductions, this may change in the near future. Although the structure and function of the avian immune system show commonalities with mammals, at the molecular level, there is often low homology across species. The cross-reactivity of mammalian immunological reagents is therefore low, but nevertheless, the list of reagents to study chicken immune cells is increasing. Recent improvement in multicolor antibody panels for chicken cells has resulted in more detailed analysis by flow cytometry and has allowed the discovery of novel leukocyte cell subpopulations. In this article, we present an overview of the reagents and guidance needed to perform multicolor flow cytometry using chicken samples and common pitfalls to avoid.

KEYWORDS

chicken, leukocytes, flow cytometry, lineages, phenotyping, single-cell biology

1 Introduction

Flow cytometry is a routine method in immunological studies incorporated in biomedical, veterinary, agricultural, and wildlife research and routinely used in veterinary clinical laboratories, albeit not for the diagnostics of poultry disease. The tremendous expansion in immunological reagents for livestock species, especially pigs and cattle, has in part been due to the availability of cross-reactive antibodies developed in the mouse and human field of immunology, as well as dedicated laboratories developing new antibodies (1–4). Although the structure and function of the avian immune system show commonalities with those of mammals, at the molecular level, there is often low sequence homology across species and low cross-reactivity of mammalian immunological reagents. Using commercially available reagents, recent improvement in multicolour antibody panels for chicken cells has resulted in more detailed analysis by flow cytometry and has allowed the discovery of novel leukocyte cell subpopulations (5–8).

Innovations in cytometry, including traditional flow, spectral flow, and mass cytometry, are driving its use for the isolation and analysis of cells for multi-omics research. Flow cytometry and cell sorting are commonly used tools to phenotype cell populations during, for example, infections and vaccine studies, whereas sorting specific cell subsets can be further analyzed using downstream transcriptomics, including bulk RNASeq (9, 10), single cell (sc)

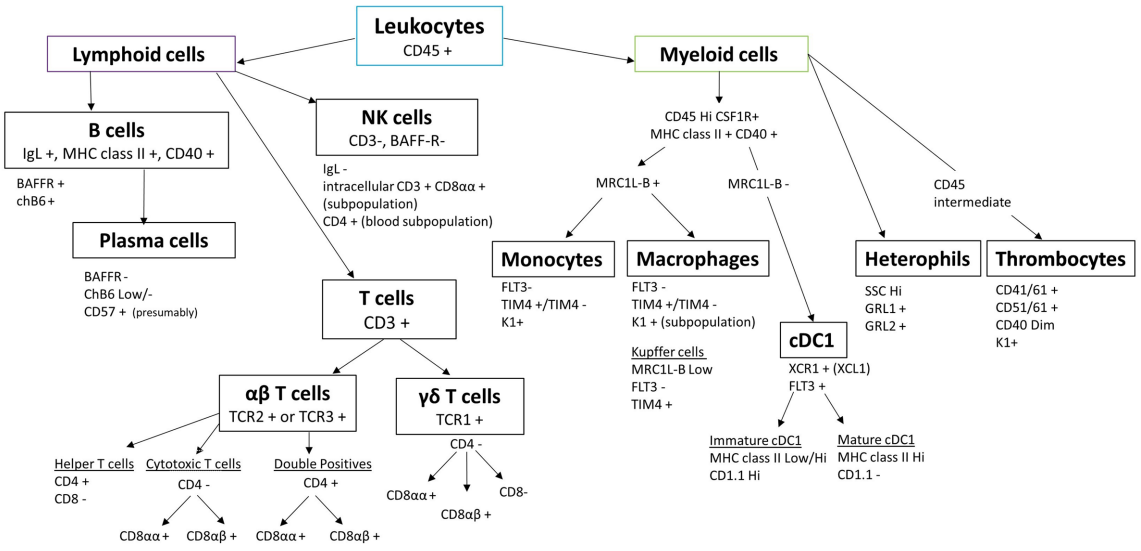

FIGURE 1
Chicken leukocyte cell lineages and their characteristic markers routinely used in flow cytometry.

(11–13), or single nucleus (sn) sequencing. High-resolution transcriptomics are instrumental to understand avian immunology and contributing to defining accurate biomarker signatures of diseases. Although not yet applied to avian immune cell flow cytometry and cell sorting, they can also be used for single-cell proteomics analysis (14, 15) and have been applied to analyse chicken sensory epithelium (16). The development of flow cytometry combined with omics technologies for avian research is rapidly enhancing and reviewed in Liu et al. (17). Validating scSeq data through flow cytometric analysis or immunohistology strengthens and verifies the data set, and thus a critical review of the single cell analysis should always be part of the quality control of sequence analysis (18). For example, recent studies (18, 19) demonstrated that due to little *de novo* mRNA production, especially avian CD4, is more difficult to detect in scSeq data, and results could be easily misinterpreted if not compared with flow cytometric CD4 staining.

The key to robust single-cell preparation is the quality of the cell sample. Sample quality is dependent on multiple steps, including the freshness of the tissue, the digestion step, either mechanical or enzymatic, and the time the preparation takes. These all affect cell viability, the amount of cell debris and aggregates, and the loss of certain cell subpopulations. The advantage of mechanical dissociation is that cell surface antigens are least affected compared to enzymatic dissociation; however, the breakdown of extracellular matrix is difficult for some tissues, such as the lung, intestine, liver, and brain, and isolation of rare cells is less likely. Different digestive enzymes, alone or in combination, can be used to break down extracellular matrix or cell–cell junction, but one method is rarely suitable for different tissues due to the large variation in cellular composition and extracellular matrix composition (17, 20). Whatever the choice of cell preparation, speed is of the essence, and awareness that changes are likely to occur should be taken into account when analysing the data. In addition, cell plasticity is widely accepted, but little is known with regard to chicken immune cells. Cells can change from one phenotype to another, for example, because the cell preparation or purification activates the cells, but also clear-cut delineation of cell subpopulations has proved challenging in livestock species (10, 21). Transgenic chickens represent a great potential to study immune cells in more detail, especially those for which few antibodies or known markers are available, increasing our capacity to distinguish different cell lineages (12, 22). In this article, we present an overview of the reagents and guidance needed to perform multicolour flow cytometry using chicken cells and common pitfalls to avoid. An overview of chicken leukocyte subsets and their delineation by flow cytometric markers is shown in Figure 1.

2 CD45—the pan leukocyte marker

The transmembrane glycoprotein CD45 is a tyrosin phosphatase that regulates a large variety of cellular functions. In mammals, it is expressed in all nucleated cells of haematopoietic origin (23). In chickens, CD45 is expressed on all leukocytes, including thrombocytes, but absent on nucleated cells of the erythroid lineage (24). The expression of CD45 on thrombocytes is significantly lower compared to other leukocytes. Depending on the cell isolation procedure, antibody, and staining protocol used, additional distinction between B cells and myeloid cells (medium expression) and T cells (high expression) can also be observed (see Figure 2) (7). Several anti-chicken CD45 mAbs are commercially available, such as LT40 (IgM), AV53 (IgG1), UM16-6 (IgG2a), and His C7 (IgG2a) (Table 1). Alternative splicing of mammalian CD45 leads to the expression of isoforms of different lengths, which are named according to the presence or absence of exons 4 (A), 5 (B), and 6 (C) (CD45RO, CD45RA, and CD45RB, respectively) (25). Expression of the isoforms varies between cell types and subsets and depends on the cellular differentiation and activation state (26, 27). For chicken CD45, expression of different isoforms caused by alternative splicing of exons 3, 5, and 7 was also demonstrated (28, 29). Whilst the above-mentioned chicken CD45 mAbs detect all isoforms, mAb 8B1 (IgM)

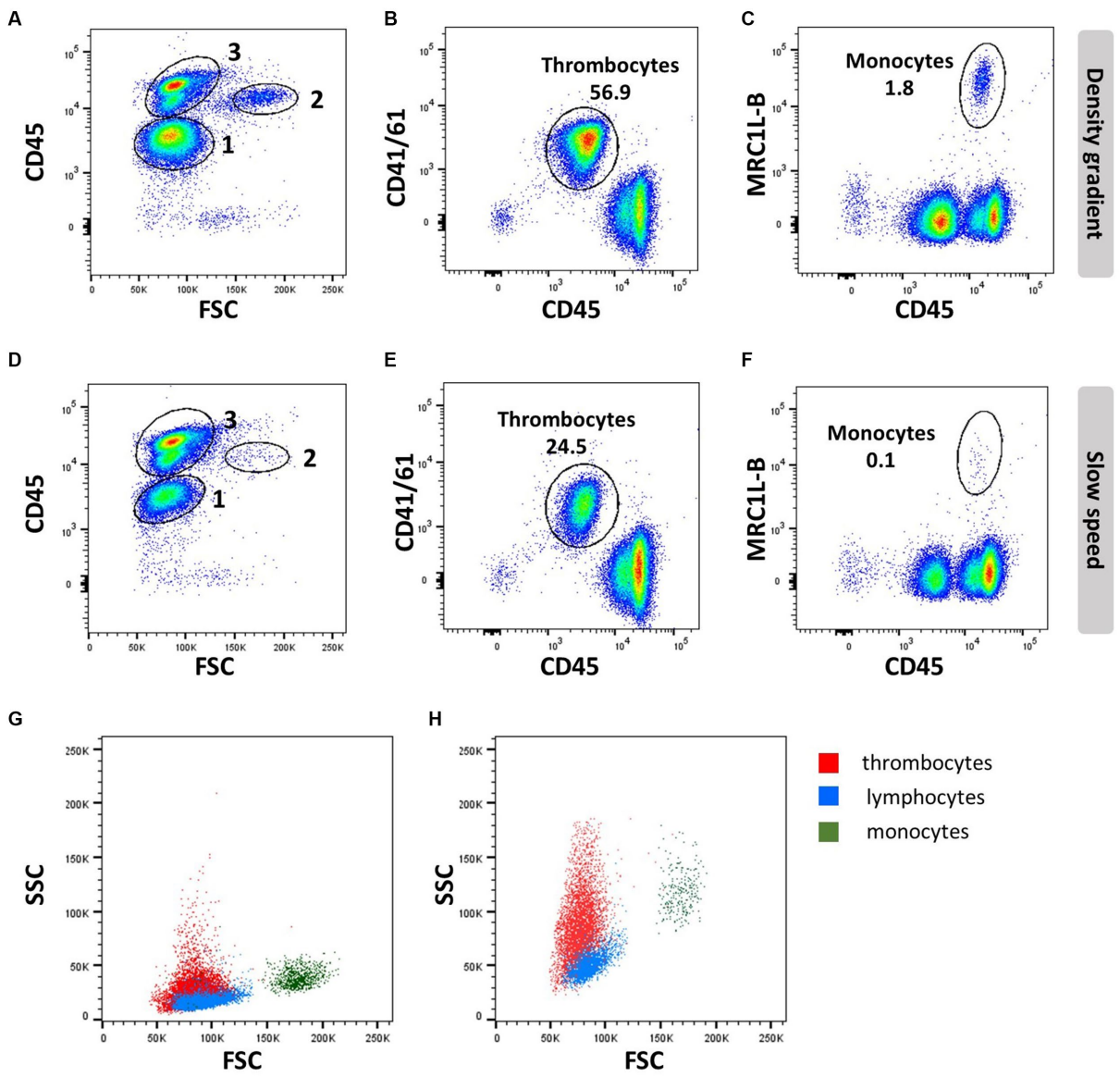

FIGURE 2
Thrombocyte characteristics: EDTA blood was processed by density gradient centrifugation **(A–C,G)** or slow speed centrifugation **(D–F,H)** and stained with anti-CD45 (16-6), followed by anti-mouse-IgG2a-FITC and anti-CD41/61 (11C3) and anti-IgG1-PE **(A,B,D,E,G,H)** or anti-MRC1L-B (clone KUL01, IgG1) and anti-IgG1-APC **(C,F–H)**. Numbers in scatter plots **(A,D)** represent 1 = thrombocytes, 2 = monocytes, and 3 = lymphocytes; FSC/SSC profile of thrombocytes (red), lymphocytes (blue), and monocytes (dark green) analyzed with common **(G)** or increased SSC voltage **(H)**.

recognises only two different short isoforms, which exhibit different expression patterns on B cells, αβ T cells, and γδ T cells (29). As activation of γδ T cells upregulated the expression of CD45 short isoforms, a varying expression system similar to that of mammals could exist in chickens, and the mAb 8B1 would be a helpful tool for its analysis. Antibody clones recognising CD45 and other relevant surface markers for leukocyte delineation are listed in Table 1.

3 Thrombocytes

Thrombocytes are the most common white blood cell population in the circulation of chickens, making up to ~80% of circulating peripheral blood mononuclear cells. In contrast to mammalian cells, avian thrombocytes are nucleated cells that display a variety of immunological functions, such as phagocytosis and tissue repair, and can release an array of bioactive proteins, including cytokines. The type of anticoagulants and isolation procedures affect the viability and number of thrombocytes; they can be isolated by PBL gradient centrifugation (Figures 2A–C), whilst slow spin or differential centrifugation (60–100× *g*) results in a major loss of thrombocytes (Figures 2D–F) (30, 31).

Differentiation of thrombocytes from lymphocytes based on morphology is difficult, although thrombocytes are slightly smaller with clear cytoplasm and more oval to spindle-shaped. Compared to erythrocytes, they are smaller and have a more rounded nucleus and an increased nucleus-to-cytoplasm ratio (32). These cellular properties present as low forward side scatter (FSC) similar to lymphocytes but

TABLE 1 Antibodies against surface markers, which are mentioned in the text.

Antigen	Clone	Isotype	Availability	Comments
Cath2	N/A	Rabbit polyclonal		
CD1.1	CB3	IgG1	Southern Biotech	
CD107a	5G10	IgG1	DSHB	
CD115 (CSF1R)	ROS-AV170	IgG1	Bio-Rad	
CD127 (IL7R)	8F10E11	IgM		Steric hindrance with CD4 when co-staining
CD15	W6D3	IgG1	BioLegend	
CD15s	CSLEX1	IgM	BD Biosciences	
CD184 (CXCR4)	9D9	IgG2a	Bio-Rad	
CD185 (CXCR5)	6A9	IgG1	S. Härtle LMU	
CD25 (IL2R-alpha)	20E5	IgG1	T. Göbel LMU	
	28–4	IgG3	T. Göbel LMU	
	AbD13504	HuCAL Fab	Southern Biotech	
	AV142	IgG1	Bio-Rad	
CD268 (BAFF-R)	2C4	IgG1	Bio-Rad	
CD28	AV7	IgG1	Southern Biotech	
CD3	CD3-12	IgG1	Thermo Fisher	
	CT-3	IgG1	Bio-Rad/Southern Biotech	
	AV36	IgG1	Immunological Toolbox	Does not bind to T cells from NARF C.B12 line
CD4	CT4	IgG1	Southern Biotech	
	EP96	IgM	Southern Biotech	
	2.35	IgG2b	Bio-Rad	
	AV29	IgG2b	RI Immunological Toolbox	
	AV30	IgG1	RI Immunological Toolbox	
CD40	IG8	IgG2a	Immunological Toolbox	
CD41/CD61	11C3	IgG1	Bio-Rad	
CD44	AV6	IgG1	Bio-Rad/Southern Biotech	
CD45	LT40	IgM	Southern Biotech	Lower discrimination between thrombocytes and lymphocytes compared to other clones
	UM16-6	IgG2a	v	
	AV53	IgG1	RI Immunological Toolbox	
	His C7	IgG2a	WUR NL	
CD45 (2 short isoforms)	8B1	IgM	T. Göbel LMU	
CD5	2–191	IgG1	Discontinued	
CD51/CD61	23C6	IgG1	Thermo Fisher/BD Biosciences/ BioLegend	
CD56	4B5	IgG1	T. Göbel LMU	
CD57	HNK-1	IgM	BioLegend	Crossreacting human antibody
CD80	AV82	IgG2a	Immunological Toolbox	
CD8α	11.39	IgG1	Bio-Rad	
	3–298	IgG2b	Southern Biotech	Superior clone recognising the majority of CD8α variants
	CT-8	IgG1	Southern Biotech	
	AV12	IgG1	Immunological Toolbox	
	AV13	IgG1	Immunological Toolbox	
	AV14	IgG2b	Immunological Toolbox	
	EP72	IgG2b	Southern Biotech	

(Continued)

TABLE 1 (Continued)

Antigen	Clone	Isotype	Availability	Comments
CD8β	EP42	IgG2a	Southern Biotech	
chB6/Bu-1	AV20	IgG1	Bio-Rad	B cells but also some IELs, subpopulation of MCR1L-B macrophages
chB6a/Bu-1a	21-1A4	IgG1	Thermo Fisher	
	L22	IgG1	Bio-Rad	
chB6b/Bu-1b	5-11G2	IgG1	Thermo Fisher	
	15H6	IgG1	Southern Biotech	
ChL12/OV	11A9	IgM	S. Härtle LMU	
CLEC-2	8G8	IgG2a	T. Göbel LMU	
FcY/CHIR-AB1	8D12	IgG2b	T. Göbel LMU	
FLT3	ROS-AV184	IgG1	RI Immunological Toolbox	High on dendritic cells and low on subpopulation of MRC1LB+ macrophages
GRL1	I-A5	IgG3	DSHB	
GRL2		IgG1	DSHB	
Ig Light chain	2G1	IgG1	Bio-Rad	
	L1	IgG1	VWR/GeneTex	
IgA	A1	IgG2b	Southern Biotech	
IgM	M1	IgG2b	Southern Biotech	
IgY	4D12	IgG1	Bio-Rad	Optimal use for ELISA/immunohistology not suitable for flow
	G1	IgG1	Southern Biotech	Detects membrane and soluble IgY
MHC I	F21-2	IgG1	Southern Biotech	
MHC I (beta 2 microglobulin)	F21-21	IgG1	Southern Biotech	
MHC II	2G11	IgG1	Southern Biotech	
	TAP1	IgG2a	DSHB	
MRC1L-B	KUL01	IgG1	Southern Biotech	
Putative CD11c	8F2	IgG1	S. Härtle LMU	
SLAMF4	8C7	IgG1	T. Göbel LMU	
TCR αβ1 (Vβ1)	TCR2	IgG1	Southern Biotech	
TCR αβ2 (Vβ2)	TCR3	IgG1	Southern Biotech	
TCRγδ	TCR1	IgG1	Southern Biotech	
TIM4	JH9	IgG1	RI Immunological TOOLBOX	
TREM-A1	14C9	IgM	T. Göbel LMU	
TREM-B1	7E8	IgG1	T. Göbel LMU	
	1E9	IgG2a	T. Göbel LMU	
Unknown	K1	IgG2a	B. Kaspers/S. Härtle LMU	

a higher side scatter (SSC) than lymphocytes, whereas monocytes have a higher FSC and SSC compared to lymphocytes (Figures 2A,D,G,H).

Avian thrombocyte surface markers have been identified and facilitate experimentation using flow cytometry mAbs specific for alpha IIb beta 3 integrin (GpIIb/IIIa complex or CD41/CD61; clone 11C3), and CD45 will distinguish thrombocytes from leukocytes based on their $CD45^{Low}$ $CD41/CD61^{+}$ phenotype (Figures 2B,E). However, CD41/61 is not exclusive for thrombocytes (33). Chicken TREM-B1 (mAb clones 7E8 and 1E9), an inhibitory receptor, is exclusively expressed in thrombocytes. The C-type lectin receptor CLEC-2 (mAb clone 8G8) (34) can be used in combination with CD8α and K1. The molecule that is recognized by mAb K1 has not been identified, but it is expressed in thrombocytes, macrophages, and monocytes. The thrombocytes can be distinguished based on size, smaller than the macrophages and monocytes, if a single cell gate is applied. In addition, thrombocytes express a CD51/CD61 integrin on their surface as

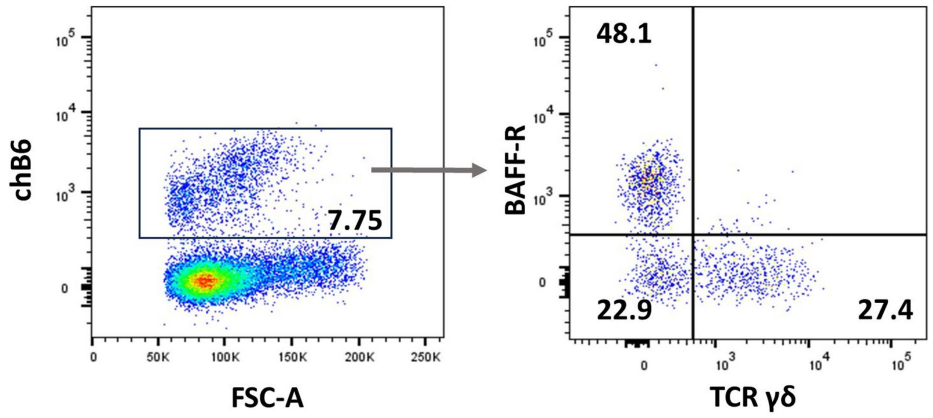

FIGURE 3
chB6 expression on non-B cells: an IEL preparation was stained with antibodies against chB6 (AV20), TCRγδ (TCR1), and BAFF-R (2C4). Cells were gated for viable, single leukocytes. Gating on chB6$^+$ cells **(A)** reveals that chB6$^+$ cells consist of three subsets: BAFF-R$^+$/TCRγδ$^-$ B cells, BAFF-R$^-$/TCRγδ$^+$ γδ T cells, and so far, uncharacterised BAFF-R$^-$/TCRγδ$^-$ cells **(B)**.

well as a signaling lymphocyte activation molecule (SLAM)F4 (35), TREM-A1 (33), CD40 (36) and MHC I (37). However, these markers have to be used in a multicolour panel to distinguish the thrombocytes from leukocytes, and in addition, a marker such as SLAMF4 is only expressed in a subpopulation of thrombocytes (35). Although it has been reported that thrombocytes express MHC II mRNA (38), accurate demonstration of MHC II surface expression is lacking so far.

4 Polymorphonuclear cells

Chickens have limited numbers of eosinophils and mast cells, and the dominant polymorphonuclear cell type is the heterophil. To the best of our knowledge, no specific flow cytometry-applicable surface markers for granulocyte subsets are available in chickens. Heterophils have been reported to lack myeloperoxidase activity; however, older literature (39) and immunocytochemical staining (40) suggest there is peroxidase activity that in the future may be detected by cross-reactive antibodies. The mAbs, anti-GRL1 and anti-GRL2, stain the granules of chicken granulocytes and thrombocytes, in addition to the surface expression of these proteins due to exocytosis (41). Increased expression can therefore be detected after permeabilisation of the cells, staining both surface and intracellular GRL1 and GRL2. Surface expression of GRL2 can also be found on activated T cells (18). Heterophils also express antimicrobial peptides, including the cathelicidin CATH-2, which can be stained with a rabbit polyclonal serum (40), which in principle could be used for intracellular staining and flow cytometry. The most applicable method to detect heterophils is through a high SSC pattern and the lack of expression of B-cell, T-cell, thrombocyte, and macrophage markers in the CD45$^+$ population. The high SSC is a consistent feature of heterophils, but the FSC pattern has been shown to be dependent on the flow cytometry equipment and the software used to analyse the data (7, 42).

Eosinophils are found in peripheral blood based on the staining of eosinophilic granules in their cytoplasm. However, chickens lack IgE isotypes and components of allergic reactions, which make it questionable if these eosinophils are functionally comparable to mammalian eosinophils. Whilst heterophils have a high SSC and low FSC pattern, eosinophils have a low SSC and higher FSC pattern (7), but a lack of specific markers hampers quantitative analysis by flow cytometry. Eosinophils have been reported to also have endogenous peroxidase activity (43), but the use of peroxidase activity in flow cytometry for chicken cells has not been demonstrated. Like eosinophils, detecting mast cells by flow cytometry is problematic due to a lack of markers. Cells containing Alcian Blue-positive granules in the lamina propria of the intestinal tract have been described (44) but the flow cytometric analysis of granulocyte subsets remains limited.

5 Natural killer cells

Natural killer (NK) cells display many different inhibitory and activating receptors that mediate a variety of functions, from the classical role of killing pathogen-infected cells to regulatory functions influencing adaptive immunity through interactions with dendritic cells (DCs) and secretion of cytokines. Chicken NK cells have been described in the embryonic spleen before the T cells enter the periphery. These cells are CD45$^+$ and lack T-cell or B-cell-specific markers on the cell surface, i.e., surface CD3$^-$, BAFF-R$^-$, and Ig Light chain$^-$, but CD3 is detected intracellularly (45). The number of NK cells in peripheral blood is low, whereas more substantial numbers can be found in tissues. Two inconsistencies in the avian NK cell literature should be highlighted before describing the recent flow cytometric data. Firstly, the mAb clone 28–4 has been used to detect chicken NK cells in the intestinal epithelium for many years, until more recently, it was shown to detect IL2Rα (CD25) (46). Therefore, although very useful in a multicolour panel, the antibody is not specific for NK cells. Secondly, chB6 has been used as a B-cell marker for decades (47). However, it is also expressed on intraepithelial leukocytes in the intestine that are CD45$^+$ CD3$^-$ Ig Light chain$^-$ and lack markers expressed on mononuclear phagocytes (Figure 3) (44).

Many antibodies have been tested to identify chicken NK cells, but none were shown to be uniquely expressed by NK cells, as these also detect subpopulations of T cells, thrombocytes, or myeloid cells (48–51). Alternatively, they only detect a subpopulation of NK cells

[reviewed in Straub et al. (52)]. Expression of receptors also varies between tissues and subpopulations of NK cells in the lung, liver, and intestinal epithelium (52). These include antibodies specific for CD56 (49) and CHIR-AB1 (53), a high-affinity IgY Fc receptor. Nonetheless, they are useful for flow cytometry in multicolour panels in combination with the lack of surface CD3, BAFF-R, or Ig Light chain staining (48). Chicken NK cells that are CD3$^-$ Ig Light chain$^-$ can express CD8αα, but the expression level alters upon activation, and expression on NK cells in peripheral blood may vary. A NK cell-like population in peripheral blood was detected, which expressed low levels of CD4, CD5, and CD11c and high levels of CHIR-AB1, CD56, and 28–4 but lacked CD3, CD8α, and chB6 (54).

To measure NK cell function, a flow cytometry-based degranulation assay can be applied that is based on the expression of CD107a (LAMP-1 or LEP100) (48). Cytotoxic activity via the perforin-granzyme pathway occurs in pre-formed lytic granules surrounded by lipid bilayers containing LAMPs that are fused with the plasma membrane. A chicken homolog of LAMP-1 (CD107a) exists (also known as LEP100), and a mAb antibody (5G10) is available, which was first used to assess the degranulation of chicken NK cells (48) and then applied to study CTLs (55). To distinguish between NK cells and CTLs, this staining must be combined with additional mAbs to exclude degranulation of cytotoxic T cells (55) and heterophils (48). More recently, flow cytometric-based staining of the release of perforin and granzyme A was developed to measure NK cell activation in ED14 embryonic splenocytes (56), but like CD107a expression, both perforin and granzyme A are not restricted to NK cells, and multicolour analysis is warranted to exclude CTLs. The lack of exclusivity is also demonstrated by perforin and granzyme A expression in the macrophage cell line HD-11 and low levels of perforin expression in the B-cell line DT-40 (56), which is in agreement with expression in human macrophages and granzyme B secretion by human B cells.

6 Mononuclear phagocytic cells

Similar to mammals, the cells of the chicken mononuclear phagocytic system (MPS) consist of monocytes, macrophages, and dendritic cells (DC). Studies into the biology of these cells using flow cytometry have focused on cells of the blood, spleen, and occasionally the liver and lung. In the blood, monocytes can be detected using the antibody KUL01, which recognises the mannose receptor C-type 1 Like B (MRC1L-B (57)). In whole blood cell preparation, monocytes are characterized by their high FSC and low SSC compared to lymphoid cells (7). MRC1L-B$^+$ monocytes also express CSF1R and MHC class II (22, 58).

TIM4 binds phosphatidylserine, a lipid normally found on the inner surface of the plasma membrane that is rapidly redistributed to the outer cell surface during apoptosis (59). Like humans, chickens express short and long isoforms of TIM4. Hu et al. generated two monoclonal antibodies against chicken TIM4. Clone JH9 was raised against the extracellular domain of TIM4 and recognises all TIM4 isoforms, whilst clone IE12 was raised against the additional linker found in some of the TIM4 long isoforms. This clone only recognises one of the long TIM4 gene products (available through the Roslin Institute, Immunological Toolbox). Currently, there is no known functional difference between the chicken TIM4 isoforms, but differential expression at the mRNA level appears to be specific to chicken lines (60). Staining chicken leukocytes with the TIM4 mAb JH9 does not provide a distinct staining pattern in flow cytometry, and it is therefore challenging to distinguish clear boundaries between TIM4$^+$ and TIM4$^-$ populations without correct unstained and FMO controls. However, in combination with MRC1L-B, the antibody has been useful in the identification of subpopulations of cells in chickens.

In chickens, the presence of monocyte subsets described in mammals, such as the classical CD14^{++} CD16$^-$ (mouse equivalent LyC6^{++} CD43$^+$), the non-classical CD14^{++} CD16^{++} (LyC6$^+$ CD43^{++}), and intermediate CD14^{++} CD16$^+$ (LyC6^{++} CD43^{++}) monocytes (61), cannot be clearly defined due to a lack of antibodies against these markers. Unlike mammalian CD14, chicken CD14 is a GPI-anchored protein rather than a transmembrane protein (62). To date, no specific staining has been demonstrated for the mAb anti-chicken CD14. However, chicken monocytes can be segregated based on their expression of TIM4. MRCL1-B$^+$ TIM4$^+$ and MRCL1-B$^+$ TIM4$^-$-cell populations both express transcripts for genes involved in murine monocyte–macrophage differentiation, indicating these cells are part of a differentiation series rather than distinct subsets (63). For *in vitro* characterization of monocytes, cells can be enriched by their adherence to glass or plastic tissue culture plates. Studies have shown that monocytes can adhere to glass after 1 h of culture. However, nucleated thrombocytes attach to these surfaces within 30 min but these cells die within 48–72 h; therefore, monocytes cultured for shorter periods of time will be contaminated with thrombocytes (64).

6.1 Macrophages

Chicken macrophages can be universally studied in tissues by flow cytometry using the MRC1L-B antibody (9, 10, 60, 65, 66). Tissue-resident macrophages exhibit diverse functionality and can be defined based on their location in the organ. For example, in the chicken spleen, several macrophage subpopulations exist. These include periarteriolar lymphoid sheaths, resident macrophages, ellipsoid-associated macrophages, and red-pulp macrophages. The ability to segregate different macrophage subsets is difficult as specific markers for each population have yet to be identified. Splenic MRC1L-B$^+$ macrophages universally express MHC class II, CD40, and CD80 and lack FLT3 expression (10, 67). Although mAbs against chicken CD83 and CD86 have been described, no convincing staining of mononuclear phagocytes has been demonstrated. In the liver, MRC1L-B$^+$ macrophages can be segregated into MRC1L-B^{Low} TIM4^{Hi} cells and MRC1L-B^{Hi} TIM4^{Low} and MRC1L-B^{Hi} TIM4$^-$ cells. Transcriptome analysis indicates that MRC1L-B^{Low} TIM4^{Hi} represent Kupffer cells, which are highly phagocytic compared to the MRC1L-B^{Hi} liver-resident macrophages (63). The TIM4 mAb JH9 stains a small population of CD3$^+$ and Bu1$^+$ cells in the liver and bursa, respectively (63).

Functional assays involving the assessment of phagocytosis can be integrated into flow cytometry experiments. Using commercially available fluorescent beads, which can be labeled with antigens such as LPS or inactive avian influenza virus, pH-sensitive pHrodo-labeled bioparticles, such as *Salmonella* or *E. coli*, or CFSE-labeled dead cells, can be utilized to determine the efficiency and specificity of chicken macrophage phagocytosis or effectorcytosis (10, 68–70). Performing phagocytosis assays at 4°C, a temperature commonly referred to as "on

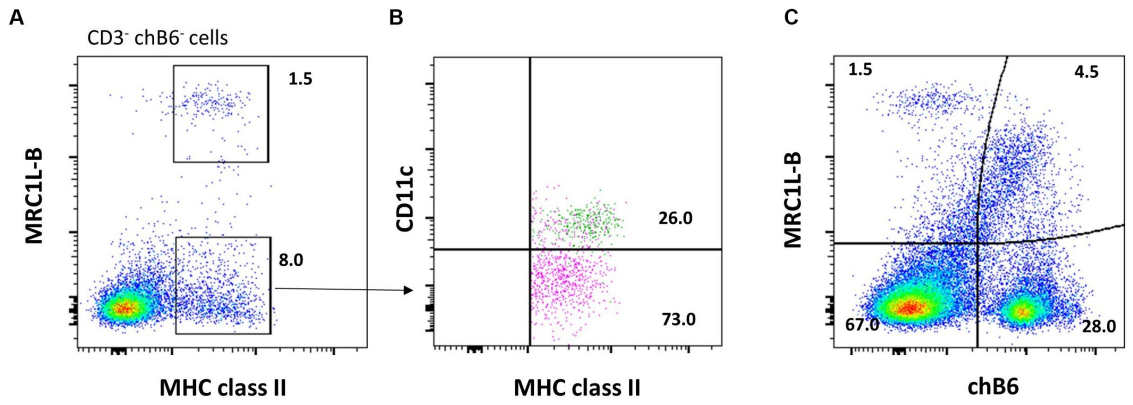

FIGURE 4
Enriching for splenic cDC1 cells without the FLT3 antibody. Splenocytes were stained for CD3 (CT3), chB6 (AV20), MRC1L-B (KUL01), MHC class II (Tap1), and putative CD11c (8F2). **(A)** Cells gated for live, single CD3⁻/chB6⁻ leukocytes, the CD3⁻ chB6⁻ cell population can be analyzed according to MHC class II and MRC1L-B expression. **(B)** Amongst the CD3⁻ chB6⁻ MRC1L-B⁻ MHC class II⁺ cells, CD11c ⁺ cDCs (green) can be addressed. **(C)** ChB6 (AV20) antibody stains MRC1L-B⁺ macrophages in the spleen.

ice," should be used to assess specific binding or adhesion of particles to cell surfaces without allowing active internalization (phagocytosis) to occur. This approach helps researchers differentiate between particles that are merely attached to the cell membrane and those that have been engulfed by the cell. It should be noted that 4°C control may not always be optimal for *in vitro* model antigen uptake studies. For example, 4°C control does not prevent bone marrow-derived macrophages from phagocytosing pH-sensitive pHrodo-labeled bioparticles. Instead, an actin polymerization inhibitor, cytochalasin D, inhibited the uptake of these bioparticles (70). The differential expression of surface markers, such as CD40 and MHC class II, can be an indicator of cell activation. In chickens, LPS-treated bone marrow-derived macrophages upregulate CD40 expression and downregulate MHC class II expression (71). In the chicken lung, MRC1L-B⁺ that phagocytosed LPS- or avian influenza-coated beads had significantly higher CD40 expression compared to cells that had taken up uncoated beads. The same study also demonstrated an increase in MHC class II expression by cells that phagocytosed LPS-coated beads (72). This observation is still to be determined for other tissue-resident macrophages, and more research is required to understand how infection alters the expression of these markers in a tissue-specific manner.

It has been well known that a small population of chicken splenic macrophages stain for chicken B-cell marker chB6 (Figure 4C) (47). Therefore, the BAFF-R mAb is a more specific reagent for chicken B cells (73). Of note, MRC1L-B may be sensitive to enzymatic digestion. To assess the impact of isolation techniques on MRC1L-B expression, researchers should examine immunohistology sections of their tissue samples to visualize the level/abundance of cells expressing the marker. Specifically, comparing the effects of non-enzymatic approaches to enzymatic methods can provide insights into how different isolation techniques influence MRC1L-B expression.

6.2 Dendritic cells

Generally, in mammals, DCs are defined by their expression levels of MHC class II, CD11c, and co-stimulatory molecules CD40 and CD86 (74). Using this general phenotype, researchers have sought to phenotype chicken DCs in this manner by flow cytometry. Vu Mahn et al. found that MHC class II⁺ putative CD11c⁺ MRC1L-B⁻ splenocytes express gene transcripts associated with mammalian cDC1 cells (75). The antibody against DEC-205, a marker for murine DC, was generated for chickens. Although useful in immunohistology, this antibody does not provide a strong staining pattern in flow cytometry (76). Recently, reagents against chicken FLT3, XCR1, and CSFR2 were developed, which aid to study chicken cDC without dependence on transgenic chickens (67). The anti-chicken FLT3 monoclonal, designated ROS-AV184, was found to label two cell populations in the spleen, FLT3^{Hi} and FLT3^{Low} cells. The FLT3^{Hi} cells, known as cDC1 cells, lack expression of the macrophage marker, MRC1L-B, and exhibit slightly lower levels of CD45 and MHC class II expression compared to the FLT3^{Low} cells. The FLT3^{Low} cells express MRC1L-B, making them macrophages. If receptor–ligand interaction is of high affinity, this offers an opportunity to analyse protein expression on cells through flow cytometry with fluorochrome-labeled ligands instead of antibodies. Recently, Wu et al. demonstrated that chicken XCL1-AF647 binds to XCR1 on FLT3⁺ cDC1 cells. In addition, to detect CSF2R expression, a CSF2-AF647 protein was generated and found not to stain chicken cDC1 cells (67). Together, this demonstrates that chicken cDC1 cells can be distinguished by staining for FLT3 or XCR1. However, if researchers do not have mAb FLT3, DC can be enriched by including MRC1L-B, CD3, and chB6 or BAFF-R staining with MCH class II to remove T and B cells and macrophages from MHC class II⁺ cell population (Figures 4A,B).

The maturation status of chicken cDC1 can be defined by their expression of CD1.1 using mAb CB3 clone (77). In the blood, a majority of XCR1⁺ cDC1 are MHC class II^{Low} and CD1.1^{Hi}, whereas small subpopulations have the MHC class II^{Hi} CD1.1^{Hi} or MHC class II^{Hi} CD1.1⁻ phenotype. In the spleen, these subpopulations are present from 1 week of hatch, with the MHC class II^{Hi} and CD1.1⁻ cells becoming the most abundant by 2-week post-hatch. It is hypothesized that the splenic XCR1⁺ MHC class II^{Hi} CD1.1^{Hi} cDC1 is derived from the blood XCR1⁺ MHC class II^{Hi} CD1.1^{Hi} cDC1 pool that lose CD1.1 expression as they mature and develop in the spleen (12).

7 B cells

Chickens use the bursa Fabricii, a gut-associated lymphoid tissue (GALT), to expand B-cell precursors and diversify the BCR repertoire. This unique primary B-cell organ is the most striking difference to B-cell development in most mammals and causes the classification of avian B-cell development into a pre-bursal, bursal, and post-bursal phase, resulting in the discrimination of pre-bursal, bursal, and post-bursal B cells (78).

7.1 Pre-bursal B cells

The earliest B-cell-specific surface marker expressed on pre-bursal B cells is Bu1/chB6, with the first chB6$^+$ cells becoming detectable simultaneously around embryonic day (ED) 10 in the embryonic bursa and spleen (79). As chB6 is strongly expressed at all stages of B-cell development except in differentiated plasma cells (47), it has become the most used marker for chicken B cells. The protein is a typical type I transmembrane protein with a highly glycosylated extracellular region and no recognizable similarity to known mammalian molecules. chB6 is recognized by several commercially available mAbs like AV20 and BoA1 (a cross-reactive guinea fowl antibody). It is an alloantigen with two alleles, Bu1a/chB6a and Bu1b/chB6b, which are recognized by anti-chB6a (clone L22) and anti-chB6b (clone 11G2) (80, 81). If using the allotype-specific antibodies to address all B cells, it is important to determine the presence of the alleles in the chicken line; otherwise, only a fraction of B cells might be stained.

Shortly after chB6 expression becomes detectable, pre-bursal B cells begin to express another pan-B-cell marker, the BAFF receptor (BAFF-R), recognized by mAb anti-BAFF-R clone 2C4 (73) and at ED14, chB6+ cells in the spleen are all BAFF-R+ (82).

Whilst most cells before their migration to the bursa are Ig-negative, very few pre-bursal cells have completed a productive BCR rearrangement and express surface Ig, detectable with anti-Ig Light chain or anti-IgM staining (82, 83). All pre-bursal B cells in the spleen express relatively high levels of CXCR4 and CXCR5 (82, 84); hence, migration of pre-bursal B cells can be mediated by their attraction toward CXCL12 and CXCL13L1-L3, respectively. Potentially also connected to their migratory behavior, pre-bursal B cells express sialyl-Lewis-X/CD15s but not Lewis-X/CD15 (85, 86). CD15s is a tetrasaccharide carbohydrate that is usually attached to O-glycans on the surface of cells and can mediate the interaction with selectins as the first step of leukocyte emigration from blood vessels. The chicken molecules can be detected with cross-reacting mAbs for the human molecules, e.g., mouse anti-human CD15s clone CSLEX1 and mouse anti-human CD15 clone W6D3 (85, 86).

7.2 Bursal B cells

Between ED9 and ED12, a small number of pre-bursal stem cells migrate to the bursa anlage and colonize the lymphoid follicles, where they start to strongly proliferate and diversify their BCR by gene conversion. From ED14 to 18, bursal B cells show a homogeneous expression of chB6, BAFF-R, MHC class II, CD40, CXCR4, and CXCR5 (36, 82, 84, 87, 88) and the initially small percentage of surface IgM-positive cells increases up to 50%. During their differentiation in the bursa, B cells lose CD15s expression and become CD15-positive (85, 86). Around hatch, the first B cells emigrate from the bursa into the periphery. The small fraction (*ca.* 5%) of emigrating cells amongst bursal B cells can be addressed as Ig Light chain$^+$, MHC class II$^+$, chL12$^+$, and CXCR4^{Low} cells (see Figure 5A) (82, 89). ChL12, or the OV antigen, is recognized by mAb 11A9. The nature of the antigen is not known, but it should always be considered that it is an alloantigen, which is not recognised by 11A9 in every chicken line (90).

7.3 Peripheral B cells

Post-emigration from the bursa, the immature B cells seed B-cell areas in secondary lymphoid organs, such as the peri-ellipsoidal white pulp in the spleen or the B-cell areas in caecal tonsils. Due to the special structure of the avian spleen, there is no histological discrimination between marginal zone and follicular B cells (91) and, to date, no markers have been described that would assign splenic B-cell subpopulations. All chicken B cells are CD5$^+$ (92) hence, CD5-based discrimination of chicken B1 and B2 cells performed in mice and with reservations in humans is not possible. Splenic B cells are quite homogeneously BAFF-R$^+$, Ig Light chain$^+$, MHC class II$^+$, and CD40$^+$ (36, 83, 93). Frequently, chB6 expression is not completely homogenous; instead, especially in the spleen, a small immunoglobulin Light chain$^+$ fraction expressing higher amounts of chB6 and a higher FSC can be observed (Figures 5B,C) (84). The BCR on the vast majority of cells (>95%) is an IgM isotype, with very few cells expressing a class-switched BCR of IgY or IgA isotype (Figure 5B). Noteworthy, not all commercially available anti-chicken IgY antibodies stain both soluble and membrane-bound IgY. Whilst clone 4D12 works optimally for ELISA and immunohistology, it does not stain membrane-bound IgY. However, anti-chicken IgY clone G1 stains both IgY variants (see Figures 5D,E) (94).

7.4 Germinal centre B cells

In the spleen and similarly in all larger secondary and tertiary lymphoid accumulations, encapsulated germinal centres (GCs) can be identified, consisting predominantly of GC B cells. It is important to be aware that in regular spleen preparations (mincing through a strainer), GCs and hence GC B cells will not be present. The GCs strongly stick to the residual artery tree and do not pass through the sieve without further measures. Imamura and colleagues have shown that chB6$^+$ GC B cells can be obtained when the splenic artery tree with adjacent GCs is freed of the red pulp and separately digested with collagenase (95). Large GCs with a comparatively thinner capsule, which are not attached to an artery, are found in the caecal tonsils (96) hence, caecal tonsil preparations potentially contain GC B cells. To date, no markers are available to address these cells specifically. However, next to a high expression of chB6, immunohistochemistry of GCs revealed a weak positivity for CD57 (using the cross-reactive anti-human CD57 clone HNK-1) (97). In addition, HNK-1 works in flow cytometry, and as PWP B cells are chB6$^+$ CD57$^-$, it could serve as a marker to identify GC B cells in cell suspensions. Indeed, despite the lack of dead cells and doublet exclusion, older flow cytometric analysis of caecal tonsil cell suspensions found a

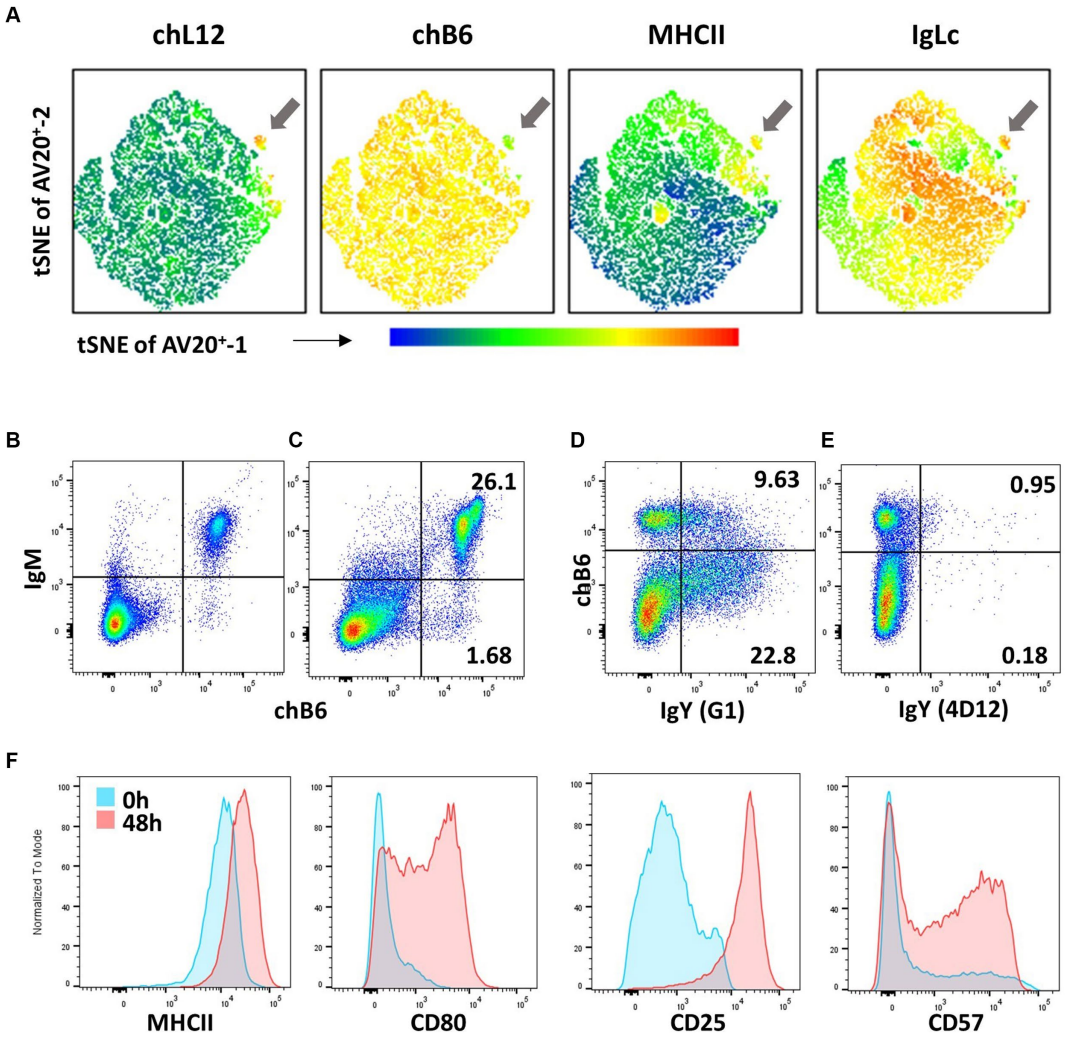

FIGURE 5
B-cell phenotypes **(A)** Bursa cells from a 5-day-old bird were stained for chL12 (11A9), chB6 (AV20), MHCII (2G11), and IgL (2G1). tSNE analysis with the FlowJo plugin was performed on viable, single, chB6^{+} cells, clearly displaying the phenotype of bursal emigrants (arrow). Leukocytes from the blood **(B)** and spleen **(C)** were stained for chB6 (AV20) and IgM (M1). Plots are gated for viable, single leukocytes. **(D,E)** Recognition of membrane-bound IgY. Spleen cells were stimulated for 6 days with CD40L and IL-10 to induce B-cell proliferation and class switch. Cells were stained with anti-chB6 (AV20) to address undifferentiated B cells and anti-IgY clone G1 **(D)** or anti-IgY clone 4D12 **(E)**. Plots are gated for viable, single leukocytes. **(F)** Immediately after isolation (blue) or after stimulation with CD40L and IL-10 for 48 h (red), splenic leukocytes were analyzed for MHC class II (2G11), CD80 (AV82), CD25 (28–4) and CD57 (HNK-1) expression. Histograms were gated for viable, single chB6+ B cells.

chB6^{high} CD57^{+} cell population, which could readily represent GC B cells (97).

7.5 Memory B cells

As with GC B cells, due to the lack of markers, it is currently not possible to identify memory B cells by flow cytometry. Here, new techniques like single-cell sequencing of B cells from different tissues and BCR sequencing will certainly help to identify these differentiation stages and potential new markers. Interestingly, scRNA sequencing of chicken blood leukocytes has identified several different B-cell subclusters (18). Though these have so far not been functionally assigned, it highlights the great value of this technique to identify chicken B-cell subpopulations.

7.6 Plasma cells

Histologically, plasma cells, the final differentiation stage of B cells, can be identified by their typical morphology with a cartwheel nucleus structure. They have been identified in the spleen and in mucosa-associated lymphoid tissues (HALT, BALT, and GALT). Immunohistochemistry has also shown that in contrast to all other known chicken B-cell stages, plasma cells do not express chB6 or show only very weak staining (47). Downregulation of chB6 has also been shown by flow cytometry when B cells were differentiated toward a plasma cell phenotype *in vitro* by the presence of CD40L (93). Based on single color immunohistochemistry, it is also suggested that splenic plasma cells express CD57, and basic flow cytometry revealed a small population of large cells in the spleen and caecal tonsils expressing chB6^{low} CD57^{+} (97). However, this

observation should be verified with further experiments, including additional markers. A rich source for plasma cells may be the Harderian gland, a lacrimal gland in the eye orbit. The gland reacts to intra-ocular vaccination, and it is described that leukocytes, including those with a plasma cell phenotype, can be isolated from the gland (98–101). Immunohistochemistry of the gut reveals a multitude of IgA-positive plasma cells in the lamina propria (LP), and with enzymatic digestion, it is possible to isolate IgA surface-positive cells (98).

Another approach to identify B-cell differentiation stages could be staining for transcription factors. Two key transcription factors for plasma cell differentiation are IRF4 and Blimp1/PRDM1. Whilst IRF4 induces plasma cell differentiation by directing immunoglobulin class switching, proliferation, and survival, BLIMP1 acts as a transcriptional repressor that represses B-cell features (102). For the rat anti-human-IRF4, clone 3E4 cross-reaction with porcine cells has been demonstrated (103) and preliminary data suggest cross-reaction with chicken cells (personal communication, Dr. W. Gerner). At least for one anti-Blimp1 antibody (mAb rabbit anti-human Blimp1, clone C14A4), cross-reactivity with the chicken protein in Western blots was demonstrated (104), and in mammals, this antibody was used in flow cytometry.

7.7 Post-bursal stem cells

In contrast to mammals, where B-cell production in the bone marrow can be a lifelong process, the bursa Fabricii, and hence the chicken's primary B-cell organ, involutes with sexual maturity (78). As analysis of older birds and studies with bursectomised birds have clearly shown the establishment of a bursa-independent dividing B-cell pool post-hatch, it is postulated that after bursa involution, the peripheral B-cell pool is maintained by post-bursal stem cells (89). Whilst after bursal emigration all B cells are chL12$^+$, with increasing age, a chB6$^+$/chL12$^-$ B-cell population becomes detectable in the spleen, which might represent these cells (105). As chL12 detects an alloantigen, it may not be useful for birds lacking the allele. With the availability of new techniques and markers, these cells can now be further analyzed.

7.8 Activation markers

As antigen-presenting cells, all B cells are MHC class II$^+$, but CD40L stimulation and mimicking T cells help further increase MHC class II (93). Whilst freshly isolated B cells from bursa, PBL, and spleen are CD80$^-$, *in vitro* activation of B cells leads to strong upregulation of CD80 and also strongly increases CD25 expression (106, 107). As mentioned, regular spleen cell preparations do not contain GC B cells, so it is possible that, like human B cells, CD80 is a marker for activated and dividing chicken GC B cells. Up to one-third of freshly isolated splenic B cells are already CD57$^+$ (97). This fraction is doubled by *in vitro* stimulation. Overall, activation of B cells can lead to an increase in already existing marker expression on all cells (MHC class II, CD25), complete *de novo* expression on a subset of B cells (CD80), or expression on an increased fraction of cells (CD57) (Figure 5F).

8 T cells

T-cell progenitors in the bone marrow express several markers like c-kit, HEMCAM, BEN, αIIbβ3, ChT1, MHC class II, and CD44 (108), and they colonize the thymus in three waves (first from paraaortic foci starting at ED6, second at ED12, and third at ED18, the two latter from bone marrow) (109). Embryonic thymocytes expressing the TCR γδ can first be detected around ED12, whereas cells expressing TCRα/vβ1 are not present until ED15 and TCRα/vβ2 around ED18 (110, 111). As in mammals, avian extra-thymic T lymphocytes all express the T-cell marker CD3. The common commercial antibody clone CT-3 recognises an extracellular domain of the chicken CD3 molecule (112). However, CT-3 staining may or may not give optimal separation between negative and positive populations, especially in whole blood. Moreover, even in isolated PBMCs, the staining can be influenced by, e.g., the chicken breed or cell activation status (7). In addition to CT-3, commercial anti-human CD3ε (clone CD3-12) antibodies exist where cross-reaction with chicken CD3 has been shown for intracellular staining (113). Reports exist on CD3 polymorphism, and another anti-chicken CD3 antibody, clone AV36, supposedly recognises a variable epitope and did not bind to splenocytes from the NARF C.B12 (B12 haplotype) inbred chicken line (114), whereas clone CT-3 could detect C.B12 splenocytes. In addition to CD3, avian T-cell subsets can be defined according to the expression of T-cell receptor variants. Avian homologs of the mammalian γδ and αβ TCR exist, but two variants of the latter were shown to differ in the variable regions in the β chain [encoded by either Vβ1 or Vβ2 genes (115)].

8.1 αβ T cells

Avian T-cell subsets expressing the variants of the αβ TCR can be identified by staining with the commercial clones TCR2 (TCR αVβ1) and TCR3 (TCR αVβ2), respectively (116). TCR2$^+$ and TCR3$^+$ subsets differ in ontogeny and tissue distribution, with TCR2$^+$ cells in general being more abundant than TCR3$^+$ cells (117). Functional differences between TCR2$^+$ and TCR3$^+$ subsets are poorly described, but interestingly, TCR2$^+$ cells but not TCR3$^+$ cells migrate to the chicken intestine, hence being of importance to mucosal IgA production (118, 119). Several subsets of αβ T cells can be identified by staining for the co-receptors CD4 and CD8 (120). As opposed to chicken CD4 and CD8β, the chicken CD8α gene is polymorphic (121). Several antibodies exist (CT-8, 3–298, EP72, AV12-14) recognising chicken CD8α, but the 3–298 clone may be superior in being the only commercial reagent recognising the majority, if not all, of CD8α variants (122). In contrast to CD8α, only a single commonly used CD8β antibody exists (EP42). Within the αβ T-cell population in, e.g., peripheral blood, the following subsets exist: CD4$^+$ CD8αα$^+$, CD4$^+$ CD8αβ$^+$, and CD4$^-$ CD8αβ$^+$, in addition to the less well-characterized subsets of CD4$^-$ CD8αα$^+$ (123) and CD4$^+$CD8αβ$^+$ cells (124).

8.2 Cytotoxic T cells

Chicken cytotoxic T lymphocytes (CTL) recognize peptides presented by MHC I molecules and show cytotoxic activity (125, 126).

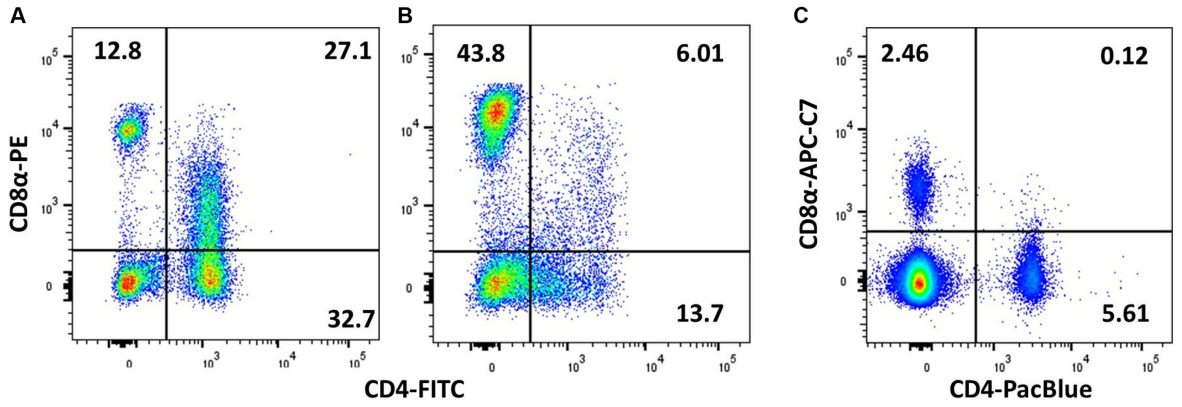

FIGURE 6
Demonstration of CD4/CD8 double-positive cells is affected by the choice of fluorochrome and the individual animal. PMBCs from adult birds were stained with TCRγδ (TCR1), CD4 (CT-4), and CD8α (3–298), and plots are shown for viable singlets and TCR1$^-$ lymphocytes. **(A)** Chicken with high level of peripheral CD4 + CD8+ cells and **(B)** a low level of double-positive cells. **(C)** Chicken with high level of CD4 + CD8+ cells, which is not picked up by the less bright APC-Cy7 staining of CD8α.

Interestingly, CD3$^+$CD8$^+$ cells in peripheral blood usually express the CD8αβ isoform, but a CD8αα-positive subset also exists and may expand, e.g., during viral infection (127). A common CTL assay in mammals is based on the detection of transient expression of lysosomal-associated membrane glycoproteins (LAMPs) on the cell surface. Cytotoxic activity via the perforin–granzyme pathway occurs in pre-formed lytic granules surrounded by lipid bilayers containing LAMPs that are fused with the plasma membrane. Hence, the LAMP-1 (CD107a) degranulation assay described above can also be used in studies of chicken cytotoxic T cells. Within the αβ T-cell population (αVβ1+ splenocytes), both CD8αα$^+$ and CD8αβ$^+$ showed potential to degranulate *in vitro* upon phorbol myristate acetate (114).

In addition to the granzyme/perforin killing pathway, evidence exists of a Fas/FasL pathway in chickens (128) and an anti-human FasL antibody (CD178, clone SB93a) was shown to cross-react with the chicken FasL by immunohistochemistry (129) but its suitability for flow cytometry is to be determined. A common parameter reported in relation to CTL responses is the production of IFN-γ. A number of monoclonal antibodies directed against chicken IFN-γ exist. Some only recognize the recombinant protein they were raised against, and others perform well in ELISA but are not suited for flow cytometry. Induction of IFN-γ production in splenocytes or PBMC by mitogens or specific antigens is reported to be detected by using antibody clones: 2B7, 11G5, 7E3, 12F12 (130, 131), mAb80 (132), and a rabbit polyclonal anti-chIFN-γ reagent (133). Clones 12F7, 12D4 (130) and EH9 (134) seem less suitable for intracellular staining (ICS) and flow cytometry. The anti-chicken IFN-γ antibody (clone 5C.123.02/08) from the commercial chicken IFN-γ Invitrogen ELISA kit works for intracellular staining (ICS) of the recombinant protein expressed by CHO cells (133). However, although some report staining of the native protein using these antibodies, others observe only weak staining with the ELISA reagents (135) or fail to reproduce even a dim signal (136). Additional clones MT6C2 and MT7C1 from Mabtech, as well as four Chinese clones, were found not suitable for ICS (136, 137). Unfortunately, the two superior antibody clones for intracellular staining and flow cytometry, mAb80 and 5G11, are not commercially available.

8.3 T helper cells

Several reagents recognising chicken CD4 are available, e.g., the clones CT4, EP96, AV29, and 2–35. In other species, CD4 may also be expressed by monocytes, but this is not the case in chickens (138). However, a small CD3$^-$ CD4$^+$ NK population (with slightly higher FSC/SSC than resting lymphocytes) is sometimes identified in peripheral blood (54) and hence at least TCRαβ or CD3 in combination with CD4 should be used to identify chicken Th cells. Interestingly, some lines of chickens have a high abundance of CD4$^+$CD8$^+$ double-positive TCRαβ$^+$ lymphocytes, and there is a genetic influence on levels in peripheral blood but not necessarily in the intestine (121, 123, 138). The double-positive subset exists either as CD4$^+$CD8αα$^+$ or CD4$^+$CD8αβ$^+$ with a dimmer CD8 signal than CD4$^-$ CD8$^+$ cells (127); hence, using bright fluorochromes for CD8 detection is crucial to obtain good separation between CD8$^-$, CD8^{dim}, and CD8^{Hi} subpopulations (Figure 6).

In mammals, major Th subsets can be differentiated by intracellular staining for the transcription factors T-bet (Th1), GATA-3 (Th2), RORγt (Th17), and Foxp3 (Treg). To the best of our knowledge, no reagents are available for staining important chickens Th transcription factors, despite the obvious value of developing such reagents for flow cytometry. The success rate of identifying cross-reacting mammalian reagents is generally poor for chicken surface markers (139, 140), but for highly conserved intracellular proteins such as transcription factors, the chances may be higher. However, testing of two widely used anti-murine Foxp3 clones, FJK-16 s and MF-14, proved they were unsuitable for Foxp3 detection in chicken cells (141).

The basic Th1 response system appears to be conserved in chickens (142), and CD4$^+$ cells producing IFN-γ are often interpreted as Th1 cells. Indeed, the Th1/Th2 paradigm was early on made probable through gene expression analysis of tissue from Newcastle disease virus and *Ascaridia galli*, infected chickens, respectively (143). However, flow cytometry studies addressing production of multiple cytokines and linking Th1 or Th2 profiles to, e.g., TCR αVβ1 or TCR αVβ2 expression are still missing. The limited quality of the chicken

cytokine antibodies is often a problem that has inspired the use of alternative methods such as identification of intracellular cytokine RNA by the PrimeFlow™ system (130).

Putative chicken regulatory T cells that can suppress T-cell proliferation *in vitro* were identified by co-expression of CD4 and CD25 (144). However, the CD4$^+$ CD25$^+$ population includes other subsets than just Tregs. More recently, *FOXP3* was identified in the chicken genome, and Foxp3 mRNA was shown to be abundant in CD4$^+$ CD25$^+$ in contrast to CD4$^+$ CD25$^-$ subsets in the spleen and caecal tonsils (141). The gene expression studies identified two CD4$^+$ CD25$^+$ subsets where the cells expressing high levels of IL-10 and Foxp3 were suggested as mature Tregs, whereas cells expressing low levels of IL-10 in combination with IL-2 were rather activated Th cells (141). Staining with CD4 and CD25 will hence provide a mixed population, and the production of chicken Foxp3 antibodies is expected to give better opportunities for studying Treg subsets in the future. Several chicken CD25 antibodies exist where AV142 and the bivalent human recombinant Fab AbD13504 are widely used. In addition, clones like 6C9, chCD25-32, and chCD25-54 exist (145), as well as 28–4, which was originally described as an NK cell marker but later identified as recognising CD25 (46).

Various *in vitro* and *in vivo* models have shown chicken IL-17 mRNA gene expression and suggested the presence of Th17 cells (146–149) but only recently have monoclonal antibodies useful for ICS been developed, namely the 1E7 clone recognising IL-17F (with slight cross-reactivity to IL-17A) and the two IL-17A-specific clones 9F11 and 10D5 (150). The IL-17 antibodies were all able to stain a small population of CD4$^+$ splenocytes upon PMA activation. The 10D5 clone was furthermore used to show that IL-17A was primarily expressed by CD3$^+$ CD4$^+$ T cells in the spleen and PBMC, but staining of smaller subsets of γδ T cells was also evident (151). Interestingly, IEL staining patterns were slightly different with IL-17A$^+$ cells largely CD4$^-$, CD8$^-$, and TCR1$^-$ but for the most part expressing CD3 and CD25 (150). In addition, the same antibody was used to show weak signals of IL-17A in lung T-cell populations (131).

8.4 γδ T cells

The commercially available antibody TCR1 recognises the TCRγδ variant, and hence all TCR1$^+$ cells are actually γδ T cells (111). However, whether all γδ TCRs indeed express the TCR1 epitope is still not proven but might be solved in the near future with the availability of new TCR sequencing protocols (152). As shown by frequency within a lymphocyte gate, γδ T cells are abundant in peripheral blood, immune organs, and bone marrow, and a CD8$^+$ subset is often seen in the lung and spleen (137), as well as in the intestinal mucosa (153). In the intestine, γδ T cells are present both in the intraepithelial and the lamina propria areas, and interestingly, in addition to the CD4$^-$ CD8$^-$, CD4$^-$ CD8αα$^+$, and CD4$^-$ CD8αβ$^+$ populations, the presence of an additional small CD4$^+$ CD8$^-$ population has been suggested. The CD8$^+$ population has received much attention and has been reported as being slightly larger in size and more prone to activation by mitogens (154). Interestingly, chB6-positive intraepithelial lymphocytes in the small intestine contain a population of TCR1$^+$ cells, as shown in Figure 3.

Some molecules are differentially expressed between γδ T cells and αβ T cells but cannot be used as unique lineage identifiers. For example, CD5 was shown to be expressed on virtually all CD4$^+$ αβ T cells and on the majority of γδ T cells, but the mean fluorescence intensities were low/intermediate on the γδ T cells isolated from spleen and peripheral blood (92). The CD5 antibody clone 2–191 unfortunately appears to be discontinued. CD28 is another molecule expressed on virtually all CD4$^+$ αβ1 T cells but is absent from the majority of γδ T cells; however, by using the clone MoAb 2–4, a small subset was found to be CD28$^+$ (mostly CD8α$^+$ but also a minor CD8$^-$ population) (155). The clone used by Koskela et al. may no longer be accessed, but clone AV7 recognises CD28 and is commercially available (156).

Data from scRNA-seq suggest the presence of multiple γδ T-cell subsets that may represent either phenotypic subsets or differentiation and activation states (18). A range of molecules may be differentially expressed by various γδ T subsets, but a comprehensive multiparameter immunophenotyping study has not yet been published. As the percentage of TCR1+, TCR2+, and TCR3$^+$ cells does not completely add up to 100% of the CD3 population, there may be a small yet unidentified T-cell subpopulation. Hence, interesting surface marker antibodies for a future multiparameter staining panel may include TIM4 (ROS-JH9 (60)), SLAMF4 (8C7 (35)), CD25 (AbD13504 (157)). Moreover, chicken γδ T cells have the ability to secrete a number of cytokines such as IFN-γ, IL-17A, IL-6, IL-10, and IL-13 (151, 158, 159), and including cytokine staining in multiparameter staining is of value to characterize various γδ T-cell subsets.

8.5 T-cell activation and memory cell markers

Extensive knowledge about T-cell activation and memory cell markers is still lacking in the avian research field. In mammals, activated proliferating T cells express several molecules that are expressed to a lesser extent or even absent on resting cells, including various chemokine receptors, adhesion molecules, co-stimulatory molecules, and MHC antigens (160). The same appears to be the case for chicken lymphocytes, but most of the published data include observations made using *in vitro* polyclonal/mitogen-stimulated cells rather than *in vivo* activated cells from infected animals. For example, *in vitro* ConA-induced T-cell proliferation of PBMC confirmed CD25 and MHC class II as T-cell activation markers for both CD4$^+$ and CD8α$^+$ cells and CD28 only for CD8α$^+$ cells when looking at activation marker-positive frequencies of cells (6). Interestingly, most of the tested putative activation markers (e.g., CD44, CD45, CD25, and CD28) showed increased surface expression (mean fluorescent intensity, MFI) over time, whereas the MFI of MHC class II was upregulated only 24-h post-stimulation, followed by MFI downregulation, especially in CD8α$^+$ T cells, where the MFI stayed below baseline from 48- to 96-h post-stimulation.

In mammals, constitutive expression of MHC class II is confined to professional antigen-presenting cells, including DCs, B cells, monocytes, and macrophages, and upon activation, MHC class II expression (all isotypes) is also seen on the surface of T cells in various species except in mice (161). The Naghizadeh chicken PBMC study mentioned above (160) showed virtually no MHC class II expression pre-stimulation, but 24-h post-stimulation, it was readily induced in 20–25% of the CD4$^+$ and CD8α$^+$ cells. Although the CD8α$^+$ antibody would have picked up a small subset of γδ T cells, the majority of γδ

T cells ($CD8^-$) were excluded from the mentioned study. Interestingly, others have reported that the majority of γδ T cells in peripheral blood express MHC class II even in a resting state, and increased MFI was shown in an *in vivo* experiment where chickens were provided high doses of Ulvan in their drinking water (162). CD25 is constitutively expressed on a subset of γδ T cells but is also described as an activation marker because frequencies of $CD25^+$ cells within the γδ T population are increased upon activation with, e.g., *Salmonella* and *Eimeria* (124, 157). Furthermore, chickens immunized with the model antigen mycobacterial purified protein derivative or *Mycobacterium tuberculosis* sonicate showed increased frequencies of $CD28^+$ γδ T-cell frequencies combined with increased surface expression of CD28, CD5, CD25, and MHC class II (155).

CD57 (clone HNK-1) has been identified as a B-cell activation marker (44, 97, 163, 164). We have shown higher degranulation of $CD57^+$ CTLs than of $CD57^-$ CTLs, which supports CD57 as chicken T-cell activation marker (165). Furthermore, frequencies of $CD57^+$ cells increase within both αβ and γδ T-cell populations in PBMC stimulated with mitogens or anti-CD3 (T. Dalgaard, manuscript in preparation). Several additional potential activation markers are available, but their expression on activated chicken T cells is poorly characterized. Examples include CD276 (AV95/EH7), CD30 (AV37 (166)), CRTAM (8A10 (167)), and GITR (9C5 (168)). In addition to activated T cells, chicken memory cells are also poorly defined in terms of phenotypes. Despite the fact that different CD45 isoforms exist (29), the equivalents of CD45RA and CD45RO have not been identified in chickens. CD127 is the α chain of the IL-7 receptor, and in mammals, it is differentially expressed depending on T-cell differentiation state (naïve, effector, memory) (169). A monoclonal antibody against chicken CD127 exists (clone 8F10E11) and was used to show that the majority of $CD4^+$ cells in the peripheral blood and spleen of healthy animals expressed CD127. In contrast, only 10–60% of the $CD8\alpha^+$ cells expressed CD127, and the frequency declines with age (170). To establish the value of this marker for the discrimination of T-cell differentiation stages, CD127 staining must be further investigated, e.g., on tetramer-positive cells and in conjunction with other activation or memory cell markers. In other species, CD44 expression is higher on effector and memory T cells as compared to naive. This is not yet established for chicken cells, although some studies suggest increased CD44 expression in the memory stages of *in vivo* vaccine or challenge experiments (5, 171).

8.6 Antigen-specific T cells

To evaluate host–pathogen interaction and vaccine responses, it is important to understand the role of antigen-specific T cells. Few avian MHC multimer flow cytometry reports exist (172, 173) and the reagents are not commercially available in various MHC–peptide combinations as they are for human and mouse models. Hence, most analyses of avian T-cell biology have relied on proliferation, degranulation, or cytokine detection in PBMC or splenocytes after antigen re-stimulation *in vitro*/*ex vivo* for quantitative and qualitative studies of antigen-specific T-cell responses. Interestingly, a subset of activation markers in mammals are exclusively expressed by T cells activated via MHC–TCR interaction, like the commonly used marker CD154 (CD40L) for antigen-activated T cells in humans and mice (174, 175). Transient CD154 surface expression or intracellular expression stabilized with the secretion inhibitor Brefeldin can be exploited for enrichment of antigen-specific T cells before further analysis (176, 177). An avian orthologue of mammalian CD154 exists, and the gene was identified and a set of monoclonal antibodies named AV71-76 were generated (UK Immunological Toolbox). Initial analysis of splenocytes activated by PMA/IO showed binding of the antibodies and suggested CD154 expression on activated T cells. In this early study, it was evident that the IgG1 antibodies AV71 and AV74 bound weakly to CD154, whereas the IgG2a antibodies AV72, AV73, and AV75 showed slightly higher affinity; however, further in-depth analysis is warranted (36).

9 Pitfalls

In the current study, we have focused on the spleen and peripheral blood; hence, this is not a comprehensive overview of cell subsets found in other tissues and organs. Moreover, it is important to note that both absolute numbers and relative frequencies of cellular subsets are influenced by, e.g., chicken breed and age (7). In addition, even the same tissue can give different results with different isolation techniques (choice of enzyme, slow speed/Ficoll gradient, etc.). Careful optimisation is therefore needed for each application, with a special focus on understanding potential epitope degradation by the digest or fixation protocol in question. Moreover, fixed samples may require different gating as compared to fresh samples, as fixation may compress FSC/SSC profiles and create problems with autofluorescence, which is, e.g., very pronounced in PFA-fixed thrombocytes. Biotinylated antibodies are often used in flow cytometric experiments with chickens due to the limited choice of directly conjugated antibodies. Since avidin is a biotin-binding protein with a possible antimicrobial effect and is upregulated after stress and infection (178), appropriate controls must be included. To check for non-specific biotin binding, an irrelevant biotinylated antibody (a non-chicken target antigen) should be included. Another well-known technique that works well for mammalian samples is lysis of erythrocytes before flow cytometry acquisition. Several groups have published data where attempts to lyse erythrocytes were made, e.g., by prolonging exposure to commercial lysis buffers with suboptimal results. However, whereas this strategy may not be possible for peripheral blood, it may work for tissues such as the bone marrow, where erythrocyte content is lower. In any case, careful validation and assessment of any effect on the phenotype and function of the remaining leukocytes is necessary.

In-depth transcriptome analysis will certainly identify further subpopulations and potential markers, and flow cytometry and cell morphology will not necessarily match with them. Hence, carefully controlled cross-validation of all sources should be a prerequisite for a successful combination of all techniques.

Author contributions

SH: Conceptualization, Visualization, Writing – original draft, Investigation, Funding acquisition, Methodology, Writing – review & editing. KS: Conceptualization, Writing – original draft, Visualization. LV: Conceptualization, Visualization, Writing – original draft,

Funding acquisition, Writing – review & editing. TD: Conceptualization, Visualization, Writing – original draft, Investigation, Methodology, Writing – review & editing.

Funding

The author(s) declare that financial support was received for the research, authorship, and/or publication of this article. TD and LV received funding from the European Union's Horizon 2020 Research and Innovation Programme under grant agreement No. 731014 (VetBioNet—Veterinary Biocontained Facility Network). LV and KS received funding from the Biotechnology and Biological Sciences Research Council under project numbers BBS/E/D/10002071 and BBS/E/D/20002174. SH received funding from the Deutsche Forschungsgemeinschaft in the framework of the Research Unit ImmunoChick (FOR5130) through the project HA-8037/2–1. We would like to thank the British Society of Immunology and the Comparative and Veterinary Immunology group for their funding and contributions to the organization of the Avian Flow Cytometry Workshop.

Acknowledgments

We thank Dominik von LaRoche and Marina Kohn for excellent technical assistance and wish to thank the animal caretakers of the National Avian Research Facility for the supply of birds.

Conflict of interest

The authors declare that the research was conducted in the absence of any commercial or financial relationships that could be construed as a potential conflict of interest.

Publisher's note

References

1. Entrican G, Lunney JK, Rutten VP, Baldwin CL. A current perspective on availability of tools, resources and networks for veterinary immunology. *Vet Immunol Immunopathol*. (2009) 128:24–9. doi: 10.1016/j.vetimm.2008.10.291

2. Gerner W, Talker SC, Koinig HC, Sedlak C, Mair KH, Saalmüller A. Phenotypic and functional differentiation of porcine Aβ T cells: current knowledge and available tools. *Mol Immunol*. (2015) 66:3–13. doi: 10.1016/j.molimm.2014.10.025

3. Sopp P, Kwong LS, Howard CJ. Cross-reactivity with bovine cells of monoclonal antibodies submitted to the 6th international workshop on human leukocyte differentiation antigens. *Vet Immunol Immunopathol*. (2001) 78:197–206. doi: 10.1016/s0165-2427(00)00262-2

4. Wagar LE, DiFazio RM, Davis MM. Advanced model systems and tools for basic and translational human immunology. *Genome Med*. (2018) 10:73. doi: 10.1186/s13073-018-0584-8

5. Dalgaard TS, Norup LR, Pedersen AR, Handberg KJ, Jørgensen PH, Juul-Madsen HR. Flow cytometric assessment of chicken T cell-mediated immune responses after Newcastle disease virus vaccination and challenge. *Vaccine*. (2010) 28:4506–14. doi: 10.1016/j.vaccine.2010.04.044

6. Naghizadeh M, Hatamzade N, Larsen FT, Kjaerup RB, Wattrang E, Dalgaard TS. Kinetics of activation marker expression after in vitro polyclonal stimulation of chicken peripheral T cells. *Cytometry A*. (2022) 101:45–56. doi: 10.1002/cyto.a.24304

7. Seliger C, Schaerer B, Kohn M, Pendl H, Weigend S, Kaspers B, et al. A rapid high-precision flow cytometry based technique for Total white blood cell counting in chickens. *Vet Immunol Immunopathol*. (2012) 145:86–99. doi: 10.1016/j.vetimm.2011.10.010

8. Sutton K, Costa T, Alber A, Bryson K, Borowska D, Balic A, et al. Visualisation and characterisation of mononuclear phagocytes in the chicken respiratory tract using Csf 1r-transgenic chickens. *Vet Res*. (2018) 49:104. doi: 10.1186/s13567-018-0598-7

9. Alber A, Morris KM, Bryson KJ, Sutton KM, Monson MS, Chintoan-Uta C, et al. Avian pathogenic *Escherichia Coli* (Apec) strain-dependent immunomodulation of respiratory granulocytes and mononuclear phagocytes in Csf 1r-reporter transgenic chickens. *Front Immunol*. (2019) 10:3055. doi: 10.3389/fimmu.2019.03055

10. Sutton KM, Morris KM, Borowska D, Sang H, Kaiser P, Balic A, et al. Characterization of conventional dendritic cells and macrophages in the spleen using the Csf 1r-reporter transgenic chickens. *Front Immunol*. (2021) 12:12. doi: 10.3389/fimmu.2021.636436

11. Geirsdottir L, David E, Keren-Shaul H, Weiner A, Bohlen SC, Neuber J, et al. Cross-species single-cell analysis reveals divergence of the primate microglia program. *Cell*. (2019) 179:1609–22.e16. doi: 10.1016/j.cell.2019.11.010

12. Wu Z, Shih B, Macdonald J, Meunier D, Hogan K, Chintoan-Uta C, et al. Development and function of chicken Xcr 1(+) conventional dendritic cells. *Front Immunol*. (2023) 14:1273661. doi: 10.3389/fimmu.2023.1273661

13. Qu X, Li X, Li Z, Liao M, Dai M. Chicken peripheral blood mononuclear cells response to avian Leukosis virus subgroup J infection assessed by single-cell Rna sequencing. *Front Microbiol*. (2022) 13:800618. doi: 10.3389/fmicb.2022.800618

14. Luo J, Erb CA, Chen K. Simultaneous measurement of surface proteins and gene expression from single cells. *Methods Mol Biol*. (2020) 2111:35–46. doi: 10.1007/978-1-0716-0266-9_3

15. Peterson VM, Zhang KX, Kumar N, Wong J, Li L, Wilson DC, et al. Multiplexed quantification of proteins and transcripts in single cells. *Nat Biotechnol*. (2017) 35:936–9. doi: 10.1038/nbt.3973

16. Zhu Y, Scheibinger M, Ellwanger DC, Krey JF, Choi D, Kelly RT, et al. Single-cell proteomics reveals changes in expression during hair-cell development. *eLife*. (2019) 8:e50777. doi: 10.7554/eLife.50777

17. Liu Y, Liang S, Wang B, Zhao J, Zi X, Yan S, et al. Advances in single-cell sequencing technology and its application in poultry science. *Genes (Basel)*. (2022) 13. doi: 10.3390/genes13122211

18. Maxwell M, Söderlund R, Härtle S, Wattrang E. Single-cell Rna-Seq mapping of chicken peripheral blood leukocytes. *BMC Genomics*. (2024) 25:124. doi: 10.1186/s12864-024-10044-4

19. Warren WC, Rice ES, Meyer A, Hearn CJ, Steep A, Hunt HD, et al. The immune cell landscape and response of Marek's disease resistant and susceptible chickens infected with Marek's disease virus. *Sci Rep*. (2023) 13:5355. doi: 10.1038/s41598-023-32308-x

20. Montanari M, Burattini S, Ciacci C, Ambrogini P, Carloni S, Balduini W, et al. Automated—mechanical procedure compared to gentle enzymatic tissue dissociation in cell function studies. *Biomol Ther*. (2022) 12:701. doi: 10.3390/biom12050701

21. Talker SC, Baumann A, Barut GT, Keller I, Bruggmann R, Summerfield A. Precise delineation and transcriptional characterization of bovine blood dendritic-cell and monocyte subsets. *Front Immunol*. (2018) 9:2505. doi: 10.3389/fimmu.2018.02505

22. Balic A, Garcia-Morales C, Vervelde L, Gilhooley H, Sherman A, Garceau V, et al. Visualisation of chicken macrophages using transgenic reporter genes: insights into the development of the avian macrophage lineage. *Development*. (2014) 141:3255–65. doi: 10.1242/dev.105593

23. Woodford-Thomas T, Thomas ML. The leukocyte common antigen, Cd45 and other protein tyrosine phosphatases in hematopoietic cells. *Semin Cell Biol*. (1993) 4:409–18. doi: 10.1006/scel.1993.1049

24. Paramithiotis E, Tkalec L, Ratcliffe MJ. High levels of Cd45 are coordinately expressed with Cd4 and Cd8 on avian Thymocytes. *J Immunol*. (1991) 147:3710–7. doi: 10.4049/jimmunol.147.11.3710

25. Streuli M, Hall LR, Saga Y, Schlossman SF, Saito H. Differential usage of three exons generates at least five different Mrnas encoding human leukocyte common antigens. *J Exp Med*. (1987) 166:1548–66. doi: 10.1084/jem.166.5.1548

26. Akbar AN, Terry L, Timms A, Beverley PC, Janossy G. Loss of Cd45r and gain of Uchl 1 reactivity is a feature of primed T cells. *J Immunol*. (1988) 140:2171–8. doi: 10.4049/jimmunol.140.7.2171

27. Powrie F, Mason D. Subsets of rat Cd4+ T cells defined by their differential expression of variants of the Cd45 antigen: developmental relationships and in vitro and in vivo functions. *Curr Top Microbiol Immunol*. (1990) 159:79–96. doi: 10.1007/978-3-642-75244-5_5

28. Houssaint E, Tobin S, Cihak J, Lösch U. A chicken leukocyte common antigen: biochemical characterization and ontogenetic study. *Eur J Immunol*. (1987) 17:287–90. doi: 10.1002/eji.1830170221

29. Huhle D, Hirmer S, Göbel TW. Splenic Γδ T cell subsets can be separated by a novel Mab specific for two Cd45 isoforms. *Dev Comp Immunol*. (2017) 77:229–40. doi: 10.1016/j.dci.2017.08.013

30. Lavoie ET, Grasman KA. Isolation, cryopreservation, and Mitogenesis of peripheral blood lymphocytes from chickens (Gallus Domesticus) and wild herring gulls (*Larus Argentatus*). *Arch Environ Contam Toxicol*. (2005) 48:552–8. doi: 10.1007/s00244-004-0128-7

31. Barta O, Barta V, Pierson FW. Optimum conditions for the chicken lymphocyte transformation test. *Avian Dis*. (1992) 36:945–55. doi: 10.2307/1591554

32. Jones MP. Avian hematology. *Clin Lab Med*. (2015) 35:649–59. doi: 10.1016/j.cll.2015.05.013

33. Turowski V, Sperling B, Hanczaruk MA, Göbel TW, Viertlboeck BC. Chicken Trem-B1, an inhibitory Ig-like receptor expressed on chicken thrombocytes. *PLoS One*. (2016) 11:e0151513. doi: 10.1371/journal.pone.0151513

34. Neulen ML, Göbel TW. Identification of a chicken Clec-2 homologue, an activating C-type lectin expressed by thrombocytes. *Immunogenetics*. (2012) 64:389–97. doi: 10.1007/s00251-011-0591-z

35. Straub C, Neulen M-L, Viertlboeck BC, Göbel TW. Chicken Slamf 4 (Cd244, 2b4), a receptor expressed on thrombocytes, monocytes, Nk cells, and subsets of Aβ-, Γδ- T cells and B cells binds to Slamf 2. *Develop Comp Immunol*. (2014) 42:159–68. doi: 10.1016/j.dci.2013.09.007

36. Tregaskes CA, Glansbeek HL, Gill AC, Hunt LG, Burnside J, Young JR. Conservation of biological properties of the Cd40 ligand, Cd154 in a non-mammalian vertebrate. *Dev Comp Immunol*. (2005) 29:361–74. doi: 10.1016/j.dci.2004.09.001

37. Ferdous F, Scott T. The immunological capacity of thrombocytes. *Int J Mol Sci*. (2023) 24. doi: 10.3390/ijms241612950

38. Paul M, Paolucci S, Barjesteh N, Wood RD, Schat KA, Sharif S. Characterization of chicken thrombocyte responses to toll-like receptor ligands. *PLoS One*. (2012) 7:e43381. doi: 10.1371/journal.pone.0043381

39. Lam KM. Myeloperoxidase activity in chicken Heterophils and adherent cells. *Vet Immunol Immunopathol*. (1997) 57:327–35. doi: 10.1016/S0165-2427(96)05751-0

40. van Dijk A, Tersteeg-Zijderveld MHG, Tjeerdsma-van Bokhoven JLM, Jansman AJM, Veldhuizen EJA, Haagsman HP. Chicken Heterophils are recruited to the site of Salmonella infection and release antibacterial mature Cathelicidin-2 upon stimulation with Lps. *Mol Immunol*. (2009) 46:1517–26. doi: 10.1016/j.molimm.2008.12.015

41. Thomas JL, Pourquie O, Coltey M, Vaigot P, Le Douarin NM. Identification in the chicken of Grl 1 and Grl 2: two granule proteins expressed on the surface of activated leukocytes. *Exp Cell Res*. (1993) 204:156–66. doi: 10.1006/excr.1993.1020

42. Bílková B, Bainová Z, Janda J, Zita L, Vinkler M. Different breeds, different blood: cytometric analysis of whole blood cellular composition in chicken breeds. *Vet Immunol Immunopathol*. (2017) 188:71–7. doi: 10.1016/j.vetimm.2017.05.001

43. Olah I, Kendall C, Glick B. Endogenous peroxidase- and vimentin-positive cells accumulate at the Corticomedullary border of the chicken Thymus 1, 2. *Poult Sci*. (1991) 70:1144–52. doi: 10.3382/ps.0701144

44. Vervelde L, Jeurissen SH. Postnatal development of intra-epithelial leukocytes in the chicken digestive tract: phenotypical characterization in situ. *Cell Tissue Res*. (1993) 274:295–301. doi: 10.1007/bf00318748

45. Göbel TW, Chen CL, Shrimpf J, Grossi CE, Bernot A, Bucy RP, et al. Characterization of avian natural killer cells and their intracellular Cd3 protein complex. *Eur J Immunol*. (1994) 24:1685–91. doi: 10.1002/eji.1830240734

46. Fenzl L, Göbel TW, Neulen ML. Γδ T cells represent a major spontaneously cytotoxic cell population in the chicken. *Dev Comp Immunol*. (2017) 73:175–83. doi: 10.1016/j.dci.2017.03.028

47. Houssaint E, Diez E, Pink JR. Ontogeny and tissue distribution of the chicken Bu-1a antigen. *Immunology*. (1987) 62:463–70.

48. Jansen CA, van de Haar PM, van Haarlem D, van Kooten P, de Wit S, van Eden W, et al. Identification of new populations of chicken natural killer (Nk) cells. *Develop Comp Immunol*. (2010) 34:759–67. doi: 10.1016/j.dci.2010.02.009

49. Neulen M-L, Göbel TW. Chicken Cd56 defines Nk cell subsets in embryonic spleen and lung. *Develop Comp Immunol*. (2012) 38:410–5. doi: 10.1016/j.dci.2012.08.001

50. Viertlboeck BC, Wortmann A, Schmitt R, Plachý J, Göbel TW. Chicken C-type lectin-like receptor B-Nk, expressed on Nk and T cell subsets, binds to a ligand on activated Splenocytes. *Mol Immunol*. (2008) 45:1398–404. doi: 10.1016/j.molimm.2007.08.024

51. Zhang L, Katselis GS, Moore RE, Lekpor K, Goto RM, Hunt HD, et al. Mhc class I target recognition, Immunophenotypes and proteomic profiles of natural killer cells within the spleens of Day-14 Chick embryos. *Develop Comp Immunol*. (2012) 37:446–56. doi: 10.1016/j.dci.2012.03.007

52. Straub C, Neulen M-L, Sperling B, Windau K, Zechmann M, Jansen CA, et al. Chicken Nk cell receptors. *Develop Comp Immunol*. (2013) 41:324–33. doi: 10.1016/j.dci.2013.03.013

53. Viertlboeck BC, Schweinsberg S, Hanczaruk MA, Schmitt R, Du Pasquier L, Herberg FW, et al. The chicken leukocyte receptor complex encodes a primordial, activating, high-affinity Igy fc receptor. *Proc Natl Acad Sci USA*. (2007) 104:11718–23. doi: 10.1073/pnas.0702011104

54. Neulen M-L, Viertlboeck BC, Straub C, Göbel TW. Identification of novel chicken Cd4+ Cd3− blood population with Nk cell like features. *Develop Comp Immunol*. (2015) 49:72–8. doi: 10.1016/j.dci.2014.11.012

55. Wattrang E, Dalgaard TS, Norup LR, Kjærup RB, Lundén A, Juul-Madsen HR. Cd107a as a marker of activation in chicken cytotoxic T cells. *J Immunol Methods*. (2015) 419:35–47. doi: 10.1016/j.jim.2015.02.011

56. Ijaz A, Broere F, Rutten V, Jansen CA, Veldhuizen EJA. Perforin and Granzyme a release as novel tool to measure Nk cell activation in chickens. *Dev Comp Immunol*. (2023) 149:105047. doi: 10.1016/j.dci.2023.105047

57. Staines K, Hunt LG, Young JR, Butter C. Evolution of an expanded mannose receptor gene family. *PLoS One*. (2014) 9:e110330. doi: 10.1371/journal.pone.0110330

58. Garcia-Morales C, Rothwell L, Moffat L, Garceau V, Balic A, Sang HM, et al. Production and characterisation of a monoclonal antibody that Recognises the chicken Csf 1 receptor and confirms that expression is restricted to macrophage-lineage cells. *Dev Comp Immunol*. (2014) 42:278–85. doi: 10.1016/j.dci.2013.09.011

59. Bratton DL, Fadok VA, Richter DA, Kailey JM, Guthrie LA, Henson PM. Appearance of phosphatidylserine on apoptotic cells requires calcium-mediated nonspecific Flip-flop and is enhanced by loss of the Aminophospholipid translocase. *J Biol Chem*. (1997) 272:26159–65. doi: 10.1074/jbc.272.42.26159

60. Hu T, Wu Z, Vervelde L, Rothwell L, Hume DA, Kaiser P. Functional annotation of the T-cell immunoglobulin mucin family in birds. *Immunology*. (2016) 148:287–303. doi: 10.1111/imm.12607

61. Ziegler-Heitbrock L, Ancuta P, Crowe S, Dalod M, Grau V, Hart DN, et al. Nomenclature of monocytes and dendritic cells in blood. *Blood*. (2010) 116:e74–80. doi: 10.1182/blood-2010-02-258558

62. Wu Z, Rothwell L, Hu T, Kaiser P. Chicken Cd14, unlike mammalian Cd14, is trans-membrane rather than Gpi-anchored. *Dev Comp Immunol*. (2009) 33:97–104. doi: 10.1016/j.dci.2008.07.008

63. Hu T, Wu Z, Bush SJ, Freem L, Vervelde L, Summers KM, et al. Characterization of subpopulations of chicken mononuclear phagocytes that express Tim 4 and Csf 1r. *J Immunol*. (2019) 202:1186–99. doi: 10.4049/jimmunol.1800504

64. Sutton JS, Weiss L. Transformation of monocytes in tissue culture into macrophages, epithelioid cells, and multinucleated Giant cells. An Electron microscope study. *J Cell Biol*. (1966) 28:303–32. doi: 10.1083/jcb.28.2.303

65. Mast J, Goddeeris BM, Peeters K, Vandesande F, Berghman LR. Characterisation of chicken monocytes, macrophages and interdigitating cells by the monoclonal antibody Kul 01. *Vet Immunol Immunopathol*. (1998) 61:343–57. doi: 10.1016/s0165-2427(97)00152-9

66. Yu K, Gu MJ, Pyung YJ, Song KD, Park TS, Han SH, et al. Characterization of splenic Mrc 1 (hi) Mhcii (Lo) and Mrc 1 (Lo) Mhcii (hi) cells from the monocyte/macrophage lineage of white Leghorn chickens. *Vet Res*. (2020) 51:73. doi: 10.1186/s13567-020-00795-9

67. Wu Z, Hu T, Chintoan-Uta C, Macdonald J, Stevens MP, Sang H, et al. Development of novel reagents to chicken Flt 3, Xcr 1 and Csf 2r for the identification and characterization of avian conventional dendritic cells. *Immunology*. (2022) 165:171–94. doi: 10.1111/imm.13426

68. de Geus ED, Rebel JM, Vervelde L. Induction of respiratory immune responses in the chicken; implications for development of mucosal avian influenza virus vaccines. *Vet Q*. (2012) 32:75–86. doi: 10.1080/01652176.2012.711956

69. van den Biggelaar R, Arkesteijn GJA, Rutten V, van Eden W, Jansen CA. In vitro chicken bone marrow-derived dendritic cells comprise subsets at different states of maturation. *Front Immunol*. (2020) 11:141. doi: 10.3389/fimmu.2020.00141

70. Borowska D, Sives S, Vervelde L, Sutton KM. Chicken Csf 2 and Il-4-, and Csf 2-dependent bone marrow cultures differentiate into macrophages over time. *Front Immunol*. (2022) 13:1064084. doi: 10.3389/fimmu.2022.1064084

71. Wu Z, Rothwell L, Young JR, Kaufman J, Butter C, Kaiser P. Generation and characterization of chicken bone marrow-derived dendritic cells. *Immunology*. (2010) 129:133–45. doi: 10.1111/j.1365-2567.2009.03129.x

72. de Geus ED, Jansen CA, Vervelde L. Uptake of particulate antigens in a nonmammalian lung: phenotypic and functional characterization of avian respiratory phagocytes using bacterial or viral antigens. *J Immunol*. (2012) 188:4516–26. doi: 10.4049/jimmunol.1200092

73. Jax E, Werner E, Müller I, Schaerer B, Kohn M, Olofsson J, et al. Evaluating effects of Aiv infection status on ducks using a flow cytometry-based differential blood count. *Microbiol Spectr*. (2023) 11:e0435122. doi: 10.1128/spectrum.04351-22

74. Helft J, Böttcher J, Chakravarty P, Zelenay S, Huotari J, Schraml BU, et al. Gm-Csf mouse bone marrow cultures comprise a heterogeneous population of Cd11c(+) Mhcii(+) macrophages and dendritic cells. *Immunity*. (2015) 42:1197–211. doi: 10.1016/j.immuni.2015.05.018

75. Vu Manh TP, Marty H, Sibille P, Le Vern Y, Kaspers B, Dalod M, et al. Existence of conventional dendritic cells in *Gallus Gallus* revealed by comparative gene expression profiling. *J Immunol*. (2014) 192:4510–7. doi: 10.4049/jimmunol.1303405

76. Staines K, Young JR, Butter C. Expression of chicken Dec 205 reflects the unique structure and function of the avian immune system. *PLoS One*. (2013) 8:e51799. doi: 10.1371/journal.pone.0051799

77. Salomonsen J, Sørensen MR, Marston DA, Rogers SL, Collen T, van Hateren A, et al. Two Cd1 genes map to the chicken Mhc, indicating that Cd1 genes are ancient and likely to have been present in the primordial Mhc. *Proc Natl Acad Sci USA*. (2005) 102:8668–73. doi: 10.1073/pnas.0409213102

78. Ratcliffe MJ. Antibodies, immunoglobulin genes and the Bursa of Fabricius in chicken B cell development. *Dev Comp Immunol*. (2006) 30:101–18. doi: 10.1016/j.dci.2005.06.018

79. Dóra D, Fejszák N, Goldstein AM, Minkó K, Nagy N. Ontogeny of ramified Cd45 cells in chicken embryo and their contribution to bursal secretory dendritic cells. *Cell Tissue Res*. (2017) 368:353–70. doi: 10.1007/s00441-017-2595-y

80. Veromaa T, Vainio O, Eerola E, Toivanen P. Monoclonal antibodies against chicken Bu-1a and Bu-1b Alloantigens. *Hybridoma*. (1988) 7:41–8. doi: 10.1089/hyb.1988.7.41

81. Veromaa T, Vainio O, Jalkanen S, Eerola E, Granfors K, Toivanen P. Expression of B-L and Bu-1 antigens in chickens Bursectomized at 60 H of incubation. *Eur J Immunol*. (1988) 18:225–30. doi: 10.1002/eji.1830180207

82. Nagy N, Busalt F, Halasy V, Kohn M, Schmieder S, Fejszak N, et al. In and out of the Bursa-the role of Cxcr 4 in chicken B cell development. *Front Immunol*. (2020) 11:1468. doi: 10.3389/fimmu.2020.01468

83. Kothlow S, Morgenroth I, Graef Y, Schneider K, Riehl I, Staeheli P, et al. Unique and conserved functions of B cell-activating factor of the Tnf family (Baff) in the chicken. *Int Immunol*. (2007) accepted) 19:203–15. doi: 10.1093/intimm/dxl137

84. Haertle S, Alzuheir I, Busalt F, Waters V, Kaiser P, Kaufer BB. Identification of the receptor and cellular Ortholog of the Marek's disease virus (mdv) cxc chemokine. *Front Microbiol*. (2017) 8:2543. doi: 10.3389/fmicb.2017.02543

85. Masteller EL, Larsen RD, Carlson LM, Pickel JM, Nickoloff B, Lowe J, et al. Chicken B cells undergo discrete developmental changes in surface carbohydrate structure that appear to play a role in directing lymphocyte migration during embryogenesis. *Development*. (1995) 121:1657–67. doi: 10.1242/dev.121.6.1657

86. Masteller EL, Lee KP, Carlson LM, Thompson CB. Expression of Sialyl Lewis (X) and Lewis (X) defines distinct stages of chicken B cell maturation. *J Immunol*. (1995) 155:5550–6. doi: 10.4049/jimmunol.155.12.5550

87. Schneider K, Kothlow S, Schneider P, Tardivel A, Gobel T, Kaspers B, et al. Chicken BAFF--a highly conserved cytokine that mediates B cell survival. *Int Immunol*. (2004) 16:139–48. doi: 10.1093/intimm/dxh015

88. Paramithiotis E, Ratcliffe MJ. B cell emigration directly from the cortex of lymphoid follicles in the Bursa of Fabricius. *Eur J Immunol*. (1994) 24:458–63. doi: 10.1002/eji.1830240229

89. Paramithiotis E, Ratcliffe MJ. Bursa-dependent subpopulations of peripheral B lymphocytes in chicken blood. *Eur J Immunol*. (1993) 23:96–102. doi: 10.1002/eji.1830230116

90. Houssaint E, Mansikka A, Vainio O. Early separation of B and T lymphocyte precursors in Chick embryo. *J Exp Med*. (1991) 174:397–406. doi: 10.1084/jem.174.2.397

91. Igyarto BZ, Magyar A, Olah I. Origin of follicular dendritic cell in the chicken spleen. *Cell Tissue Res*. (2007) 327:83–92. doi: 10.1007/s00441-006-0250-0

92. Koskinen R, Göbel TW, Tregaskes CA, Young JR, Vainio O. The structure of avian Cd5 implies a conserved function. *J Immunol*. (1998) 160:4943–50. doi: 10.4049/jimmunol.160.10.4943

93. Kothlow S, Morgenroth I, Tregaskes CA, Kaspers B, Young JR. Cd40 ligand supports the long-term maintenance and differentiation of chicken B cells in culture. *Dev Comp Immunol*. (2008) 32:1015–26. doi: 10.1016/j.dci.2008.01.012

94. Petkov DI, Linnemann EG, Kapczynski DR, Sellers HS. Identification and characterization of two distinct bursal B-cell subpopulations following infectious bursal disease virus infection of white Leghorn chickens. *Avian Dis*. (2009) 53:347–55. doi: 10.1637/8456-082208-Reg.1

95. Imamura K, Yasuda M, Riwar B, Inui S, Ekino S. Characteristic cellular composition of germinal centers. *Comp Immunol Microbiol Infect Dis*. (2009) 32:419–28. doi: 10.1016/j.cimid.2007.12.002

96. Nagy N, Olah I, Vervelde L. Structure of the avian lymphoid system In: B Kaspers, KA Schat, TW Göbel and L Vervelde, editors. *Avian immunology*. *3rd* ed: Elsevier (2021). 11–44.

97. Mast J, Goddeeris BM. Cd57, a marker for B-cell activation and splenic ellipsoid-associated reticular cells of the chicken. *Cell Tissue Res*. (1998) 291:107–15. doi: 10.1007/s004410050984

98. Scott TR, Savage ML, Olah I. Plasma cells of the chicken Harderian gland. *Poult Sci*. (1993) 72:1273–9. doi: 10.3382/ps.0721273

99. Scott TR, Savage ML. Immune cell proliferation in the Harderian gland: an avian model. *Microsc Res Tech*. (1996) 34:149–55. doi: 10.1002/(SICI)1097-0029(19960601)34:2<149::AID-JEMT9>3.0.CO;2-N

100. Gallego M, Glick B. The proliferative capacity of the cells of the avian Harderian gland. *Dev Comp Immunol*. (1988) 12:157–66. doi: 10.1016/0145-305X(88)90033-X

101. Mansikka A, Sandberg M, Veromaa T, Vainio O, Granfors K, Toivanen P. B cell maturation in the chicken Harderian gland. *J Immunol*. (1989) 142:1826–33. doi: 10.4049/jimmunol.142.6.1826

102. Tang TF, Chan YT, Cheong HC, Cheok YY, Anuar NA, Looi CY, et al. Regulatory network of blimp 1, Irf 4, and Xbp 1 triad in Plasmacytic differentiation and multiple myeloma pathogenesis. *Cell Immunol*. (2022) 380:104594. doi: 10.1016/j.cellimm.2022.104594

103. Villanueva-Hernández S, Adib Razavi M, van Dongen KA, Stadler M, de Luca K, Beyersdorf N, et al. Co-expression of the B-cell key transcription factors Blimp-1 and Irf 4 identifies plasma cells in the pig. *Front Immunol*. (2022) 13:854257. doi: 10.3389/fimmu.2022.854257

104. Wan Z, Rui L, Li Z. Expression patterns of Prdm 1 during chicken embryonic and germline development. *Cell Tissue Res*. (2014) 356:341–56. doi: 10.1007/s00441-014-1804-1

105. Paramithiotis E, Ratcliffe MJ. Survivors of bursal B cell production and emigration. *Poult Sci*. (1994) 73:991–7. doi: 10.3382/ps.0730991

106. Lee SH, Lillehoj HS, Park MS, Baldwin C, Tompkins D, Wagner B, et al. Development and characterization of mouse monoclonal antibodies reactive with chicken Cd80. *Comp Immunol Microbiol Infect Dis*. (2011) 34:273–9. doi: 10.1016/j.cimid.2011.01.003

107. Postrak L. *Untersuchungen Zum Einfluss Der Zytokine Cd40l, Baff, Il10 Und Il21 Auf Proliferation, Überleben Und Phänotypänderungen Von B-Zellen Des Haushuhns in Vitro. [thesis]*. Munich: LMU München (2017).

108. Ody C, Alais S, Corbel C, McNagny KM, Davison TF, Vainio O, et al. Surface molecules involved in avian T-cell progenitor migration and differentiation. *Dev Immunol*. (2000) 7:267–77. doi: 10.1155/2000/13850

109. Coltey M, Bucy RP, Chen CH, Cihak J, Lösch U, Char D, et al. Analysis of the first two waves of Thymus homing stem cells and their T cell progeny in Chick-quail chimeras. *J Exp Med*. (1989) 170:543–57. doi: 10.1084/jem.170.2.543

110. Coltey M, Jotereau FV, Le Douarin NM. Evidence for a cyclic renewal of lymphocyte precursor cells in the embryonic Chick Thymus. *Cell Differ*. (1987) 22:71–82. doi: 10.1016/0045-6039(87)90414-3

111. Sowder JT, Chen CL, Ager LL, Chan MM, Cooper MD. A large subpopulation of avian T cells express a homologue of the mammalian T gamma/Delta receptor. *J Exp Med*. (1988) 167:315–22. doi: 10.1084/jem.167.2.315

112. Chen CL, Ager LL, Gartland GL, Cooper MD. Identification of a T3/T cell receptor complex in chickens. *J Exp Med*. (1986) 164:375–80. doi: 10.1084/jem.164.1.375

113. Mitra T, Gerner W, Kidane FA, Wernsdorf P, Hess M, Saalmüller A, et al. Vaccination against Histomonosis limits pronounced changes of B cells and T-cell subsets in turkeys and chickens. *Vaccine*. (2017) 35:4184–96. doi: 10.1016/j.vaccine.2017.06.035

114. Bryson KJ, Sives S, Lee HM, Borowska D, Smith J, Digard P, et al. Comparative analysis of different inbred chicken lines highlights how a hereditary inflammatory state affects susceptibility to avian influenza virus. *Viruses*. (2023) 15. doi: 10.3390/v15030591

115. Tjoelker LW, Carlson LM, Lee K, Lahti J, McCormack WT, Leiden JM, et al. Evolutionary conservation of antigen recognition: the chicken T-cell receptor Beta chain. *Proc Natl Acad Sci USA*. (1990) 87:7856–60. doi: 10.1073/pnas.87.20.7856

116. Chen CH, Sowder JT, Lahti JM, Cihak J, Lösch U, Cooper MD. Tcr 3: a third T-cell receptor in the chicken. *Proc Natl Acad Sci USA*. (1989) 86:2351–5. doi: 10.1073/pnas.86.7.2351

117. Char D, Sanchez P, Chen CL, Bucy RP, Cooper MD. A third sublineage of avian T cells can be identified with a T cell Receptor-3-specific antibody. *J Immunol*. (1990) 145:3547–55.

118. Cihak J, Hoffmann-Fezer G, Wasl M, Merkle H, Kaspers B, Vainio O, et al. Inhibition of the development of spontaneous autoimmune thyroiditis in the obese strain (Os) chickens by in vivo treatment with anti-Cd4 or anti-Cd8 antibodies. *J Autoimmun*. (1998) 145:3547–55. doi: 10.4049/jimmunol.145.11.3547

119. Chen CH, Göbel TW, Kubota T, Cooper MD. T cell development in the chicken. *Poult Sci*. (1994) 73:1012–8. doi: 10.3382/ps.0731012

120. Chan MM, Chen CL, Ager LL, Cooper MD. Identification of the avian homologues of mammalian Cd4 and Cd8 antigens. *J Immunol*. (1988) 140:2133–8. doi: 10.4049/jimmunol.140.7.2133

121. Luhtala M, Tregaskes CA, Young JR, Vainio O. Polymorphism of chicken Cd8-alpha, but not Cd8-Beta. *Immunogenetics*. (1997) 46:396–401. doi: 10.1007/s002510050293

122. Norup LR, Dalgaard TS, Pedersen AR, Juul-Madsen HR. Assessment of Newcastle disease-specific T cell proliferation in different inbred Mhc chicken lines. *Scand J Immunol*. (2011) 74:23–30. doi: 10.1111/j.1365-3083.2011.02534.x

123. Luhtala M, Lassila O, Toivanen P, Vainio O. A novel peripheral Cd4+ Cd8+ T cell population: inheritance of Cd8alpha expression on Cd4+ T cells. *Eur J Immunol*. (1997) 27:189–93. doi: 10.1002/eji.1830270128

124. Wattrang E, Lundén A, Ibrahim O, Dalgaard TS. Phenotypic characterization of Eimeria Tenella-specific chicken T-cells responding to in vitro parasite antigen re-stimulation. *J Med Microbiol*. (2023) 72. doi: 10.1099/jmm.0.001650

125. Seo SH, Collisson EW. Specific cytotoxic T lymphocytes are involved in in vivo clearance of infectious bronchitis virus. *J Virol*. (1997) 71:5173–7. doi: 10.1128/jvi.71.7.5173-5177.1997

126. Schat KA. Cell-mediated immune effector functions in chickens. *Poult Sci*. (1994) 73:1077–81. doi: 10.3382/ps.0731077

127. Dai M, Zhao L, Li Z, Li X, You B, Zhu S, et al. The transcriptional differences of avian Cd4(+)Cd8(+) double-positive T cells and Cd8(+) T cells from peripheral blood of Alv-J infected chickens revealed by smart-Seq 2. *Front Cell Infect Microbiol*. (2021) 11:747094. doi: 10.3389/fcimb.2021.747094

128. Wattrang E, Magnusson SE, Näslund K, Thebo P, Hagström Å, Smith AL, et al. Expression of perforin, Granzyme a and Fas ligand Mrna in Caecal tissues upon Eimeria Tenella infection of Naïve and immune chickens. *Parasite Immunol*. (2016) 38:419–30. doi: 10.1111/pim.12329

129. Rauf A, Khatri M, Murgia MV, Saif YM. Fas/Fasl and perforin-Granzyme pathways mediated T cell cytotoxic responses in infectious bursal disease virus infected chickens. *Results Immunol*. (2012) 2:112–9. doi: 10.1016/j.rinim.2012.05.003

130. Lagler J, Mitra T, Schmidt S, Pierron A, Vatzia E, Stadler M, et al. Cytokine production and phenotype of *Histomonas Meleagridis*-specific T cells in the chicken. *Vet Res*. (2019) 50:107. doi: 10.1186/s13567-019-0726-z

131. Bagheri S, Paudel S, Wijewardana V, Kangethe RT, Cattoli G, Hess M, et al. Production of interferon gamma and interleukin 17a in chicken T-cell subpopulations hallmarks the stimulation with live, irradiated and killed avian pathogenic *Escherichia Coli*. *Dev Comp Immunol*. (2022) 133:104408. doi: 10.1016/j.dci.2022.104408

132. Ariaans MP, van de Haar PM, Lowenthal JW, van Eden W, Hensen EJ, Vervelde L. Elispot and intracellular cytokine staining: novel assays for quantifying T cell responses in the chicken. *Dev Comp Immunol*. (2008) 32:1398–404. doi: 10.1016/j.dci.2008.05.007

133. Andersen SH, Vervelde L, Sutton K, Norup LR, Wattrang E, Juul-Madsen HR, et al. Quantification and phenotypic characterisation of peripheral Ifn-Γ producing leucocytes in chickens vaccinated against Newcastle disease. *Vet Immunol Immunopathol*. (2017) 193-194:18–28. doi: 10.1016/j.vetimm.2017.10.001

134. Ruiz-Hernandez R, Peroval M, Boyd A, Balkissoon D, Staines K, Smith A, et al. An infected chicken kidney cell co-culture Elispot for enhanced detection of T cell responses to avian influenza and vaccination. *J Immunol Methods*. (2015) 416:40–8. doi: 10.1016/j.jim.2014.10.012

135. Qin Y, Tu K, Teng Q, Feng D, Zhao Y, Zhang G. Identification of novel T-cell epitopes on infectious bronchitis virus N protein and development of a multi-epitope vaccine. *J Virol*. (2021) 95:e0066721. doi: 10.1128/jvi.00667-21

136. Hao X, Zhang F, Yang Y, Shang S. The evaluation of cellular immunity to avian viral diseases: methods, applications, and challenges. *Front Microbiol*. (2021) 12:794514. doi: 10.3389/fmicb.2021.794514

137. Hao X, Li S, Chen L, Dong M, Wang J, Hu J, et al. Establishing a multicolor flow cytometry to characterize cellular immune response in chickens following H7n9 avian influenza virus infection. *Viruses*. (2020) 12. doi: 10.3390/v12121396

138. Luhtala M. Chicken Cd4, Cd8alphabeta, and Cd8alphaalpha T cell co-receptor molecules. *Poult Sci*. (1998) 77:1858–73. doi: 10.1093/ps/77.12.1858

139. Saalmüller A, Lunney JK, Daubenberger C, Davis W, Fischer U, Göbel TW, et al. Summary of the animal homologue section of Hlda 8. *Cell Immunol*. (2005) 236:51–8. doi: 10.1016/j.cellimm.2005.08.009

140. Conrad ML, Davis WC, Koop BF. Tcr and Cd3 antibody cross-reactivity in 44 species. *Cytometry A*. (2007) 71:925–33. doi: 10.1002/cyto.a.20435

141. Burkhardt NB, Elleder D, Schusser B, Krchlíková V, Göbel TW, Härtle S, et al. The discovery of chicken Foxp 3 demands redefinition of avian regulatory T cells. *J Immunol*. (2022) 208:1128–38. doi: 10.4049/jimmunol.2000301

142. Göbel TW, Schneider K, Schaerer B, Mejri I, Puehler F, Weigend S, et al. Il-18 stimulates the proliferation and Ifn-gamma release of Cd4+ T cells in the chicken: conservation of a Th1-like system in a nonmammalian species. *J Immunol*. (2003) 171:1809–15. doi: 10.4049/jimmunol.171.4.1809

143. Degen WG, Daal N, Rothwell L, Kaiser P, Schijns VE. Th1/Th2 polarization by viral and helminth infection in birds. *Vet Microbiol*. (2005) 105:163–7. doi: 10.1016/j.vetmic.2004.12.001

144. Shanmugasundaram R, Selvaraj RK. Regulatory T cell properties of chicken Cd4+Cd25+ cells. *J Immunol*. (2011) 186:1997–2002. doi: 10.4049/jimmunol.1002040

145. Lu M, Lee Y, Lillehoj HS. Evolution of developmental and comparative immunology in poultry: the regulators and the regulated. *Dev Comp Immunol*. (2023) 138:104525. doi: 10.1016/j.dci.2022.104525

146. Min W, Lillehoj HS. Isolation and characterization of chicken Interleukin-17 Cdna. *J Interf Cytokine Res*. (2002) 22:1123–8. doi: 10.1089/10799900260442548

147. Hong YH, Lillehoj HS, Lee SH, Dalloul RA, Lillehoj EP. Analysis of chicken cytokine and chemokine gene expression following Eimeria Acervulina and Eimeria Tenella infections. *Vet Immunol Immunopathol*. (2006) 114:209–23. doi: 10.1016/j.vetimm.2006.07.007

148. Kim WH, Jeong J, Park AR, Yim D, Kim S, Chang HH, et al. Downregulation of chicken Interleukin-17 receptor a during Eimeria infection. *Infect Immun*. (2014) 82:3845–54. doi: 10.1128/iai.02141-14

149. Kim WH, Jeong J, Park AR, Yim D, Kim Y-H, Kim KD, et al. Chicken Il-17f: identification and comparative expression analysis in Eimeria-infected chickens. *Dev Comp Immunol*. (2012) 38:401–9. doi: 10.1016/j.dci.2012.08.002

150. Walliser I, Göbel TW. Generation of glycosylphosphatidylinositol linked chicken Il-17 to generate specific monoclonal antibodies applicable for intracellular cytokine staining. *Dev Comp Immunol*. (2017) 73:27–35. doi: 10.1016/j.dci.2017.03.006

151. Walliser I, Göbel TW. Chicken Il-17a is expressed in Aβ and Γδ T cell subsets and binds to a receptor present on macrophages, and T cells. *Dev Comp Immunol*. (2018) 81:44–53. doi: 10.1016/j.dci.2017.11.004

152. Linti AE, Göbel TW, Früh SP. Chicken Γδ T cells proliferate upon Il-2 and Il-12 treatment and show a restricted receptor repertoire in cell culture. *Front Immunol*. (2024) 15:1325024. doi: 10.3389/fimmu.2024.1325024

153. Imhof BA, Dunon D, Courtois D, Luhtala M, Vainio O. Intestinal Cd8 alpha alpha and Cd8 alpha Beta intraepithelial lymphocytes are Thymus derived and exhibit subtle differences in Tcr Beta repertoires. *J Immunol*. (2000) 165:6716–22. doi: 10.4049/jimmunol.165.12.6716

154. Kasahara Y, Chen CH, Cooper MD. Growth requirements for avian Gamma Delta T cells include exogenous cytokines, receptor ligation and in vivo priming. *Eur J Immunol*. (1993) 23:2230–6. doi: 10.1002/eji.1830230927

155. Koskela K, Arstila TP, Lassila O. Costimulatory function of Cd28 in avian Gammadelta T cells is evolutionarily conserved. *Scand J Immunol*. (1998) 48:635–41. doi: 10.1046/j.1365-3083.1998.00441.x

156. Young JR, Davison TF, Tregaskes CA, Rennie MC, Vainio O. Monomeric homologue of mammalian Cd28 is expressed on chicken T cells. *J Immunol*. (1994) 152:3848–51. doi: 10.4049/jimmunol.152.8.3848

157. Braukmann M, Methner U, Berndt A. Avian Cd25(+) Gamma/Delta (Γδ) T Cells after Salmonella Exposure. *Vet Immunol Immunopathol*. (2015) 168:14–8. doi: 10.1016/j.vetimm.2015.09.010

158. Pieper J, Methner U, Berndt A. Heterogeneity of avian Gammadelta T cells. *Vet Immunol Immunopathol*. (2008) 124:241–52. doi: 10.1016/j.vetimm.2008.03.008

159. Laursen AMS, Kulkarni RR, Taha-Abdelaziz K, Plattner BL, Read LR, Sharif S. Characterizaton of Gamma Delta T cells in Marek's disease virus (Gallid herpesvirus 2) infection of chickens. *Virology*. (2018) 522:56–64. doi: 10.1016/j.virol.2018.06.014

160. Wieland E, Shipkova M. Lymphocyte surface molecules as immune activation biomarkers. *Clin Biochem*. (2016) 49:347–54. doi: 10.1016/j.clinbiochem.2015.07.099

161. Holling TM, Schooten E, van Den Elsen PJ. Function and regulation of Mhc class ii molecules in T-lymphocytes: of mice and men. *Hum Immunol*. (2004) 65:282–90. doi: 10.1016/j.humimm.2004.01.005

162. Guriec N, Bussy F, Gouin C, Mathiaud O, Le Goff M, Delarue J, et al. Activation of chicken Gamma-Delta T lymphocytes by a purified Ulvan extract. *Vet Immunol Immunopathol*. (2021) 237:110255. doi: 10.1016/j.vetimm.2021.110255

163. Peault B, Chen CL, Cooper MD, Barbu M, Lipinski M, Le Douarin NM. Phylogenetically conserved antigen on nerve cells and lymphocytes resembles myelin-associated glycoprotein. *Proc Natl Acad Sci USA*. (1987) 84:814–8. doi: 10.1073/pnas.84.3.814

164. Ratcliffe MJ, Boyd R, Chen CL, Vainio O. Avian cd nomenclature workshops, Montreal, June 1991, Budapest, august 1992 and Tours, September 1992. *Vet Immunol Immunopathol*. (1993) 38:375–86. doi: 10.1016/0165-2427(93)90095-l

165. Wattrang E, Norup LR, Juul-Madsen HR, Dalgaard TS. Preliminary characterisation of Cd107a and Cd57 as potential activation markers of chicken cytotoxic T-cells In: *XII avian immunology research group meeting*. Edinburgh, UK: (2012). 43.

166. Burgess SC, Young JR, Baaten BJ, Hunt L, Ross LN, Parcells MS, et al. Marek's disease is a natural model for lymphomas overexpressing Hodgkin's disease antigen (Cd30). *Proc Natl Acad Sci USA*. (2004) 101:13879–84. doi: 10.1073/pnas.0305789101

167. Zechmann M, Reese S, Göbel TW. Chicken Crtam binds Nectin-like 2 ligand and is upregulated on Cd8+ Aβ and Γδ T lymphocytes with different kinetics. *PLoS One*. (2013) 8:e81942. doi: 10.1371/journal.pone.0081942

168. Scherer S, Huhle D, Göbel TW. Identification of chicken Gitr and Gitr ligand, proof of their mutual interaction, and analysis of chicken Gitr tissue distribution by a novel antibody that reveals expression on activated T cells and erythrocytes. *Immuno Horizons*. (2018) 2:324–37. doi: 10.4049/immunohorizons.1800065

169. Osborne LC, Dhanji S, Snow JW, Priatel JJ, Ma MC, Miners MJ, et al. Impaired Cd8 T cell memory and Cd4 T cell primary responses in Il-7r alpha mutant mice. *J Exp Med*. (2007) 204:619–31. doi: 10.1084/jem.20061871

170. van Haarlem DA, van Kooten PJ, Rothwell L, Kaiser P, Vervelde L. Characterisation and expression analysis of the chicken Interleukin-7 receptor alpha chain. *Dev Comp Immunol*. (2009) 33:1018–26. doi: 10.1016/j.dci.2009.05.001

171. Gurjar RS, Gulley SL, van Ginkel FW. Cell-mediated immune responses in the head-associated lymphoid tissues induced to a live attenuated avian coronavirus vaccine. *Dev Comp Immunol*. (2013) 41:715–22. doi: 10.1016/j.dci.2013.08.002

172. Liu G, Wang Q, Tong T, Xiao Y, Bai Y, Liu S, et al. Construction and functional test of a chicken Mhc-I (Bf2*15)/peptide tetramer. *Vet Immunol Immunopathol*. (2008) 122:1–7. doi: 10.1016/j.vetimm.2007.10.019

173. Liu G, Wang Q, Liu N, Xiao Y, Tong T, Liu S, et al. Infectious bronchitis virus nucleoprotein specific Ctl response is generated prior to serum igg. *Vet Immunol Immunopathol*. (2012) 148:353–8. doi: 10.1016/j.vetimm.2012.06.028

174. Meier S, Stark R, Frentsch M, Thiel A. The influence of different stimulation conditions on the assessment of antigen-induced Cd154 expression on Cd4+ T cells. *Cytometry A*. (2008) 73:1035–42. doi: 10.1002/cyto.a.20640

175. Chattopadhyay PK, Yu J, Roederer M. Live-cell assay to detect antigen-specific Cd4+ T-cell responses by Cd154 expression. *Nat Protoc*. (2006) 1:1–6. doi: 10.1038/nprot.2006.1

176. Frentsch M, Arbach O, Kirchhoff D, Moewes B, Worm M, Rothe M, et al. Direct access to Cd4+ T cells specific for defined antigens according to Cd154 expression. *Nat Med*. (2005) 11:1118–24. doi: 10.1038/nm1292

177. Mura M, Chaudhury S, Farooq F, Duncan EH, Beck K, Bergmann-Leitner ES. Optimized flow cytometric protocol for the detection of functional subsets of low frequency antigen-specific Cd4(+) and Cd8(+) T cells. *Methods X*. (2020) 7:101005. doi: 10.1016/j.mex.2020.101005

178. Röll S, Härtle S, Lütteke T, Kaspers B, Härtle S. Tissue and time specific expression pattern of interferon regulated genes in the chicken. *BMC Genomics*. (2017) 18:264. doi: 10.1186/s12864-017-3641-6

frontiers | Frontiers in Veterinary Science

TYPE Original Research
PUBLISHED 28 May 2024
DOI 10.3389/fvets.2024.1378826

OPEN ACCESS

EDITED BY
Francesco Grandoni,
Council for Agricultural and Economics Research (CREA), Italy

REVIEWED BY
Valeria Martini,
University of Milan, Italy
Kelly Hughes,
Colorado State University, United States

*CORRESPONDENCE
Barbara C. Rütgen
barbara.ruetgen@vetmeduni.ac.at

RECEIVED 30 January 2024
ACCEPTED 02 May 2024
PUBLISHED 28 May 2024

CITATION
Rütgen BC, Wolfesberger B, Baumgartner D, Hammer SE, Groiss S, Hittmair KM, Gradner G, Fuchs-Baumgartinger A, Donovan TA and Schwendenwein I (2024) Flowcytometric data of intermediate-large cell gastrointestinal lymphoma presenting a gross mass in 32 cats – "let them glow in the flow".
Front. Vet. Sci. 11:1378826.
doi: 10.3389/fvets.2024.1378826

Flowcytometric data of intermediate-large cell gastrointestinal lymphoma presenting a gross mass in 32 cats – "let them glow in the flow"

Barbara C. Rütgen[1]*, Birgitt Wolfesberger[2], Daniel Baumgartner[1], Sabine E. Hammer[3], Sandra Groiss[3], Katharina M. Hittmair[4], Gabriele Gradner[5], Andrea Fuchs-Baumgartinger[6], Taryn A. Donovan[7] and Ilse Schwendenwein[1]

[1]Clinical Pathology, Department of Biological Sciences and Pathobiology, University of Veterinary Medicine Vienna, Vienna, Austria, [2]Clinical Unit of Internal Medicine Small Animals, Department for Companion Animals and Horses, University of Veterinary Medicine Vienna, Vienna, Austria, [3]Institute of Immunology, Department of Biological Sciences and Pathobiology, University of Veterinary Medicine Vienna, Vienna, Austria, [4]Diagnostic Imaging, Department for Companion Animals and Horses, University of Veterinary Medicine Vienna, Vienna, Austria, [5]Small Animal Hospital Clinic, Department for Companion Animals and Horses, University of Veterinary Medicine Vienna, Vienna, Austria, [6]Institute of Pathology, Department of Biological Sciences and Pathobiology, University of Veterinary Medicine Vienna, Vienna, Austria, [7]The Schwarzman Animal Medical Center, New York, NY, United States

Gastrointestinal lymphoma is the most common form of lymphoma in domestic cats. Aggressive phenotypes are much less common but do bear and unfavorable prognosis. Immunophenotyping by flow cytometry (FCM) is not systematically performed in these patients, because of difficulties in the acquisition of suitable sample material from the gastrointestinal tract. A multimodal diagnostic approach is recommended to improve identification of subtypes targeting patient tailored therapeutic strategies. The aim of this prospective study was to present results of multicolor FCM immunophenotyping in surgically removed gastrointestinal mass and relate them with histopathology using the World Health Organization (WHO) classification and clonality PCR testing. Thirty-two patients were included. Eight cats (25%) had gastric, 23 (72%) had intestinal lymphoma and 1 (3%) had gastric/jejunal lymphoma. Intestinal lymphoma sites were represented by 18 small intestinal, 4 ileocaecal, 1 large intestinal. All gastric lymphomas were diffuse large B-cell lymphoma (DLBCL). Small intestinal lymphomas were 10 enteropathy associated T-cell lymphoma type I (EATL I), 2 enteropathy associated T-cell lymphoma type II (EATL II), 2 peripheral T-cell lymphoma (PTCL), 3 DLBCL and one DLBCL+EATL II. The most common small intestinal FCM T-cell phenotype was $CD3^{+}CD21^{-}$ $CD4^{-}CD8^{-}CD18^{+}$ $CD5^{-}CD79^{-}$ in 7/10 EATL I and one EATL II. The most frequent FCM B-cell phenotype was $CD3^{-}CD21^{+}$ $CD4^{-}CD8^{-}CD18^{+}$ $CD5^{-}CD79^{+}$ in 13/17 DLBCL and the DLBCL+EATL II. Clonality PCR results were positive in 87.5% (28/32) of all cases. No cross-lineage rearrangement was observed. IHC and FCM results agreed in 87.5% (28/32) of all cases. When all 3 methods were combined, consistent results were seen in 75% (24/32). This is the first demonstration of a multicolor FCM approach set in context to the gold standard histopathology and clonality testing results.

KEYWORDS

feline lymphoma, flow cytometry, immunophenotyping, gastrointestinal, WHO classification

1 Introduction

Lymphoma is a common neoplasia of domestic cats, affecting multiple organ systems (1). In felines the gastrointestinal tract is the most common anatomic site of manifestation (2). Low-grade small intestinal T-cell lymphoma was recently described in detail (3, 4), but aggressive subtypes bearing an unfavorable prognosis are also observed (5, 6).

Currently, the World health organization (WHO) histologic classification is the diagnostic gold standard for feline lymphoma (7, 8) requiring a full thickness biopsy specimen, which is invasive and time-consuming (9). In contrast to the dog, feline gastrointestinal lymphoma, with the stomach and small intestines as the most commonly affected gastrointestinal regions, is not routinely diagnosed with rapid tools such as flow cytometry (FCM). An important reason for this is that fine needle aspirates of sufficient quantity and quality for FCM are difficult to obtain from these sites, thus, FCM is not an integral part of diagnostic workup. For this reason, descriptions of immunophenotypic expression patterns including CD4CD8 expression are scarce.

However, the fact that feline antibodies against CD4 and CD8 are only available for FCM or frozen biopsy samples, and not for paraffin embedded material, makes this method interesting for gaining basic insights into expression patterns and to expand knowledge (3, 10).

So far four retrospective studies on feline lymphoma mentioned FCM analysis in intestinal tissue, however, no systematically collected data is available (9, 11–13).

Roccabianca et al. (11) used FCM for the first time in feline intestinal tissues characterizing the non-malignant intraepithelial compartment (IEC) and the lamina propria compartment (LPC) lymphocytes in the intestines of 22 specific pathogen free (SPF) cats. The most comprehensive retrospective overview on FCM in feline lymphoma elucidates pre-analytic factors affecting the sample quality of peripheral lymph nodes, as well as abdominal or thoracic lymph nodes and masses (9). Guzera et al. (12) retrospectively analyzed 19 FNA samples of lymphoid material and documented the immunophenotype. Thirteen lymphoma cases consisted of 6 alimentary lymphoma samples of which five were of B-cell and one of T-cell origin (12). The most recent publication reported FCM data of different anatomic sites including GI-tract but also spleen and tarsus of seven cats and six dogs (13). FCM was only used in one patient. In this recent publication, four-color staining was chosen. In the other aforementioned papers, a single- or two-color approach was used.

In summary FCM data characterizing feline intestinal lymphoma is based on 6 cases in a single color stain (12). There is no information available about provable eg CD4CD8 double expression or multicolor staining.

Herewith we present FCM results gained by a multi-color approach from thirty-two cats with GI-lymphoma. Data are presented in relation to WHO classification and PCR clonality testing obtained from identical sampling sites. Multicolor FCM might be useful for identifying different expression patterns of feline alimentary lymphoma, aiding potential future patient tailored therapeutic approaches.

2 Materials and methods

2.1 Patient selection

Inclusion criteria for this study were presence of a surgically removable lymphoma mass exclusively present in the gastrointestinal tract, which was confirmed during the staging process. Lymphoma cases with diffuse wall thickening were not included in this series.

An initial tentative diagnosis was obtained by cytologic evaluation of an ultrasound guided fine needle aspiration smear of a suspect tumor mass from cats that were presented to the Clinic for Small Animals at the University of Veterinary Medicine, Vienna, Austria, between April 2016 and January 2021. With informed owners consent for further diagnostic workup and therapy, sample material was obtained via surgical procedures in which gross gastrointestinal masses were removed completely.

Data about the 3D size of the material used for the study was documented in cm^3.

The study was approved by an Ethics Committee and the Federal Ministry for Science and Research (referring number: GZ 68.205/0173-WF/V/3b/2015).

2.2 Patient material

Within 1 h of surgery, the excised neoplastic gastrointestinal material was processed. Immediately after excision the material was transferred into a 15 mL vial (Greiner Bio-One, Kremsmünster, Austria) containing 10 mL cell culture medium (RPMI, PAA, Pasching, Austria) supplemented with 10% inactivated fetal calf serum (FCS, PAA) and 100 U/mL penicillin/0.1 mg/mL streptomycin (PAA). The material was stored at 4°C for a maximum of 1 h until further processing, depending on the time of surgery. All tissue from each cat was then trimmed clean of surrounding fat and connective tissue and was cut in half. Tissue imprints were prepared for cytologic evaluation to affirm the presence of lymphoid cells in tumor material before immunophenotyping. Representative tumor mass was separately transferred into 4% buffered formaldehyde solution and prepared for histopathology and immunohistochemistry. From the neoplastic intestinal material in the cell culture medium, a single cell suspension was prepared by mincing the tissue through a sieve (mesh size 40 µm) and flushing bigger tissue parts with a syringe (BD Micro-Fine 0.5 mL Insulin syringe U-100, New Jersey, United States) using phosphate buffered saline (1 × PBS) without Ca2+ and Mg2+ (PAA). The single cell suspension was transferred to phosphate buffered saline and was centrifuged at 1300 U/min (353 g) for 6 min (Heraeus Multifuge 1 s-R,

Kendro, Osterode, Germany). The cell pellet was resuspended in 1 mL 1 × PBS and was used for Flow Cytometric immunophenotyping and PCR-based lymphocyte clonality testing.

2.3 Total nucleated cell count of single cell suspension for FCM

The total nucleated cell count (TNCC) was determined by an ADVIA 2120™ (Siemens, Austria) hematology analyzer with the veterinary software setting for cats.

2.4 Cytology

Cytocentrifuge preparations with approximately 5×10^5 cells from the single cell suspensions were stained by a Romanowsky dip stain (LT-Sys Haema-Schnellfaerbung™, Labor+ Technik, Berlin, Germany). All cytologic samples were microscopically inspected by the principal investigator (BR) and a board-certified clinical pathologist (IS). Cellularity, overall preservation of cells and morphology were evaluated. Criteria for cell differentiation included cell size, amount, color, granulation and vacuolization of cytoplasm, and topography, size, shape, and chromatin pattern of the nucleus, as previously described (14).

2.5 Flow cytometry

For immunophenotyping aliquots of the single cell suspensions were labelled with anti-feline, anti-human or anti-canine cross-reactive monoclonal antibodies (mAbs) listed in Tables 1, 2. The viability dye eBioscience™ Fixable Viability Dye eFluor™ 780 (Thermo Fischer Scientific, Life Technologies, Carlsbad, CA) was used for live/dead discrimination. Cells only and corresponding isotype controls to all corresponding antibodies were used as controls. All mAbs were directly conjugated to fluorochromes. For each analysis 5×10^5–1×10^6 cells were incubated with the specific mAbs or the isotype controls for 20 min on ice. After a washing step all labelled cells were immediately analyzed in a FACSCanto II flow cytometer™ (BD Biosciences, San Jose, CA, United States). For fixation and permeabilization prior to labelling intracellular antigens, anti CD79acy and anti CD3, the IntraStain-Kit™ (Dako, Glostrup, Denmark) was used according to the manufacturers' instructions. Combinations of monoclonal antibodies used for multi-color staining and the isotype controls are listed in Table 2.

Gating was performed for all samples using the forward scatter/side scatter (FSC/SSC) dot plot representing the size and the granularity of the cells/events. The target lymphoid population was gated, doublet discrimination was done, and the dead cells excluded by viability stain. The remaining living cells within the gate were used for the analysis of their antigen expression.

As there is no definite proved cut off published for a "monomorphic" expression pattern and a reactive pattern in FCM – in our lab we have the cut off with >90% of the gated cells showing the same expression pattern (eg all $CD3^+CD21^-$ $CD4^-CD8^-CD18^+$ $CD5^-CD79^-$) – as done in a former publication (12). The only reference available based on feline normal and mildly reactive peripheral lymph nodes describes a range of: $CD3^+$ 54.81% ± 11.10%, $CD5^+$ 57.39% ± 12.66%, $CD21^+$ 40.42% ± 12.40%, $CD79\alpha cy^+$ 30.41% ± 13.49%; 30.88% ± 13.48% $CD4^+$, 12.91% ± 6.68% $CD8^+$ cells (19). Cases eventually presenting with <90% uniformity and subpopulations within the reported ranges were not considered as lymphomas.

2.6 Histopathology and immunohistochemistry

The formalin-fixed samples of the gastrointestinal material were embedded in paraffin (FFPE samples), cut in 2 µm sections, stained with haematoxylin and eosin (H&E) and all examined microscopically by two veterinary anatomic pathologists (AFB, TAD).

Immunohistochemistry was performed with a LabVision-Autostainer (Thermo Fisher Scientific, Fremont, United States) using the Bright Vision HRP- Polymer method. FFPE samples were cut in 2 µm sections, deparaffinized, rehydrated and pre-treated with heat in pH 6 citrate for 20 min, incubated in Hydrogen Peroxidase Block (Thermo Fisher Scientific) for 5 min and in Ultra Vision Protein Block (Thermo Fisher Scientific) for another 10 min. A polyclonal rabbit

TABLE 1 List of monoclonal antibodies used for flow cytometric phenotyping of single cell suspension from gastrointestinal feline lymphoma biopsy material including clone, isotype, fluorescent label, source and target species/cross reactivity.

	Clone	Isotype	Fluorescence labelling	Source[a]	Target species / species cross reactivity
CD3	CD3-12	rIgG1	FITC	Bio-Rad	Anti-human (15)
CD4	vpg34	mIgG1	APC	Bio-Rad	Anti-feline
CD5	FE1.1B11	mIgG1	FITC	Bio-Rad	Anti-feline
CD8	vpg9	mIgG1	PE	Bio-Rad	Anti-feline
CD18	CA1.4E9	mIgG1	Alexa647	Bio-Rad	Anti-canine (16)
CD21	CA2.1D6	mIgG1	Alexa647	Bio-Rad	Anti-canine(16, 17)
CD79αcy	HM57	mIgG1	APC	Dako	Anti-human (18)

m, mouse; r, rat; FITC, fluorescein isothiocyanate; APC, allophycocyanin; PE, phycoerythrin.
[a]Bio-Rad, Hercules, CA, United States; Dako Cytomation, Glostrup, Denmark.

TABLE 2 Antibody combinations used for multi-color flow cytometric phenotyping of feline gastrointestinal lymphoma cells.

Tube Nr.	mAb	Source[a]
1	mIgG1-FITC	Bio-Rad
	mIgG1-PE	Bio-Rad
	mIgG1-Alexa647	Bio-Rad
2	CD4-FITC	Bio-Rad
	CD8-PE	Bio-Rad
	CD18-Alexa647	Bio-Rad
3	mIgG1-FITC	Bio-Rad
	mIgG1-APC	Dako
4	CD5-FITC	Bio-Rad
	CD79-APC	Dako
5	rIgG1-FITC	Bio-Rad
	mIgG1-Alexa647	Bio-Rad
6	CD3-FITC	Bio-Rad
	CD21-Alexa647	Bio-Rad

The tubes with the numbers 1, 3, 5 are the isotype controls followed by the respective specific antibody combinations in tubes 2, 4, 6. All tubes contained exclusively directly conjugated antibodies. Column 1 describes the number of the respective tubes, column 2 the monoclonal antibody, column 3 the company source of the antibody. The cells only and life dead staining control tube is not listed in the Table. In all tubes shown, the eBioscience™ Fixable Viability Dye eFluor™ 780 staining was added. m, mouse; r, rat; FITC, fluorescein isothiocyanate, APC, allophycocyanin; PE, phycoerythrin.
[a]Bio-Rad, Hercules, CA, United States; Dako Cytomation, Glostrup, Denmark, SouthernBiotech, Birmingham, Alabama, United States.

anti-human antibody against CD3 (Dako, Glostrup, Denmark; diluted 1:1000) and a polyclonal rabbit anti-human antibody against CD20 (Spring Biosciences, diluted 1:1000) was used. The samples were incubated with the primary antibodies for 30 min, and subsequently with the secondary antibodies (Bright Vision poly HRP anti rabbit IgG, Immunologic, Duiven, Netherlands) for 30 min. For visualization, DAB Quanto (Thermo Fisher Scientific) for 5 min was used and counterstained with Mayer's haematoxylin. A feline peripheral lymph node was used as positive control.

All samples were evaluated by one experienced veterinary anatomic pathologist (AFB) and one board certified anatomic pathologist (TAD). Consensus diagnosis was performed using the WHO classification (7).

2.7 Lymphocyte clonality testing

For the PCR-based lymphocyte clonality assay, total genomic DNA (gDNA) was extracted from 5×10^6 cells of the feline tissue with 200 µL elution buffer using a commercial kit following the manufacturers' instructions (E.Z.N.A Tissue DNA Kit™, Omega Biotech, Norcross, Georgia). Genomic DNA concentration and quality were determined using the NanoDrop 2000c™ spectrophotometer (Thermo Fisher Scientific, Waltham, MA, United States) in pedestal mode. The threshold was set to 30 ng/µL with desired 260/280 ratios of 1.8–2.0 and 260/230 ratios above or equal two (2.0–2.2) (20). The gDNA samples were assayed by amplifying a 189 base pair fragment of the feline androgen receptor gene (fAR), the immunoglobulin heavy chain (IGH-VDJ) gene rearrangements with the primer sets V1F2, V3F3 and V3F4 and the T-cell receptor gamma chain (TRG-VJ) gene rearrangements with the primer sets TRG-J1, TRG-J2 and TRG-J3 (20–22). Each PCR reaction was carried out in triplicate including positive and negative PCR controls in each PCR run (20, 23).

After PCR, 10 µL of DNA Dilution Buffer (Qiagen, Hilden, Germany) were added to each PCR reaction and size separated using the QIAxcel Advanced System capillary electrophoresis analyzer with the QIAxcel DNA High Resolution Kit and the QX Alignment Marker 15 bp/1000 bp (Qiagen). The presence and size of obtained PCR products was accurately determined using QIAxcel ScreenGel Software (Qiagen). Identical PCR triplicates verified the reproducibility of the clonality patterns, which were interpreted as described previously (20, 23, 24).

3 Results

3.1 Patient material

In total, gastrointestinal material from 32 cats with feline lymphoma was collected. Samples originated from 27 (84.5%) domestic shorthair cats, one (3.1%) Maine Coon, one (3.1%) Persian, one (3.1%) Abyssinian, one Norwegian forest cat (3.1%) and one (3.1%) Siamese cat. Ages ranged between 7 months and 14 years (mean 9.1 years, median 9 years). There were 12 (37.5%) castrated males, and 20 (62.5%) spayed females. The 7-month-old patient was FeLV positive. The 3D size of the removed gross gastrointestinal masses was from 3 to 729cm^3 (mean 84cm^3, median 20cm^3). All 32 samples were analyzed by FCM, clonality PCR and histopathology (Figure 1A).

3.2 Anatomic site

Eight out of 32 cats (25%) had gastric, 23 (72%) had intestinal lymphoma and 1 (3%) had gastric+jejunal lymphoma. Intestinal lymphoma sites were represented by 18 small intestinal, 4 ileocaecal, 1 large intestinal.

The 18 small intestinal lymphoma sites were 4 duodenum, 13 jejunum, one ileum (Figure 1A).

3.3 Total nucleated cell count of single cell suspension for FCM

Numbers of cells harvested from sampled gastrointestinal material of 27/32 patients ranged from 0.26×10^7 to 49×10^7 cells (mean 17.8×10^7, median 17.4×10^7). The gated population for the FCM analyses was from 11.3 to 99% (mean 39%, median 41.8%), cells alive were ranging from 38 to 99% (mean 87%, median 71%).

3.4 Cytology

The cytomorphologic evaluation of the gastrointestinal material was performed in all 32 cases as part of inclusion into the study using FNA material and was repeated with the solid material

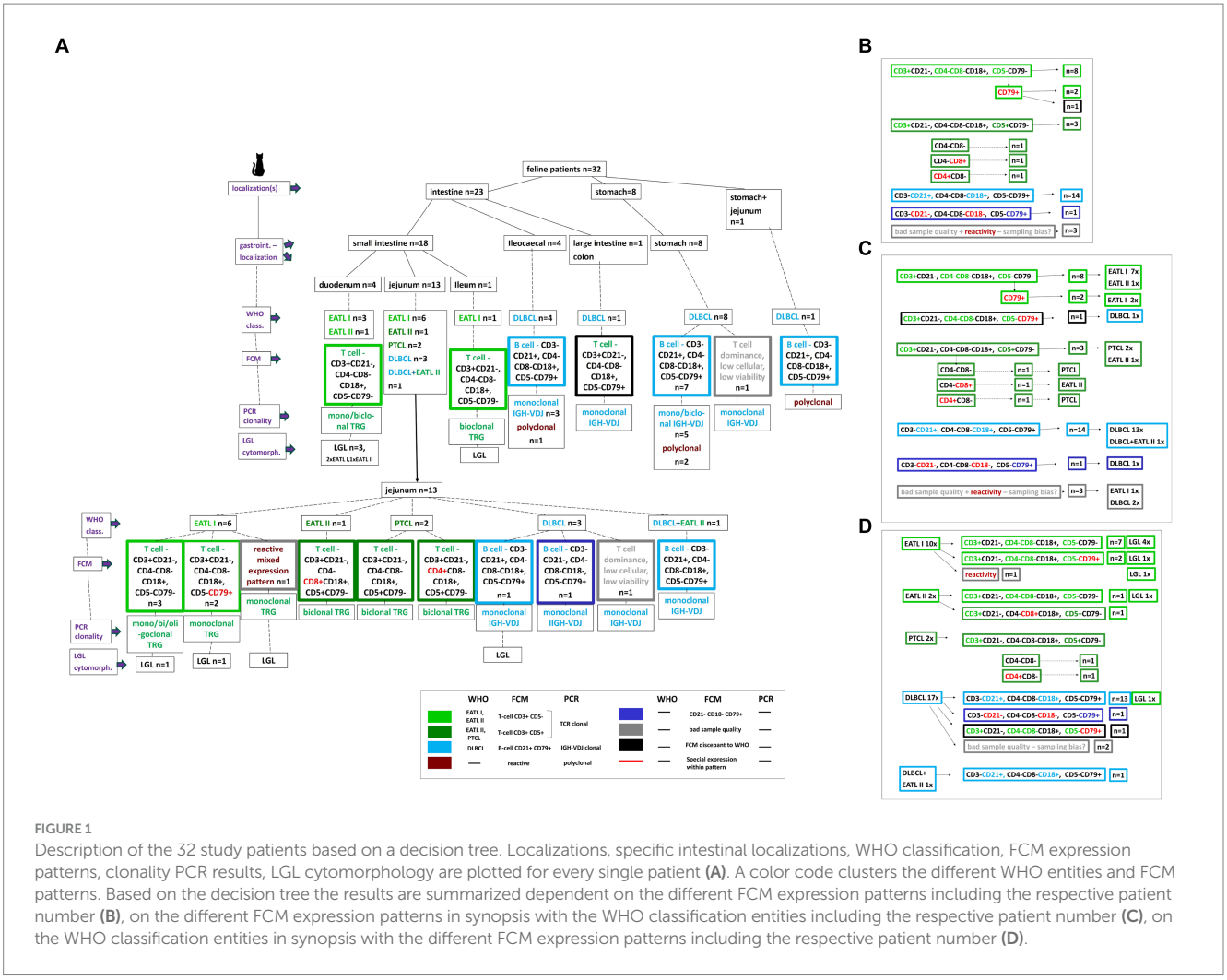

FIGURE 1
Description of the 32 study patients based on a decision tree. Localizations, specific intestinal localizations, WHO classification, FCM expression patterns, clonality PCR results, LGL cytomorphology are plotted for every single patient **(A)**. A color code clusters the different WHO entities and FCM patterns. Based on the decision tree the results are summarized dependent on the different FCM expression patterns including the respective patient number **(B)**, on the different FCM expression patterns in synopsis with the WHO classification entities including the respective patient number **(C)**, on the WHO classification entities in synopsis with the different FCM expression patterns including the respective patient number **(D)**.

from the surgically removed mass with cytospins and impression smears. Cytology was consistent with lymphoma in all cases. All samples showed intermediate to large size lymphoid cells with immature chromatin (Figures 2Aa+b). Morphologically inconclusive needing additional confirmation with clonality PCR prior to further diagnostics or therapy were not included. Large granulocyte lymphocyte (LGL) lymphoma was observed in 8 patients. Seven out of these eight were T-cell lymphomas. Three were in the duodenum, 4 in the jejunum and one in the ileum (Figures 1A+D).

3.5 Immunophenotyping – flow cytometry

3.5.1 Immunophenotypic expression patterns

3.5.1.1 T-cell immunophenotype

The most common T-cell phenotype was **CD3**$^+$CD21$^-$ **CD4**$^-$**CD8**$^-$**CD18**$^+$ CD5$^-$CD79$^-$ in 8 cases. Three cases were **CD3**$^+$CD21$^-$ **CD4**$^-$**CD8**$^-$**CD18**$^+$ CD5$^-$**CD79**$^+$. Three cases were positive for CD3 and CD5 but showing a variable CD4CD8 expression. One case each of these were **CD3**$^+$CD21$^-$ **CD4**$^-$**CD8**$^-$**CD18**$^+$ **CD5**$^+$CD79$^-$, **CD3**$^+$CD21$^-$ **CD4**$^+$CD8$^-$**CD18**$^+$ CD5$^-$CD79$^-$ and **CD3**$^+$CD21$^-$ CD4$^-$**CD8**$^+$**CD18**$^+$ CD5$^-$CD79$^-$ (Figure 1B).

3.5.1.2 B-cell immunophenotype

The dominating B-cell immunophenotype was CD3$^-$**CD21**$^+$ CD4$^-$CD8$^-$**CD18**$^+$ CD5$^-$**CD79**$^+$ in 14 cases. One was CD3$^-$CD21$^-$ CD4$^-$CD8$^-$CD18$^-$ CD5$^-$**CD79**$^+$.

Three cases did not show a definitive immunophenotypic pattern. Two were of T cell dominance with <10% B cells; most suggestive but not definitive of T cell lymphoma and one showed mixed lymphoid cells compatible with a reactive phenotype expression pattern.

From the values here these expression results of these patients were between published ranges and < 90% uniformity (12) – so they were not considered as definitive lymphomas in FCM.

3.5.2 Immunophenotypic expression based on localization

The most common small intestinal T-cell phenotype was **CD3**$^+$CD21$^-$ **CD4**$^-$**CD8**$^-$**CD18**$^+$ CD5$^-$CD79$^-$ (Figures 1A, 2Bb) in 8/18 cases. Four are localized in the duodenum, 3 in the jejunum and one in the ileum. Two cases showed the same expression pattern except of being **CD79+**. All these cases were CD3+ and CD5- and were localized in the jejunum. In contrast to this, 3 jejunal cases were positive for CD3 and CD5 but showing a variable CD4CD8 expression. One case each of these were **CD3**$^+$CD21$^-$ **CD4**$^-$**CD8**$^-$**CD18**$^+$ **CD5**$^+$CD79$^-$, **CD3**$^+$CD21$^-$ **CD4**$^+$CD8$^-$**CD18**$^+$ CD5$^-$CD79$^-$ and **CD3**$^+$CD21$^-$ CD4$^-$**CD8**$^+$**CD18**$^+$ CD5$^-$CD79$^-$. Of the remaining small intestinal samples, 2 showed a

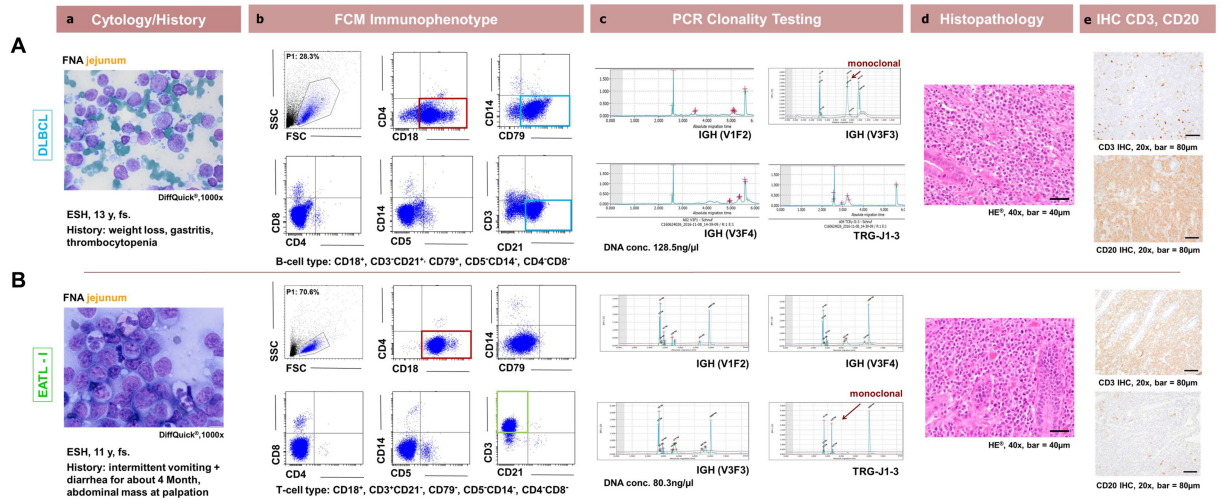

FIGURE 2
Comparison between patient cytology, flow cytometry, PCR for lymphocyte clonality testing, histopathology and immunohistochemistry in feline intestinal lymphoma immunophenotyping. Corresponding cytological (**a**, DiffQuick®1,000x), flow cytometrical plots for Immunophenotyping (**b**, showing the corresponding FSC/SSC (P1), CD18/CD4, CD79/SSC, CD4/CD8, CD5/SSC, CD21/CD3 dot plots), (**c**, capillary electropherogram traces for IGH-VDJ and TRG (V1F1, V3F3, V3F4, TRG-J1-3) including the DNA concentration in ng/µl evaluated photometrically) clonality PCR traces, histopathological (**d**, H + E, 400x) and immunohistochemical (**e**, DAB chromogen, 200x) images are shown for 2 representative patients. In the first row **(A)** represents a 13y, fs ESH cat with a jejunal DLBCL showing CD3$^-$ **CD21$^+$** CD4$^-$CD8$^-$ **CD18$^+$** CD5$^-$ **CD79$^+$** expression and a monoclonal IGH-VDJ antigen receptor rearrangement and CD20+ with IHC. In the second row **(B)** represents a 11y, fs ESH cat with a jejunal EATLI showing **CD3$^+$** CD21$^-$ CD4$^-$CD8$^-$ **CD18$^+$** CD5$^-$CD79$^-$ expression and a monoclonal TRG antigen receptor rearrangement and CD3+ with IHC. The FSC/SSC (P1) gated population is marked in blue **(Ab,Bb)** and is represented in the subsequent dot plots. It is chosen due to size and granularity and life / dead discrimination. The cytological images are consistent with lymphoma for each case. CD18 expression is marked in red, CD3 expression in green and CD21 and CD79 expression in light blue.

CD3$^-$**CD21$^+$** CD4$^-$CD8$^-$**CD18$^+$** CD5$^-$**CD79$^+$** B-cell phenotype, one was negative for all antibodies except CD79 (CD3$^-$CD21$^-$ CD4$^-$CD8$^-$CD18$^-$ CD5$^-$**CD79$^+$**), one showed a mixed lymphoid cell expression compatible with a reactive flow cytometric immunophenotype and one T cell dominance with <10% B cells; most suggestive but not definitve of T cell lymphoma. These were all located in the jejunum (Figure 1A).

All 4 lymphomas located ileocaecal had the same expression B-cell pattern of CD3$^-$**CD21$^+$** CD4$^-$CD8$^-$**CD18$^+$** CD5$^-$**CD79$^+$** (Figures 1A, 2Ba).

Seven out of the 8 gastric lymphomas the same B-cell of CD3$^-$**CD21$^+$** CD4$^-$CD8$^-$**CD18$^+$** CD5$^-$**CD79$^+$** as well. One gastric lymphoma was of T cell dominance with <10% B cells; most suggestive but not definitive of T cell lymphoma (Figure 1A).

The one large intestinal lymphoma was of T-cell expression being **CD3$^+$**CD21$^-$ **CD4$^-$CD8$^-$CD18$^+$** CD5$^-$**CD79$^+$** (Figure 1A).

The last remaining case localized in stomach/jejunum was of the dominant B-cell pattern of CD3$^-$**CD21$^+$** CD4$^-$CD8$^-$**CD18$^+$** CD5$^-$**CD79$^+$** (Figure 1A).

3.6 Histopathology and immunohistochemistry based on localization

Small intestinal lymphomas were represented by 10 EATL I, 2 EATL II, 2 PTCL, 3 DLBCL and one DLBCL+EATL II. Within the small intestinal lymphomas, the 4 duodenal lymphomas were 3 EATL I and 1 EATL II. The 13 jejunal lymphomas were 6 EATL I, 1 EATL II, 2 PTCL, 3 DLBCL and one DLBCL+EATL II. All 8 gastric lymphomas were DLBCL.

The 4 ileocaecal lymphomas were all DLBCL. Also, the one large intestinal lymphoma (colon) was a DLBCL as well as the lymphoma located in stomach and jejunum (Figures 1A, 2d+e).

Abdominal lymph node involvement was observed by histopathology in 12/17 DLBCL, 2/2 PTCL, 3/10 EATL I, 1/2 EATL II and in the DLBCL+EATL II case.

3.7 Lymphocyte clonality testing

Clonality testing, performed in all 32 patients, showed clonality for TRG in 14 cases, with IGH-VDJ clonality in 14 samples. A polyclonal result was seen in 4 B-cell lymphoma cases. Out of the TRG clonal PCR results, 8 were monoclonal, 5 were biclonal and one was oligoclonal. The clonal IGH-V DJ cases were represented by 13 monoclonal and one biclonal result (Figures 1A, 2c).

In summary clonality PCR results were positive in 87.5% (28/32) of all cases. No cross-lineage rearrangement was observed.

3.8 Immunophenotypic expression matched with localization, histopathologic who classification and clonality PCR

The most common small intestinal T-cell phenotype was **CD3$^+$**CD21$^-$ **CD4$^-$CD8$^-$**CD18$^+$ **CD5$^-$CD79$^-$** seen in 8 cases. Seven out of these were EATL I and one was EATL II in all small intestinal areas.

Three cases were **CD3**$^+$CD21$^-$ **CD4**$^-$**CD8**$^-$CD18$^+$ **CD5**$^-$**CD79**$^+$. Two of them were EATL I in the jejunum, one was a DLBCL in the colon.

The three cases being **CD5**$^+$ in contrast to the before mentioned samples were of variable CD4CD8 expression. The CD4$^-$**CD8**$^+$ cytotoxic T-cell lymphoma was jejunal EATL II, the **CD4**$^+$CD8$^-$ T-helper cell lymphoma a jejunal PTCL and the **CD4**$^-$**CD8**$^-$ lymphoma a jejunal PTCL as well.

The dominating expression pattern in the 14 B-cell lymphomas, CD3$^-$**CD21**$^+$ CD4$^-$CD8$^-$CD18$^+$ CD5$^-$**CD79**$^+$ was in all except one case diagnosed as DLBCL. Localization was ileocaecal (4), stomach (7), stomach+jejunum (1), and jejunum (1). One case was histopathologically a jejunal DLBCL+EATL II.

One jejunal DLBCL lymphoma case was CD3$^-$**CD21**$^-$ CD4$^-$CD8$^-$CD18$^-$ CD5$^-$**CD79**$^+$.

One jejunal case showed heterogeneous lymphoid cells compatible with reactive immunophenotype being diagnosed as EATL I. The two cases showing a dominant T-cell expression with <10% B cells were both diagnosed with DLBCL in histopathology. All patterns see Figures 1C +D.

A polyclonal clonality PCR result was seen in 4/32 cases representing a false negative result based on FCM and histopathology (Figure 1A). These were all DLBCL lymphoma. All other TRG and IGH-VDJ clonality results were in all cases in line with histopathology and immunohistochemistry.

IHC and FCM results were in agreement in 87.5% (28/32) of all cases. When all 3 methods were combined, consistent results were seen in 75% (24/32).

4 Discussion

This is the first report of FCM data obtained by a standardized multi-color approach aligned to WHO classification and PCR-clonality testing in cats with GI-lymphoma.

In this cohort the CD4$^-$CD8$^-$ immunophenotype predominated in both most frequently affected small intestinal sites (duodenum and jejunum). One study investigated CD4CD8 in feline low grade intestinal T-cell lymphoma (LGITL) using IHC of frozen samples in 11 cats, predominantly with jejunal LGITL (3). Four out of 11 (36%) cases were CD4$^-$CD8$^-$, four (36%) were CD4$^+$CD8$^-$ and three cases (27%) were CD4$^-$CD8$^+$. The more homogeneous distribution between CD4 and CD8 positivity in the latter report might be explained by the different WHO entities investigated in our dataset namely EATL I and EATL II. Nevertheless, in our cohort CD3$^+$CD4$^-$CD8$^-$CD5$^-$ predominated in EATL I.

Regarding the CD4CD8 expression in physiologic feline intestinal epithelial lymphocytes (IELs) Roccabianca et al. (11) reported a high prevalence (44%) of CD4$^-$CD8$^-$ IELs in specific pathogen free (SPF) healthy cats. In other species like the dog, comparable CD4$^-$CD8$^-$ IEL cell populations was reported only in neonatal healthy Swiss Beagle dogs showing TCRγδ$^+$ and representing approximately 20% of all IELs. However, the dominant remaining (80%) TCRαβ$^+$ IELs in these neonatal and adult Beagles did not comprise more than 10% CD4$^-$CD8$^-$ cells (25). This fact leads to the conclusion that in the canine species a population exceeding 10% of CD4$^-$CD8$^-$ TCRαβ$^+$ IELs is considered atypical. To the authors knowledge there is no anti-TCRαβ/γδ available for FCM in cats so that a full comparison between species is currently not possible. However, cats may contain a unique IEL phenotype as described above in Roccabianca et al. (11) in IELs in SPF healthy cats regarding their CD4CD8 expression. For this reason, a predominance of this double negative population in feline intestinal FCM might indicate neoplastic disease, if confirmed by a larger body of evidence in the future. Until then clonality testing is a helpful complementary tool, because immunophenotypic dominance cannot discriminate between a clonal versus polyclonal population. In the present study all CD4$^-$CD8$^-$ cases showed a clonal result. This fact emphasizes the necessity of a multimodal diagnostic approach and underlines the usefulness of clonality testing as an adjacent tool discriminating between reactive and malignant lymphocyte populations.

In our case series only one **CD3**$^+$CD21$^-$ **CD4**$^+$CD8$^-$**CD18**$^+$ CD5$^-$CD79$^-$ helper cell lymphoma and one **CD3**$^+$CD21$^-$ CD4$^-$**CD8**$^+$**CD18**$^+$ CD5$^-$CD79$^-$ cytotoxic T cell lymphoma was observed. The cytotoxic T-cell lymphoma was EATL II and the T-helper cell lymphoma a PTCL.

In the study by Freiche and colleagues 36% of LGITL were CD4$^+$ and 27% were CD8$^+$ (3). Again, this discrepancy is most likely caused by the different WHO entities investigated and needs further studies with an extended FCM panel including CD4 and CD8.

Nevertheless, all cases in our series showing either CD4 or CD8 positivity also expressed CD5. In contrast, all CD4$^-$CD8$^-$ negative cases except one were also negative for CD5. In addition to that, no EATL I lymphoma showed CD4, CD8 nor CD5 positivity. All CD5 positive cases were represented by EATL II or PTCL. This finding needs further investigation because it might indicate a relation between immunophenotype and WHO entities.

Three intestinal cases (21.4%) showed double positive expression for B and T-cell antigens being **CD3**$^+$CD21$^-$ CD4$^-$CD8$^-$**CD18**$^+$ CD5$^-$**CD79**$^+$. Two of them were EATL I, and one a DLBCL.

In recent years, many groups performing diagnostic FCM in the veterinary field observed non-specific binding of neoplastic T cells to CD79αcy (W Vernau, 2021, personal communication). In dogs and in cats, non-specific binding of neoplastic T cells has been observed. Thus, CD79αcy must be considered a less reliable antibody for labelling B cells than CD21 (19). The single case of DLBCL exhibiting CD3 positivity in our case series was the only one showing discrepant results with histopathology and clonality testing being monoclonal for IGH-VDJ.

In general, CD3 is considered a reliable antibody against T-cells in many species, including domestic cats. However, an aberrant expression in this case cannot be excluded. In humans a false positive CD3 expression is reported to be related with 24–72 h storage (26). This can be excluded in our case because all samples were processed within 1 hour after surgery.

When all 3 methods, FCM, WHO classification and clonality PCR were combined, consistent results were seen in 75% (24/32). One of the 8 discrepant results is the CD3$^+$ CD79$^+$ case mentioned above for which an explanation for the FCM mismatch could not be identified. For the remaining 7 discrepant results reasonable explanations were found. Three cases showed low cellularity and cell viability in FCM so that heterogeneous lymphoid cells compatible with a reactive phenotype and T-cell predominance was observed. Two of them were DLBCL, one in the stomach, one in the jejunum and the remaining case was a jejunal EATL I with consistency between WHO and clonality PCR. A preanalytical problem in processing the sample is the most likely explanation. These cases are reported to underline the fact that a multimodal approach is advisable especially when clinical findings (tumor size!) indicate neoplasia.

A probably false negative PCR result is assumed in the remaining inconsistent cases as the results are overruled by histopathology as current gold standard. The false negative rate for clonality PCR was 12.5% resulting in a diagnostic sensitivity of 87.5% which is slightly below the expected sensitivity of 90% for this assay (23). All false negative cases were DLBCL lymphomas. Somatic hypermutations which can occur with B-cell neoplasia might be a possible explanation (24). All other TRG and IGH-VDJ clonality results agreed with immunophenotyping using histopathology and immunohistochemistry, thus no cross-lineage rearrangement was observed.

Regarding the B-cell immunophenotyping, the dominant expression pattern in the 14 B-cell lymphomas was CD3$^-$**CD21**$^+$ CD4$^-$CD8$^-$**CD18**$^+$ CD5$^-$**CD79**$^+$ in the 7 stomach, all 4 ileocaecal region, 1 jejunal and the one stomach+jejunum cases. These were all DLBCL. This agrees with FCM expression patterns for DLBCL in other species (27).

One case showing the same expression as above, CD3$^-$**CD21**$^+$ CD4$^-$CD8$^-$**CD18**$^+$ CD5$^-$**CD79**$^+$, comprised two separate concurrent histopathologic populations; a small cell mucosal lymphoma (EATLII), superimposed by a DLBCL, confirmed with IHC. This entity is not described in the WHO but observed occasionally in feline intestinal lymphoma cases (A Durham, 2022, personal communication). In FCM and clonality PCR testing, the T-cell lymphoma population was not detected. Sampling bias for FCM and clonality PCR is the most likely explanation.

One jejunal DLBCL lymphoma case was CD3$^-$CD21$^-$ CD4$^-$CD8$^-$CD18$^-$ CD5$^-$**CD79**$^+$. The solitary positivity for CD79 with negativity for the pan antibody CD18 and the reliable B-cell CD21 makes this FCM result not reliable for a B-cell type. However, DLBCL diagnosis supported by monoclonality for IGH-VDJ were proof for B-cells in this case. The loss of CD18 positivity in a B-cell lymphoma has not been described so far. This should be investigated in the future. This underlines in addition inclusion of further test in such cases.

Further studies using an extended panel of antibodies in a multi-color FCM approach are needed for better understanding of different expression patterns. Nevertheless, in the preset cohort, the frequent FCM B-cell immunophenotype in 13/14 B-cell cases seems to be more uniformly expressed within the DLBCL entity even in different sites along the GI-tract. In contrast to this, more diverse expression patterns are seen in the T-cell immunophenotype throughout the different small intestinal regions.

In general, the distribution of B and T-cell phenotype with dominance of T-cell immunophenotypic EATL I in the small intestine and B-cell FCM immunophenotypic DLBCL in gastic, ileocaecal and large intestine (colon) agrees with former reports (5).

5 Conclusion

We describe different FCM expression patterns of WHO entities in feline GI-lymphoma of different sites aligned with PCRclonality results in a cohort of 32 patients. Results are intended to provide a starting point for further research attempting to match FCM expression patterns to WHO-entities as already done in other species (28). Until more data are available a multimodal approach is still recommended.

6 Limitations of the study

A low and heterogeneous case load of 32 patients is the first limitation, which prohibited in depth statistical workup. The other limitation is the inclusion of discrepant results in some cases, which raise more questions than answers. We decided to report these findings to share our experience and stimulate further discussions.

Data availability statement

The raw data supporting the conclusions of this article will be made available by the authors, without undue reservation.

Ethics statement

The animal studies were approved by Ethics Committee and the Federal Ministry for Science and Research (referring number: GZ 68.205/0173-WF/V/3b/2015). The studies were conducted in accordance with the local legislation and institutional requirements. Written informed consent was obtained from the owners for the participation of their animals in this study.

Author contributions

BR: Conceptualization, Data curation, Formal analysis, Methodology, Visualization, Writing – original draft. BW: Project administration, Supervision, Writing – review & editing. DB: Formal analysis, Writing – review & editing. SH: Writing – review & editing. SG: Writing – review & editing. KH: Writing – review & editing. GG: Writing – review & editing. AF-B: Writing – review & editing. TD: Writing – review & editing. IS: Writing – review & editing.

Funding

The author(s) declare that no financial support was received for the research, authorship, and/or publication of this article.

Conflict of interest

The authors declare that the research was conducted in the absence of any commercial or financial relationships that could be construed as a potential conflict of interest.

Publisher's note

References

1. Vail DM, Pinkerton ME, Young KM. Hematopoietic tumors In: SJ Withrow, DM Vail and RL Page, editors. *Withrow and MacEwen's small animal clinical oncology*. St Louis, MO: Elsevier Health Sciences (2013). 608–37.

2. Louwerens M, London CA, Pedersen NC, Lyons LA. Feline lymphoma in the post-feline leukemia virus era. *J Vet Intern Med*. (2005) 19:329–35. doi: 10.1892/0891-6640(2005)19[329:flitpl]2.0.co;2

3. Freiche V, Paulin MV, Cordonnier N, Huet H, Turba ME, Macintyre E, et al. Histopathologic, phenotypic, and molecular criteria to discriminate low-grade intestinal T-cell lymphoma in cats from lymphoplasmacytic enteritis. *J Vet Intern Med*. (2021) 35:2673–84. doi: 10.1111/jvim.16231

4. Marsilio S, Freiche V, Johnson E, Leo C, Langerak AW, Peters I, et al. ACVIM consensus statement guidelines on diagnosing and distinguishing low-grade neoplastic from inflammatory lymphocytic chronic enteropathies in cats. *J Vet Intern Med*. (2023) 37:794–816. doi: 10.1111/jvim.16690

5. Moore PF, Rodriguez-Bertos A, Kass PH. Feline gastrointestinal lymphoma: mucosal architecture, immunophenotype, and molecular clonality. *Vet Pathol*. (2012) 49:658–68. doi: 10.1177/0300985811404712

6. Wolfesberger B, Skor O, Hammer SE, Flickinger I, Kleiter M, Rütgen BC, et al. Does categorisation of lymphoma subtypes according to the World Health Organization classification predict clinical outcome in cats? *J Feline Med Surg*. (2017) 19:897–906. doi: 10.1177/1098612X16666119

7. Valli VEO, Kiupel M, Bienzle D. Hematopoietic system In: MG Maxie, editor. *Pathology of domestic animals*. Missouri: Elsevier Inc (2016). 213–35.

8. Wolfesberger B, Fuchs-Baumgartinger A, Greß V, Hammer SE, Gradner G, Knödl K, et al. World Health Organisation classification of lymphoid Tumours in veterinary and human medicine: a comparative evaluation of gastrointestinal lymphomas in 61 cats. *J Comp Pathol*. (2018) 159:1–10. doi: 10.1016/j.jcpa.2017.12.006

9. Martini V, Bernardi S, Marelli P, Cozzi M, Comazzi S. Flow cytometry for feline lymphoma: a retrospective study regarding pre-analytical factors possibly affecting the quality of samples. *J Feline Med Surg*. (2018) 20:494–501. doi: 10.1177/1098612X17717175

10. Paulin MV, Couronné L, Beguin J, Le Poder S, Delverdier M, Semin MO, et al. Feline low-grade alimentary lymphoma: an emerging entity and a potential animal model for human disease. *BMC Vet Res*. (2018) 14:306. doi: 10.1186/s12917-018-1635-5

11. Roccabianca P, Woo JC, Moore PF. Characterization of the diffuse mucosal associated lymphoid tissue of feline small intestine. *Vet Immunol Immunopathol*. (2000) 75:27–42. doi: 10.1016/s0165-2427(00)00181-1

12. Guzera M, Cian F, Leo C, Winnicka A, Archer J. The use of flow cytometry for immunophenotyping lymphoproliferative disorders in cats: a retrospective study of 19 cases. *Vet Comp Oncol*. (2014) 14:40–51. doi: 10.1111/vco.12098

13. Hughes KL, Rout ED, Avery PR, Pavuk AA, Avery AC, Moore AR. A series of heterogeneous lymphoproliferative diseases with CD3 and MUM1 co-expressed in cats and dogs. *J Vet Diagn Invest*. (2023) 35:22. doi: 10.1177/10406387221139799

14. Raskin RE. Hematopetic system – lymph nodes In: RE Raskin, DJ Meyer and KM Boes, editors. *Canine and feline cytopathology*. St. Louis, Missouri: Elsevier (2023). 124–49.

15. Steinberg JD, Keating JH. What is your diagnosis? Cervical mass in a cat. *Vet Clin Pathol*. (2008) 37:323–7. doi: 10.1111/j.1939-165X.2008.00033.x

16. Brodersen R, Bijlsma F, Gori K, Jensen KT, Chen W, Dominguez J, et al. Analysis of the immunological cross reactivities of 213 well characterized monoclonal antibodies with specificities against various leucocyte surface antigens of human and 11 animal species. *Vet Immunol Immunopathol*. (1998) 64:1–13. doi: 10.1016/s0165-2427(98)00117-2

17. Dean GA, Reubel GH, Moore PF, Pedersen NC. Proviral burden and infection kinetics of feline immunodeficiency virus in lymphocyte subsets of blood and lymph node. *J Virol*. (1996) 70:5165–9. doi: 10.1128/JVI.70.8.5165-5169.1996

18. Mason DY, Cordell JL, Tse AGD, van Dongen JJM, van Noesel CJM, Micklem K, et al. The IgM-associated protein mB 1 as a marker of normal and neoplastic B cells. *J Immunol*. (1991) 147:2474–82. doi: 10.4049/jimmunol.147.8.2474

19. Rütgen BC, Baszler E, Weingand N, Wolfesberger B, Baumgartner D, Hammer SE, et al. Composition of lymphocyte subpopulations in normal and mildly reactive peripheral lymph nodes in cats. *J Feline Med Surg*. (2022) 24:77–90. doi: 10.1177/1098612X211005310

20. Hammer SE, Groiss S, Fuchs-Baumgartinger A, Nedorost N, Gress V, Luckschander-Zeller N, et al. Characterization of a PCR-based lymphocyte clonality assay as a complementary tool for the diagnosis of feline lymphoma. *Vet Comp Oncol*. (2017) 15:1354–69. doi: 10.1111/vco.12277

21. Mochizuki H, Nakamura K, Sato H, Goto-Koshino Y, Sato M, Takahashi M, et al. Multiplex PCR and Genescan analysis to detect immunoglobulin heavy chain gene rearrangement in feline B-cell neoplasms. *Vet Immunol Immunopathol*. (2011) 143:38–45. doi: 10.1016/j.vetimm.2011.05.030

22. Mochizuki H, Nakamura K, Sato H, Goto-Koshino Y, Sato M, Tahashi M, et al. GeneScan analysis to detect clonality of T-cell receptor gene rearrangement in feline lymphoid neoplasms. *Vet Immunol Immunopathol*. (2012) 145:402–9. doi: 10.1016/j.vetimm.2011.12.015

23. Gress V, Wolfesberger B, Fuchs-Baumgartinger A, Nedorost N, Saalmüller A, Schwendenwein I, et al. Characterization of the T-cell receptor gamma chain gene rearrangements as an adjunct tool in the diagnosis of T-cell lymphomas in the gastrointestinal tract of cats. *Res Vet Sci*. (2016) 107:261–6. doi: 10.1016/j.rvsc.2016.07.004

24. Keller SM, Vernau W, Moore PF. Clonality testing in veterinary medicine: a review with diagnostic guidelines. *Vet Pathol*. (2016) 53:711–25. doi: 10.1177/0300985815626576

25. Luckschander N, Pfamatter NS, Sidler D, Jakob S, Burgener IA, Moore PF, et al. Phenotyping, functional characterization, and developmental changes in canine intestinal intraepithelial lymphocytes. *Vet Res*. (2009) 40:58. doi: 10.1051/vetres/2009042

26. Nagel A, Möbs C, Raifer H, Wiendl H, Hertl M, Eming R. CD3-positive B cells: a storage-dependent phenomenon. *PLoS One*. (2014) 9:e110138. doi: 10.1371/journal.pone.0110138

27. Rütgen BC, Hammer SE, Gerner W, Christian M, Guija de Arespagochaga A, Willmann M, et al. Establishment and characterization of a novel canine B-cell line derived from a spontaneously occurring diffuse large cell lymphoma. *Leuk Res*. (2010) 34:932–8. doi: 10.1016/j.leukres.2010.01.021

28. Seelig DM, Avery P, Webb T, Yoshimoto J, Bromberek J, Ehrhart EJ, et al. Canine T-zone lymphoma: unique Immunophenotypic features, outcome, and population characteristics. *J Vet Intern Med*. (2014) 28:878–86. doi: 10.1111/jvim.12343

frontiers | Frontiers in Veterinary Science

TYPE Original Research
PUBLISHED 29 May 2024
DOI 10.3389/fvets.2024.1390486

OPEN ACCESS

EDITED BY
Francesco Grandoni,
Council for Agricultural and Economics Research (CREA), Italy

REVIEWED BY
Kate M. Sutton,
University of Edinburgh, United Kingdom
Asmaa H. Mahmoud,
Washington State University, United States

*CORRESPONDENCE
Selma Schmidt
✉ selma.schmidt@pirbright.ac.uk

RECEIVED 23 February 2024
ACCEPTED 10 May 2024
PUBLISHED 29 May 2024

CITATION
Moorton M, Tng PYL, Inoue R, Netherton CL, Gerner W and Schmidt S (2024) Investigation of activation-induced markers (AIM) in porcine T cells by flow cytometry. *Front. Vet. Sci.* 11:1390486. 10.3389/fvets.2024.1390486

Investigation of activation-induced markers (AIM) in porcine T cells by flow cytometry

Madison Moorton[1,2], Priscilla Y. L. Tng[1], Ryo Inoue[3], Christopher L. Netherton[1], Wilhelm Gerner[1] and Selma Schmidt[1]*

[1]The Pirbright Institute, Woking, United Kingdom, [2]School of Biological Sciences, University of Reading, Whiteknights, Reading, United Kingdom, [3]Laboratory of Animal Science, Setsunan University, Osaka, Japan

Activation-induced markers (AIMs) are frequently analyzed to identify re-activated human memory T cells. However, in pigs the analysis of AIMs is still not very common. Based on available antibodies, we designed a multi-color flow cytometry panel comprising pig-specific or cross-reactive antibodies against CD25, CD69, CD40L (CD154), and ICOS (CD278) combined with lineage/surface markers against CD3, CD4, and CD8α. In addition, we included an antibody against tumor necrosis factor alpha (TNF-α), to study the correlation of AIM expression with the production of this abundant T cell cytokine. The panel was tested on peripheral blood mononuclear cells (PBMCs) stimulated with phorbol 12-myristate 13-acetate (PMA)/ionomycin, Staphylococcus enterotoxin B (SEB) or PBMCs from African swine fever virus (ASFV) convalescent pigs, restimulated with homologous virus. PMA/ionomycin resulted in a massive increase of CD25/CD69 co-expressing T cells of which only a subset produced TNF-α, whereas CD40L expression was largely associated with TNF-α production. SEB stimulation triggered substantially less AIM expression than PMA/ionomycin but also here CD25/CD69 expressing T cells were identified which did not produce TNF-α. In addition, CD40L-single positive and $CD25^+CD69^+CD40L^+TNF\text{-}\alpha^-$ T cells were identified. In ASFV restimulated T cells TNF-α production was associated with a substantial proportion of AIM expressing T cells but also here ASFV-reactive $CD25^+CD69^+TNF\text{-}\alpha^-$ T cells were identified. Within $CD8\alpha^+$ CD4 T cells, several CD25/CD40L/CD69/ICOS defined phenotypes expanded significantly after ASFV restimulation. Hence, the combination of AIMs tested will allow the identification of primed T cells beyond the commonly used cytokine panels, improving capabilities to identify the full breadth of antigen-specific T cells in pigs.

KEYWORDS

activation-induced markers, CD69, CD40L, CD25, ICOS, SEB, African swine fever virus, pig

1 Introduction

The identification of effector cells is a key element to understanding the contribution of T cells in immune responses. Detection of molecules or markers associated with different effector functions by polychromatic or high-dimensional flow cytometry (FCM) is one approach to detect such cells. For example, analyzing one or several cytokines can aid in the identification of Th1, Th2, Th17, or Treg cells (1). However, depending on the cytokine, release from T cells varies over time (2). In addition, for intracellular cytokine staining by FCM, the Golgi apparatus needs

to be inhibited for prevention of cytokine release from the cell (3). This makes it difficult to identify all effector T cells by intracellular cytokine staining, even if several cytokines are investigated in combination.

Due to these limitations, the investigation of Activation-induced markers (AIMs), often in combination with one or several cytokines has become the preferred method in studies on human T cell responses (4–9). However, in livestock species, the use of AIMs for identification of activated T cells is limited, mainly due to restricted availability of antibodies to detect markers used for human T cells, like OX40 (CD134), 41BB (CD137), CD200 or PD-L1 (CD274). However, for other molecules qualifying as AIMs, like CD25, CD69, CD40L (CD154) or inducible T-cell co-stimulator (ICOS, CD278), either species-specific or cross-reactive antibodies are available for porcine T cells (10–14).

CD25 is the α-chain of the IL-2 receptor and is expressed on activated CD4 T cells but also regulatory T cells (Tregs); this was also demonstrated for porcine T cells (15, 16). Due to the ubiquitous expression on Tregs, CD25 expression is analyzed in combination with other AIMs in the identification of activated T cells (8, 9). CD69 is a type II C lectin receptor. For pigs, a mAb only recently became available (12) and it was shown that subsets of CD8 T cells in lymph nodes and lung express CD69 under steady state conditions (17). In human T cells, CD69 expression already peaks about 18 h after stimulation (18). The marker is frequently analyzed in combination with CD25 or other AIMs for the identification of activated CD8 T cells (8). CD40L belongs to the tumor necrosis factor (TNF) superfamily and is typically expressed by CD4 T cells following T cell receptor (TCR) stimulation but also CD8 T cells (19–21). For pigs, it has been shown that expression of CD40L correlates in CD4 T cells with production of interferon (IFN)-γ and TNF-α both after *Staphylococcus* enterotoxin B (SEB) stimulation and restimulation with *Candida albicans, Ascaris suum* and *Streptococcus suis* antigens *in vitro* (11). ICOS has been used less frequently as an AIM. For human CD4 T cells it was investigated to identify activated circulating T follicular helper cells (Tfh) (22, 23) but also total activated CD4 T cells (23). In pigs, a cross-reactive antibody to ICOS has been used to investigate invariant natural killer T (iNKT) cells in different lymphoid and non-lymphoid organs (14). In addition, ICOS expression was studied in the context of lymph node and blood-derived porcine Tfh cells (13).

Based on this, we tested combinations of antibodies against CD25, CD69 and CD40L to identify activated CD4 and CD8 T cells in pigs, using polyclonal (phorbol 12-myristate 13-acetate [PMA]/ionomycin) and oligoclonal (SEB) stimulation. The three AIMs were also combined with ICOS and tested in the context of antigen-specific restimulation, using peripheral blood mononuclear cells (PBMCs) from African swine fever virus (ASFV) convalescent pigs. Comparing expression patterns of these AIMs against TNF-α, one of the most widely expressed porcine cytokines in the context of T cell activation (24), we show that combinations of CD25 and CD69 have the capacity to identify additional antigen-specific T cells, while CD40L was largely associated with TNF-α production.

2 Materials and methods

2.1 ASFV for *in vitro* cultivation

The moderately virulent Estonia 2014 ASFV strain [spleen homogenate kindly provided by Sandra Blome from Friedrich-Loeffler-Institute, Greifswald-Insel Riems, Germany (25)] was used for *in vitro* restimulation experiments and cultured and titrated using end point dilution on bone-marrow-derived macrophages as detailed in a previous study (26). In brief, bone marrow cells were extracted from femurs of 4–6 week old outbred pigs and cultured in EBSS (Sigma) supplemented with 4 mM HEPES, 10% heat-inactivated pig serum (BioSera), and 100 I.U./mL penicillin with 100 ug/mL streptomycin (Gibco) for 3 days prior to ASFV infection to allow the differentiation of bone-marrow-derived macrophages. Mock inoculum was prepared from the same stock of uninfected cells. Virus was collected from the cells 5 days post-infection and titrated using the Spearman-Karber method of end-point dilution, wherein 50% of infected bone-marrow-derived macrophage cultures exhibited haemadsorption caused by ASFV.

2.2 Cell isolation and animals used in the study

Peripheral blood mononuclear cells (PBMCs) were isolated from heparinized blood by density gradient centrifugation (Histopaque-1077 Hybri-Max, density 1.077 g/mL, Sigma-Aldrich, Merck KGaA, Darmstadt, Germany). Blood for *in vitro* assays with PMA/ionomycin and SEB was obtained postmortem from six outbred pigs, aged 4 to 6 weeks. The animal experiment involving ASFV was conducted under the Home Office Animals (Scientific Procedures) Act (1986) (ASPA) and was approval by the Animal Welfare and Ethical Review Board (AWERB) at The Pirbright Institute. The animals were housed in accordance with the Code of Practice for the Housing and Care of Animals Bred, Supplied, or Used for Scientific Purposes. Throughout the study, appropriate bedding and species-specific enrichment measures were implemented to uphold high standards of welfare. All procedures were performed by trained and competent Personal License holders under the authority of Project License PP8739708. In detail, four female (animals AY95, AY97, AY98 and AY99) and one male (animal AY94) 12-week-old Babraham pigs were bred at the Centre for Dairy Research, University of Reading, Whiteknights, United Kingdom. The pigs were acclimatized for a week before oronasal challenge with 1,145 HAD_{50} moderately virulent ASFV strain Estonia 2014 in spleen homogenate. The challenge dose of ASFV was confirmed by back titration on bone-marrow-derived macrophages. Clinical signs and macroscopic lesion at post-mortem were assessed as previously described (27, 28). All animals survived the viral challenge. Heparinized blood samples were obtained from the animals 21 days post viral challenge. Following careful monitoring all pigs were euthanized using an overdose of anesthetic after reaching scientific or humane endpoints.

2.3 *In vitro* cultivation and FCM staining

Round-bottom 96-well microtiter plates (Nunc MicroWell Plates, Thermo Fisher Scientific, Waltham, MA, United States) were seeded with 5×10^5 thawed (PMA and SEB) or freshly isolated PBMCs (PMA and ASFV Estonia 2014) in a final volume of 200 µL/well in RPMI-1640 Medium (Sigma-Aldrich) supplemented with 100 U/mL penicillin, 0.1 mg/mL streptomycin (Gibco, Thermo Fisher Scientific)

and 10% heat-inactivated fetal bovine serum (FBS, Life Science Production, Life Science Group, Sandy, United Kingdom). Cells were incubated with PMA (5 ng/mL) and ionomycin (500 ng/mL), SEB (500 ng/mL, all Sigma-Aldrich), or ASFV Estonia 2014 at a multiplicity of infection of 0.5 for 18 h. Cells incubated in cell culture medium only or incubated with mock inoculum served as negative controls. Brefeldin A (BD GolgiPlug™, BD Biosciences, San Jose, CA, United States) was added to the cultures for the final 6 h of cultivation at a concentration of 1 µg/mL. After 18 h, cells were harvested and re-suspended in staining buffer containing PBS with 3% FBS (Life Science Production). Cells were surface-stained with primary monoclonal antibodies (mAbs) directed against CD3 (PerCP-Cy5.5-conjugated, mouse IgG2a anti-pig, clone: BB23-8E6-8C8, BD Biosciences), CD4 (FITC-conjugated, mouse IgG1 anti-pig, clone: b38c6c7, Bio-Rad Laboratories Ltd., Hercules, CA, United States), CD8α (biotinylated, mouse IgG2a anti-pig, clone: 76–2-11, Southern Biotech, Birmingham, AL, United States), CD25 (AlexaFluor 647-conjugated, mouse IgG1 anti-pig, clone: K231.3B2, Bio-Rad) and CD69 [unconjugated, mouse IgG2b anti-pig, clone: 01-14-22-51 (12)]. Cells derived from ASFV Estonia 2014-stimulated cultures were additionally stained with a primary monoclonal antibody against ICOS (CD278, BV605-conjugated, anti-human/mouse/rat, hamster IgG, clone: C398.4A, BioLegend, San Diego, CA, United States). Streptavidin-BV421 (BioLegend) and goat anti-mouse-IgG2b-PE (Tonbo, Cytek Biosciences, Fremont, CA, United States) were added in a secondary staining step, to label CD8α and CD69, respectively. Dead cells were identified using Fixable Viability Dye eFluor780 (Thermo Fisher Scientific) after surface staining according to the manufacturer's instructions. BD Cytofix/Cytoperm™ Fixation/Permeabilization Kit (BD Biosciences) was used following the manufacturer's instructions by adding 100 µL per well of Fixation/Permeabilization solution to resuspended cells for 20 min at 4°C, followed by two washes with Perm/Wash Buffer (BD Biosciences). Intracellular staining was performed using the following mAbs: TNF-α-BV711 (mouse IgG1 anti-human, clone: Mab11, BioLegend) and CD40L-PE-Vio770 (CD154, anti-human, recombinant human IgG1, clone: REA238, Miltenyi Biotec, Bergisch Gladbach, Germany). Staining steps were carried out in 96-well round bottom plates at 4°C for 20 min with the exception of the intracellular incubation step which lasted 30 min. Following intracellular incubation, cells were washed twice and stored at 4°C overnight in 50 µL Perm/Wash Buffer (BD Biosciences). Samples were acquired the following morning on a Cytek Aurora Spectral Cytometer (Cytek Biosciences), equipped with 5 lasers (UV 355 nm, violet 405 nm, blue 488 nm, yellow-green 561 nm, red 640 nm) and 64 fluorescence detection channels UV: 16, violet: 16, blue: 14, yellow-green: 10, red: 8. Spectral unmixing was performed using SpectroFlo software (version 3.2.1, Cytek Biosciences) following the acquisition of single-stained reference samples. Autofluorescence signatures based on unstained controls were extracted from the samples. Data of a minimum of 1×10^5 live lymphocytes per sample were recorded and analyzed on FlowJo Software for Windows (Version 10.9.0, BD Biosciences). Boolean "AND" combination gates were used to define co-expression of $CD25^+$, $CD40L^+$, $CD69^+$, TNF-α^+ and $ICOS^+$ in T cells. Boolean gating resulted in 16 possible phenotypes for combination gates including CD25, CD40L, CD69 and TNF-α as well as 32 possible phenotypes for combination gates including CD25, CD40L, CD69, TNF-α and ICOS.

2.4 Statistical analysis

Statistical analysis was performed using GraphPad Prism 9 (GraphPad Software, Dotmatics, Boston, MA, United States). Data sets were analyzed for normality. A paired t-test was used to test for statistical differences between groups where the data was normally distributed. A Wilcoxon matched-pairs signed rank test was used for data sets that were not normally distributed. A p-value of ≤ 0.05 was considered statistically significant. t-SNE plots were generated in R (version 4.2.3). t-SNE algorithm was run on live $CD3^+$ T cells using the parameters CD4, CD8α, CD25, CD40L, CD69 and TNF-α with samples of five pigs per stimulation condition (Medium, SEB, PMA). The script used was developed by the group of Adrian Liston (29) and is available on GitHub at https://github.com/AdrianListon/Cross-Entropy-test.

3 Results

3.1 PMA/ionomycin leads to strong upregulation of AIMs in pigs

To investigate the suitability of CD25, CD69 and CD40L as AIMs in pigs, we started by stimulating PBMCs from healthy animals with PMA/ionomycin. PMA works through the activation of protein kinase C while ionomycin triggers calcium release, thus bypassing TCR engagement. In combination, PMA/ionomycin is a very potent polyclonal stimulant for T cell activation. Cells cultured in medium only served as negative controls. To focus on T cells, $CD3^+$ cells were gated within live lymphocytes (Supplementary Figure 1).

The investigated AIMs CD25, CD69 and CD40L were strongly upregulated in PMA-stimulated samples compared to the medium control (Figure 1A). In addition, a large proportion of AIM^+ cells showed co-expression of TNF-α. To elucidate individual T cell phenotypes further, $CD3^+$ T cells were further gated for $CD25^+$, $CD69^+$, $CD40L^+$ and TNF-α^+ cells, resulting in 16 possible phenotypes identified by Boolean gating (Supplementary Figure 2). PMA/ionomycin stimulation resulted in substantial upregulation of the AIMs under investigation, with 85 to 95% of T cells showing an AIM^+ phenotype (Supplementary Table 1). Most prominent phenotypes induced by PMA/ionomycin were $CD25^+CD69^+$ (green), $CD25^+CD40L^+CD69^+$ (light blue), CD69 $single^+$ (orange) and CD25 $single^+$ (dark blue) T cells (Figure 1B). AIM^+ T cell phenotypes co-expressing TNF-α (collectively highlighted in gray) only constituted between 26% and 43% of total T cells (Supplementary Table 1), showing that analysis of AIMs identifies additional PMA-responding T cells.

We further used a t-SNE algorithm to explore T cell phenotypes induced by PMA stimulation and visualize these in contrast to medium control samples. t-SNE plots revealed three clusters that were uniquely present in PMA-stimulated samples (Figure 1C; Supplementary Figure 3): cluster 3 ($CD25^{high}CD69^+$partially$CD40L^+$), cluster 6 ($CD25^{high}CD69^+CD40L^+$TNF-α^+) and cluster 7 ($CD25^{high}CD69^+$). While CD69 and CD40L expression was almost entirely restricted to PMA-stimulated samples, variable level CD25 expression was also present in medium controls. Most of these cells

10.3389/fvets.2024.1390486

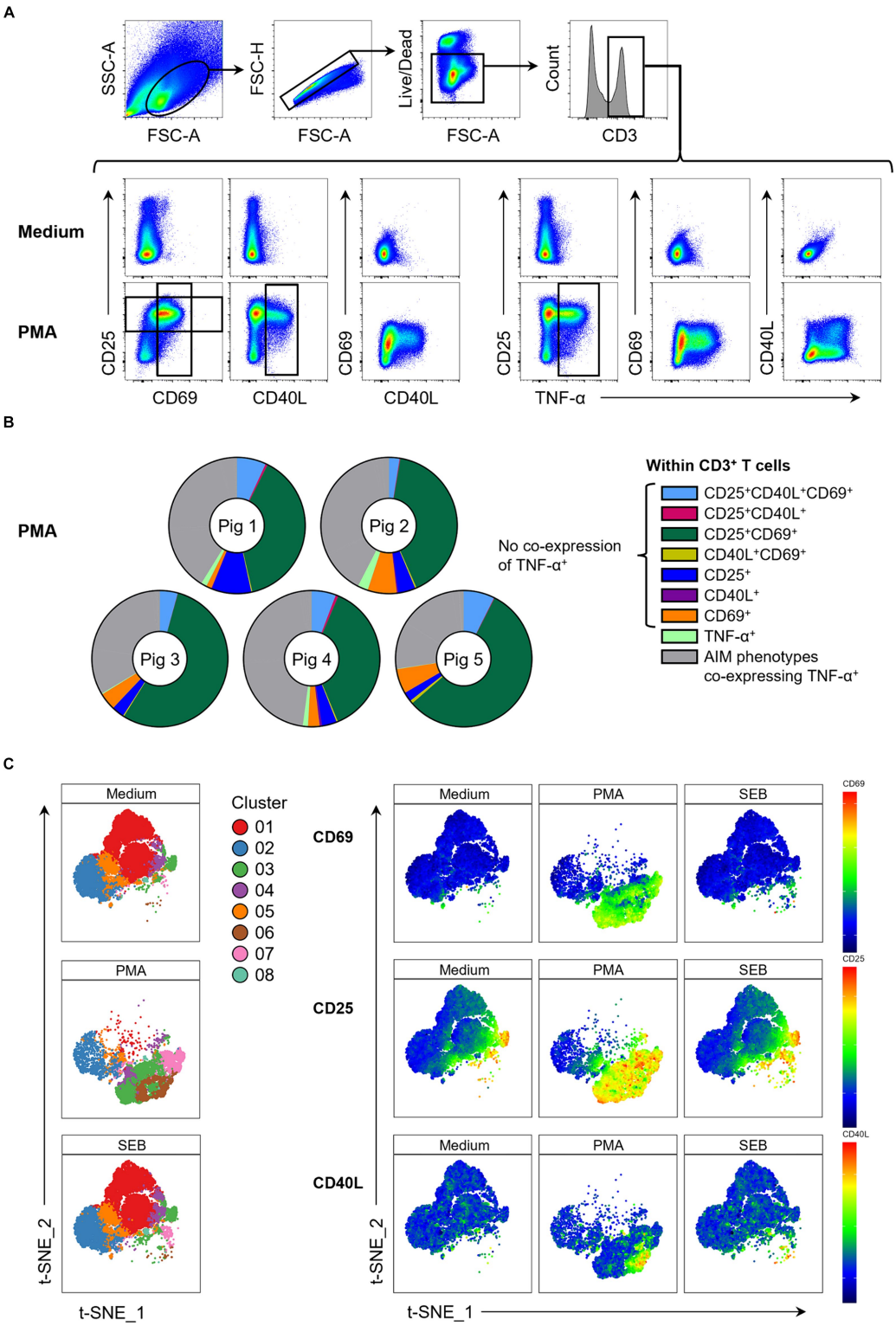

FIGURE 1
Expression of AIMs in blood-derived CD3+ T cells after stimulation with PMA/ionomycin. **(A)** Representative FCM plots depicting expression of CD25, CD69, CD40L and TNF-α in CD3+ T cells when PBMC samples were unstimulated (Medium, top row) or stimulated with PMA/ionomycin (PMA, bottom row) for 18 h. Surface staining was performed for antibodies against CD3, CD4, CD8α, CD25 and CD69. Intracellular staining was performed for CD40L and TNF-α. Gates shown are representative of gating for total CD25+, total CD69+, total CD40L+ and total TNF-α+ T cells applied to PMA-stimulated samples and used in Boolean gating to create doughnut charts. **(B)** Doughnut charts of AIM phenotypes in PMA-stimulated samples generated by Boolean gating. Each doughnut represents the PBMC sample of one pig. Different phenotypes are indicated by different colors with all AIM phenotypes co-expressing TNF-α summarized in gray. CD25−CD40L−CD69−TNF-α− T cells are not shown. **(C)** Live CD3+ T cells from unstimulated (Medium), SEB-stimulated and PMA-stimulated cultures were clustered using the t-SNE algorithm with generated clusters shown in a colored overlay (left side). Relative expression levels of CD69, CD25 and CD40L within clusters (right side) are colored from high (red) to low (blue).

co-expressed CD4 (Supplementary Figure 3). Cluster 3 in medium consisted almost exclusively of CD25^{high} CD4$^+$ T cells, most likely representing Tregs. Thus, PMA/ionomycin stimulation of porcine PBMCs strongly upregulated expression of CD25, CD69 and CD40L, confirming these as suitable AIMs in the pig.

3.2 AIMs are predominant in CD4$^+$CD8α$^+$ T cells after SEB stimulation

Next, we investigated AIM expression after stimulation of PBMCs with SEB. SEB is a superantigen that binds to the α-chain of MHC class II molecules on antigen-presenting cells and specific Vβ chains of the TCR which leads to activation of T cells and cytokine release (30, 31). While still non-specific, SEB activates TCR signaling via similar pathways to when T cells are activated by their cognate MHC peptides (32, 33). t-SNE analysis showed that overall AIM expression levels within total T cells after SEB stimulation were much lower compared to PMA stimulation, however more CD25$^+$, CD40L$^+$ and CD69$^+$ T cells were visible in clusters 6 and 7 compared to medium controls (Figure 1C). As SEB is known to predominantly activate CD4$^+$ T cells (34), CD3$^+$ T cells were further sub-gated into three populations based on their expression of CD4 and CD8α: CD4$^-$CD8α$^+$, CD4$^+$CD8α$^+$ and CD4$^+$CD8α$^-$ T cells (Figure 2A).

Analysis of AIMs within these subsets revealed that SEB-stimulation led to expression of all AIMs as well as TNF-α production in all three T cell subsets. Frequencies of AIM$^+$ T cells within the CD4$^-$CD8α$^+$ T cell subset, which mostly contains CD8 T cells, were higher in SEB-stimulated samples compared to medium controls (Figure 2B). Due to high animal-to-animal variation, however, only CD69$^+$ CD4$^-$CD8α$^+$ T cells reached a significant difference. CD8α$^+$ CD4$^+$ T cells are a special subset in the pig with high percentages in blood increasing with age and consisting mainly of activated and/ or memory T cells (35, 36). Among the investigated T cell subsets, highest overall frequencies of AIM-expressing and TNF-α producing cells were observed within CD4$^+$CD8α$^+$ T cells with all markers expressed in significantly higher frequencies in SEB-stimulated samples than in medium controls. SEB also induced AIM upregulation in the CD4$^+$CD8α$^-$ T cell subset, largely formed by naïve CD4$^+$ T cells (35), with the exception of one pig that showed a decrease in CD69 expression after stimulation.

3.3 ASFV induces expression of multiple AIMs

While the *in vitro* stimulation experiments using PMA/ionomycin and SEB confirmed the potential of an AIM assay in the pig, the ultimate goal was to utilize the AIMs for the detection of antigen-specific T cells after immunization or infection. To that end, we employed ASFV-primed cells from five pigs that had undergone a challenge infection with the moderately virulent ASFV strain Estonia 2014. Fresh blood samples were collected 21 days post viral challenge and isolated PBMCs were subjected to 18 h *in vitro* restimulation with ASFV Estonia 2014. Cells incubated with mock inoculum served to determine background expression.

Identical to SEB-stimulated samples, ASFV Estonia-stimulated samples were gated on live CD3$^+$ T cells (Supplementary Figure 1, bottom) which were further divided into three CD4/CD8α-defined T cell subsets (Figure 3A). In addition to the analysis of CD25, CD69 and CD40L, ICOS was included as a further potential AIM. Although not traditionally used in human AIM studies, ICOS is known to be expressed at low levels on naïve T cells and upregulated following T cell activation in both CD4 and CD8 T cells (37–39). As predicted when using an antigen-specific stimulation approach, overall levels of AIM expression were lower than those observed with PMA/ionomycin or SEB stimulation (Figure 3B).

Interestingly, highest frequencies of TNF-α in response to ASFV Estonia stimulation were found in CD4$^-$CD8α$^+$ T cells. Significance was not reached for this phenotype since data from the mock control was not normally distributed. Of note, we observed increases in ICOS$^+$ and CD40L$^+$ expressing cells in CD4$^-$CD8α$^+$ T cells, with ICOS even reaching significance, although both molecules are more associated with CD4 T cells. While overall percentages of CD40L expressing cells were low, ASFV Estonia stimulation induced significant CD40L upregulation above mock controls in CD4$^+$CD8α$^+$ T cells of all pigs. In line with results for SEB, increased frequencies of CD25, CD69 and ICOS expressing cells after ASFV Estonia stimulation were detected in the CD4$^+$CD8α$^+$ T cell subset. Consistent with the notion that CD4$^+$CD8α$^-$ cells represent naïve CD4 T cells, no consistent increase of AIM expressing T cells was found in this subset following ASFV stimulation. Similarly, an increase in TNF-α producing cells was found in CD4$^+$CD8α$^+$ T cells (though not significant) but not in the CD4$^+$CD8α$^-$ subpopulation. Therefore, ASFV stimulation induced the expression of multiple AIMs, most prominently in the CD4$^+$CD8α$^+$ T cell subset.

3.4 CD25$^+$CD69$^+$ is a prominent AIM T cell phenotype for SEB and ASFV stimulation

To compare AIM$^+$ T cell phenotypes elicited by SEB with the antigen-specific stimulation of ASFV-primed cells, the 16 phenotypes defined by expression of CD25$^+$, CD69$^+$, CD40L$^+$ and TNF-α$^+$ cells were analyzed by Boolean gating within CD4$^-$CD8α$^+$, CD4$^+$CD8α$^+$ and CD4$^+$CD8α$^-$ T cells. For both stimulations, CD25 single$^+$ T cells strongly dominated in all three T cell subsets (Supplementary Figures 4A,B). As the CD25 single$^+$ T cell subset was in its majority likely composed of Tregs, we decided to exclude these cells from further analysis.

Omitting CD25 single$^+$ T cells, CD25$^+$CD69$^+$ (dark green), CD25$^+$CD40L$^+$ (pink) and CD40L single$^+$ (purple) constituted the most frequent AIM$^+$ T cell phenotypes after SEB stimulation (Figure 4A) with CD25$^+$CD69$^+$ in CD4$^+$CD8α$^+$ T cells reaching an average of 34.7% when AIM^{neg}TNF-α^{neg} and CD25 single$^+$ T cells were excluded from the calculation (referred to as "ATC excluded" [from **A**IM^{neg}**T**NF-α^{neg} **C**D25 single$^+$] from now on; percentages in total T cells given in Supplementary Table 1). While CD25$^+$CD40L$^+$ (pink, average 11.5% in CD4$^-$CD8α$^+$, 12.3% in CD4$^+$CD8α$^+$, 18.6% in CD4$^-$CD8α$^+$ of ATC-excluded) and CD40L single$^+$ (purple, average 20.3% in CD4$^-$CD8α$^+$, 9% in CD4$^+$CD8α$^+$, 23.3% in CD4$^-$CD8α$^+$ of ATC-excluded) AIM phenotypes were frequent in all T cell subsets,

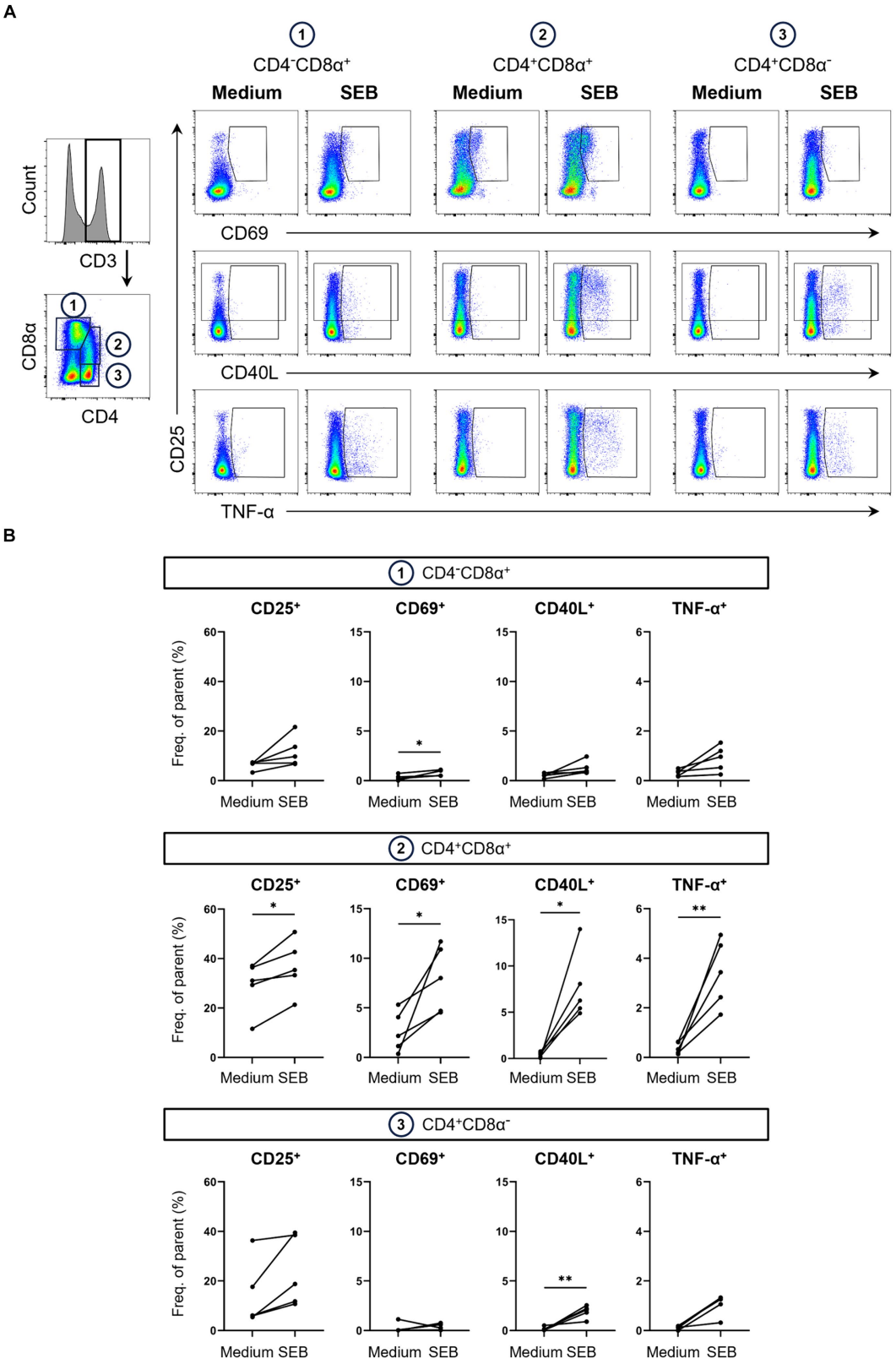

FIGURE 2
Expression of AIMs in blood-derived CD4/CD8α-defined T cell subsets after stimulation with SEB. **(A)** Representative FCM plots depicting expression of CD25, CD69, CD40L and TNF-α in $CD4^{-}CD8\alpha^{+}$, $CD4^{+}CD8\alpha^{+}$ and $CD4^{+}CD8\alpha^{-}$ T cells. PBMC samples were unstimulated (Medium, left columns) or stimulated with SEB (SEB, right columns) for 18 h. Cells were pre-gated in the following order: live, single and $CD3^{+}$. Gates shown indicate gating applied to calculate frequencies of AIM^{+} and TNF-α^{+} cells. **(B)** Frequencies of $CD25^{+}$, $CD69^{+}$, $CD40L^{+}$ and TNF-α^{+} cells within CD4/CD8α-defined T cell subsets in unstimulated (Medium) and SEB-stimulated samples. Each dot represents data from one animal ($n = 5$). Asterisks indicate significant differences between groups ($^{*}p \leq 0.05$, $^{**}p \leq 0.01$).

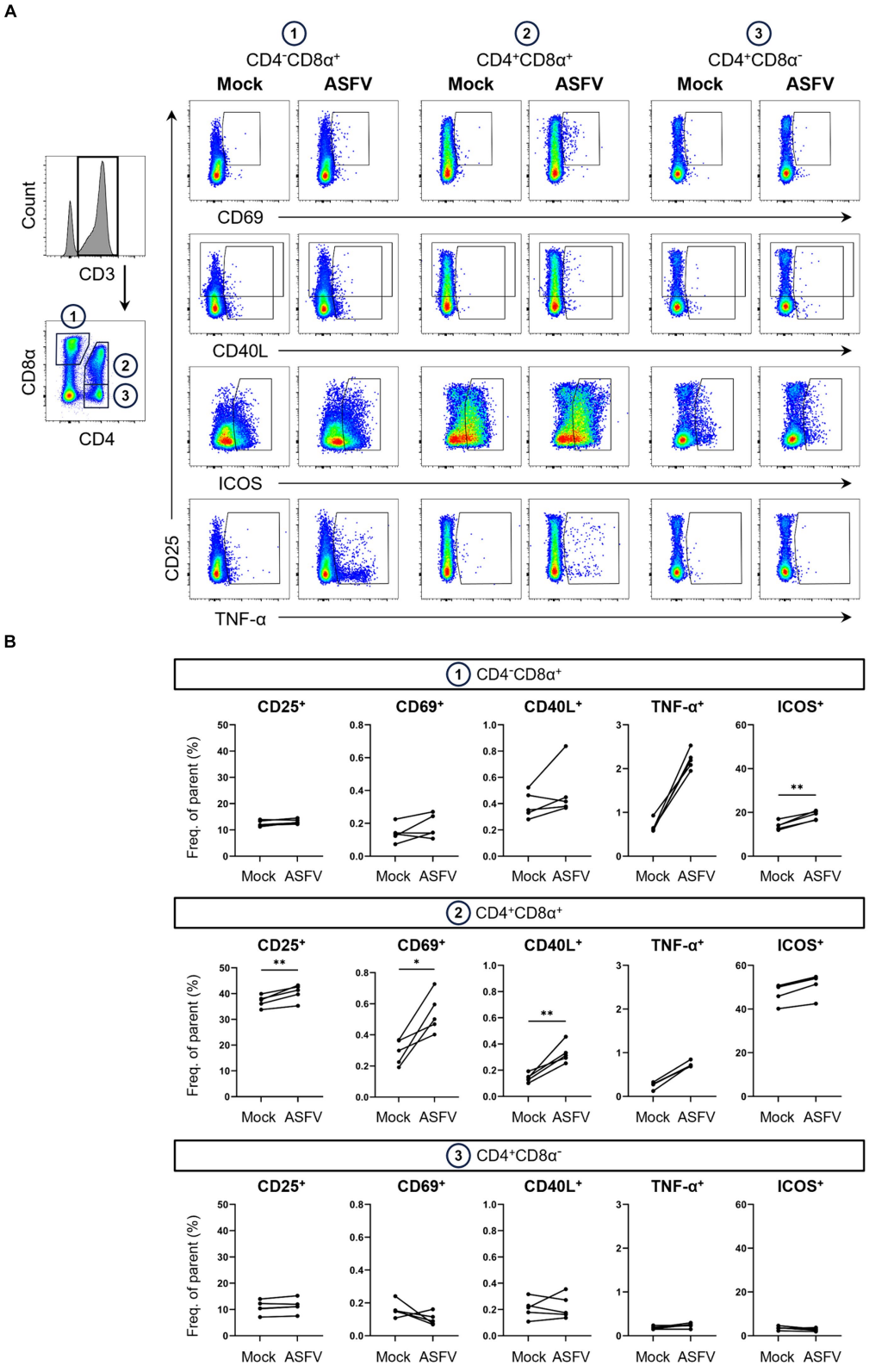

FIGURE 3
Expression of AIMs in blood-derived CD4/CD8α-defined T cell subsets after stimulation with ASFV Estonia 2014. **(A)** Representative FCM plots depicting expression of CD25, CD69, CD40L, ICOS and TNF-α in $CD4^{-}CD8\alpha^{+}$, $CD4^{+}CD8\alpha^{+}$ and $CD4^{+}CD8\alpha^{-}$ T cells. PBMC samples were incubated with mock inoculum (Mock, left columns) or ASFV Estonia 2014 (ASFV, right columns) for 18 h. Cells were pre-gated in the following order: live, single and $CD3^{+}$. Gates shown indicate gating applied to calculate frequencies of AIM^{+} and $TNF\text{-}\alpha^{+}$ cells. Dot size was enlarged to improve visibility of AIM^{+} and $TNF\text{-}\alpha^{+}$ cells. **(B)** Frequencies of $CD25^{+}$, $CD69^{+}$, $CD40L^{+}$, $ICOS^{+}$ and $TNF\text{-}\alpha^{+}$ cells within CD4/CD8α-defined T cell subsets in mock-inoculated (Mock) and ASFV Estonia 2014 (ASFV)-stimulated samples. Each dot represents data from one animal (n = 5). Asterisks indicate significant differences between groups (*$p \leq 0.05$, **$p \leq 0.01$).

FIGURE 4
Relative distribution of AIM phenotypes within CD4/CD8α-defined T cell subsets in SEB-stimulated vs. ASFV-stimulated PBMC cultures. **(A)** Doughnut charts of AIM phenotypes in SEB-stimulated samples generated by Boolean gating in $CD4^{-}CD8\alpha^{+}$ (top row), $CD4^{+}CD8\alpha^{+}$ (middle row) and $CD4^{+}CD8\alpha^{-}$ (bottom row) T cells. Each doughnut represents the PBMC sample of one pig. Different phenotypes are indicated by different colors with all AIM phenotypes co-expressing TNF-α summarized in gray. $CD25^{-}CD40L^{-}CD69^{-}TNF\text{-}\alpha^{-}$ and CD25 single^{+} T cell phenotypes are not shown. **(B)** Doughnut charts of AIM phenotypes in ASFV Estonia 2014-stimulated samples generated by Boolean gating in $CD4^{-}CD8\alpha^{+}$ (top row), $CD4^{+}CD8\alpha^{+}$ (middle row) and $CD4^{+}CD8\alpha^{-}$ (bottom row) T cells. Each doughnut represents the PBMC sample of one pig. Different phenotypes are indicated by different colors with all AIM phenotypes co-expressing TNF-α summarized in gray. $CD25^{-}CD40L^{-}CD69^{-}TNF\text{-}\alpha^{-}$ and CD25 single^{+} T cell phenotypes are not shown.

$CD25^{+}CD40L^{+}CD69^{+}$ (light blue, average 3.6% in $CD4^{-}CD8\alpha^{+}$, 16.2% in $CD4^{+}CD8\alpha^{+}$, 4% in $CD4^{-}CD8\alpha^{+}$ of ATC-excluded) were mostly found within $CD4^{+}CD8\alpha^{+}$ T cells.

Among ASFV Estonia-stimulated samples, TNF-α single^{+} (light green) and $CD25^{+}CD69^{+}$ (dark green) T cells were the most prominent phenotypes (Figure 4B). In contrast to SEB, however, differences between CD4/CD8α-defined T cell subsets were more pronounced. TNF-α single^{+} (light green) vastly dominated within $CD4^{-}CD8\alpha^{+}$ T cells with an average of 60.9% within ATC-excluded. While $CD25^{+}CD69^{+}$ T cells (dark green) were frequent within both

$CD4^+CD8\alpha^+$ (31.2% of ATC-excluded) and $CD4^+CD8\alpha^-$ T cells (15.1% of ATC-excluded), CD40L single$^+$ were largely confined to the $CD4^+CD8\alpha^-$ T cell subset (purple, average 25.9% of ATC-excluded). Overall, $CD25^+CD69^+$ and CD40L single$^+$ were the most prominent AIM^+ phenotypes elicited by SEB and ASFV Estonia stimulation.

Of note, frequencies of AIM^+ T cell phenotypes co-expressing TNF-α (gray) varied between T cell subsets and stimulations (SEB: 23.4% in $CD4^-CD8\alpha^+$, 24% in $CD4^+CD8\alpha^+$, 40.1% in $CD4^-CD8\alpha^+$ of ATC-excluded; ASFV: 25.7% in $CD4^-CD8\alpha^+$, 36.7% in $CD4^+CD8\alpha^+$, 34% in $CD4^-CD8\alpha^+$of ATC-excluded). Focusing in more detail on AIM^+ $TNF\text{-}\alpha^+$ T cell phenotypes revealed further differences between SEB and ASFV Estonia-stimulated PBMC cultures (Supplementary Figures 5A,B). While AIM^+ $TNF\text{-}\alpha^+$ T cell phenotypes in SEB-stimulated samples were dominated by $CD40L^+TNF\text{-}\alpha^+$ (rust-red) and $CD25^+CD40L^+TNF\text{-}\alpha^+$ (light blue) T cells, $CD25^+TNF\text{-}\alpha^+$ T cells (green) were the most prominent phenotype in ASFV Estonia samples. $CD25^+CD40L^+CD69^+TNF\text{-}\alpha^+$ T cells (maroon) were mostly restricted to $CD4^+$ T cells, being present in $CD4^+CD8\alpha^+$ and $CD4^+CD8\alpha^-$ subsets after both stimulations. Therefore, TNF-α production in SEB-stimulated cells seems to be largely associated with CD40L expression, whereas it is rather affiliated with CD25 in ASFV Estonia-stimulated samples. In accordance with this, when analyzing $ICOS^+$ T cell phenotypes in combination with the other AIMs and TNF-α in ASFV Estonia-samples, ICOS was preferentially co-expressed with CD25 (Supplementary Figure 6).

3.5 Multiple AIM^+ phenotypes expand in response to ASFV

Finally, we dissected which combinations of AIMs expanded in response to ASFV stimulation and therefore prove valuable for the identification of antigen-specific T cells. Consequently, we applied further Boolean gating of $CD25^+$, $CD40L^+$ and $CD69^+$ within CD4/CD8α-defined T cell subsets, omitting analysis of TNF-α expression to focus exclusively on expression of AIMs. Significant increases in frequencies were observed for $CD25^+CD40L^+CD69^+$, $CD25^+CD40L^+$ and $CD25^+CD69^+$ phenotypes in $CD4^+CD8\alpha^+$ T cells (Figure 5A). For $CD4^+CD8\alpha^-$ T cells, consisting mainly of naïve CD4 T cells in pigs (35), no significant differences between mock and ASFV-treated cultures were found (data not shown). When including ICOS in the AIM panel, $CD25^+CD40L^+ICOS^+$, $CD25^+ICOS^+$ and $ICOS^+$ phenotypes were significantly upregulated in the $CD4^-CD8\alpha^+$ T cell subset in ASFV-cultures (Figure 5B, top). Within $CD4^+CD8\alpha^+$ T cells, five AIM^+ phenotypes co-expressing ICOS showed significant expansion following ASFV restimulation: $CD25^+CD40L^+CD69^+ICOS^+$, $CD25^+CD40L^+ICOS^+$, $CD25^+CD69^+ICOS^+$, $CD25^+ICOS^+$ and $CD40L^+ICOS^+$ (Figure 5B, bottom). This suggests that the addition of ICOS improves the breadth of the investigated AIM panel. In summary, multiple AIM^+ phenotypes expanded in ASFV-primed cells after ASFV restimulation, most notably within $CD4^+CD8\alpha^+$ T cells.

4 Discussion

AIMs have become a widely used tool to identify the full breadth of antigen-specific CD4 and CD8 T cells following short-term *in vitro* restimulation (8). However, in livestock species, their use has been very limited, probably due to a perceived lack of antibodies addressing AIMs established for human T cells. Here, we made use of species specific or cross-reactive antibodies for pigs, binding to CD25, CD69, CD40L and ICOS to investigate activated T cells following polyclonal, oligoclonal or antigen (re-)stimulation.

PMA/ionomycin stimulation resulted in a substantial increase of T cells expressing CD25, CD69 and CD40L, suggesting that all three molecules are suitable for the identification of activated T cells. Previously, we reported similar results for ICOS following ConA stimulation (13). However, stimulation by either PMA/ionomycin or ConA is very potent in T cells and therefore does not allow immediate conclusions on the suitability of CD25, CD69, CD40L or ICOS to identify antigen-specific T cells. As an intermediate to antigen recall, we initially tested our AIM panel on SEB stimulated PBMCs. SEB is a group II superantigen, binding to the α-chain of MHC class II molecules and the Vβ chain of the TCR (40). In human PBMCs, stimulation with SEB (1 μg/mL) results in up to 10% TNF-α producing (41) and 30% CD40L expressing CD4 T cells (9). Although we and others worked with similar concentrations for porcine PBMC [500 ng/mL to 1 ug/mL (11, 42)], percentages of activated phenotypes in porcine T cells are lower, e.g., in total CD4 T cells approx. 1% of cells become $CD40L^+$ (11). In our study 5%–14% and 1.7%–5% within $CD4^+CD8\alpha^+$ T cells expressed CD40L or TNF-α, respectively (Figure 2B). This suggests that SEB could have a lower affinity for porcine MHC-II α-chains or TCR-Vβ similar to what has been reported for mice (43). Although this could be seen as a disadvantage on the overall suitability of SEB to stimulate porcine T cells, it might be beneficial for the overall goal: to use AIMs to identify memory T cells capable of recall responses, where affinity between MHC/peptide and the TCR is also rather low. Indeed, our results show that $CD25^+CD69^+$ is a prominent phenotype induced by both SEB and ASFV (re-)stimulation, at least in $CD4^+CD8\alpha^+$ T cells.

At the beginning of our work on AIMs for porcine T cells, we also tested antibodies against CD71, CD137 and CD274. Although CD71 is less frequently analyzed in human T cells (8), its suitability as an AIM for T cells from mice and humans has been suggested (44) and a cross-reactive antibody (clone T56/14) for pig was reported (45). However, in our hands, the antibody did not show any binding on resting or ConA-stimulated T cells (data not shown). Similarly, cross-reactive antibodies for human AIMs CD137 (clone 4B4-1) and CD274 (PD-L1, clone 29E.2A3) have been mentioned (46), but again both antibodies did not bind to T cells or other cells in porcine PBMCs in our hands. A pig specific mAb for porcine CD137 has been reported (47) but to our knowledge is currently not commercially available and was not investigated in this study. Collectively, this illustrates that the toolbox for AIMs in pigs is still limited but our work shows that addressing CD25, CD69, CD40L and ICOS in combination should allow the identification of activated CD4 and CD8 T cells in different experimental settings.

Different to cytokines, which for FCM analysis require intracellular staining, AIMs are membrane bound molecules. This allows for cell sorting and further downstream analyses, for example *in vitro* testing or bulk transcriptome analysis. However, as in previous studies on equine and porcine T cells (11, 48), CD40L expression was investigated after fixation and permeabilization of cells. This is due to the extremely short half-life of CD40L on the cell membrane (49), limiting possibilities to

10.3389/fvets.2024.1390486

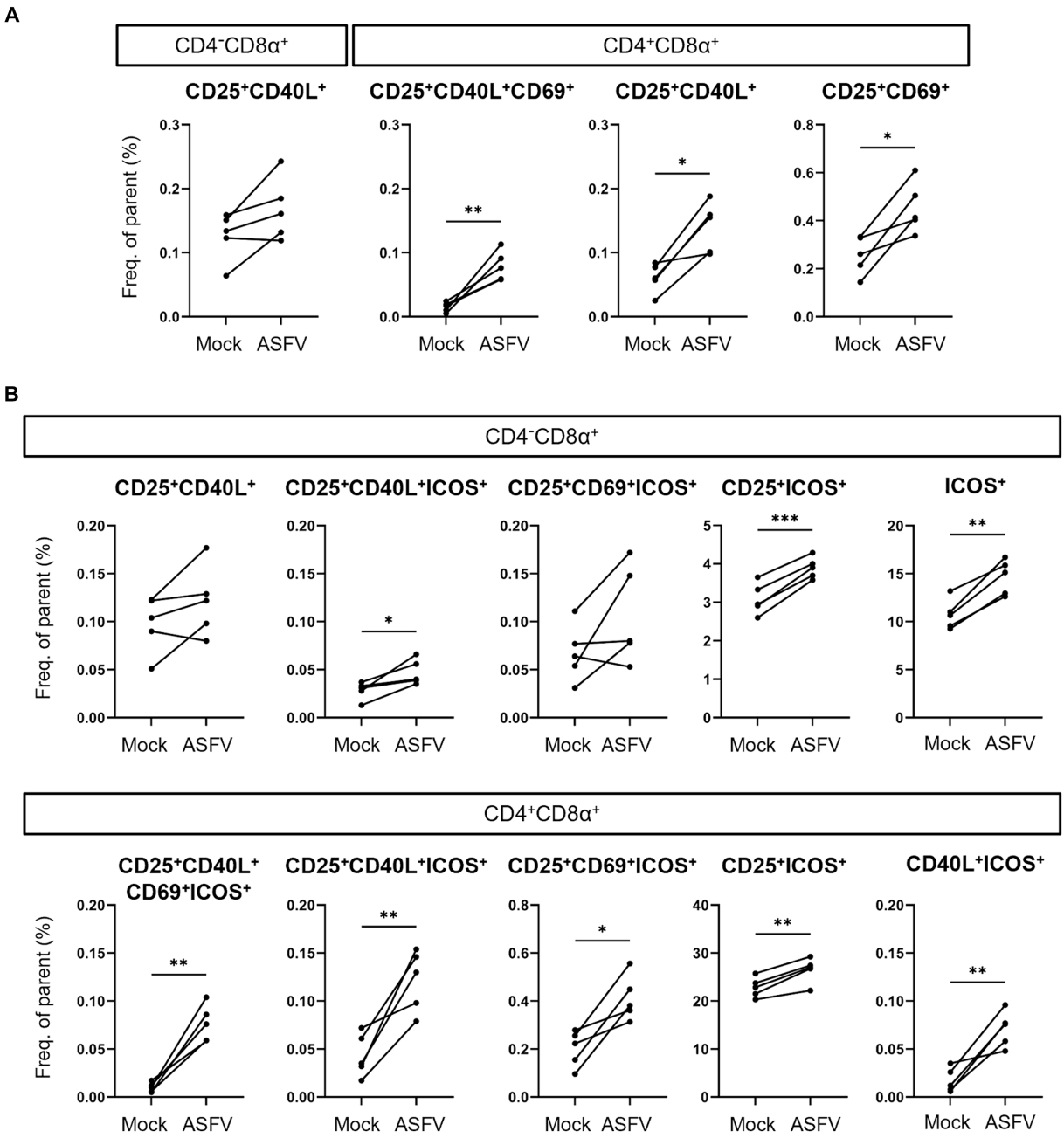

FIGURE 5
Induction of AIM⁺ CD4/CD8α-defined T cell phenotypes after ASFV Estonia 2014 stimulation. **(A,B)** Frequencies of selected AIM⁺ phenotypes within CD4⁻CD8α⁺ and CD4⁺CD8α⁺ T cells in mock-inoculated (Mock) vs. ASFV Estonia 2014 (ASFV)-stimulated samples. Boolean gating of AIMs was performed excluding **(A)** or including analysis of ICOS expression **(B)**. Each dot represents data from one animal ($n = 5$). Asterisks indicate significant differences between groups (*$p \leq 0.05$, **$p \leq 0.01$, ***$p \leq 0.001$).

identify it while on the cell surface. To overcome the need of permeabilization for sensitive CD40L detection, two strategies have been developed in the past. One is to place CD40L mAbs into the culture during the period of *in vitro* stimulation. This requires addition of monensin to the culture, to prevent degradation of the fluorochromes which partially become internalized together with their antibodies during the cultivation period (19). This approach was also successfully used for porcine CD4 T cells, allowing the combined analysis of CD40L in combination with either TNF-α or IFN-γ (50). However, when we tried this in combination with the analysis of CD25 and CD69, the expression of these molecules was severely impaired by the monensin (data not shown). An alternative to this is the addition of CD40 blocking antibodies (9, 20), a standard procedure in human AIM assays when CD40L is included. We have not tested this approach in our experiments, but several putatively pig cross-reactive antibodies (rabbit polyclonal PA5-27419; rabbit polyclonal PA1-31075; mouse anti-human, clone 647CT13.2.4; mouse anti-human, clone LOB7/6;

mouse anti-human, clone 9G10) were already unsuccessfully tested by Ebner and colleagues (F. Ebner, personal communication). Hence, a sorting of antigen-specific porcine T cells could either be performed based on CD25/CD69/ICOS co-expression (or subsets thereof, our findings) or on CD40L only (50). Nevertheless, further testing of antibodies for blocking porcine CD40 would strengthen AIM guided sorting of re-activated memory T cells.

In our experiments we compared AIM expressing T cells against the capacity for TNF-α production. TNF-α was chosen based on previous work, showing that frequencies of TNF-α and IFN-γ producing CD4 and CD8 T cells are similar following PMA/ionomycin stimulation. However, TNF-α production was also found in $CD4^+CD8\alpha^-$ T cells, while IFN-γ production was largely confined to $CD4^+CD8\alpha^+$ and $CD4^-CD8\alpha^+$ T cells (24). In addition, IFN-γ and TNF-α are often co-produced, both after PMA/ionomycin stimulation (24) and for example in influenza or porcine reproductive and respiratory syndrome virus (PRRSV) recall assays (51–54). Nevertheless, all those publications show that IFN-γ single producing T cells are frequently present, suggesting that IFN-γ production will also correlate with the AIMs investigated in our work. This clearly warrants future investigations. Of note, TNF-α has been subject to limited investigation in the context of ASFV restimulation (55), but our data show that a considerable proportion of $CD4^-CD8\alpha^+$ T cells can produce this cytokine in a recall assay. The $CD4^-CD8\alpha^+$ T cells in our phenotyping panel should largely consist of conventional CD8 T cells, although a minor subset of $CD2^+$ γδ T cells can also have this phenotype (56). However recall stimulation of cells from animals recovered from a low virulent isolate of ASFV did not induce secretion of IFN-γ or TNF-α from $CD3^+\gamma\delta TCR1^+$ cells (55). Nonetheless, a more detailed analysis of TNF-α production in CD8 T cells in the context of different ASFV infections is of interest and should be addressed in future studies.

Finally, our data show that AIM combinations of CD25, CD40L, CD69 and ICOS identify phenotypes that expand significantly within $CD4^+CD8\alpha^+$ T cells following ASFV restimulation. The high percentage of $CD25^+ICOS^+$ cells within $CD4^+CD8\alpha^+$ T cells (also within mock cultures, Figure 5B, bottom) suggests that this phenotype contains a considerable proportion of Treg cells. Porcine Treg cells mainly have a $CD25^{high}$ phenotype but also subsets of $CD25^{dim/intermediate}$ CD4 T cells can express Foxp3 (57). This demonstrates the need to combine CD25 with other AIMs. Indeed, combinations of three or four AIMs identified much smaller subsets of $CD4^+CD8\alpha^+$ T cells showing an increase after ASFV restimulation (Figure 5B, bottom) with frequencies being closer to what can be expected in the context of *in vitro* antigen recall. Of note, we also identified ASFV induced increases of $CD25^+ICOS^+$ and single $ICOS^+$ $CD4^-CD8\alpha^+$ T cells (Figure 5B, top), potentially arising from $ICOS^{low}$ $CD4^-CD8\alpha^+$ T cells (Figure 3A). Mouse splenic and blood-derived CD8 T cells have been reported to be largely $ICOS^-$ (39, 58), but more recently it was shown that ICOS drives the generation of CD8 tissue resident memory T (Trm) cells (59). This indicates that further investigations on ICOS expressing CD8 T cells and its role as an AIM in pigs are justified. Together, this shows the versatility of our panel, providing avenues to investigate those CD25/CD40L/CD69/ICOS AIM phenotypes in pigs in future experiments, both in the context of infection and immunization studies.

Data availability statement

The raw data supporting the conclusions of this article will be made available by the authors, without undue reservation.

Ethics statement

The animal study was approved by the Animal Welfare and Ethical Review Board (AWERB) at The Pirbright Institute. The study was conducted in accordance with the local legislation and institutional requirements.

Author contributions

MM: Writing – review & editing, Methodology, Investigation. PT: Writing – review & editing, Supervision, Project administration, Methodology, Investigation, Funding acquisition. RI: Writing – review & editing, Resources. CN: Writing – review & editing, Supervision, Project administration, Funding acquisition. WG: Writing – original draft, Supervision, Project administration, Funding acquisition, Conceptualization. SS: Writing – original draft, Visualization, Supervision, Project administration, Funding acquisition, Formal analysis, Conceptualization.

Funding

The author(s) declare that financial support was received for the research, authorship, and/or publication of this article. This work was supported by the Biotechnology and Biological Sciences Research Council (BBSRC) Strategic Programme and Core Capability Grants to The Pirbright Institute (BBS/E/I/00007031, BBS/E/I/00007037, BBS/E/I/00007038, BBS/E/I/00007039, BBS/E/PI/230001A, BBS/E/PI/230001B, and BBS/E/PI/23NB0004) as well as BB/X511134/1. The Pirbright Institute Flow Cytometry Science Technology platform and support through the BBSRC Core capability grant and National Bioscience Research Infrastructure grant (BBS/E/I/00007039 and BBS/E/PI/23NB0004, respectively) is gratefully acknowledged.

Acknowledgments

The authors thank Laila Al-Adwani for her assistance with the animal study and cell isolation. Additionally, we acknowledge the following members of the Animal Services Team at The Pirbright Institute: Ollie Trussler, Louise Carder, Zach Skoumbourdis, Jake Scales, Dave Selby, Henry Steele, Luke Fitzpatrick, and Billy Matthews. We are grateful to the Flow Cytometry Unit at The Pirbright Institute for their support. The advice by Friederike Ebner, Technical University of Munich, Germany, on optimization of CD40L labeling is gratefully acknowledged.

Conflict of interest

The authors declare that the research was conducted in the absence of any commercial or financial relationships that could be construed as a potential conflict of interest.

Publisher's note

All claims expressed in this article are solely those of the authors and do not necessarily represent those of their affiliated organizations, or those of the publisher, the editors and the reviewers. Any product that may be evaluated in this article, or claim that may be made by its manufacturer, is not guaranteed or endorsed by the publisher.

Supplementary material

The Supplementary material for this article can be found online at: https://www.frontiersin.org/articles/10.3389/fvets.2024.1390486/full#supplementary-material

References

1. Yin Y, Mitson-Salazar A, Prussin C. Detection of intracellular cytokines by flow cytometry. *Curr Protoc Immunol*. (2015) 110:6.24.1. doi: 10.1002/0471142735.im0624s110

2. Han Q, Bagheri N, Bradshaw EM, Hafler DA, Lauffenburger DA, Love JC. Polyfunctional responses by human T cells result from sequential release of cytokines. *Proc Natl Acad Sci USA*. (2012) 109:1607–12. doi: 10.1073/pnas.1117194109

3. Lovelace P, Maecker HT. Multiparameter intracellular cytokine staining. *Methods Mol Biol*. (2018) 1678:151–66. doi: 10.1007/978-1-4939-7346-0_9

4. Brasu N, Elia I, Russo V, Montacchiesi G, Stabile SA, De Intinis C, et al. Memory CD8(+) T cell diversity and B cell responses correlate with protection against SARS-CoV-2 following mRNA vaccination. *Nat Immunol*. (2022) 23:1445–56. doi: 10.1038/s41590-022-01313-z

5. Dan JM, Lindestam Arlehamn CS, Weiskopf D, da Silva AR, Havenar-Daughton C, Reiss SM, et al. A cytokine-independent approach to identify antigen-specific human germinal center T follicular helper cells and rare antigen-specific CD4+ T cells in blood. *J Immunol*. (2016) 197:983–93. doi: 10.4049/jimmunol.1600318

6. Elias G, Ogunjimi B, Van Tendeloo V. Activation-induced surface proteins in the identification of antigen-responsive CD4 T cells. *Immunol Lett*. (2020) 219:1–7. doi: 10.1016/j.imlet.2019.12.006

7. Painter MM, Mathew D, Goel RR, Apostolidis SA, Pattekar A, Kuthuru O, et al. Rapid induction of antigen-specific CD4(+) T cells is associated with coordinated humoral and cellular immunity to SARS-CoV-2 mRNA vaccination. *Immunity*. (2021) 54:2133–42.e3. doi: 10.1016/j.immuni.2021.08.001

8. Poloni C, Schonhofer C, Ivison S, Levings MK, Steiner TS, Cook L. T-cell activation-induced marker assays in health and disease. *Immunol Cell Biol*. (2023) 101:491–503. doi: 10.1111/imcb.12636

9. Reiss S, Baxter AE, Cirelli KM, Dan JM, Morou A, Daigneault A, et al. Comparative analysis of activation induced marker (AIM) assays for sensitive identification of antigen-specific CD4 T cells. *PLoS One*. (2017) 12:e0186998. doi: 10.1371/journal.pone.0186998

10. Bailey M, Stevens K, Bland PW, Stokes CR. A monoclonal antibody recognising an epitope associated with pig interleukin-2 receptors. *J Immunol Methods*. (1992) 153:85–91. doi: 10.1016/0022-1759(92)90309-H

11. Ebner F, Schwiertz P, Steinfelder S, Pieper R, Zentek J, Schütze N, et al. Pathogen-reactive T helper cell analysis in the pig. *Front Immunol*. (2017) 8:565. doi: 10.3389/fimmu.2017.00565

12. Hayashi Y, Okutani M, Ogawa S, Tsukahara T, Inoue R. Generation of anti-porcine CD69 monoclonal antibodies and their usefulness to evaluate early activation of cellular immunity by flow cytometric analysis. *Anim Sci J*. (2018) 89:825–32. doi: 10.1111/asj.12989

13. Hoog A, Villanueva-Hernández S, Razavi MA, van Dongen K, Eder T, Piney L, et al. Identification of CD4(+) T cells with T follicular helper cell characteristics in the pig. *Dev Comp Immunol*. (2022) 134:104462. doi: 10.1016/j.dci.2022.104462

14. Schäfer A, Hühr J, Schwaiger T, Dorhoi A, Mettenleiter TC, Blome S, et al. Porcine invariant natural killer T cells: functional profiling and dynamics in steady state and viral infections. *Front Immunol*. (2019) 10:1380. doi: 10.3389/fimmu.2019.01380

15. Käser T, Gerner W, Hammer SE, Patzl M, Saalmüller A. Phenotypic and functional characterisation of porcine CD4(+)CD25(high) regulatory T cells. *Vet Immunol Immunopathol*. (2008) 122:153–8. doi: 10.1016/j.vetimm.2007.08.002

16. Saalmüller A, Werner T, Fachinger V. T-helper cells from naive to committed. *Vet Immunol Immunopathol*. (2002) 87:137–45. doi: 10.1016/S0165-2427(02)00045-4

17. Martini V, Edmans M, Gubbins S, Jayaraman S, Paudyal B, Morgan S, et al. Spatial, temporal and molecular dynamics of swine influenza virus-specific CD8 tissue resident memory T cells. *Mucosal Immunol*. (2022) 15:428–42. doi: 10.1038/s41385-021-00478-4

18. Wu H, Witzl A, Ueno H. Assessment of TCR signal strength of antigen-specific memory CD8(+) T cells in human blood. *Blood Adv*. (2019) 3:2153–63. doi: 10.1182/bloodadvances.2019000292

19. Chattopadhyay PK, Yu J, Roederer M. A live-cell assay to detect antigen-specific CD4+ T cells with diverse cytokine profiles. *Nat Med*. (2005) 11:1113–7. doi: 10.1038/nm1293

20. Frentsch M, Arbach O, Kirchhoff D, Moewes B, Worm M, Rothe M, et al. Direct access to CD4+ T cells specific for defined antigens according to CD154 expression. *Nat Med*. (2005) 11:1118–24. doi: 10.1038/nm1292

21. Stark R, Hartung A, Zehn D, Frentsch M, Thiel A. IL-12-mediated STAT4 signaling and TCR signal strength cooperate in the induction of CD40L in human and mouse CD8+ T cells. *Eur J Immunol*. (2013) 43:1511–7. doi: 10.1002/eji.201243218

22. Herati RS, Muselman A, Vella L, Bengsch B, Parkhouse K, Del Alcazar D, et al. Successive annual influenza vaccination induces a recurrent oligoclonotypic memory response in circulating T follicular helper cells. *Sci Immunol*. (2017) 2:2152. doi: 10.1126/sciimmunol.aag2152

23. Rodda LB, Netland J, Shehata L, Pruner KB, Morawski PA, Thouvenel CD, et al. Functional SARS-CoV-2-specific immune memory persists after mild COVID-19. *Cell*. (2021) 184:169–83.e17. doi: 10.1016/j.cell.2020.11.029

24. Gerner W, Talker SC, Koinig HC, Sedlak C, Mair KH, Saalmüller A. Phenotypic and functional differentiation of porcine αβ T cells: current knowledge and available tools. *Mol Immunol*. (2015) 66:3–13. doi: 10.1016/j.molimm.2014.10.025

25. Zani L, Forth JH, Forth L, Nurmoja I, Leidenberger S, Henke J, et al. Deletion at the 5′-end of Estonian ASFV strains associated with an attenuated phenotype. *Sci Rep*. (2018) 8:6510. doi: 10.1038/s41598-018-24740-1

26. Netherton CL, Goatley LC, Reis AL, Portugal R, Nash RH, Morgan SB, et al. Identification and immunogenicity of African swine fever virus antigens. *Front Immunol*. (2019) 10:1318. doi: 10.3389/fimmu.2019.01318

27. Galindo-Cardiel I, Ballester M, Solanes D, Nofrarías M, López-Soria S, Argilaguet JM, et al. Standardization of pathological investigations in the framework of experimental ASFV infections. *Virus Res*. (2013) 173:180–90. doi: 10.1016/j.virusres.2012.12.018

28. King K, Chapman D, Argilaguet JM, Fishbourne E, Hutet E, Cariolet R, et al. Protection of European domestic pigs from virulent African isolates of African swine fever virus by experimental immunisation. *Vaccine*. (2011) 29:4593–600. doi: 10.1016/j.vaccine.2011.04.052

29. Roca CP, Burton OT, Neumann J, Tareen S, Whyte CE, Gergelits V, et al. A cross entropy test allows quantitative statistical comparison of t-SNE and UMAP representations. *Cell Rep Methods*. (2023) 3:100390. doi: 10.1016/j.crmeth.2022.100390

30. Fries BC, Varshney AK. Bacterial toxins-staphylococcal enterotoxin B. *Microbiol Spectr*. (2013) 1:2. doi: 10.1128/microbiolspec.AID-0002-2012

31. Pinchuk IV, Beswick EJ, Reyes VE. Staphylococcal enterotoxins. *Toxins*. (2010) 2:2177–97. doi: 10.3390/toxins2082177

32. Bueno C, Lemke CD, Criado G, Baroja ML, Ferguson SS, Rahman AK, et al. Bacterial superantigens bypass Lck-dependent T cell receptor signaling by activating a Galpha11-dependent. *PLC Beta Mediated Pathway Immun*. (2006) 25:67–78. doi: 10.1016/j.immuni.2006.04.012

33. Niedergang F, Dautry-Varsat A, Alcover A. Cooperative activation of TCRs by enterotoxin superantigens. *J Immunol*. (1998) 161:6054–8. doi: 10.4049/jimmunol.161.11.6054

34. Fleischer B. Superantigens. *APMIS*. (1994) 102:3–12. doi: 10.1111/j.1699-0463.1994.tb04839.x

35. Gerner W, Käser T, Saalmüller A. Porcine T lymphocytes and NK cells--an update. *Dev Comp Immunol*. (2009) 33:310–20. doi: 10.1016/j.dci.2008.06.003

36. Rodríguez-Gómez IM, Talker SC, Käser T, Stadler M, Hammer SE, Saalmüller A, et al. Expression of T-bet, Eomesodermin and GATA-3 in porcine αβ T cells. *Dev Comp Immunol*. (2016) 60:115–26. doi: 10.1016/j.dci.2016.02.022

37. Hutloff A, Dittrich AM, Beier KC, Eljaschewitsch B, Kraft R, Anagnostopoulos I, et al. ICOS is an inducible T-cell co-stimulator structurally and functionally related to CD28. *Nature*. (1999) 397:263–6. doi: 10.1038/16717

38. McAdam AJ, Chang TT, Lumelsky AE, Greenfield EA, Boussiotis VA, Duke-Cohan JS, et al. Mouse inducible costimulatory molecule (ICOS) expression is enhanced by CD28 costimulation and regulates differentiation of CD4+ T cells. *J Immunol*. (2000) 165:5035–40. doi: 10.4049/jimmunol.165.9.5035

39. Watanabe M, Hara Y, Tanabe K, Toma H, Abe R. A distinct role for ICOS-mediated co-stimulatory signaling in CD4+ and CD8+ T cell subsets. *Int Immunol*. (2005) 17:269–78. doi: 10.1093/intimm/dxh206

40. Spaulding AR, Salgado-Pabón W, Kohler PL, Horswill AR, Leung DY, Schlievert PM. Staphylococcal and streptococcal superantigen exotoxins. *Clin Microbiol Rev*. (2013) 26:422–47. doi: 10.1128/CMR.00104-12

41. Guerreiro M, Na IK, Letsch A, Haase D, Bauer S, Meisel C, et al. Human peripheral blood and bone marrow Epstein-Barr virus-specific T-cell repertoire in latent infection reveals distinct memory T-cell subsets. *Eur J Immunol*. (2010) 40:1566–76. doi: 10.1002/eji.200940000

42. Pernold CPS, Lagumdzic E, Stadler M, Dolezal M, Jäckel S, Schmitt MW, et al. Species comparison: human and minipig PBMC reactivity under the influence of immunomodulating compounds in vitro. *Front Immunol*. (2023) 14:1327776. doi: 10.3389/fimmu.2023.1327776

43. Fraser JD, Proft T. The bacterial superantigen and superantigen-like proteins. *Immunol Rev*. (2008) 225:226–43. doi: 10.1111/j.1600-065X.2008.00681.x

44. Motamedi M, Xu L, Elahi S. Correlation of transferrin receptor (CD71) with Ki67 expression on stimulated human and mouse T cells: the kinetics of expression of T cell activation markers. *J Immunol Methods*. (2016) 437:43–52. doi: 10.1016/j.jim.2016.08.002

45. Tripathi RC, Kolli SP, Borisuth NS, Tripathi BJ. Identification and quantification of transferrin receptors on trabecular cells. *Invest Ophthalmol Vis Sci*. (1992) 33:3449–54.

46. Dawson HD, Lunney JK. Porcine cluster of differentiation (CD) markers 2018 update. *Res Vet Sci*. (2018) 118:199–246. doi: 10.1016/j.rvsc.2018.02.007

47. Subramaniam S, Overend C, Yugo DM, Heffron CL, Matzinger SR, Rogers AJ, et al. Isolation of peripheral blood CD8 T cells specific to porcine reproductive and respiratory syndrome virus utilizing porcine CD137 activation marker. *Viral Immunol*. (2018) 31:333–7. doi: 10.1089/vim.2017.0189

48. Schnabel CL, Fletemeyer B, Lübke S, Marti E, Wagner B, Alber G. CD154 expression indicates T cell activation following tetanus toxoid vaccination of horses. *Front Immunol*. (2022) 13:805026. doi: 10.3389/fimmu.2022.805026

49. Yellin MJ, Sippel K, Inghirami G, Covey LR, Lee JJ, Sinning J, et al. CD40 molecules induce down-modulation and endocytosis of T cell surface T cell-B cell activating molecule/CD40-L. potential role in regulating helper effector function. *J Immunol*. (1994) 152:598–608. doi: 10.4049/jimmunol.152.2.598

50. Schmidt S, Ebner F, Rosen K, Kniemeyer O, Brakhage AA, Löffler J, et al. The domestic pig as human-relevant large animal model to study adaptive antifungal immune responses against airborne *Aspergillus fumigatus*. *Eur J Immunol*. (2020) 50:1712–28. doi: 10.1002/eji.201948524

51. de Brito RCF, Holtham K, Roser J, Saunders JE, Wezel Y, Henderson S, et al. An attenuated herpesvirus vectored vaccine candidate induces T-cell responses against highly conserved porcine reproductive and respiratory syndrome virus M and NSP5 proteins that are unable to control infection. *Front Immunol*. (2023) 14:1201973. doi: 10.3389/fimmu.2023.1201973

52. Edmans M, McNee A, Porter E, Vatzia E, Paudyal B, Martini V, et al. Magnitude and kinetics of T cell and antibody responses during H1N1pdm09 infection in inbred Babraham pigs and outbred pigs. *Front Immunol*. (2020) 11:604913. doi: 10.3389/fimmu.2020.604913

53. Mokhtar H, Pedrera M, Frossard JP, Biffar L, Hammer SE, Kvisgaard LK, et al. The non-structural protein 5 and matrix protein are antigenic targets of T cell immunity to genotype 1 porcine reproductive and respiratory syndrome viruses. *Front Immunol*. (2016) 7:40. doi: 10.3389/fimmu.2016.00040

54. Talker SC, Stadler M, Koinig HC, Mair KH, Rodríguez-Gómez IM, Graage R, et al. Influenza a virus infection in pigs attracts multifunctional and cross-reactive T cells to the lung. *J Virol*. (2016) 90:9364–82. doi: 10.1128/JVI.01211-16

55. Goatley LC, Nash RH, Andrews C, Hargreaves Z, Tng P, Reis AL, et al. Cellular and humoral immune responses after immunisation with low virulent African swine fever virus in the large white inbred Babraham line and outbred domestic pigs. *Viruses*. (2022) 14:1487. doi: 10.3390/v14071487

56. Sedlak C, Patzl M, Saalmüller A, Gerner W. CD2 and CD8α define porcine γδ T cells with distinct cytokine production profiles. *Dev Comp Immunol*. (2014) 45:97–106. doi: 10.1016/j.dci.2014.02.008

57. Käser T, Gerner W, Hammer SE, Patzl M, Saalmüller A. Detection of Foxp3 protein expression in porcine T lymphocytes. *Vet Immunol Immunopathol*. (2008) 125:92–101. doi: 10.1016/j.vetimm.2008.05.007

58. Blair T, Baird J, Bambina S, Kramer G, Gostissa M, Harvey CJ, et al. ICOS is upregulated on T cells following radiation and agonism combined with radiation results in enhanced tumor control. *Sci Rep*. (2022) 12:14954. doi: 10.1038/s41598-022-19256-8

59. Peng C, Huggins MA, Wanhainen KM, Knutson TP, Lu H, Georgiev H, et al. Engagement of the costimulatory molecule ICOS in tissues promotes establishment of CD8(+) tissue-resident memory T cells. *Immunity*. (2022) 55:98–114.e5. doi: 10.1016/j.immuni.2021.11.017

frontiers | Frontiers in Veterinary Science

TYPE Original Research
PUBLISHED 26 June 2024
DOI 10.3389/fvets.2024.1377414

OPEN ACCESS

EDITED BY
Fulvio Riondato,
University of Torino, Italy

REVIEWED BY
Ellen Sparger,
University of California, Davis, United States
Davis Seelig,
University of Minnesota Twin Cities,
United States

*CORRESPONDENCE
Katharina Zwicklbauer
k.zwicklbauer@medizinische-kleintierklinik.de

†These authors have contributed equally to this work and share last authorship

RECEIVED 27 January 2024
ACCEPTED 05 June 2024
PUBLISHED 26 June 2024

CITATION
Zwicklbauer K, von la Roche D, Krentz D, Kolberg L, Alberer M, Zablotski Y, Hartmann K, von Both U and Härtle S (2024) Adapting the SMART tube technology for flow cytometry in feline full blood samples.
Front. Vet. Sci. 11:1377414.
doi: 10.3389/fvets.2024.1377414

Adapting the SMART tube technology for flow cytometry in feline full blood samples

Katharina Zwicklbauer[1]*, Dominik von la Roche[2], Daniela Krentz[1], Laura Kolberg[3], Martin Alberer[3], Yury Zablotski[1], Katrin Hartmann[1], Ulrich von Both[3,4†] and Sonja Härtle[2†]

[1]LMU Small Animal Clinic, Centre for Clinical Veterinary Medicine, LMU Munich, Munich, Germany, [2]Department of Veterinary Sciences, AG Immunology, LMU Munich, Planegg, Germany, [3]Division of Paediatric Infectious Diseases, Dr. von Hauner Children's Hospital, University Hospital, LMU Munich, Munich, Germany, [4]German Center for Infection Research (DZIF), Partner Site Munich, Munich, Germany

Flow cytometry of blood samples is a very valuable clinical and research tool to monitor the immune response in human patients. Furthermore, it has been successfully applied in cats, such as for infections with feline immune deficiency virus (FIV). However, if cells are not isolated and frozen, analysis of anticoagulated blood samples requires mostly prompt processing following blood collection, making later analysis of stored full blood samples obtained in clinical studies often impossible. The SMART Tube system (SMART TUBE Inc., California, United States; SMT) allows fixation and long-term preservation of whole blood samples at −80°C. However, this system has so far only been applied to human biological samples. In the present study, a new flow cytometry SMART Tube protocol adapted for feline whole blood samples was successfully established allowing quantification of T-helper cells, cytotoxic T-cells, B-cells, monocytes, and neutrophils up to 2 years post sampling. Results obtained from frozen stabilized and fresh blood samples were compared for validation purposes and correlated to differential blood counts from a conventional hematology analyzer. Clinical applicability of the new technique was verified by using samples from a treatment study for feline infectious peritonitis (FIP). Using the new SMT protocol on retained samples, it could be demonstrated that long-term storage of these SMT tubes is also possible. In summary, the newly adapted SMT protocol proved suitable for performing flow cytometry analysis on stored feline whole blood samples, thus opening up new avenues for veterinary research on a variety of aspects of clinical interest.

KEYWORDS

flow cytometry, smart tube system (SMT), feline, full blood sample, long-term storage

1 Introduction

Flow cytometry is a very sophisticated and highly developed technique for analyzing the qualitative and quantitative characteristics of individual whole cells and cellular components (1). The physical properties (e.g., size, complexity/granularity, membrane integrity) and the expression of specific molecules (e.g., antigens on or in the cell) can be recorded quickly and simultaneously for each individual cell. Cells, therefore, can be divided into different populations and subpopulations. Flow cytometry is often used to

characterize diseases in clinical settings in order to monitor the immune response in human patients (2, 3). The multiparametric, quantitative analysis also makes flow cytometry a powerful tool in biological sciences. Peripheral blood, bone marrow and lymph node aspirates, and cerebrospinal fluid are among the multitude of specimens that can be analyzed. Clinical flow cytometry in cats is currently primarily used for diagnosis and prognosis of hematopoietic neoplasms (lymphoma and leukemia) (4). It also has been successfully applied for infections with feline immune deficiency virus (FIV), in order to analyze diagnostic approaches or to monitor the immune responses in these cats (5).

However, only viable cells should be subjected to the initial staining process (6). For peripheral whole blood samples collected in ethylenediaminetetraacetic acid (EDTA)-anticoagulated tubes, cell stability has been demonstrated for a maximum of 48 h after collection (7) with only mild changes in leukocytes, lymphocytes and neutrophils, but in some cases significant changes in monocytes when measuring with automatic analyzers (8). This leaves only a very small time-window for analysis, especially for samples from clinical trials; this window is often too short, as in-house devices performing flow cytometry are rarely available, and samples from different sites often have to be shipped and stored before analysis. Although it is possible to isolate feline peripheral blood mononuclear cells (PBMC) using density gradient centrifugation and use traditional cryopreservation protocols to allow subsequent analysis by flow cytometry, a comparably large amount of blood is necessary to extract enough cells for conservation. In addition, isolation and freezing can alter cellular composition and impact the expression of certain markers.

The SMART Tube system (SMART TUBE Inc., California, United States; SMT) was developed for fixation and long-term storage of whole blood samples. This system has already been used in some mass and flow cytometry studies, but so far, only on human biological samples (9–12). An important benefit of whole blood storage and staining is the requirement for significantly smaller blood volumes compared to volumes needed for classical isolation techniques. This advantage is especially important in studies with longitudinal sampling in smaller animals such as cats, where the possible volume for blood withdrawal is severely restricted.

Therefore, the aim of this study was to establish a protocol for routine use of the SMT system with feline full blood samples and apply this protocol to samples of a clinical treatment study for cats with feline infectious peritonitis (FIP) after long-term storage.

2 Materials and methods

2.1 Sampling of feline blood

Spare EDTA-anticoagulated samples from peripheral whole blood of 20 healthy cats were collected at the LMU Small Animal Clinic in Munich. For fresh blood (FB) analysis, EDTA samples were stored at 4°C overnight and processed the next morning. For stored samples, 200 µL of EDTA whole blood was fixed and stabilized within a few hours after collection by mixing it with 270 µL of Proteomic Stabilizer Prot1 (SMART TUBE Inc., California, United States) in cryovials [micro screw-in tube 2 mL (Sarstedt AG & Co. KG, Nümbrecht, Germany)] according to the manufacturer's instructions. After incubation for 10 min at room temperature (RT) the samples were immediately transferred to −80°C. The individual storage periods (at −80°C) for all SMT blood samples are shown in Supplementary Table S1.

2.2 Automatic hematologic analyzer for feline blood

Hematology examination from all collected fresh-blood EDTA samples of the healthy cats was performed at the LMU Small Animal Clinic in Munich using the in-house automatic analyzer ProCyte Dx (IDEXX Laboratories, Inc., Maine, United States). Hematology examination from samples of cats with FIP was performed using the automatic analyzer Cell-Dyn 3,500 (Abott Laboratories, IL, United States). When an invalid separation of leukocyte populations was present, additional microscopical examination of blood smears (for the validation study and the clinical application) was performed.

2.3 Antibodies

For flow cytometry, seven commercially available monoclonal antibodies (mAbs) were tested: anti-cat CD4- Fluorescein isothiocyanate (FITC) (clone 3-4F4) (SouthernBiotech, Birmingham, United States), anti-cat CD4-FITC (clone vpg34) (BioRad Laboratories, Feldkirchen, Germany), anti-cat CD8-PE (clone fCD8) (SouthernBiotech), anti-dog CD21 (clone CA2.1D6) (BioRad Laboratories), anti-human CD21-APC (clone B-ly4) (BD PharmingenTM, Heidelberg, Germany), anti-human CD14-PacificBlue (clone TÜK14) (BioRad Laboratories), and anti-cat MHCII (clone PF6J-6D) (BioRad Laboratories). Anti-cat MHCII was only available purified and was therefore conjugated to CF405M using the Mix-n-StainTM CFTM405M Antibody Labeling Kit (Sigma-Aldrich®, St. Louis, United States). Purified anti-dog CD21 was conjugated to PerCP-Cy5.5 using the Lynx Rapid Antibody Conjugation Kit (BioRad Laboratories) according to the manufacturer's instructions. All mAbs were titrated prior to the start of the experiment for optimal working dilutions (see Table 1).

2.4 Sample processing for flow cytometry

For flow cytometric analysis of FB samples, 100 µL blood was mixed with 2 mL of 10X RBC Lysis Buffer (ThermoFisher Scientific, Massachusetts, United States) and incubated for 15 min at RT in the dark. After centrifugation at 550 × g for 5 min at 18°C, the supernatant was discarded and the cell pellet was resuspended in 500 µL of staining buffer (PBS pH 7.2, 1% BSA, 0.1% NaN3).

To thaw the stored tubes, the manufacturers protocol was modified as follows: the tubes were thawed in a cold-water bath (10°C to 15°C) for 5 min. Thawed content was transferred to a new tube, mixed with 2 mL of 1X Thaw-Lyse Buffer (SMART TUBE Inc.) and incubated for 10 min at RT under constant rotation. After this, leukocytes were pelleted at 560 × g for 5 min at RT. The pellet was resuspended with 3 mL of 1X Thaw-Lyse Buffer and incubated at RT

TABLE 1 Commercially available antibodies for cats and cross-reactive antibodies from other species (dog and human) tested for functionality for Smart Tubes with flow cytometry.

Antibody	Clone	Fluorochrome	Target cells	Reference	Dilution	SMART Tube
Mouse anti-cat CD4-FITC	3-4F4	FITC	T-helper cells	Ackley et al. (13)	1:50	no
Mouse anti-cat CD4-FITC	vpg34	FITC	T-helper cells	Callanan et al. (14)	1:40	yes
Mouse anti-feline CD8-PE	fCD8	PE	cytotoxic T-cells	Klotz and Cooper (15)	1:100	yes
Mouse anti-human CD14-PacificBlue	TÜK14	PacificBlue	monocytes, granulocytes	Jacobsen et al. (16)	1:50	no
Mouse anti-cat MHCII	PF6J-6D	CF405M*	lymphocytes, monocytes	Hunt et al. (17)	1:20	yes
Mouse anti-human CD21-APC	B-ly4	APC	B-cells	Fischer et al. (18)	1:5	yes
Mouse anti-dog CD21	CA2.1D6	PerCP-Cy5.5#	B-cells	Cobbold and Metcalfe (19)	1:500	no

no, antibody did work on fresh blood cells but not on the SMT-fixed cells; yes, antibody did work on both, the fresh blood cells and the SMT-fixed cells. *This antibody is only available purified; so, it was conjugated to CF405M using the Mix-n-StainTM CFTM405M Antibody Labeling Kit (Sigma-Aldrich®, St. Louis, United States). #This antibody was obtained purified; so, it was conjugated to PerCP-Cy5.5 using the Lynx Rapid Antibody Conjugation Kit (BioRad Laboratories, Feldkirchen, Germany).

for 10 min under rotation. After another centrifugation at 560 × g for 5 min at RT the cell pellet was resuspended with 500 µL of staining buffer (PBS pH 7.2, 1% BSA, 0.1% NaN3).

From both fresh and stored samples, 1×10^5 cells were transferred into a 96-well plate and incubated with 50 µL of the mAbs mixture (each antibody was titrated individually for optimal staining to generate a final panel in section 3.1; also, see Table 1) for 20 min in the dark on ice, followed by washing with 100 µL staining buffer and centrifugation at 725 × g for 1 min at 18°C. Pellets were resuspended in 400 µL staining buffer, transferred to a new tube and analyzed by flow cytometry. Due to the presence of a fixative in SMT tubes, which alters cell membrane integrity and precludes the use of viability dyes, we refrained from employing viability dyes for any of the samples to maintain consistency in treatment.

Flow cytometry was performed on a BD FACS Canto II Flow Cytometer (Becton Dickinson, Heidelberg, Germany). For each sample, 10,000 single cells were acquired. BD FACS DIVA and FlowJo (Tree Star Inc., OR, United States) software were used for data analysis.

The absolute numbers of each leukocyte subset were calculated as previously published (20): to obtain absolute cell numbers from flow cytometry samples, the determined percentage of the respective cell population was multiplied by the hematology analyzers leukocyte count. Lymphocyte numbers were calculated by adding up the numbers of CD4+, CD8+, CD21+, and marker negative/MHCII+/ small cells.

2.5 Analyzing intra-assay precision and accuracy of the feline SMT protocol

To determine intra-assay precision for the cell numbers obtained by the new feline SMT protocol, a blood sample of one healthy cat was split into five FB and five SMT samples, which were frozen afterwards and analyzed by flow cytometry processing. Coefficients of variation (CVs, in percent) were calculated as standard deviation (SD)/ mean × 100.

To test for accuracy of the newly established feline SMT protocol, blood samples of 20 cats were split into triplicates and subsequently analyzed with conventional automated hematology analyzer (Diff) and by flow cytometry on either FB or SMT-fixed samples to compare numbers of lymphocytes, monocytes, and neutrophils. The cell numbers were calculated as described above.

2.6 Clinical application of the established protocol to cats from a FIP treatment study

In a recent clinical treatment study, five cats suffering from FIP received orally for 84 days the multi component drug Xraphconn® (Mutian Life Sciences Limited, Nantong, China) containing the nucleoside analogue GS-441524 as previously published (21). During this treatment study, EDTA samples were collected with the SMT system according to the manufacturer's instructions at six different time points from day 0 (before treatment initiation) through days 7, 14, 28, 56, and 83 (last day of treatment). In addition, EDTA samples of five healthy cats were collected with the SMT system. These cats were anti-feline coronavirus (FCoV) antibody-negative in serum and had no fecal FCoV shedding, both of which was determined as previously described (21–23).The SMTs of healthy and diseased cats were thawed and processed as described above. Storage times are given in Supplementary Table S1.

2.7 Statistical analysis

For a first comparison of Diff, FB, and SMT, Box plots were visualized for distribution of the data using MS Excel (version 2313). Data were analyzed using R statistical language (version 4.0.3; R Core Team, 2020). Pearson's correlation coefficient [with the rules tiny to small correlation $r < 0.2$, medium correlation $r < 0.3$, large correlation $r < 0.4$, and very large correlation $r \geq 0.4$ (24)], Bland–Altman plots depicting the mean bias ± 2 SD, and results of a Passing-Bablok regression analysis were reported.

3 Results

3.1 Antibody panel

Main objective of the used staining panel was to discriminate the different leukocyte subsets and, in addition to classical hematologic analysis, to address different lymphocyte subsets. Therefore, commercially available mAbs were tested for their functionality on SMT samples (see Table 1). Several mAbs resulted in a good staining pattern on FB. However, they did not work on SMT samples [anti-CD4-FITC (clone 3-4F4), anti-CD21-PerCP-Cy5.5 (clone CA2.1D6)],

most likely due to the fixation process of the SMT system (see Supplementary Figures S1A,B). The anti-CD14 mAb showed good results on both FB and SMT samples but stained monocytes and neutrophils equally, so the desired differentiation of monocytes within the population of large cells was not possible (see Supplementary Figure S1C).

Four of the tested mAbs, either cat-specific or described as cross-reactive, gave good results likewise on FB and SMT samples and stained the intended cell populations (see Supplementary Figure S2). Hence, the final flow cytometry protocol included the following mAbs: anti-cat-CD4- FITC (vpg34) to stain T-helper cells, anti-cat-CD8-PE (fCD8) for cytotoxic T cells, anti-human-CD21-APC (B-ly4) for B cells, and anti-cat-MHCII-PacificBlue (PF6J-6D) to discriminate monocytes from neutrophils.

Although for all mAbs, mean fluorescence intensity (MFI) was significantly lower on cells from SMT than FB samples (40–45% for CD4, CD21 and MHCII, 25% for CD8), clear discrimination of even the most affected dim target populations was still possible (Supplementary Figure S2).

3.2 Gating strategy for flow cytometry

Strikingly, flow cytometric analysis of SMT samples revealed FSC/SSC scatter plots, which differed considerably from that of FB and between individual cats. While discrimination between neutrophils and lymphocytes became more difficult after fixation, visibility of the otherwise hardly distinguishable monocyte population was often improved (Figure 1).

To address the different subpopulations, the following gating strategy was applied: First, feline leukocytes were identified by their FSC/SSC scatter profiles (Figure 2A), followed by doublet exclusion (Figure 2B). CD4 and CD8 were used to address CD4+ helper T cells and CD8+ cytotoxic T cells. Double positive cells were not observed (Figure 2C, I and II).

From the CD4/CD8 double-negative population neutrophils were identified through high SSC and a negative MHCII staining (Figure 2D, III). B cells and monocytes were addressed in a CD21/MHCII plot (Figure 2E) with CD21+/MHCII+ B cells and a CD21-/MHCII+ cell population. When the latter was further examined according to its FSC/SSC scatter characteristics (Figure 2F), two distinct populations could be identified: a more homogeneous population of large cells, which we regarded as monocytes (Figure 2F, V) and an additional population of smaller cells. Since these CD4-/CD8-/CD21-/MHCII+ cells have a lymphocyte scatter profile (Figure 2F, VI), they were regarded as "marker-negative lymphocytes." As no natural killer (NK) cell marker was included in the applied antibody panel, a proportion of those "unstained" lymphocytes were supposedly NK cells but other lymphocyte populations could equally contribute.

3.3 Validation of the protocol

In order to analyze intra-assay precision of the applied protocol, one blood sample of a healthy cat was split into five FB and five SMT samples and analyzed by flow cytometry. As shown in Table 2, SD for all cell populations was very low (0.01–0.02 $\times 10^9$ c/L) and CV of intra-assay precision was below 1% for all cell types (Table 2).

For accuracy of the newly established feline SMT protocol, the numbers of lymphocytes, monocytes, and neutrophils analyzed with Diff, FB and SMT were compared to each other.

In general, a first juxtaposition of cell numbers revealed similar mean cell counts for all cell populations although flow cytometry-based analysis resulted in slightly lower cell counts, which was most pronounced for lymphocytes [mean Diff 3.6 $\times 10^9$ c/L vs. 3.2 $\times 10^9$ c/L (FB and SMT) (Figure 3A; Supplementary Table S2)]. The correlation between the different methods was very large for all cell populations with Pearson's r ranging from 0.979 to 0.997. Results of Passing–Bablok regression showed slopes for all comparisons between 0.80–1.11. All 95% coefficients of variation (CIs) included 1.00 indicating that there was no proportional bias between the methods for any of the cell populations tested. All intercepts included 0.0 within the 95% CIs (ranging from −0.91–0.23) indicating that there was no significant constant error between the methods for any cell count (Figures 4A–C and Table 3). The Bland–Altman plots showed that all but a few values were within the limits of agreement (LoA), and only a single value when comparing neutrophil counts between SMT and FB, was outside the 95% CI of the upper LoA (Supplementary Figures S3A–C).

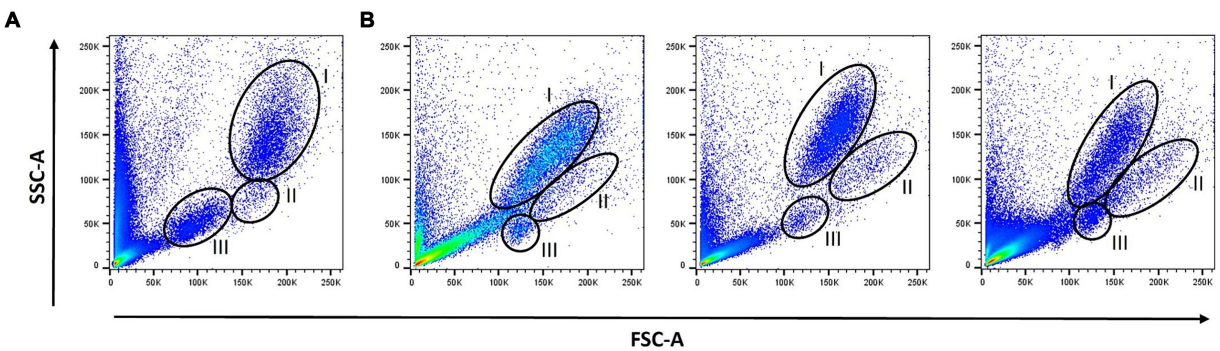

FIGURE 1
Scatter profiles: Forward scatter/Side scatter (FSC /SSC) profiles of lyzed fresh blood **(A)** and lyzed SMART Tube (SMT)-fixed blood samples from three different cats **(B)** were determined by flow cytometry. The different leukocyte populations were gated according to their FSC/SSC scatter profiles: neutrophils (I), monocytes (II), and lymphocytes (III).

10.3389/fvets.2024.1377414

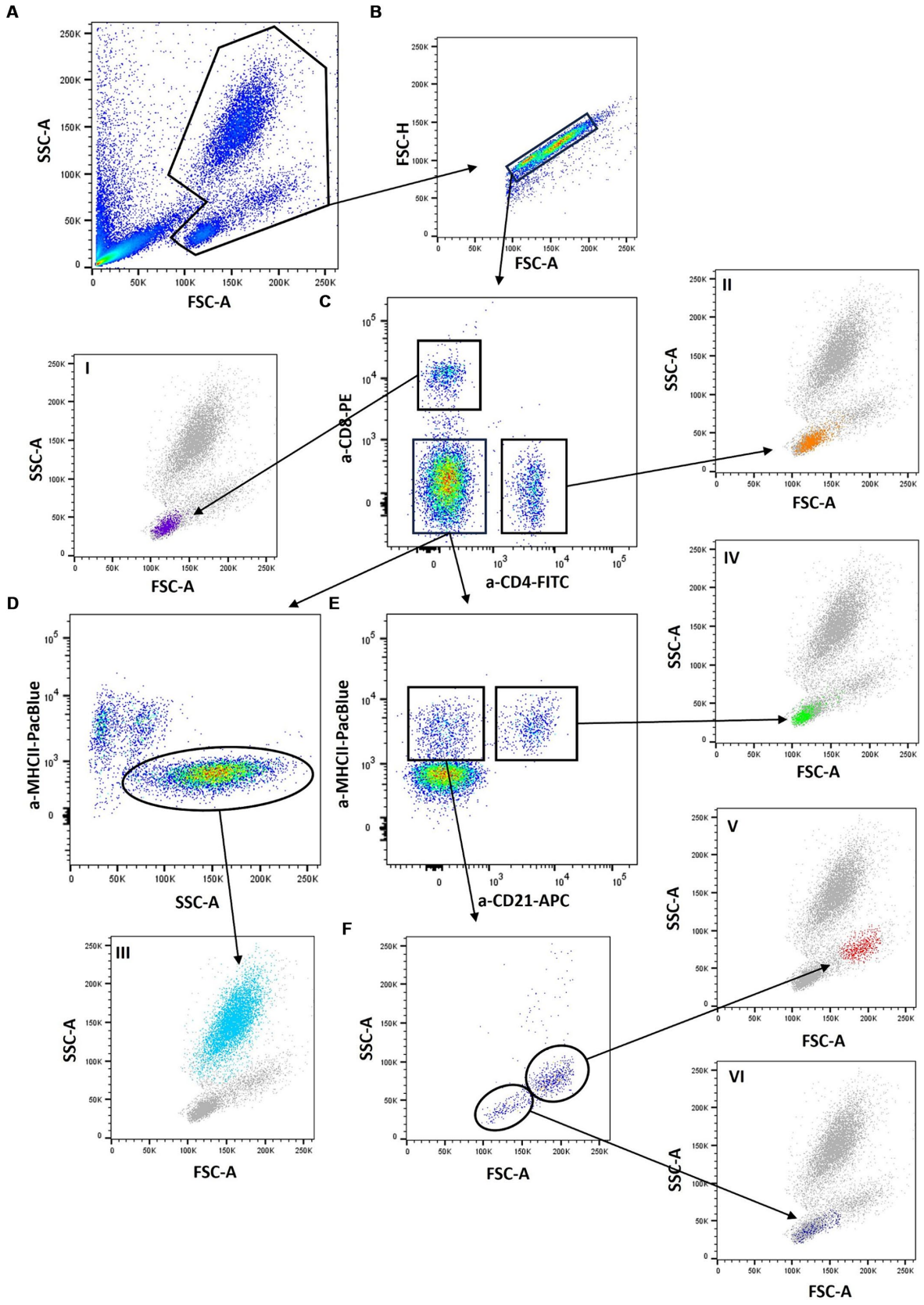

FIGURE 2
Gating strategy: A lyzed SMART Tube (SMT) blood sample was stained with anti-cat-CD4- FITC (vpg34), anti-cat-CD8-PE (fCD8), anti-huCD21-APC (B-ly4), and anti-cat-MHCII-PacificBlue (PF6J-6D) and analyzed by flow cytometry. First, feline leukocytes were identified by their Forward scatter/Side scatter (FSC /SSC) profiles **(A)**, followed by doublet exclusion **(B)**. CD4 and CD8 were used to address CD4+ helper T cells and CD8+ cytotoxic T cells.

(Continued)

FIGURE 2 (Continued)
Double-positive cells were not observed (**C**, I and II). From the CD4/CD8 double-negative population neutrophils were identified through high SSC and a negative MHCII staining (**D**, III). B cells and monocytes were addressed in a CD21/MHCII plot **(E)** with CD21+/MHCII+ B cells and a CD21-/MHCII+ cell population. When the latter was further examined according to its FSC/SSC scatter characteristics **(F)**, two distinct populations could be identified: a more homogeneous population of large cells, which we regard as monocytes (V) and an additional population of smaller cells. Since these CD4-/CD8-/CD21-/MHCII+ cells have a lymphocyte scatter profile (VI), they were regarded as "marker negative lymphocytes."

TABLE 2 **Intra-assay precision estimated from 5 fresh blood and 5 fixed aliquots from a blood sample of a single cat analyzed by flow cytometry.**

	Neutrophils	Monocytes	CD4+	CD8+	CD21+
Samples	Mean ± SD (CV in %)	Mean ± SD (CV in %)	Mean ± SD (CV in %)	Mean ± SD (CV in %)	Mean ± SD (CV in %)
Fresh blood	2.93 ± 0.02 (0.62)	0.29 ± 0.00 (0.84)	0.91 ± 0.01 (0.61)	1.03 ± 0.01 (0.73)	0.92 ± 0.01 (0.60)
Smart tube	3.34 ± 0.01 (0.26)	0.25 ± 0.00 (0.75)	0.73 ± 0.00 (0.65)	0.84 ± 0.00 (0.43)	0.75 ± 0.00 (0.48)

SD, standard deviation; CV, coefficient of variation. The absolute leukocyte counts determined by routine hematologic procedures using the in-house automatic analyzer ProCyte Dx (IDEXX Laboratories, Inc., Maine, United States) were multiplied by the percentage of the respected subpopulations from total single cells determined by flow cytometry; all means of the cell counts of each subpopulation are given in x109/l.

In detail, comparison of neutrophil and monocyte counts revealed Pearson's r $0.985 \geq r \leq 0.994$ (neutrophils) and $0.982 \geq r \leq 0.990$ (monocytes) showing no significant biases between all methods (Figures 4A,B and Supplementary Figures S3A,B). As already assumed from the mean cell counts, the comparison between lymphocyte counts from the different methods revealed the lowest correlation coefficient with $r = 0.979$ (Diff vs. FB/SMT), which, however, still indicates a very large correlation; the biases were significant at 0.33 and 0.43 $\times 10^9$ c/L (differences ranging from −0.32–1.58 $\times 10^9$ c/L), and with the values plotted particularly above the 0 line, it is again indicated that Diff values tended to be higher than FB/SMT. For FB vs. SMT we found $r = 0.997$ with a bias of only −0.1 $\times 10^9$ c/L and differences ranging from −0.58–0.19 $\times 10^9$ c/L (Figure 4C and Supplementary Figure S3C). Since discrimination of lymphocyte subpopulations is not possible using Diffs, CD4+, CD8+ and CD21+ cell counts were only compared between FB and SMT samples (Figure 3B). Here, too, the 95% CI of all slopes and intercepts included 1.00 and 0.00 indicating no proportional bias or constant error. For the three lymphocyte subpopulations, the direct comparison between FB and SMT cells revealed a very large correlation with $r \geq 0.983$. With a few exceptions, the values were within the upper and lower LoA; comparing SMT vs. FB for CD4+, one value was without the 95% CI of the lower LoA. Biases were between −0.08 and − 0.01 $\times 10^9$ c/L (differences ranging from −0.63–0.42 $\times 10^9$ c/L), with minimal significance for CD4+ (Figure 4D; Supplementary Figure S3D and Table 3). Overall, with the anticipated exception of lymphocyte numbers, comparison between Diff counts and flow cytometry of both FB and fixed, frozen SMT samples revealed high correlation and agreement between methods. Comparison of lymphocyte subpopulations between FB and SMT samples showed only minimal differences, demonstrating that fixation and storage of blood samples in SMT tubes is possible.

3.4 Application to long-term stored clinical samples

Finally, we tested the applicability of our protocol for clinical samples using samples from an earlier FIP treatment study. Feline infectious peritonitis (FIP) is a fatal feline coronavirus (FCoV)-induced and immunologically mediated disease characterized by systemic granulomatous vasculitis and perivasculitis (25). Treatment of FIP diseased cats with oral GS-441524 led to a complete recovery of cats with a significant improvement of most clinicopathological parameters [hematological and clinical chemistry parameters including the acute phase protein serum amyloid A (SAA)], which can be highly elevated in cats with FIP during the initial 14 days of treatment (21). Throughout the study, SMT blood samples were obtained and stored at −80°C. The mean sample storage time was 2 years (plus/minus a few weeks, depending on when the cats were included into the study, see Supplementary Table S1 for detailed information). We analyzed SMT samples from five healthy cats (not infected with FCoV) and five cats with FIP on days 0, 7, 14, 28, 56, and 83 after treatment initiation and compared the obtained results with Diff performed on the day of sampling.

Strikingly, the thawing process of SMT samples from the FIP-diseased cats did not work successfully for any sample from days 0 and 7. Samples appeared visibly clotted and, after thawing and lysis, contained large amounts of debris from which no intact cells could be isolated (see Figure 5A, D0 + D7 for representative scatter plots). Accordingly, no comparison between Diff and flow cytometry could be made for D0 and D7 (Figure 5B).

In contrast, control samples and samples from days 28, 56, and 83 could be thawed and processed without any problems, including samples with even longer storage times than D0 and D7 (see Figure 5A, D14–D83 and Supplementary Table S1). On day 14, samples of three cats showed minor signs of clotting, which, however, did not affect further processing.

Owing to the limited sample size, a comprehensive statistical analysis was not conducted. Mean and distribution for neutrophils and monocytes was similar between Diff and SMT, while values for lymphocyte numbers obtained for SMT samples were consistently lower than those from the initial Diff (Figure 5B and Supplementary Table S3).

Importantly, it was possible to determine the number of lymphocyte subpopulations in all non-clotted samples, which revealed a largely identical number of CD8+ cells between control cats and the

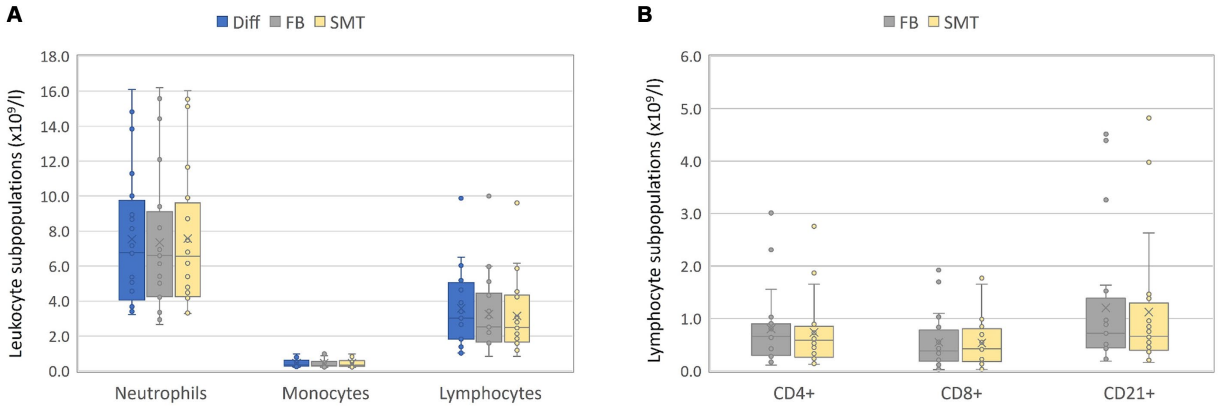

FIGURE 3
Validation – absolute counts: Blood of 20 healthy cats was split in three and objected to automated hematology analysis (Diff), analyzed by flow cytometry within 24 h (FB) or fixed/frozen in a SMART Tube (SMT) before flow cytometric analysis. For FB and SMT samples, the absolute numbers of each leukocyte subset were calculated by multiplication of Diff. Absolute blood cell counts from all three techniques for monocytes, lymphocytes, and neutrophils are presented in **(A)**; lymphocyte subpopulations obtained by flow cytometry are shown in **(B)**. Box plots include the second and the third quantile, whiskers include all values within the 1.5 interquartile range, dots outside the box represent outliers, dots inside the box the values; the horizontal line represents the median, the mean is presented as a cross.

treatment group and considerable differences for CD4+ and CD21+ cells (Figure 5C).

4 Discussion

On-site sample processing during clinical trials is challenging. However, until now, EDTA samples from cats and other species had to be processed within a maximum of 48 h (7). The SMT system for whole blood was developed to allow for fixation and conservation at −80°C for a long period, but this technique had so far been only applied to human biological samples. In this study, the SMT protocol was successfully adapted for feline blood samples. A new flow cytometry protocol to address leukocytes, monocytes, neutrophils, and lymphocytes was established accurately separating lymphocytes into CD4+ T-helper cells, CD8+ cytotoxic T cells and CD21+ B cells even after prolonged storage of samples.

Only commercially available mAbs were used in the staining panel aiming for a wide availability. As the range of cat-specific and cross-reactive commercially available mAbs is currently very limited, while highly desirable to identify all T cells, no surface anti-CD3 or anti-TCR staining could be included. Though a feline CD3 monoclonal antibody recognizing a surface epitope has been described (26) this antibody is not commercially available and has so far rarely been used due to difficulties with conjugation. The anti-human CD3 monoclonal antibody clone CD3-12, targeting an intracytoplasmic epitope of CD3e and cross-reactive with CD3 molecules of multiple species, has been used and reported with success for the detection of feline T cells, and is commercially available conjugated to several different fluorochromes (27). However, this antibody requires permeabilization for intracytoplasmic staining, a step which we did not want to include in our initial protocol. But that could be an option for its further refinement. As potential alternative, staining for CD5 expression was reported as option to address all feline T cells (28) and several mAbs (f43; FE1.1B11) are commercially available. Both should be tested in future for their suitability in staining SMT-fixed cells.

From the tested mAbs, the potential monocyte marker anti-CD14 had to be omitted eventually as it did not show the desired staining specificity but instead resulted in an undistinguishable staining of monocytes and neutrophils. Some mAbs (an anti-CD4 and an anti-CD21 clone) worked well on FB but staining patterns were altered by fixation to a great extent, a well-known phenomenon, as fixation can affect cell membrane permeability leading to unspecific staining or disrupts the antibody's epitopes leading to loss of staining (29, 30).

Finally, four mAbs specific for CD4, CD8, CD21 and MHC class II were identified showing excellent performance on both FB and SMT samples. Staining for CD4 and CD8 to address T-helper cells and cytotoxic T cells is common practice in cats (31–33). CD4 and CD8 expression on feline PBMC CD3+ cells are mutually exclusive and hardly any double positive cells were found in the present study as well as in previous studies (34). Still, it must be considered that in many species, e.g., dogs and pigs (35, 36), CD8 is also expressed on a subset of γδ T cells and in some species additional CD8 is found on NK cells (37–40). Due to the lack of feline TCR-specific mAbs to discriminate between αβ and γδ T cells and commercially available surface markers for NK cells, we could not address these cells. However, in dogs, a related species, with more available markers, only 0.5–3% of peripheral blood lymphocytes are CD8 expressing γδ T cells CD8 (41). Assuming that cats are also a γδ-low species and considering that about 15% of lymphocytes were CD8+, the content of CD8+ γδ T cells is probably only marginal. In addition, Vermeulen and colleagues showed, that feline NK cells represent only about 1–5% of PBL and only 10% of these cells express CD8, resulting in only 0.1–0.5% of CD8 expressing non-T cells (42). Thus, despite some limitations it seems justified to refer to the gated CD8+ cells as cytotoxic T cells. Unfortunately, the lack of CD3 staining prevents the identification of a potential small CD4-/CD8- double negative T cell population which was reported in other species (35).

CD21 is an established B cell marker in many species (19, 43, 44) and although the cat-specific anti-CD21 mAb did not work on SMT, the cross-reactive human clone with identical staining on FB could be included into the antibody panel. Nevertheless, as in other species,

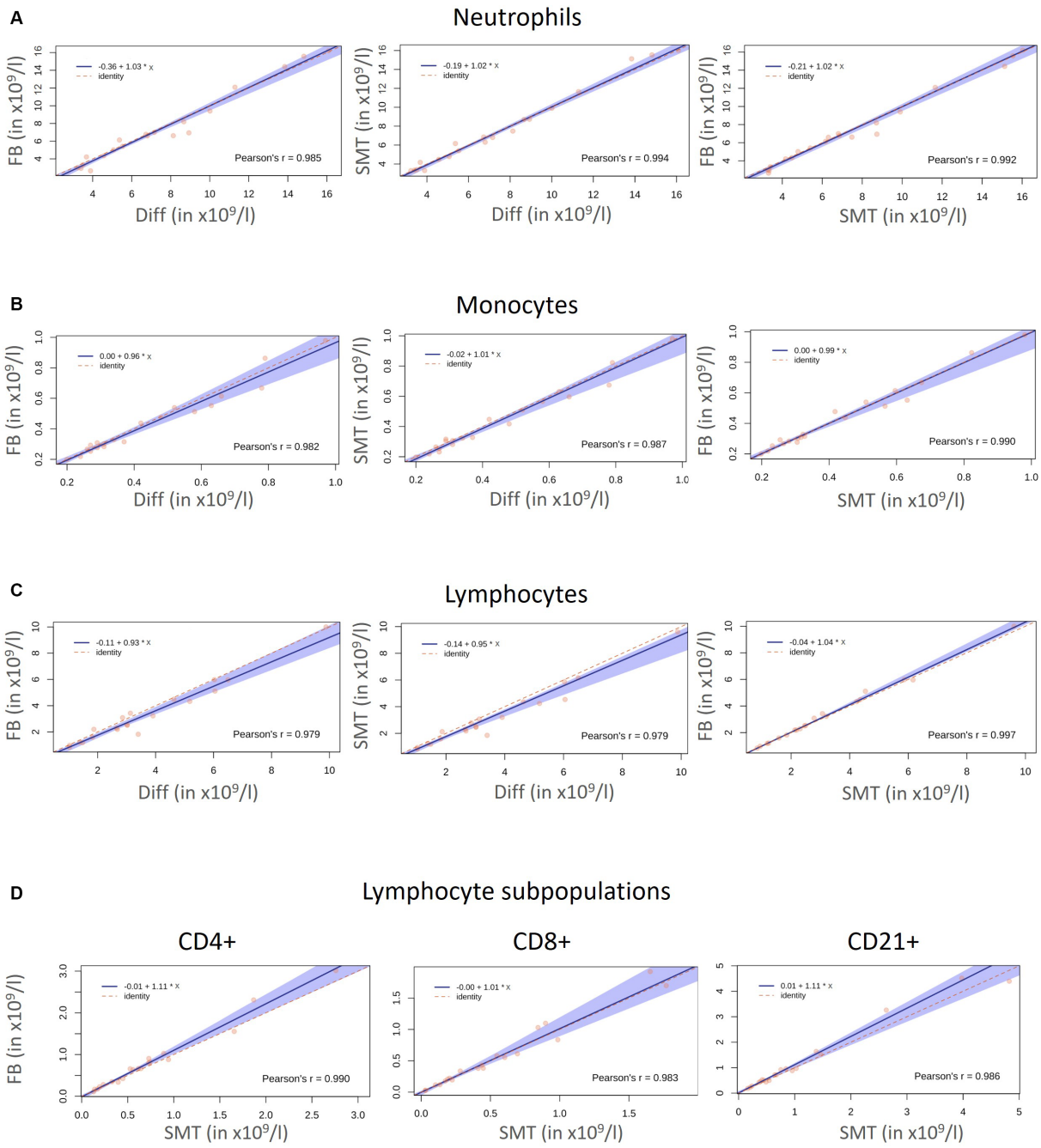

FIGURE 4
Correlation Diff/FB/SMT: Correlation and agreement between the absolute cell numbers (x10^9/l) for neutrophils **(A)**, monocytes **(B)**, and lymphocytes **(C)** of 20 healthy cats obtained with an automated hematology analyzer (Diff), by flow cytometry within 24 h (FB) and with fixed/frozen Smart Tubes (SMTs). Side scatter diagrams with the red dots represent measured values. The solid blue line represents the regression line, the dashed red line represents the line of identity, and 95% confidence intervals (CI) are represented by the blue shaded area. Comparison for lymphocyte subpopulations obtained by flow cytometry with FB and SMT are shown in **(D)**. Pearson's correlation coefficient (r) is given in each diagram.

anti-CD21 staining probably does not address all stages of feline B cell differentiation. In other species like humans, B cells lose CD21 expression when they differentiate into plasmablasts (45) and the presence of some CD21−/immunoglobulin+ B cells, which is larger in cell size (FSC) and probably resembles plasmablasts was reported in feline blood (46). Activated memory B cells in humans and non-human primates also lose CD21 expression (47). It is therefore quite possible that CD21+ cells represent not all differentiation states of feline B cells and staining for the B cell receptor complex (e.g., with anti-CD79) might be an option to address further B cell subpopulations in the future.

However, it is highly likely that these CD21−B cell stages cells express MHCII and hence could be part of the MHCII+/marker-negative small cell population in the gating strategy.

In addition to B cells and monocytes, almost all other feline lymphocytes express MHC class II without prior activation, but

TABLE 3 Passing-Bablok [with 95% confidence intervals (CI)] regression analysis between the different methods for neutrophils, monocytes, and lymphocytes and Pearson's correlation coefficient (r).

	Neutrophils r Slope (CI)/ Intercept (CI)	Monocytes r Slope (CI)/ Intercept (CI)	Lymphocytes* r Slope (CI)/ Intercept (CI)	CD4+ r Slope (CI)/ Intercept (CI)	CD8+ r Slope (CI)/ Intercept (CI)	CD21+ r Slope (CI)/ Intercept (CI)
FB/ Diff	0.985 1.03 (0.94–1.11)/ −0.36 (−0.91–0.23)	0.982 0.96 (0.81–1.10)/ 0.00 (−0.04–0.05)	0.979 0.93 (0.84–1.04)/ −0.11 (−0.47–0.08)	–	–	–
SMT/Diff	0.994 1.02 (0.97–1.09)/ −0.19 (−0.72–0.11)	0.987 1.01 (0.85–1.08)/ −0.01 (−0.05–0.04)	0.979 0.95 (0.80–1.01)/ −0.14 (−0.41–0.12)	–	–	–
SMT/ FB	0.992 1.02 (0.95–1.08)/ −0.21 (−0.66–0.18)	0.990 1.00 (0.84–1.05)/ 0.00 (−0.02–0.05)	0.997 1.04 (1.01–1.11)/ −0.04 (−0.16–0.01)	0.990 1.11 (0.99–1.25)/ −0.01 (−0.09–0.03)	0.983 1.01 (0.88–1.23)/ −0.00 (−0.05–0.02)	0.986 1.11 (0.91–1.20)/ 0.00 (−0.04–0.08)

r, Pearson's correlation coefficient; CI, 95% confidence intervals; SMT, fixed cells with Smart Tube System; Diff, differential blood count with automatic hemocytometer, FB, fresh blood.
*Lymphocyte numbers were calculated by adding up the numbers of CD4+, CD8+, CD21+ and "marker-negative" lymphocytes.

neutrophils are MHC class II-negative (17). Hence, anti-MHCII staining were used to discriminate neutrophils and monocytes in the present study. Though comparison of monocyte numbers from an automated analyzer and the gating strategy of the SMT protocol showed a very large correlation, it must be mentioned that in many species monocytes express to a different extent CD4 (48). For example, in dogs next to the majority of MHCII+/CD4− monocytes two minor subsets of MHCII+/CD4+ and even MHCII−/CD4+ monocytes were identified (49). Hence, the small subset of larger cells in our CD4+ gate, instead being activated T helper cells, could also be monocytes. If antibodies are available, a possible solution to overcome this problem in the future studies would be the inclusion of a specific T cell or monocyte marker.

For validation of the used staining protocol with blood samples obtained from healthy cats, flow cytometry derived numbers of FB and SMT samples were compared to cell counts obtained by an automatic hematology analyzer. It is known that accuracy of automated leukocyte differentials particularly for animal species and especially the quantification of monocytes and basophils does not reach the accuracy of microscopic review. Though microscopic review of blood smears in this study was only performed when the automated differential was inconclusive, we have put up with this limitation as automated leukocyte counts were only used to verify agreement between methods and not accuracy of the real values.

The comparison revealed a very good agreement for the quantification of monocytes and neutrophils. Flow cytometry-based lymphocyte counts were generally lower than the automated counts, but still showed a very large correlation. A possible explanation for the reduced numbers could be that lymphocyte numbers were calculated as the sum of CD4+, CD8+, CD21+ and MHCII+/marker-negative/small cells, which does not include potential additional MHCII− lymphocytes, such as CD4−/CD8− T cells, NK cells and CD21− B cell subsets. In future studies, addition of an anti-CD18 mAb, which is reported as panleukocyte marker with good lymphocyte discrimination (50), might help to solve this issue, provided it works on fixed cells. However, considering a study evaluating the ProCyte Dx, one of the automated analyzers used in this study, the results showed good to excellent correlations for most different leukocyte counts, but deviations of up to 30% for lymphocyte counts (51). Therefore, results of the used flow cytometry protocol without anti-CD18 were satisfactory.

Comparison of lymphocyte subpopulations between FB and SMT samples showed a very large correlation and agreement with only minimal biases, demonstrating that fixation, freezing, and thawing and a second lysis step in the SMT protocol did not affect the number of T and B cells. Thus, the SMT technology can be successfully applied to feline blood samples. Though the validation was carried out on samples that had only been frozen for an average time of 2 days, the comparable results of the FB samples and the paired long-term SMT-fixed and frozen samples from FIP diseased (at the later study timepoints) and healthy control cats suggests that long-term preservation and processing is also possible with reliable results.

Availability of the SMT technology is of paramount importance for trial purposes, allowing for collection of biological samples during routine business and analysis of respective samples at a later time point. In addition, collection of samples can now be performed at various study site with sample analysis taking place in a different site or laboratory.

To assess applicability of the new feline SMT protocol in practice, SMT samples from cats in a FIP treatment study were investigated. Strikingly, in contrast to samples from healthy cats, not a single sample from a cat with FIP from day 0 to day 7 after treatment initiation could be analyzed. Regular thawing of SMTs was not possible, as the stabilized samples were visibly clotted and contained only large amounts of debris following lysis, and no intact cells could be isolated. Interestingly, one human study using SMTs for hospitalized COVID-19 patients reported similar results. The SMTs worked very well with healthy donor samples, but performance was poor with samples of a large number of acute COVID-19 patients. This was discussed to be related to polymerized fibrin or other plasma factors associated with COVID-19-associated coagulopathy (9). Cats with FIP can also develop disseminated intravascular coagulopathy due to activation of complement and clotting factors and marked vasculitis during the inflammatory process (52). Indeed, it is already known that inflammatory markers, such as SAA and alpha-1-acid glycoprotein (53), can be highly elevated in cats with FIP, which indicates a severe inflammatory response (54–57). Cats in the treatment study had very high SAA concentrations before and up to 7 days of treatment, which then decreased rapidly and were in the reference range by day 14 (21). The marked decrease of inflammatory markers in response to treatment indicates a strong attenuation of the hyperinflammatory

10.3389/fvets.2024.1377414

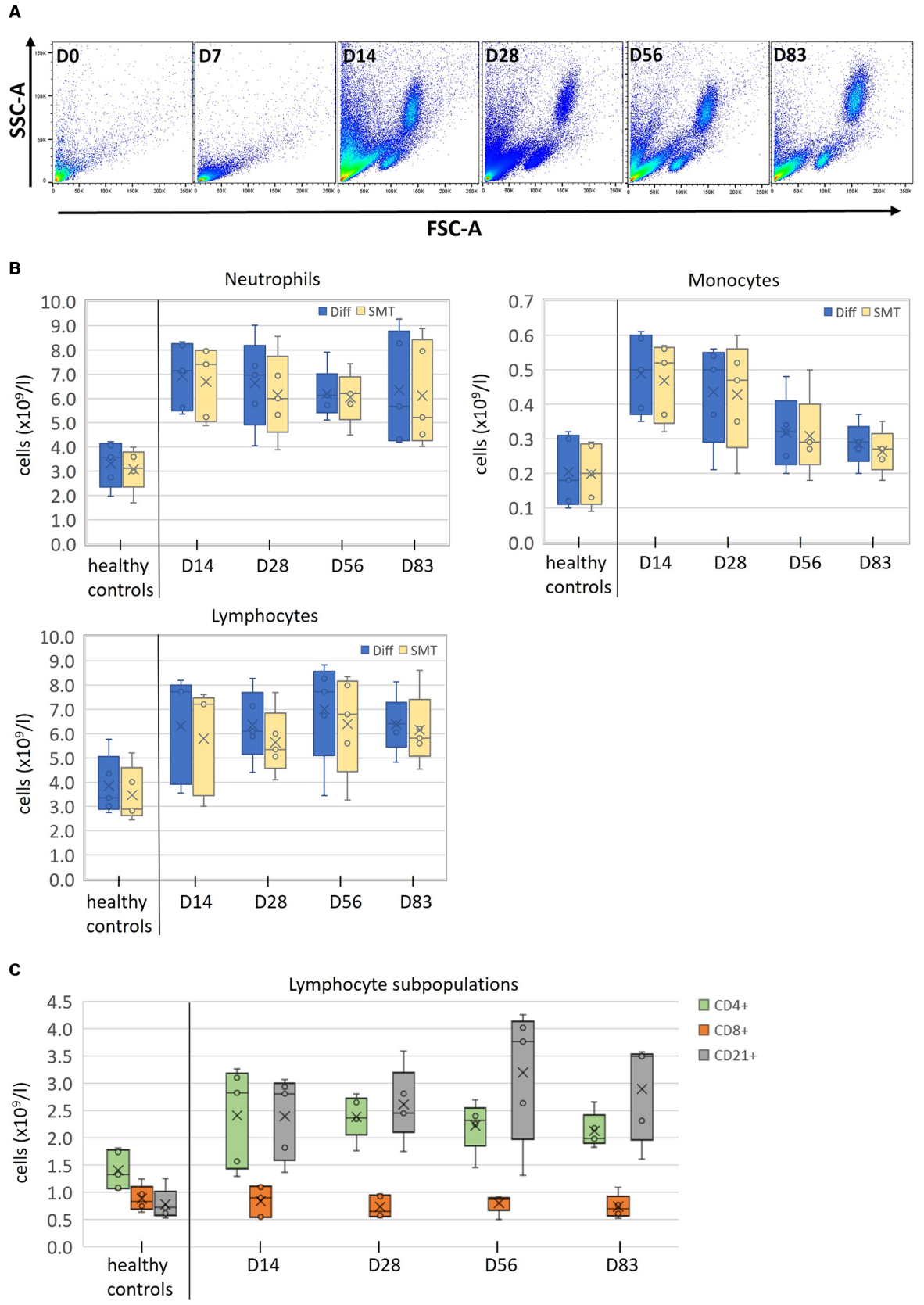

FIGURE 5
Measurement of clinical SMT samples after long time storage **(A)** FSC/SSC profiles of SMT blood samples from one representative cat suffering from feline infectious peritonitis (FIP) before (D0), and during (D7, 14, 28, 56, and 83) antiviral treatment. **(B)** Absolute counts of all cell populations

(Continued)

FIGURE 5 (Continued)
(neutrophils, monocytes, and lymphocytes) from five healthy control cats collected at a single timepoint and from five FIP cats at the indicated timepoints, analyzed with an automated hematology analysis at the day of sampling (Diff; blue Box plots) or by flow cytometry with fixed/frozen SMART Tubes (SMT; orange Box plots) up to 2 years post sampling. **(C)** Lymphocyte subpopulations (CD4+, CD8+, and CD21+) of indicated SMT samples after long time storage. Box plots include the second and the third quantile, whiskers include all values within the 1.5 interquartile range, dots outside the box represent outliers, dots inside the box the values; the horizontal line represents the median, the mean is presented as a cross.

FIP-mediated stage, and from the day of normalization of inflammatory markers on, SMT samples could be analyzed without problems. Although COVID-19 can also cause a strong inflammatory response in humans, affected SMT samples in the above-mentioned study were still processable with protocol modifications, which however, did not work with affected cat SMT samples of the present study. This might be explained by an even more pronounced inflammatory status in cats with FIP or an amplification of the effect by feline platelets, which, even in healthy cats, generally have a high tendency to clump after blood collection regardless of the collection technique (58).

Taken together, this first application of the newly established feline SMT flow cytometry protocol demonstrates a general possibility for flow cytometric analysis after long-term storage of full blood samples, and that in its current form can probably not be used for samples taken during a highly inflammatory state of a patient. Future experiments will need to address whether this phenomenon also occurs in other acute diseases such as septic conditions and severe bacterial infections or whether this is FIP-specific. In a next step it should be evaluated whether the sampling procedure can be modified for samples from such conditions.

In conclusion, in the present study we demonstrate for the first time that the SMT system is successfully applicable for feline full blood samples. Using our newly established protocol, samples can be collected, stabilized, sent to a laboratory for flow cytometric analysis, or stored to address later arising questions. In addition, the successful technology transfer from human to veterinary medicine will likely pave the way to its, albeit slightly modified, application in other animal species. This holds the potential to significantly improve and simplify workflows, subsequently enhancing the amount of knowledge that can be obtained from animal studies.

Data availability statement

The original contributions presented in the study are included in the article/Supplementary material, further inquiries can be directed to the corresponding author.

Ethics statement

The animal studies were approved by Government of Upper Bavaria, reference number 55.2-2532.Vet_02-20-52 and ethical committee (reference number 261-19-03-2021) of the Centre for Clinical Veterinary Medicine of the LMU Munich. The studies were conducted in accordance with the local legislation and institutional requirements. Written informed consent was obtained from the owners for the participation of their animals in this study.

Author contributions

KZ: Conceptualization, Formal analysis, Investigation, Methodology, Resources, Validation, Visualization, Writing – original draft, Writing – review & editing. DR: Investigation, Methodology, Writing – review & editing. DK: Resources, Writing – review & editing. LK: Resources, Writing – review & editing. MA: Conceptualization, Writing – review & editing. YZ: Statistical Analysis, Writing – review & editing. KH: Conceptualization, Funding acquisition, Writing – review & editing. UB: Conceptualization, Funding acquisition, Writing – review & editing. SH: Conceptualization, Formal analysis, Funding acquisition, Methodology, Validation, Visualization, Writing – original draft, Writing – review & editing.

Funding

The author(s) declare that no financial support was received for the research, authorship, and/or publication of this article.

Acknowledgments

The authors would like to thank Marina Kohn for her excellent technical support and assistance whenever it was necessary, and Kaspar Matiasek for arranging the contact.

Conflict of interest

The authors declare that the research was conducted in the absence of any commercial or financial relationships that could be construed as a potential conflict of interest.

Publisher's note

Supplementary material

The Supplementary material for this article can be found online at: https://www.frontiersin.org/articles/10.3389/fvets.2024.1377414/full#supplementary-material

References

1. Herzenberg LA, Parks D, Sahaf B, Perez O, Roederer M, Herzenberg LA. The history and future of the fluorescence activated cell sorter and flow cytometry: a view from Stanford. *Clin Chem*. (2002) 48:1819–27. doi: 10.1093/clinchem/48.10.1819

2. Bariogie B, Raber MN, Schumann J, Johnson TS, Drewinko B, Swartzendruber DE, et al. Flow cytometry in clinical cancer research. *Cancer Res*. (1983) 43:3982–97.

3. Ibrahim SF, Van Den Engh G. Flow cytometry and cell sorting. *Adv Biochem Eng Biotechnol*. (2007) 106:19–39. doi: 10.1007/10_2007_073

4. Martini V, Bernardi S, Marelli P, Cozzi M, Comazzi S. Flow cytometry for feline lymphoma: a retrospective study regarding pre-analytical factors possibly affecting the quality of samples. *J Feline Med Surg*. (2018) 20:494–501. doi: 10.1177/1098612X17717175

5. Murphy B, Hillman C, McDonnel S. Peripheral immunophenotype and viral promoter variants during the asymptomatic phase of feline immunodeficiency virus infection. *Virus Res*. (2014) 179:34–43. doi: 10.1016/j.virusres.2013.11.017

6. Trewhitt KG. Bone marrow aspiration and biopsy: collection and interpretation. *Oncol Nurs Forum*. (2001) 28:1415.

7. Davis BH, Dasgupta A, Kussick S, Han JY, Estrellado A. Validation of cell-based fluorescence assays: practice guidelines from the ICSH and ICCS – part II – preanalytical issues. *Cytometry B Clin Cytom*. (2013) 84:286–90. doi: 10.1002/cyto.b.21105

8. Granat F., Geffré A., Bourgès-Abella N., Braun J-P., Trumel C. Changes in haematology measurements with the Sysmex XT-2000iV during storage of feline blood sampled in EDTA or EDTA plus CTAD. *J Feline Med Surg* (2013) 15:433–444. doi: 10.1177/1098612X12469967

9. Geanon D, Lee B, Gonzalez-Kozlova E, Kelly G, Handler D, Upadhyaya B, et al. A streamlined whole blood CyTOF workflow defines a circulating immune cell signature of COVID-19. *Cytometry A*. (2021) 99:446–61. doi: 10.1002/cyto.a.24317

10. Chen L, Youssef Y, Robinson C, Ernst GF, Carson MY, Young KA, et al. CD56 expression marks human group 2 innate lymphoid cell divergence from a shared NK cell and group 3 innate lymphoid cell developmental pathway. *Immunity*. (2018) 49:464–476.e4. doi: 10.1016/j.immuni.2018.08.010

11. Aghaeepour N, Ganio EA, Mcilwain D, Tsai AS, Tingle M, van Gassen S, et al. An immune clock of human pregnancy. *Sci Immunol*. (2017) 2:2. doi: 10.1126/sciimmunol.aan2946

12. Spitzer MH, Carmi Y, Reticker-Flynn NE, Kwek SS, Madhireddy D, Martins MM, et al. Systemic immunity is required for effective cancer immunotherapy. *Cell*. (2017) 168:487–502.e15. doi: 10.1016/j.cell.2016.12.022

13. Ackley CO, Hoover LA, Cooper MD. Identification of a CD4 homologue in the cat. *Tissue Antigens*. (1990) 35:92–8. doi: 10.1111/j.1399-0039.1990.tb01762.x

14. Callanan JJ, Racz P, Thompson H, Jarrett O. Morphologic characterization of the lymph node changes in feline immunodeficiency virus infection as an animal model of AIDS1 In: P Racz, NL Letvin and JC Gluckman, editors. *Animal Models of HIV and Other Retroviral Infections* (1993). (Basel, CHE: S.Karger AG), 115–36.

15. Klotz FW, Cooper MD. A feline thymocyte antigen defined by a monoclonal antibody (FT2) identifies a subpopulation of non-helper cells capable of specific cytotoxicity. *J Immunol*. (1986) 136:2510–4. doi: 10.4049/jimmunol.136.7.2510

16. Jacobsen CN, Aasted B, Broe MK, Petersen JL. Reactivities of 20 anti-human monoclonal antibodies with leucocytes from ten different animal species. *Vet Immunol Immunopathol*. (1993) 39:461–6. doi: 10.1016/0165-2427(93)90075-F

17. Hunt P, Mcconnell I, Grant CK, Else RW, Hopkins J. Variable expression of major histocompatibility complex class II in the domestic cat. *Res Vet Sci*. (1995) 59:195–200. doi: 10.1016/0034-5288(95)90001-2

18. Fischer E, Delibrias C, Kazatchkine MD. Expression of CR2 (the C3dg/EBV receptor, CD21) on normal human peripheral blood T lymphocytes. *J Immunol*. (1991) 146:865–9. doi: 10.4049/jimmunol.146.3.865

19. Cobbold S, Metcalfe S. Monoclonal antibodies that define canine homologues of human CD antigens: summary of the first international canine leukocyte antigen workshop (CLAW). *Tissue Antigens*. (1994) 43:137–54. doi: 10.1111/j.1399-0039.1994.tb02315.x

20. Holznagel E, Hofmann-Lehmann R, Leutenegger CM, Allenspach K, Huettner S, Forster U, et al. The role of in vitro-induced lymphocyte apoptosis in feline immunodeficiency virus infection: correlation with different markers of disease progression. *J Virol*. (1998) 72:9025–33. doi: 10.1128/JVI.72.11.9025-9033.1998

21. Krentz D, Zenger K, Alberer M, Felten S, Bergmann M, Dorsch R, et al. Curing cats with feline infectious peritonitis with an oral multi-component drug containing GS-441524. *Viruses*. (2021) 13:2228. doi: 10.3390/v13112228

22. Meli ML, Spiri AM, Zwicklbauer K, Krentz D, Felten S, Bergmann M, et al. Fecal feline coronavirus RNA shedding and spike gene mutations in cats with feline infectious peritonitis treated with GS-441524. *Viruses*. (2022) 14:1069. doi: 10.3390/v14051069

23. Zwicklbauer K, Krentz D, Bergmann M, Felten S, Dorsch R, Fischer A, et al. Long-term follow-up of cats in complete remission after treatment of feline infectious peritonitis with oral GS-441524. *J Feline Med Surg*. (2023) 25:25. doi: 10.1177/1098612X231183250

24. Funder DC, Ozer DJ. Evaluating effect size in psychological research: sense and nonsense. *Adv Methods Pract Psychol Sci*. (2019) 2:156–68. doi: 10.1177/2515245919847202

25. Kipar A, May H, Menger S, Weber M, Leukert W, Reinacher M. Morphologic features and development of granulomatous vasculitis in feline infectious peritonitis. *Vet Pathol*. (2005) 42:321–30. doi: 10.1354/vp.42-3-321

26. Nishimura Y, Shimojima M, Sato E, Izumiya Y, Tohya Y, Mikami T, et al. Downmodulation of CD3ε expression in CD8α + β − T cells of feline immunodeficiency virus-infected cats. *J Gen Virol*. (2004) 85:2585–9. doi: 10.1099/vir.0.80102-0

27. Rütgen BC, Baszler E, Weingand N, Wolfesberger B, Baumgartner D, Hammer SE, et al. Composition of lymphocyte subpopulations in normal and mildly reactive peripheral lymph nodes in cats. *J Feline Med Surg*. (2022) 24:77–90. doi: 10.1177/1098612X211005310

28. Ackley CD, Cooper MD. Characterization of a feline T-cell-specific monoclonal antibody reactive with a CD5-like molecule. *Am J Vet Res*. (1992) 53:466–71. doi: 10.2460/ajvr.1991.53.04.466

29. de Ruiter K, van Staveren S, Hilvering B, Knol E, Vrisekoop N, Koenderman L, et al. A field-applicable method for flow cytometric analysis of granulocyte activation: cryopreservation of fixed granulocytes. *Cytometry A*. (2018) 93:540–7. doi: 10.1002/cyto.a.23354

30. Maecker HT, McCoy JP Jr , FOCIS Human Immunophenotyping ConsortiumAmos M, Elliott J, Gaigalas A, et al. A model for harmonizing flow cytometry in clinical trials. *Nat Immunol*. (2010) 11:975–8. doi: 10.1038/ni1110-975

31. Byrne KM, Kim HW, Chew BP, Reinhart GA, Hayek MG. A standardized gating technique for the generation of flow cytometry data for normal canine and normal feline blood lymphocytes. *Vet Immunol Immunopathol*. (2000) 73:167–82. doi: 10.1016/s0165-2427(99)00163-4

32. Walker C, Canfield PJ, Love DN. Analysis of leucocytes and lymphocyte subsets for different clinical stages of naturally acquired feline immunodeficiency virus infection. *Vet Immunol Immunopathol*. (1994) 44:1–12. doi: 10.1016/0165-2427(94)90165-1

33. Roosje PJ, van Kooten PJS, Thepen T, Bihari IC, Rutten VPMG, Koeman JP, et al. Increased numbers of CD4+ and CD8+ T cells in lesional skin of cats with allergic dermatitis. *Vet Pathol*. (1998) 35:268–73. doi: 10.1177/030098589803500405

34. Dean GA, Quackenbush SL, Ackley CD, Cooper MD, Hoover EA. Flow cytometric analysis of T-lymphocyte subsets in cats. *Vet Immunol Immunopathol*. (1991) 28:327–35. doi: 10.1016/0165-2427(91)90124-u

35. Rabiger FV, Rothe K, von Buttlar H, Bismarck D, Büttner M, Moore PF, et al. Distinct features of canine non-conventional CD4−CD8α− double-negative TCRαβ+ vs. TCRγδ+ T cells. *Front Immunol*. (2019) 10:2748. doi: 10.3389/fimmu.2019.02748. eCollection 2019

36. Yang H, Parkhouse RME. Differential expression of CD8 epitopes amongst porcine CD8-positive functional lymphocyte subsets. *Immunology*. (1997) 92:45–52. doi: 10.1046/j.1365-2567.1997.00308.x

37. Addison EG, North J, Bakhsh I, Marden C, Haq S, al-Sarraj S, et al. Ligation of CD8α on human natural killer cells prevents activation-induced apoptosis and enhances cytolytic activity. *Immunology*. (2005) 116:354–61. doi: 10.1111/j.1365-2567.2005.02235.x

38. Trinchieri G. Biology of natural killer cells. *Adv Immunol*. (1989) 47:187–376. doi: 10.1016/S0065-2776(08)60664-1

39. Boysen P, Gunnes G, Pende D, Valheim M, Storset AK. Natural killer cells in lymph nodes of healthy calves express CD16 and show both cytotoxic and cytokine-producing properties. *Dev Comp Immunol*. (2008) 32:773–83. doi: 10.1016/j.dci.2007.11.006

40. Ferlazzo G, Thomas D, Lin SL, Goodman K, Morandi B, Muller WA, et al. The abundant NK cells in human secondary lymphoid tissues require activation to express killer cell Ig-like receptors and become cytolytic. *J Immunol*. (2004) 172:1455–62. doi: 10.4049/jimmunol.172.3.1455

41. Galler A, Rütgen BC, Haas E, Saalmüller A, Hirt RA, Gerner W, et al. Immunophenotype of peripheral blood lymphocytes in dogs with inflammatory bowel disease. *J Vet Intern Med*. (2017) 31:1730–9. doi: 10.1111/jvim.14812

42. Vermeulen BL, Devriendt B, Olyslaegers DA, Dedeurwaerder A, Desmarets LM, Grauwet KL, et al. Natural killer cells: frequency, phenotype and function in healthy cats. *Vet Immunol Immunopathol*. (2012) 150:69–78. doi: 10.1016/j.vetimm.2012.08.010

43. Moore PF, Rossitto PV, Danilenko DM, Wielenga JJ, Raff RF, Severns E. Monoclonal antibodies specific for canine CD4 and CD8 define functional T-lymphocyte subsets and high-density expression of CD4 by canine neutrophils. *Tissue Antigens*. (1992) 40:75–85. doi: 10.1111/j.1399-0039.1992.tb01963.x

44. Dean GA, Reubel GH, Moore PF, Pedersen NC. Proviral burden and infection kinetics of feline immunodeficiency virus in lymphocyte subsets of blood and lymph node. *J Virol*. (1996) 70:5165–9. doi: 10.1128/JVI.70.8.5165-5169.1996

45. Tedder TF, Clement LT, Cooper MD. Expression of C3d receptors during human B cell differentiation: immunofluorescence analysis with the HB-5 monoclonal antibody. *J Immunol*. (1984) 133:678–83. doi: 10.4049/jimmunol.133.2.678

46. Takano T, Azuma N, Hashida Y, Satoh R, Hohdatsu T. B-cell activation in cats with feline infectious peritonitis (FIP) by FIP-virus-induced B-cell differentiation/survival factors. *Arch Virol*. (2009) 154:27–35. doi: 10.1007/s00705-008-0265-9

47. Chang WL, Gonzalez DF, Kieu HT, Castillo LD, Messaoudi I, Shen X, et al. Changes in circulating B cell subsets associated with aging and acute SIV infection in Rhesus macaques. *PLoS One*. (2017) 12:e0170154. doi: 10.1371/journal.pone.0170154. PMID: 28095513

48. Ziegler-Heitbrock L. Monocyte subsets in man and other species. *Cell Immunol*. (2014) 289:135–9. doi: 10.1016/j.cellimm.2014.03.019

49. Rzepecka A, Żmigrodzka M, Witkowska-Piłaszewicz O, Cywińska A, Winnicka A. CD4 and MHCII phenotypic variability of peripheral blood monocytes in dogs. *PLoS One*. (2019) 14:e0219214. doi: 10.1371/journal.pone.0219214

50. Martini V, Bernardi S, Giordano A, Comazzi S. Flow cytometry expression pattern of CD44 and CD18 markers on feline leukocytes. *J Vet Diagn Invest*. (2020) 32:706–9. doi: 10.1177/1040638720945670

51. Goldmann F, Bauer N, Moritz A. Evaluation of the IDEXX ProCyte dx analyzer for dogs and cats compared to the Siemens ADVIA 2120 and manual differential. *Comp Clin Path*. (2014) 23:283–96. doi: 10.1007/s00580-012-1608-1

52. Pedersen NC. A review of feline infectious peritonitis virus infection: 1963-2008. *J Feline Med Surg*. (2009) 11:225–58. doi: 10.1016/j.jfms.2008.09.008

53. Saverio P, Alessia G, Vito T, Stefano G. Critical assessment of the diagnostic value of feline alpha1-acid glycoprotein for feline infectious peritonitis using the likelihood ratios approach. *J Vet Diagn Invest*. (2007) 19:266–72. doi: 10.1177/104063870701900306

54. Tecles F, Caldín M, Tvarijonaviciute A, Escribano D, Martínez-Subiela S, Cerón JJ. Serum biomarkers of oxidative stress in cats with feline infectious peritonitis. *Res Vet Sci*. (2015) 100:12–7. doi: 10.1016/j.rvsc.2015.02.007

55. Hazuchova K, Held S, Neiger R. Usefulness of acute phase proteins in differentiating between feline infectious peritonitis and other diseases in cats with body cavity effusions. *J Feline Med Surg*. (2017) 19:809–16. doi: 10.1177/1098612X16658925

56. Sasaki K, Ma Z, Khatlani TS, Okuda M, Inokuma H, Onishi T. Evaluation of feline serum amyloid a (SAA) as an inflammatory marker. *J Vet Med Sci*. (2003) 65:545–8. doi: 10.1292/jvms.65.545

57. Giordano A, Spagnolo V, Colombo A, Paltrinieri S. Changes in some acute phase protein and immunoglobulin concentrations in cats affected by feline infectious peritonitis or exposed to feline coronavirus infection. *Vet J*. (2004) 167:38–44. doi: 10.1016/s1090-0233(03)00055-8

58. Riond B, Waßmuth AK, Hartnack S, Hofmann-Lehmann R, Lutz H. Study on the kinetics and influence of feline platelet aggregation and deaggregation. *BMC Vet Res*. (2015) 11:276. doi: 10.1186/s12917-015-0590-7

frontiers | Frontiers in Veterinary Science

TYPE Original Research
PUBLISHED 26 July 2024
DOI 10.3389/fvets.2024.1412227

OPEN ACCESS

EDITED BY
Fernando Costa Ferreira,
University of Lisbon, Portugal

REVIEWED BY
Serenella Silvestri,
Centre for Haemato-Oncology Research (CREO), Italy
William Kisseberth,
The Ohio State University, United States

*CORRESPONDENCE
Valeria Martini
✉ valeria.martini@unimi.it

RECEIVED 04 April 2024
ACCEPTED 15 July 2024
PUBLISHED 26 July 2024

CITATION
Ubiali A, Cesar Conti L, Dall'Ara P, De Maria R, Aresu L, Moretti P, Sini F, Riondato F, Stefanello D, Comazzi S and Martini V (2024) Exploring the dynamics of Programmed Death-Ligand 1 in canine lymphoma: unraveling mRNA amount, surface membrane expression and plasmatic levels. *Front. Vet. Sci.* 11:1412227. doi: 10.3389/fvets.2024.1412227

Exploring the dynamics of Programmed Death-Ligand 1 in canine lymphoma: unraveling mRNA amount, surface membrane expression and plasmatic levels

Alessandra Ubiali[1], Luiza Cesar Conti[2], Paola Dall'Ara[1], Raffaella De Maria[2], Luca Aresu[2], Pierangelo Moretti[1], Federica Sini[2], Fulvio Riondato[2], Damiano Stefanello[1], Stefano Comazzi[1] and Valeria Martini[1]*

[1]Department of Veterinary Medicine and Animal Sciences, University of Milan, Lodi, Italy, [2]Department of Veterinary Sciences, University of Turin, Grugliasco, TO, Italy

Introduction: Programmed Death-Ligand 1 is a well-known immune checkpoint molecule. Recent studies evaluated its expression in different canine cancer types through different laboratory techniques. The present study aims to evaluate the surface membrane protein expression (mPD-L1) by means of flow cytometry (FC) in different canine lymphoma immunophenotypes. Furthermore, in a subset of cases, mRNA and plasmatic soluble protein (sPD-L1) have been assessed in the same patient, and correlations among results from the three analyses investigated.

Methods: Samples obtained for diagnostic purpose from untreated dogs with a confirmed lymphoma immunophenotype were included: surface protein was assessed via FC and quantified with median fluorescence index ratio (MFI ratio), gene expression was evaluated by real time quantitative polymerase chain reaction (RT-qPCR) and plasmatic concentration of soluble protein (sPD-L1) measured with ELISA. Statistical analyses were performed to investigate any difference among FC immunophenotypes, updated Kiel cytological classes, and in the presence of blood infiltration.

Results: Considering FC, most B-cell lymphomas (BCL) were positive, with higher MFI ratios than other subtypes (81%, median MFI ratio among positive samples = 1.50, IQR 1.21–2.03, range 1.01–3.47). Aggressive T-cell lymphomas had a lower percentage of positive samples (56%) and showed low expression (median MFI ratio in positive samples = 1.14, IQR 1.07–1.32, range 1.02–2.19), while T-zone lymphomas (TZL) were frequently positive (80%) but with low expression (median MFI ratio in positive samples = 1.19, IQR 1.03–1.46, range 1.02–6.03). Cellular transcript and sPD-L1 were detected in all samples, without differences among immunophenotypes. No correlation between results from different techniques was detected, but sPD-L1 resulted significantly increased in FC-negative lymphomas ($p = 0.023$).

Discussion: PD-L1 molecule is involved in canine lymphoma pathogenesis, with differences among immunophenotypes detected by FC. Specifically, BCL have

the highest expression and aggressive T-cell lymphomas the lowest, whereas TZL need further investigations.

KEYWORDS

Programmed Death-Ligand 1, lymphoma, dog, flow cytometry, polymerase chain reaction, immunoassay

1 Introduction

In both human and, more recently, veterinary oncology, therapeutic approaches for cancer are shifting from traditional chemotherapeutics to innovative strategies focused on anti-tumor immunity (1–5). The increasing interest in cancer immunotherapy has prompted a deeper exploration of molecules that influence the immune system, promoting or avoiding its reactivation and thus regulating cancer growth (6, 7).

Programmed Death-Ligand 1 (PD-L1) is a well-established immune checkpoint molecule, typically expressed by antigen-presenting cells. Its binding to Programmed Death-1 (PD-1) on T-lymphocytes initiates a signaling cascade culminating in the suppression of T-cell activation (8). When tumoral cells express PD-L1, the activation of immunosuppressive pathways through the PD-1/PD-L1 axis facilitates immune system evasion by cancer cells, thereby contributing to tumor progression (9–11). The use of inhibitors that block the interaction between PD-L1 and the PD-1 has demonstrated potential in preventing this phenomenon in several cancer types (3, 12, 13). In addition, the safety profile and clinical efficacy of an anti-canine PD-L1 monoclonal antibody were recently tested in a pilot study on 12 dogs with recurrent, metastatic, or resistant tumors following surgery, radiation, or chemotherapy, with significant results (5).

In dogs, either membrane PD-L1 (mPD-L1), mRNA and soluble protein concentration (sPD-L1) have been evaluated in various cancers, including mammary tumors, melanomas, and lymphomas (14–17). Considering canine lymphoma, Hartley and colleagues utilized flow cytometry (FC) to investigate PD-1 and PD-L1 expression both at the time of diagnosis and at relapse in nodal aspirates from dogs with B-cell lymphoma (BCL), T-cell lymphoma and healthy controls. The findings revealed an increase of PD-L1 expression in BCL, but not in T-cell lymphoma (18). In a separate study, Aresu et al. applied the RNA-scope technique to canine diffuse large B-cell lymphoma (DLBCL) histopathological sections and observed that an increasing amount of mRNA encoding for PD-L1 was associated with a worse prognosis (19). Finally, a study by Song et al. reported a significant difference in sPD-L1 plasmatic levels between healthy dogs and those with different tumors, including lymphoma (20). Notably, none of these studies assessed plasmatic, membrane protein expression, and cellular transcript in the same dog. Thus, nothing is known about the link among different forms of expression of PD-L1, leading to possible misinterpretation of results when considering studies using different techniques.

Here, our primary goal was to evaluate the different stages of PD-L1 expression in different canine lymphoma immunophenotypes. Results about transcript amount and sPD-L1 were compared to those obtained via FC in the same patient. This multiple approach aims to enhance the knowledge about the biological role of PD-L1 in dogs presenting with different lymphoma subtypes.

2 Materials and methods

Samples for the present study were prospectively enrolled at the FC service of the Veterinary Teaching Hospital (VTH), University of Milan, from August 2022 to December 2023. All samples were obtained for diagnostic purposes from lymph node (LN) aspirates of privately-owned dogs with suspect of lymphoma. An informed consent of the owner was always obtained. Thus, specific Ethical Committee approval to use leftover specimens for research purposes was not required (Ethical Committee decision 29 October 2012, renewed with protocol 02–2016, University of Milan).

Nodal aspirates were collected and processed for diagnostic FC as already described (21). If provided by the referring veterinarian, peripheral blood (PB) samples were processed as well, and infiltration by neoplastic cells was quantified as the percentage of cells showing the same morphological and phenotypical properties shown in the LN. A cutoff of ≥0.56% was applied to define positive PB samples. This cut-off was chosen in alignment with recommendations in the literature for DLBCL (22). However, it was uniformly applied to all samples, as no definitive analytic cutoff has been established for any other lymphoma subtype.

Cases were enrolled in the study if fulfilled the following inclusion criteria: (1) diagnosis of lymphoma based on clinical presentation, cytology and FC; and (2) adequate quality and cellularity for FC assessment of mPD-L1 expression. Cases were excluded if they were submitted for minimal residual disease (MRD) assessment in a dog already diagnosed and treated for lymphoma, or in the event of suspected relapse in a treated patient. Additionally, patients who had already undergone a chemotherapeutic agent before receiving a definitive lymphoma diagnosis were excluded.

Following FC assessment of mPD-L1 expression, when feasible, excess nodal material underwent centrifugation. The supernatant was removed, and the cell pellet was re-suspended in RNA-later (Invitrogen™ RNAlater Stabilization Solution™, catalog number AM7020) and stored at −20°C for assessment of transcript amount. If PB was available, centrifugation was performed, and plasma was separated and stored at −20°C for sPD-L1 quantification.

For each included case, the following data were recorded, if available: sex (female, spayed female, male, neutered male), breed (mixed, purebred), age (years), cytological subtype according to the updated Kiel classification (23), FC PB infiltration (presence/absence).

2.1 Flow cytometry

For FC assessment of mPD-L1, the LN sample was divided into three tubes, each containing 500,000 cells. Subsequently, 25 µL of a blocking solution containing 10% fetal bovine serum (FBS) and 0.2%

sodium azide in RPMI 1640 (catalog number R0883) were added to each tube. The first tube served as an unstained control, the second as an isotypic control (Clone39, adivo GmbH, Germany), and the third was utilized to assess mPD-L1 expression (Clone1, adivo GmbH, Germany).

Both Clone39 and Clone1 were isolated from adivo's proprietary fully canine antibody library using phage display methodologies (adivo GmbH, Germany). Antibodies are fully canine and belong to the IgG HC-B subtype and containing a lambda light chain. Clone1 was selected against recombinant canine PD-L1 and tested for binding recombinant antigen in Enzyme-Linked Immunosorbent Assay (ELISA) as well as for its ability to recognize native canine PD-L1 expressed on HEK-293 cells and endogenous PD-L1 on the squamous cell carcinoma cell line SCC1. In addition, the antibody was checked for unspecific binding to unrelated proteins, such as protein that were present during the antibody selection process, e.g., FBS and other blocking reagents. Moreover, binding to untransfected HEK-239 cells was tested demonstrating no stickiness/binding to unrelated proteins on the surface of cells (data not shown). Clone39 was raised against an unrelated protein by similar methodologies. Antibodies were biotinylated using No-Weigh™ EZ-Link Sulfo-NHS-LC-Biotin kit (Thermo Fisher Scientific, catalog number A39256) according to the manufacturer instructions and were tested side-by-side with the non-biotinylated variant to ensure that biotinylation did not impair antigen binding. Antibodies used in FC experiments were diluted to achieve the same concentration.

After 10 min of incubation at room temperature and a washing step, 1 µL of an avidin kit (Avidin, Alexa Fluor™ 488 conjugate, Thermo Fisher Scientific, Waltham, Massachusetts, USA, catalog number A21370) was added to each tube. Both antibodies and avidin kit were titrated before use to determine the optimal working dilutions, utilizing a canine lymphoma cell line (CLBCL-1) previously reported to express PD-L1 (14). The tubes incubated for 10 min and finally were washed and resuspended with Phosphate Buffered Saline Solution (PBS) for acquisition at the flow cytometer. All samples were acquired with the same flow cytometer (BriCyte E6, Mindray, Shenzen, China), with constant settings and compensation matrices and data were analyzed with "MRflow" software (Mindray) by a single experienced operator (VM). Analyses were restricted to neoplastic cells, by setting a gate in an FSC versus SSC scattergram after doublets exclusion (Figure 1). The degree of mPD-L1 expression was calculated as the ratio between the Median Fluorescence Index (MFI) of the anti-PD-L1 antibody-stained tube and the isotypic control one (MFI ratio). Samples were considered positive if MFI ratio was >1, negative if it was =1.

2.2 Enzyme-linked immunosorbent assay (ELISA)

Plasmatic sPD-L1 levels were quantified using the specific Canine PD-L1 ELISA kit (MyBioSource Inc., San Diego, USA, catalog number MBS9349782) following the manufacturer's protocol as suggested by Song et al. (20). This kit applies the competitive ELISA technique, using a polyclonal anti-PD-L1 antibody and a PD-L1- HorseRadish Peroxidase (HRP) conjugate, where the sample PD-L1 and PD-L1-HRP conjugate compete for binding to the anti-PD-L1 antibody site. Undiluted canine plasma samples and standard sPD-L1 samples (ranging from 10 to 0.5 ng/mL), always tested in duplicates, were incubated together with the PD-L1-HRP conjugate in an anti-sPD-L1 pre-coated plate for 1 h at 37°C. After washing the wells five times, the plate was incubated with the HRP enzyme substrate for 15–20 min at 37°C avoiding sunlight. At the end of the incubation, a stop solution (sulfuric acid, 0.18 M) was added, causing wells to change color from blue to yellow. The color intensity was measured with an ELISA microplate reader (Titertek Multiskan, Flow Laboratories, McLean, VA, USA) at 450 nm, expressing the results as Optical Density (OD). Given the competitive nature of the ELISA, the color intensity was inversely proportional to the concentration of PD-L1. The concentrations of canine plasma sPD-L1 were interpolated from the standard curve.

2.3 RNA extraction and RT-qPCR

Total RNA was extracted by using TRIzol reagent (Invitrogen, catalog number 15596026), according to manufacturer's instructions for tissue samples. After quantification by QUBIT Fluorimeter, cDNA was synthesized starting from 1 µg of total RNA using the QuantiTect Reverse Transcription kit (Qiagen, catalog number 205311).

To assess the relative amounts of the PD-L1 gene expression, real-time quantitative PCR (RT-qPCR) was performed using IQ SYBR Green Supermix (BioRad, catalog number 1708882) and IQ5 Thermocycle (BioRad). GAPDH was used as housekeeping gene and RT-qPCR experiments were performed in duplicate. Quantitative RT-PCR primer sequences were as follows: primer pair PD-L1 5′-GAGAATCACAGGCACCTACAA-3′ (forward) and 5′-CGACAA GACTCCAAAGACTCAA-3′ (reverse) and primer pair GAPDH 5′-GGCACAGTCAAGGCTGAGAAC-3′ (forward) and 5′-CCAGCA TCACCCCATTTGAT-3′ (reverse).

Gene expression was calculated using the formula of $2^{-\Delta\Delta Ct}$ (fold increase), where $\Delta\Delta Ct = \Delta Ct\left(sample\right) - \Delta Ct\left(control\right)$ and ΔCt is the Ct of the target gene subtracted from the Ct of the housekeeping gene.

2.4 Statistical analysis

For statistical purposes, enrolled cases were subdivided into BCL, T-zone lymphomas (TZL) and T-cell lymphoma-Not Otherwise Specified (T-NOS) as previously reported (24). This was due to the distinctive morphology and phenotype of TZL, which predict an indolent clinical behavior (25–27). Conversely, despite marginal-zone lymphomas (MZL) being traditionally classified as an indolent subtype, they were included in the BCL group, due to their FC features, clinical behavior, and prognosis overlapping with those of DLBCL (28).

Data distribution for continuous variables was assessed with a Shapiro–Wilk test and visual inspection of histograms and q-q plots. Normally distributed data are presented as mean and standard deviation, whereas non-normally distributed data are presented as median and range. Thereafter, differences in MFI ratio, transcript amount and sPD-L1 concentration among the three lymphoma immunophenotypes (BCL, T-NOS and TZL) and among different cytological subtypes were assessed with Kruskal-Wallis or ANOVA

10.3389/fvets.2024.1412227

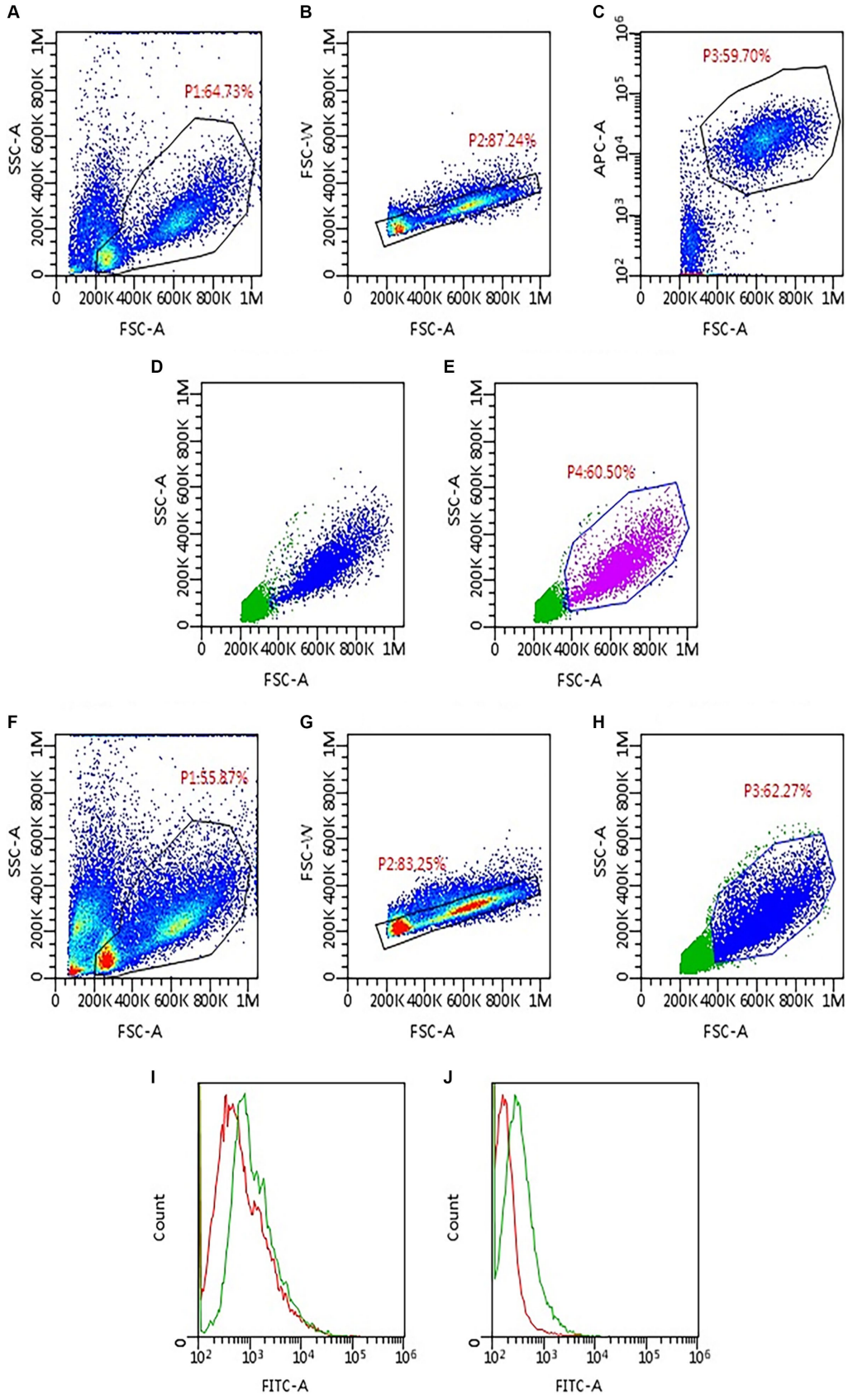

FIGURE 1
Gating strategy applied to assess PD-L1 expression via flow cytometry in 93 lymph node aspirates from dogs with lymphoma. First, samples were labeled to identify neoplastic cells based on phenotype **(A–E)**. Then, the same gating strategy was applied to the tubes incubated with anti-PD-L1

(Continued)

FIGURE 1 (Continued)

antibody and the respective isotypic control **(F–H)**. **(A)** Density plot, all events are shown; a gate (P1) was set to exclude platelet and debris. **(B)** Density plot, P1 events are shown; a gate (P2) was set to exclude doublets. **(C)** Density plot, P2 events are shown; neoplastic cells are identified based on cell size and phenotype; in the example shown, a gate (P3) was set to include only large CD21-positive cells. **(D)** Dot plot, P2 events are shown; P3 neoplastic cells are back-colored (blue dots). **(E)** Dot plot, P2 events are shown; a gate P4 was set to include only neoplastic cells based on the distribution of blue dots in panel **(D)**. **(F)** Density plot, all events are shown; P1 gate was copied and pasted from panel **(A)**, to exclude platelet and debris. **(G)** Density plot, P1 events are shown; P2 gate was copied and pasted from panel **(B)**, to exclude doublets. **(H)** Dot plot, P2 events are shown; the gate (P3) was copied and pasted from panel **(E)** (P4) to include only neoplastic cells. **(I,J)** Histogram overlay showing FITC-fluorescence in PD-L1 stained tubes (green line) compared with the respective isotypic control (red line); both samples shown were considered positive for PD-L1 expression, with lower **(I)** and higher **(J)** median fluorescence intensity (MFI) ratio.

test and appropriate post-hoc analyses (Mann Whitney test with Bonferroni correction for multiple comparisons).

Two contingency tables were prepared to calculate possible differences in FC positive and negative samples among different immunophenotypes and cytological subtypes, respectively. Fisher's exact test was applied.

Mann–Whitney and Student t test were applied to assess differences in PD-L1 transcript amount and sPD-L1 concentration between FC positive and negative samples, and possible difference in sPD-L1 concentration between infiltrated and non-infiltrated PB samples. Spearman non-parametric correlation was applied to assess possible correlation between MFI ratio, fold increase in transcript amount, and sPD-L1 concentration. Immunophenotype was not considered for these tests.

All analyses were performed with SPSS v 28.0 for Windows, and significance was set at $p \leq 0.05$ for all tests.

3 Results

In total, 93 dogs were enrolled in the present study. PD-L1 expression was investigated in all cases via FC, in 41 (44.1%) via ELISA, and in 31 (33.3%) via qPCR. Twenty-one (22.6%) cases were tested with all techniques.

Among the enrolled dogs, there were 30 (33.3%) mixed-breed and 60 (66.7%) purebred dogs, whereas the breed was not reported in 3 cases. Sex was reported for 90 dogs, including 39 (43.3%) males, 27 (30.0%) spayed females, 16 (17.8%) females, and 8 (8.9%) neutered males. The mean age at diagnosis was 8.8 ± 3.0 years.

Considering lymphoma subtype, 58 (62.4%) dogs were diagnosed with BCL, 25 (26.9%) with T-NOS, and 10 (10.7%) with TZL. In 64 cases, a cytological smear was available for review, leading to the following classification: 27 (42.2%) centroblastic polymorphic, 10 (15.6%) pleomorphic mixed, 8 (12.5%) centroblastic monomorphic, 8 (12.5%) small clear, 4 (6.2%) plasmacytoid, 3 (4.7%) pleomorphic large, 3 (4.7%) marginal zone, and 1 (1.6%) was defined as unclassified. Peripheral blood infiltration was tested in 71 cases (54 positive, 76%).

3.1 Flow cytometry

Surface membrane expression of PD-L1 was detected in 69 (74.2%) samples via FC, with a median MFI ratio of 1.38 (IQR 1.12–1.80; range 1.01–6.03) among positive samples. The remaining 24 (25.8%) samples had an MFI ratio equal to 1 and were considered negative. Results among different lymphoma immunophenotypes are shown in Figures 2, 3. Based on the Fisher's exact test, the prevalence of mPD-L1-positive samples among the three lymphoma categories was not significantly different ($p = 0.063$; Figure 2 and Table 1). Considering positive samples, the median MFI ratio significantly varied among BCL, T-NOS and TZL ($p = 0.011$; Figure 3A and Table 1). In particular, post-hoc analyses revealed a significantly higher MFI ratio in BCL than in T-NOS ($p = 0.023$), but no difference either between BCL and TZL or between T-NOS and TZL. One TZL sample had an outlier MFI ratio of 6.03. When considering Kiel subtypes, no difference in the prevalence of positive samples and median MFI ratio was detected ($p > 0.050$ for both analyses).

3.2 qPCR

PD-L1 transcript was detected in all 31 samples tested via qPCR. Among them, 19 (61.3%) were BCL, 8 (25.8%) were T-NOS and 4 (12.9%) were TZL. Overall median fold-increase in transcript amount was 0.23 (IQR 0.16–1.40; range, 0.01–5.45), with no differences among lymphoma immunophenotypes ($p = 0.247$; Figure 3B and Table 1) and Kiel subtypes ($p = 0.597$). However, none of the T-NOS samples had a fold-increase >1, differently from BCL (8 samples out of 19, 42.1%) and TZL (1 sample out of 4, 25.0%). The TZL sample with an outlier MFI ratio had a 5.45-fold increase in PD-L1 transcript amount.

3.3 ELISA

Plasmatic sPD-L1 was detected in all 41 samples tested via ELISA. Among them, 28 (68.3%) were BCL, 9 (22.0%) were T-NOS and 4 (9.7%) were TZL. The overall mean sPD-L1 concentration was 7.88 ± 3.78 ng/mL, with no differences observed among lymphoma immunophenotypes ($p = 0.993$; Figure 3C and Table 1) and Kiel subtypes ($p = 0.360$). Finally, sPD-L1 concentration did not vary between dogs with and without PB infiltration ($p > 0.050$).

3.4 Comparison among techniques

When comparing FC positive and negative samples, no difference in fold increase of transcript amount was detected (31 samples, $p = 0.486$), whereas sPD-L1 concentration was significantly higher in FC negative samples (41 samples, $p = 0.023$). Indeed, mean sPD-L1 concentration was 6.95 ± 3.39 ng/mL in FC positive samples and 10.13 ± 3.87 ng/mL in FC negative samples.

When restricting analyses to FC positive samples alone, 22 samples were included to compare MFI ratio and fold increase in

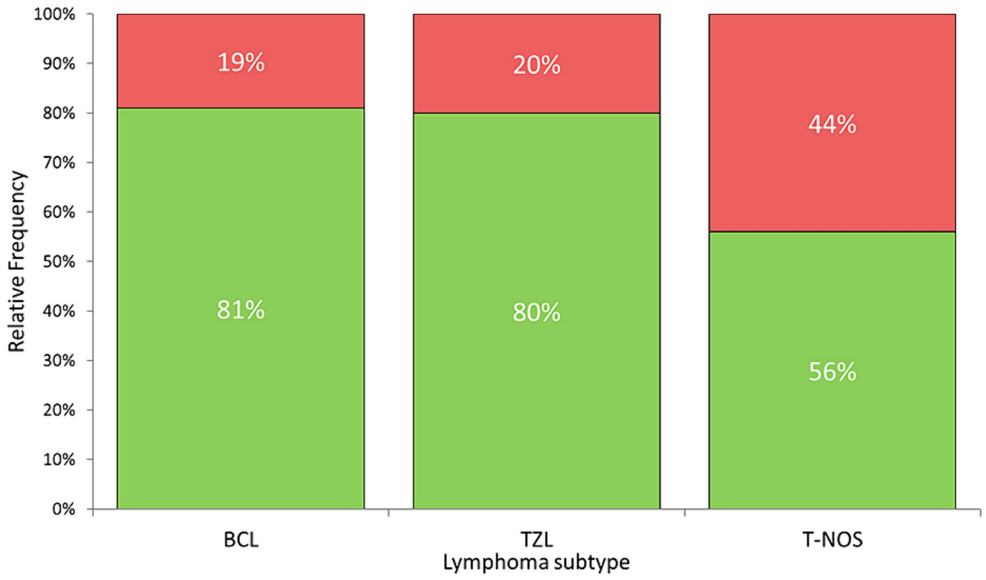

FIGURE 2
Stacked bar plots showing the percentage of samples expressing PD-L1 protein on the surface of neoplastic cells, assessed via flow cytometry on nodal aspirates from 93 dogs, according to lymphoma subtype. Green column: positive samples. Red column: negative samples. BCL, B-cell lymphoma; TZL, T-Zone lymphoma; T-NOS, T-cell lymphoma-Not Otherwise Specified.

transcript amount, while 29 were included to compare MFI ratio and sPD-L1. No significant correlation between MFI ratio and either fold increase in transcript amount or sPD-L1 concentration was found ($p = 0.254$ and $p = 0.150$, respectively).

4 Discussion

To the authors' knowledge this is the first comprehensive assessment of PD-L1, combining evaluation of surface membrane expression, cellular transcript amount, and plasmatic concentration within the same patient in different canine lymphoma subtypes.

Overall, surface membrane protein expression by FC was detected in the majority of samples (74.2%). However, even among positive samples, the median MFI ratio was quite low, thus suggesting that canine lymphomas often express PD-L1, but with a substantial low level. This result aligns with previously published data, indicating lower PD-L1 expression in canine lymphomas compared to other cancers examined *in vitro* (29). Speculatively, this might suggest that lymphomas may exhibit a mild to low response to immunotherapy targeting PD-L1/PD-1 axis. Higher PD-L1 expression has been reported in chemotherapy-resistant than non-chemotherapy selected lymphoma cells in dogs (18). Thus, future studies including lymphoma relapses, may lead to results different from ours. In this perspective, PD-L1 immunotherapy could represent a more reliable rescue treatment than a first-line option.

Herein, BCL exhibited a significantly higher likelihood of being positive, and when positive, demonstrated a higher degree of expression compared to T-NOS, in line with the literature (14, 18). In particular, Hartley et al. (18) reported a higher expression of surface protein in neoplastic B-cells compared to their non-neoplastic counterparts, whereas this phenomenon was not observed in T-cells. Taken together, the data suggest a more significant role of PD-L1 in BCL than in T-NOS, possibly due to its suppressive activity on non-neoplastic anti-cancer T-cells (8). Concerning TZL, there is currently a lack of data on PD-L1 expression. In our case series, they showed a high prevalence of positive samples, comparable to BCL (80 and 81%, respectively) (Figure 2). Conversely, they exhibited a low MFI ratio, similar to T-NOS (Figure 3A). Most likely, the lack of statistical significance regarding TZL could be attributed to the relatively low number of cases enrolled.

Interestingly, among the 10 TZL samples assessed by FC, an outlier case with an extremely high MFI ratio and transcript amount was observed. In this dog, the concentration of sPD-L1 was only slightly over the mean value. The dog, a 13-years-old Akita Inu neutered female, received no treatment after diagnosis, and unfortunately died of causes unrelated to the neoplasm within 35 days. Consequently, no further insights could be drawn regarding the clinical relevance of the outlier PD-L1 expression. Nevertheless, reporting this case may provide valuable information related to either the biological variability of the cancer or the patient itself.

Concerning PD-L1 transcript, Ambrosius et al. (30) reported a greater expression in LN from dogs with DLBCL than from healthy controls, even if no statistical analysis was performed. Based on the lack of differences among lymphoma subtypes in the present study, it is plausible that the results obtained by Ambrosius and colleagues were associated with the presence or absence of lymphoma rather than the specific subtype considered. The same study failed to identify a prognostic role for PD-L1 transcript amount (30). Conversely, Aresu et al. found that the increased PD-L1 score quantified by RNAscope was associated with a higher risk of progression and tumor-related death in dogs with DLBCL (19). In the present study, prognostic evaluations were not performed. Thus, prognostic relevance of PD-L1 transcript amount is still controversial.

As for soluble protein, Song et al. (20) reported a difference of plasmatic concentrations between healthy and tumor-bearing dogs

10.3389/fvets.2024.1412227

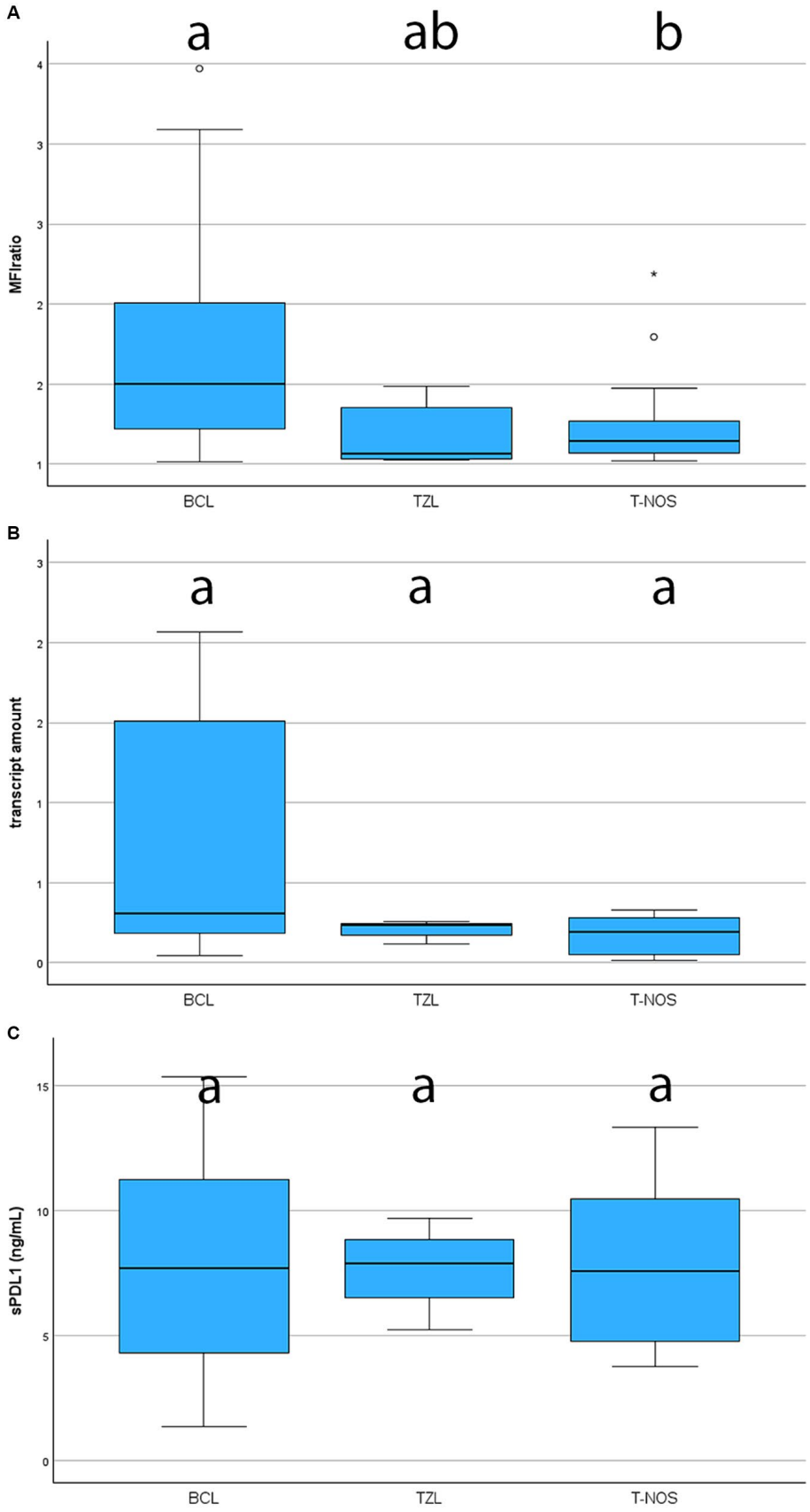

FIGURE 3
Boxplots showing the level of expression of PD-L1 assessed with different techniques, according to lymphoma subtype. BCL, B-cell lymphoma; TZL, T-Zone lymphoma; T-NOS, T-cell lymphoma-Not Otherwise Specified. The boxes with different superscript letters are significantly different.

(Continued)

FIGURE 3 (Continued)
(A) Degree of expression on the surface of neoplastic cells, assessed via flow cytometry and quantified as the ratio between the Median Fluorescence Index (MFI) of the anti-PD-L1 antibody-stained tube and the isotypic control one (MFI ratio). Only positive samples are shown (69 dogs). One TZL case with an extremely high MFI ratio was excluded from the figure to ameliorate the graphical aspect. **(B)** Fold increase in transcript amount, assessed via RT-qPCR in 31 cases. One TZL [same case excluded in panel **(A)**] with an extremely fold increase was excluded from the figure to ameliorate the graphical aspect. **(C)** Plasmatic concentration of soluble PD-L1, assessed via ELISA in 41 cases.

TABLE 1 Median MFI ratio, fold increase in the transcript amount and mean plasmatic concentration of sPD-L1 in a group of dogs with lymphoma, according to immunophenotype of neoplastic cells.

	Lymphoma immunophenotype			
	All	BCL	T-NOS	TZL
Number of FC positive samples	69 (74.2%)	47 (81.0%)	14 (56.0%)	8 (80.0%)
Median MFI ratio of positive samples	1.38 IQR 1.12–1.80 range 1.01–6.03	1.50 IQR 1.21–2.03 range 1.01–3.47	1.14 IQR 1.07–1.32 range 1.02–2.19	1.19 IQR1.03–1.46 range 1.02–6.03
Median fold increase in transcript amount	0.23 IQR 0.16–1.40 range 0.01–5.45	0.31 IQR 0.17–1.53 range 0.05–2.06	0.19 IQR 0.05–0.30 range 0.01–0.33	0.24 IQR 0.14–4.16 range 0.11–5.46
Plasmatic concentration of sPD-L1 (ng/mL) (mean ± SD)	7.88 ± 3.78	7.89 ± 4.10	7.95 ± 3.66	7.68 ± 1.83

IQR, interquartile range; SD, standard deviation; FC, flow cytometry; MFI, median fluorescence index; BCL, B-cell lymphoma; T-NOS, T-cell lymphoma-Not Otherwise Specified; TZL, T-Zone Lymphoma.

without assessing whether any difference existed among cancer histotypes. In the present study, no healthy dogs were included for comparison, since we only focused on lymphoma-bearing dogs. The sPD-L1 values we obtained were higher than those reported in literature (20), with no differences based on lymphoma subtype or presence of PB infiltration. This is likely due to the fact that, differently from the study of Song et al. (20), patients with comorbidities were retained in the present study, possibly leading the lymphoma-unrelated increase of sPD-L1. Inclusion of such dogs was aimed at enrolling a case-load representative of the standard population of oncological patients, with possible co-morbidities often linked to aging. Pairwise, the same cause might explain the lack of correlation between surface expression and soluble protein, as also documented in human medicine (31, 32). Unfortunately, most of the samples included in the present study were sent from referring veterinarians across Italy, and a complete anamnesis was scarcely available, preventing us from assessing the influence of other clinical variables on the concentration of sPD-L1. Nevertheless, the presence of sPD-L1, irrespective of its biological origin, should be considered in the context of immunotherapies, as it has the potential to bind and saturate the administered antibodies. Therefore, investigating its variation in a patient's plasma and assessing it before initiating anti-PD-L1 therapies might aid in planning treatment dosage to achieve optimal effects during clinical trials.

When comparing the three techniques, the only significant result was found with sPD-L1 and FC. In particular, the sPD-L1 resulted significantly more concentrated in FC-negative cases. This could be explained by different mechanisms, including sPD-L1 release by non-neoplastic cells (i.e., dendritic cells) (33), and enzymatic cleavage of the protein on the surface of neoplastic cells (34, 35), leading to higher amount of soluble protein, while less surface protein remained.

Another interesting result is that the amount of cellular transcript does not seem to correlate with either mPD-L1 or sPD-L1. This has implications when selecting the technique to evaluate PD-L1 during future clinical trial involving immunotherapy. In the therapeutic context of human medicine, this has been already considered, and assessing surface proteins is recommended (36, 37). Relying only on mRNA expression might be misleading when trying to predict expected results of PD-L1 antibody administration.

The major pitfall of the present study is linked to the low caseload for some specific lymphoma subtypes, which might have affected the significance of statistical analyses. Anyway, the sample pool was representative of the reported prevalence of lymphoma subtypes in the canine population, with BCL being more frequent than T-NOS and TZL (38, 39). Similarly, the low number of samples analyzed by qPCR and ELISA could have impacted on the significance of those results, and it would be interesting in the future to collect a larger number of cases to eventually confirm our results.

A second limitation is that the population of neoplastic cells in FC was identified based on morphological properties (FSC) without employing a multicolor approach. This was due to the fact that the staining kit showed an undesired fluorescent signal in different channels, which was difficult to remove even with relevant compensation. The identification of neoplastic cells via FSC is usually straightforward in clinically aggressive lymphomas, mostly constituted by large cells. On the other hand, identification of neoplastic cells based on FSC is more challenging for TZL and it is possible that a proportion of residual lymphocytes has been included in the analysis, while a proportion of neoplastic cells has been excluded. However, such a condition is not likely to have grossly biased MFI ratio analysis, since TZL cells represented the vast majority of the population within each sample, and their FSC is actually higher than the one of residual

lymphocytes (40), although perhaps less immediately identifiable by unexperienced operators. No further small cell lymphoma was included in the present study.

Lastly, clinical and follow-up data, when retrieved, were fragmentary, thus preventing us from including them. Future studies assessing correlations between the variables evaluated and prognosis are warranted.

5 Conclusion

PD-L1 is often expressed on cells' surface in canine lymphomas, typically with low intensity. BCL are frequently positive and have the highest amount of surface protein compared to TZL and T-NOS. Although cellular transcript resulted present in all samples, no correlation with lymphoma categories or other techniques was found. sPD-L1 is higher in the samples with no surface protein expression, as possible result of the cleavage and release of surface proteins in the plasma.

Future studies should carefully consider the technique for assessing PD-L1 expression, since results are not correlated and interchangeable. This consideration is crucial when admitting dogs with lymphoma to immunotherapies targeting the surface membrane PD-L1.

Data availability statement

The raw data supporting the conclusions of this article will be made available by the authors, without undue reservation.

Ethics statement

The requirement of ethical approval was waived by Ethical Committee, University of Milan, Italy for the studies involving animals because all samples were obtained for diagnostic purposes from lymph node (LN) aspirates of privately-owned dogs with suspect of lymphoma. An informed consent of the owner was always requested. Thus, specific EC approval to use leftover specimens for research purposes was not required (EC decision 29 October 2012, renewed with protocol 02-2016, University of Milan). The studies were conducted in accordance with the local legislation and institutional requirements. Written informed consent was obtained from the owners for the participation of their animals in this study.

Author contributions

AU: Data curation, Investigation, Validation, Writing – original draft. LC: Investigation, Writing – review & editing. PD: Investigation, Writing – review & editing. RM: Investigation, Writing – review & editing. LA: Writing – review & editing. PM: Visualization, Writing – review & editing. FS: Writing – review & editing. FR: Writing – review & editing. DS: Writing – review & editing. SC: Writing – review & editing. VM: Formal analysis, Investigation, Project administration, Supervision, Writing – review & editing.

Funding

The author(s) declare that financial support was received for the research, authorship, and/or publication of this article. The authors also acknowledge support from the University of Milan through the Article Publication Charge (APC) initiative.

Acknowledgments

The authors wish to thank all private vets who sent their sample to our FC facility for diagnostic purposes, with prof Laura Marconato above all. A special thank to Markus Waldhuber, Philipp Baer, and Felix Funck from adivo GmbH for their technical support in setting up FC experiment.

Conflict of interest

The authors declare that the research was conducted in the absence of any commercial or financial relationships that could be construed as a potential conflict of interest.

The author(s) declared that they were an editorial board member of Frontiers, at the time of submission. This had no impact on the peer review process and the final decision.

Publisher's note

References

1. Pardoll DM. The blockade of immune checkpoints in cancer immunotherapy. *Nat Rev Cancer*. (2012) 12:252–64. doi: 10.1038/nrc3239

2. Schadendorf D, Hodi FS, Robert C, Weber JS, Margolin K, Hamid O, et al. Pooled analysis of long-term survival data from phase II and phase III trials of ipilimumab in unresectable or metastatic melanoma. *J Clin Oncol*. (2015) 33:1889–94. doi: 10.1200/JCO.2014.56.2736

3. Ansell SM, Lesokhin AM, Borrello I, Halwani A, Scott EC, Gutierrez M, et al. PD-1 blockade with nivolumab in relapsed or refractory Hodgkin's lymphoma. *N Engl J Med*. (2015) 372:311–9. doi: 10.1056/NEJMoa1411087

4. Minoli L, Licenziato L, Kocikowski M, Cino M, Dziubek K, Iussich S, et al. Development of monoclonal antibodies targeting canine PD-L1 and PD-1 and their clinical relevance in canine apocrine gland anal sac adenocarcinoma. *Cancers*. (2022) 14:6188. doi: 10.3390/cancers14246188

5. Maekawa N, Konnai S, Hosoya K, Kim S, Kinoshita R, Deguchi T, et al. Safety and clinical efficacy of an anti-PD-L1 antibody (c4G12) in dogs with advanced malignant tumours. *PLoS One*. (2023) 18:e0291727. doi: 10.1371/journal.pone.0291727

6. Hanahan D, Weinberg RA. Hallmarks of cancer: the next generation. *Cell*. (2011) 144:646–74. doi: 10.1016/j.cell.2011.02.013

7. Marcucci F, Rumio C, Corti A. Tumor cell-associated immune checkpoint molecules – drivers of malignancy and stemness. *Biochim Biophys Acta Rev Cancer*. (2017) 1868:571–83. doi: 10.1016/j.bbcan.2017.10.006

8. Shklovskaya E, Rizos H. Spatial and temporal changes in PD-L1 expression in cancer: the role of genetic drivers, tumor microenvironment and resistance to therapy. *Int J Mol Sci*. (2020) 21:7139. doi: 10.3390/ijms21197139

9. Iwai Y, Ishida M, Tanaka Y, Okazaki T, Honjo T, Minato N. Involvement of PD-L1 on tumor cells in the escape from host immune system and tumor immunotherapy by PD-L1 blockade. *Proc Natl Acad Sci U S A*. (2002) 99:12293–7. doi: 10.1073/pnas.192461099

10. Butte MJ, Keir ME, Phamduy TB, Sharpe AH, Freeman GJ. Programmed death-1 ligand 1 interacts specifically with the B7-1 costimulatory molecule to inhibit T cell responses. *Immunity*. (2007) 27:111–22. doi: 10.1016/j.immuni.2007.05.016

11. Kythreotou A, Siddique A, Mauri FA, Bower M, Pinato DJ. PD-L1. *J Clin Pathol*. (2018) 71:189–94. doi: 10.1136/jclinpath-2017-204853

12. Weber JS, D'Angelo SP, Minor D, Hodi FS, Gutzmer R, Neyns B, et al. Nivolumab versus chemotherapy in patients with advanced melanoma who progressed after anti-CTLA-4 treatment (CheckMate 037): a randomised, controlled, open-label, phase 3 trial. *Lancet Oncol*. (2015) 16:375–84. doi: 10.1016/S1470-2045(15)70076-8

13. Garon EB, Rizvi NA, Hui R, Leighl N, Balmanoukian AS, Eder JP, et al. Pembrolizumab for the treatment of non-small-cell lung cancer. *N Engl J Med*. (2015) 372:2018–28. doi: 10.1056/NEJMoa1501824

14. Shosu K, Sakurai M, Inoue K, Nakagawa T, Sakai H, Morimoto M, et al. Programmed cell death ligand 1 expression in canine cancer. *In Vivo*. (2016) 30:195–204.

15. Stevenson VB, Perry SN, Todd M, Huckle WR, LeRoith T. PD-1, PD-L1, and PD-L2 gene expression and tumor infiltrating lymphocytes in canine melanoma. *Vet Pathol*. (2021) 58:692–8. doi: 10.1177/03009858211011939

16. Kumar SR, Kim DY, Henry CJ, Bryan JN, Robinson KL, Eaton AM. Programmed death ligand 1 is expressed in canine B cell lymphoma and downregulated by MEK inhibitors. *Vet Comp Oncol*. (2017) 15:1527–36. doi: 10.1111/vco.12297

17. Maekawa N, Konnai S, Okagawa T, Nishimori A, Ikebuchi R, Izumi Y, et al. Immunohistochemical analysis of PD-L1 expression in canine malignant cancers and PD-1 expression on lymphocytes in canine oral melanoma. *PLoS One*. (2016) 11:e0157176. doi: 10.1371/journal.pone.0157176

18. Hartley G, Elmslie R, Dow S, Guth A. Checkpoint molecule expression by B and T cell lymphomas in dogs. *Vet Comp Oncol*. (2018) 16:352–60. doi: 10.1111/vco.12386

19. Aresu L, Marconato L, Martini V, Fanelli A, Licenziato L, Foiani G, et al. Prognostic value of PD-L1, PD-1 and CD8A in canine diffuse large B-cell lymphoma detected by RNAscope. *Vet Sci*. (2021) 8:120. doi: 10.3390/vetsci8070120

20. Song DW, Ro WB, Park HM. Evaluation of circulating PD-1 and PD-L1 as diagnostic biomarkers in dogs with tumors. *J Vet Sci*. (2021) 22:e75. doi: 10.4142/jvs.2021.22.e75

21. Gelain ME, Mazzilli M, Riondato F, Marconato L, Comazzi S. Aberrant phenotypes and quantitative antigen expression in different subtypes of canine lymphoma by flow cytometry. *Vet Immunol Immunopathol*. (2008) 121:179–88. doi: 10.1016/j.vetimm.2007.09.018

22. Riondato F, Miniscalco B, Poggi A, Aricò A, Aresu L, Comazzi S, et al. Analytical and diagnostic validation of a flow cytometric strategy to quantify blood and marrow infiltration in dogs with large B-cell lymphoma. *Cytometry B Clin Cytom*. (2016) 90:525–30. doi: 10.1002/cyto.b.21353

23. Ponce F, Marchal T, Magnol JP, Turinelli V, Ledieu D, Bonnefont C, et al. A morphological study of 608 cases of canine malignant lymphoma in France with a focus on comparative similarities between canine and human lymphoma morphology. *Vet Pathol*. (2010) 47:414–33. doi: 10.1177/0300985810363902

24. Celant E, Marconato L, Stefanello D, Moretti P, Aresu L, Comazzi S, et al. Clinical and clinical pathological presentation of 310 dogs affected by lymphoma with aberrant antigen expression identified via flow cytometry. *Vet Sci*. (2022) 9:184–96. doi: 10.3390/vetsci9040184

25. Seelig DM, Avery P, Webb T, Yoshimoto J, Bromberek J, Ehrhart EJ, et al. Canine T-zone lymphoma: unique immunophenotypic features, outcome, and population characteristics. *J Vet Intern Med*. (2014) 28:878–86. doi: 10.1111/jvim.12343

26. Martini V, Poggi A, Riondato F, Gelain ME, Aresu L, Comazzi S. Flow-cytometric detection of phenotypic aberrancies in canine small clear cell lymphoma. *Vet Comp Oncol*. (2015) 13:281–7. doi: 10.1111/vco.12043

27. Martini V, Marconato L, Poggi A, Riondato F, Aresu L, Cozzi M, et al. Canine small clear cell/T-zone lymphoma: clinical presentation and outcome in a retrospective case series. *Vet Comp Oncol*. (2016) 14:117–26. doi: 10.1111/vco.12155

28. Cozzi M, Marconato L, Martini V, Aresu L, Riondato F, Rossi F, et al. Canine nodal marginal zone lymphoma: descriptive insight into the biological behaviour. *Vet Comp Oncol*. (2018) 16:246–52. doi: 10.1111/vco.12374

29. Hartley G, Faulhaber E, Caldwell A, Coy J, Kurihara J, Guth A, et al. Immune regulation of canine tumour and macrophage PD-L1 expression. *Vet Comp Oncol*. (2017) 15:534–49. doi: 10.1111/vco.12197

30. Ambrosius LA, Dhawan D, Ramos-Vara JA, Ruple A, Knapp DW, Childress MO. Quantification and prognostic value of programmed cell death ligand-1 expression in dogs with diffuse large B-cell lymphoma. *Am J Vet Res*. (2018) 79:643–9. doi: 10.2460/ajvr.79.6.643

31. Ruf M, Moch H, Schraml P. PD-L1 expression is regulated by hypoxia inducible factor in clear cell renal cell carcinoma. *Int J Cancer*. (2016) 139:396–403. doi: 10.1002/ijc.30077

32. Rossille D, Gressier M, Damotte D, Maucort-Boulch D, Pangault C, Semana G, et al. High level of soluble programmed cell death ligand 1 in blood impacts overall survival in aggressive diffuse large B-cell lymphoma: results from a French multicenter clinical trial. *Leukemia*. (2014) 28:2367–75. doi: 10.1038/leu.2014.137

33. Frigola X, Inman BA, Krco CJ, Liu X, Harrington SM, Bulur PA, et al. Soluble B7-H1: differences in production between dendritic cells and T cells. *Immunol Lett*. (2012) 142:78–82. doi: 10.1016/j.imlet.2011.11.001

34. Dezutter-Dambuyant C, Durand I, Alberti L, Bendriss-Vermare N, Valladeau-Guilemond J, Duc A, et al. A novel regulation of PD-1 ligands on mesenchymal stromal cells through MMP-mediated proteolytic cleavage. *Onco Targets Ther*. (2016) 5:e1091146. doi: 10.1080/2162402X.2015.1091146

35. Hira-Miyazawa M, Nakamura H, Hirai M, Kobayashi Y, Kitahara H, Bou-Gharios G, et al. Regulation of programmed-death ligand in the human head and neck squamous cell carcinoma microenvironment is mediated through matrix metalloproteinase-mediated proteolytic cleavage. *Int J Oncol*. (2018) 52:379–88. doi: 10.3892/ijo.2017.4221

36. O'Malley DP, Yang Y, Boisot S, Sudarsanam S, Wang JF, Chizhevsky V, et al. Immunohistochemical detection of PD-L1 among diverse human neoplasms in a reference laboratory: observations based upon 62, 896 cases. *Mod Pathol*. (2019) 32:929–42. doi: 10.1038/s41379-019-0210-3

37. Polioudaki H, Chantziou A, Kalyvianaki K, Malamos P, Notas G, Mavroudis D, et al. Nuclear localization of PD-L1: artifact or reality? *Cell Oncol (Dordr)*. (2019) 42:237–42. doi: 10.1007/s13402-018-00419-7

38. Ruslander DA, Gebhard DH, Tompkins MB, Grindem CB, Page RL. Immunophenotypic characterization of canine lymphoproliferative disorders. *In Vivo*. (1997) 11:169–72.

39. Valli VE, San Myint M, Barthel A, Bienzle D, Caswell J, Colbatzky F, et al. Classification of canine malignant lymphomas according to the World Health Organization criteria. *Vet Pathol*. (2011) 48:198–211. doi: 10.1177/0300985810379428

40. Riondato F, Poggi A, Miniscalco B, Sini F, Marconato L, Martini V. Flow cytometric features of B- and T-Lmphocytes in reactive lymph nodes compared to their neoplastic counterparts in dogs. *Vet Sci*. (2023) 10:374–86. doi: 10.3390/vetsci10060374

frontiers | Frontiers in Veterinary Science

TYPE Original Research
PUBLISHED 19 August 2024
DOI 10.3389/fvets.2024.1405297

OPEN ACCESS

EDITED BY
Fulvio Riondato,
University of Torino, Italy

REVIEWED BY
Valeria Martini,
University of Milan, Italy
E. Villiers,
Dick White Referrals, United Kingdom

*CORRESPONDENCE
Tracy Stokol
ts23@cornell.edu

RECEIVED 22 March 2024
ACCEPTED 03 July 2024
PUBLISHED 19 August 2024

CITATION
Stokol T, Thomas SI, Hoffman M and Zhao S (2024) Flow cytometric-based detection of CD80 is a useful diagnostic marker of acute myeloid leukemia in dogs. *Front. Vet. Sci.* 11:1405297. doi: 10.3389/fvets.2024.1405297

Flow cytometric-based detection of CD80 is a useful diagnostic marker of acute myeloid leukemia in dogs

Tracy Stokol*, Sophie Isabella Thomas, Martha Hoffman and Shay Zhao

Department of Population Medicine and Diagnostic Sciences, College of Veterinary Medicine, Cornell University, Ithaca, NY, United States

Introduction: CD80, a co-stimulatory molecule required for optimal T cell activation, is expressed on antigen-presenting cells, including monocytes and dendritic cells, in dogs and humans. We hypothesized that CD80 would be expressed on tumor cells in dogs from acute myeloid leukemia (AML) but not dogs with lymphoid neoplasms.

Methods and results: We first evaluated the cellular staining pattern of a hamster anti-murine CD80 antibody (clone 16-10A1, ThermoFisher Scientific Cat# 17–0801-82, RRID: AB_469417) in blood and bone marrow aspirates from healthy dogs. Using flow cytometric analysis and examination of modified Wright's-stained cytologic smears of unsorted and flow cytometric or immunomagnetic bead-sorted leukocytes, we show that the antibody binds to mature and immature neutrophils and monocytes, but not lymphocytes or eosinophils, in blood and bone marrow. We then added the antibody to routine flow cytometric panels for immunophenotyping hematopoietic neoplasms in dogs. We found that the antibody labeled tumor cells in 72% of 39 dogs with AML and 36% of 11 dogs with acute leukemia expressing lymphoid and myeloid markers ("mixed lineage") but none of the dogs with B ($n = 37$) or T ($n = 35$) lymphoid neoplasms. A higher proportion of tumor cells in dogs with AML were labeled with the anti-CD80 antibody vs antibodies against other myeloid-associated antigens, including CD4 (36%, $p = 0.003$), CD11b (44%), CD11c (46%), CD14 (38%, $p = 0.006$) and CD18 (59%, clone YFC118). In contrast, antibodies against CD11b and CD11c bound to tumor cells in 8–32% of the lymphoid neoplasms.

Discussion: We show that CD80, as detected by antibody clone 16-10A1, is a sensitive and specific marker for AML and would be useful to include in flow cytometric immunophenotyping panels in dogs.

KEYWORDS

acute leukemia, hematopoietic neoplasia, canine, immunophenotyping, flow cytometry, diagnostic testing, lymphoma, B7-1

1 Introduction

Immunophenotyping with flow cytometry is a powerful tool used to help determine the cell lineage of hematopoietic neoplasms, including acute leukemia and lymphoma, in dogs. To identify normal and neoplastic canine leukocytes, diagnostic laboratories offer immunophenotyping panels, which typically include antibodies against the following surface antigens: T cell—CD3, CD5, CD4, CD8; B cell—CD21; monocyte—CD14; stem cell—CD34;

common leukocyte—CD45; and major histocompatibility class II (MHCII), which is expressed on lymphocytes and monocytes in healthy dogs. Individual laboratories or investigators may also test for other antigens, such as CD22 (B cell) (1–3), CD25 (activated T and B cells or regulatory T cells) (4–8), CD11b and/or CD11c (neutrophils and monocytes) (2, 3, 9–12), CD61 (megakaryocytes) (3, 12, 13) and myeloperoxidase (an intracellular enzyme in neutrophils, eosinophils and monocytes) (9).

Acute leukemia in dogs is generally categorized as acute myeloid leukemia (AML), acute lymphoblastic leukemia (ALL), and acute undifferentiated leukemia (AUL). In humans, there are also acute leukemias of ambiguous lineage, which include AUL and mixed phenotype acute leukemia (MPAL), where the tumor expresses markers of more than one lineage on the same or different cell populations (14, 15). The entity of MPAL has not been definitively described in dogs, although we have seen dual expression of lymphoid and myeloid antigens in individual dogs with acute leukemia (2, 3). In dogs with acute leukemias, regardless of lineage, tumor cells often express the stem cell marker, CD34, while lacking MHCII (2, 3, 16), thus the different types are distinguished by expression of lineage-associated antigens. To diagnose an AML with flow cytometric analysis, tumor cells should express one or more of the myeloid-associated antigens (CD11b, CD11c, CD14, or CD4 without CD3 or CD5) (2, 3, 9–13, 16). Recently, a specific clone against human CD18 (YFC118.3) was found to be a useful antibody for the flow cytometric diagnosis of AML (16), because this clone primarily labels monocytes and neutrophils in normal dogs (17). A cut-off of >18% $CD18^+$/$MCHII^-$/$CD4^-$ cells was used in a proposed algorithm to diagnose AML in dogs with an acute leukemia consisting of >10% or $>1 \times 10^9$/L $CD34^+$/$MHCII^-$ cells (16). B- and T-ALL are distinguished by the solitary or combined expression of CD21 or CD22 and CD3 or CD5, respectively. However, it is difficult to distinguish B or T cell lymphoma from an ALL when tumor cells from lymphoma are found in high proportions in blood or bone marrow or both. Per WHO criteria, a blast cut-off of 25% in bone marrow is used to distinguish between a T and B precursor ALL from lymphoma (15). Acute leukemias that lack lineage-associated antigens are often categorized as AUL as a diagnosis of exclusion (11, 18). However, the term "acute leukemia-un-phenotyped" is preferred instead of AUL, because we lack antibodies against other lineage-associated markers in dogs (e.g., CD133, CD13, CD2, CD7, CD19), and cytochemical staining may help facilitate a diagnosis of AML in such cases (2, 3). It can be difficult to conclusively diagnose AML on flow cytometric analysis. Myeloid-associated antigens are not expressed on all cases of AML and may not be included in flow cytometric panels, which can result in a diagnosis of AML being based on lack of expression of classic lymphoid-associated antigens (usually CD3, CD5, and CD21) (13). There are only a limited number of antibodies that detect canine myeloid antigens and several of these antigens are also expressed on T cells, such as CD11d (19), or are intracellular antigens, requiring additional steps of fixation and permeabilization, such as myeloperoxidase (9). In addition, there is cross-lineage expression of markers, including CD5, CD22 and CD18, on leukemic cells in ALL and AML (2, 3, 16), which can confound determination of the involved lineage in an acute leukemia. Distinction between AML and ALL is important because dogs may be treated with different chemotherapeutic protocols, such as doxorubicin-cytosine arabinoside- and cyclophosphamide-doxorubicin-vincristine-prednisolone (CHOP)-based protocols, respectively (20, 21). To improve our ability to confidently diagnose AML on flow cytometric analysis, it would be useful to find antibodies against other myeloid antigens that could be added to standard flow cytometric panels.

CD80 (also known as B7.1/B7-1/BB1) is part of the B7 family of immunoglobulin-like proteins that is expressed on antigen-presenting cells, including monocytes, macrophages, and dendritic cells, in humans and mice. CD80 functions as a co-stimulatory molecule for T cells, via binding to CD28 or CD152 (CTLA4) in T cell membranes (22, 23). In dogs, CD80 expression has mostly been described in dendritic cells, including those from the skin, Peyer's patches, and mesenteric lymph nodes, using flow cytometric analysis and immunostaining of tissue sections (24, 25). In addition, cytokine-stimulated cultured dendritic cells and polarized inflammatory macrophages derived from peripheral blood mononuclear cells (PBMCs) upregulate CD80 on flow cytometric analysis (26, 27). A subset of monocytes in blood express CD80 with flow cytometry (28). Since monocytic variants are the most common subtype of AML in dogs (2, 3, 11, 13), we reasoned that if CD80 is expressed on normal canine monocytes, it may be a helpful flow cytometric marker to confirm AML in a dog with acute leukemia. We performed a generic search for commercially available anti-CD80 antibodies that are cross-reactive for canine cells and found an Armenian Hamster anti-murine CD80 antibody (clone 16-10A1, ThermoFisher Scientific Cat# 17–0801-82, RRID: AB_469417). Preliminary testing showed this antibody labeled canine monocytes and, unexpectedly, neutrophils in residual blood samples that were submitted for routine hematologic analysis in the Clinical Pathology laboratory of the Animal Health Diagnostic Center (AHDC) at Cornell University. Even though the expression pattern was different than expected, given that the antibody bound to neutrophils and monocytes in canine blood, we hypothesized that when using this antibody, CD80 would be a flow cytometric marker of AML, but not lymphoid neoplasms, in the dog. We had these study objectives: (1) Verify the leukocyte labeling pattern of the anti-CD80 antibody using flow cytometric analysis on blood from healthy dogs, (2) Determine which cells in bone marrow aspirates from healthy dogs were labeled with the anti-CD80 antibody, and (3) Test our hypothesis by including the anti-CD80 antibody in flow cytometric panels used to immunophenotype canine hematopoietic neoplasms, including leukemia and lymphoma.

2 Materials and methods

2.1 Collection and source of samples

For objective 1, blood from healthy dogs was collected into EDTA anticoagulant-containing vacutainer tubes (BD Biosciences, Franklin Lakes, NJ, United States) by jugular or cephalic venipuncture. The healthy dogs were research animals housed at our institution or owned by students, faculty, and staff, and blood was obtained with owner consent. For objective 2, bone marrow was aspirated from the humeri of research beagles housed at our institution. Blood and bone marrow sample collection was approved by the Institutional Animal Care and Use Committee (#2009–0085). For objective 3, we used data from two sources: (1) Blood, aspirates from bone marrow, lymph node or masses, and body cavity fluid samples collected from dogs with hematopoietic neoplasia that were submitted to the AHDC for

immunophenotyping as part of routine diagnostic service. These samples and data become the property of the AHDC after submission; (2) Blood, bone marrow or lymph node aspirates collected from dogs, with client consent, as part of an ongoing research study on acute leukemia. Data collection for the study herein ceased on July 6, 2023. Two immunophenotyping panels were used: One for acute leukemia and one for lymphoma. For routine immunophenotyping, the panel was chosen by the requesting clinician, with or without consultation with a clinical pathologist at our institution. Typically, lymphoma panels were requested for lymph node aspirates, acute leukemia panels were requested for bone marrow, mass or body cavity fluid aspirates, and both panels were run on blood samples. The acute leukemia panel was used for the research study. Each panel consisted of antibodies against various markers, with all panels including the anti-CD80 antibody. In cases phenotyped after April 2021, including all cases in the research study, we used triple-marker antibody combinations; before April 2021, the same antibodies were used as single markers with a few double-marker combinations (Tables 1, 2). Additional conjugated and unconjugated antibodies against other antigens were used as single markers in the acute leukemia panel, e.g., CD61-phycoerythrin (Beckman Coulter Cat# IM3605, RRID:AB 131237) and the α and β chain of the T cell receptor (TCRαβ, Peter Moore, clone CA15.8G7).

2.2 Antibody labeling of normal canine leukocytes in blood and bone marrow aspirates

Because the intended application of the antibody was for flow cytometric-based immunophenotyping, we used flow cytometric analysis to verify the labeling pattern of the anti-CD80 antibody in healthy canine blood in three ways: (1) Double- or triple-labeled analysis of normal dog leukocytes; (2) Flow cytometric-based sorting of anti-CD80 and -CD14 double-labeled leukocytes followed by cytologic analysis of sorted cells, using CD14 as a monocyte marker; and (3) Isolation of leukocytes followed by flow cytometric labeling with the anti-CD80 antibody. Monocytes, T cells and B cells were isolated by immunomagnetic bead-labeling, whereas neutrophils were isolated by double-density centrifugation followed by red blood cell (RBC) lysis. The same antibodies were used for verification of staining pattern of the anti-CD80 antibody and immunophenotyping of clinical cases (Table 1).

For the bone marrow aspirates, we labeled bone marrow mononuclear cells (BMMC) with the anti-CD80 antibody and then performed: (1) Flow cytometric analysis; and (2) Sorting for cells labeled with the anti-CD80 antibody followed by cytologic analysis of the positively and negatively stained sorted cells. All reagents were from Sigma-Aldrich (St Louis, MO, United States), unless otherwise specified.

2.2.1 Double- or triple-labeled flow cytometric analysis of normal dog leukocytes with CD80 and monocyte, T and B cell markers

After lysis of RBCs with ammonium chloride, cells were resuspended in phosphate-buffered saline (PBS) containing 1% bovine serum albumin (BSA) and 0.05% sodium azide (PBSA). The following antibody combinations were then incubated with the cells for 30 min on ice with the anti-murine CD80-allophycocyanin (APC) antibody (0.01 mg/mL final antibody concentration): (1) Antihuman-CD14-phycoerythrin (PE) (final concentration 0.6 ug/mL) for monocytes; and (2) Anti- human CD21-PE (1:25 dilution) and anti-canine CD5-fluoroscein isothiocyanate (FITC) (1:100 dilution) for B and T cells, respectively. The cells were washed in PBSA and resuspended in PBS for analysis with a flow cytometer (BD FACSCalibur™, BD Biosciences), using appropriate compensation settings. Isotype and unlabeled cells were included in separate tubes. FloJo™ software was used for analysis (version 10, Ashland, OR, United States), excluding lysed RBCs and cellular debris. For the CD80 vs. CD14 double labels, the cells were separated into different gates (lymphocytes, monocytes and neutrophils), based on their characteristic forward (FSC) and side scatter (SSC) and the percentage of cells labeled with the anti-CD80

TABLE 1 Conjugated antibodies used for triple-labeling cells in acute leukemia immunophenotyping panels after April 2021, including their target antigen and registry number (when available) or source.

Target antigen	Registry number or source
CD3-FITC/CD4-PE/CD8-APC	Bio-Rad Cat# TC014, RRID:AB_808411
CD5-FITC/CD21-PE/CD45-APC	**CD5**: Bio-Rad Cat# MCA1037F, RRID:AB_322643; **CD21**: BD Biosciences Cat# 555422; RRID:AB_395816 **CD45**: Bio-Rad Cat# MCA1042APC, RRID:AB_324810
MHCII-FITC/CD34-PE/CD80-APC	**MHCII**: Bio-Rad Cat# MCA1044F, RRID:AB_322642; **CD34**: BD Biosciences Cat# 559369, RRID:AB_397238; **CD80**: ThermoFisher Scientific Cat# 17–0801-82, RRID: AB_469417.
CD4-FITC/CD14-PE/MHCII-A647	**CD4**: Bio-Rad Cat# MCA1038F, RRID:AB_321271, **CD14**: Agilent Cat# R086401, RRID:AB_579551; **MHCII**: Bio-Rad Cat#MCA1044A647, RRID: NA
CD11b-FITC*/CD22-PE or CD34-PE/CD11c-APC*	**CD11b**: Cell Signaling Technology Cat# 24442S, RRID: NA; **CD22:** Abcam Cat# ab23620, RRID:AB_447570, **CD11c:** BioLegend Cat# 117310 (also 117,309), RRID:AB_313779
CD11b-FITC/CD34-PE/CD18-A647*	**CD18**: Bio-Rad Cat# MCA503A647, RRID:AB_324799

This panel was used for routine diagnostic testing and for samples submitted as part of an acute leukemia research study. Before April 2021, the same antibody clones (exceptions noted) were used with the same or different fluorophores as single labels, with limited double labeling (MHCII and CD34 in some cases, CD14 and CD4, CD4 and CD8), for routine diagnostic testing. *The antibodies against CD18 and CD11c were not used in all cases acquired after April 2021. In single color panels before April 2021, unconjugated antibodies were used to detect CD11b (Biorad Cat# MCA1777, RRID:AB_322922), CD11c (Bio-Rad Cat# MCA1778S, RRID:AB_3229420), and CD18 (Bio-Rad Cat# MCA1780, RRID:AB_2128639). Note the latter antibody is a different clone [CA1.4E9] from the anti-human CD18 antibody in the table and labels all leukocytes (29), so results for this antibody are not included in this study. A647, Alexa Fluor™ 647; APC, Allophycocyanin, FITC, Fluorescein isothiocyanate, NA, Not available, PE, Phycoerythrin.

TABLE 2 Conjugated antibodies used for triple-labeling cells in a lymphoma immunophenotyping panel used for routine diagnostic testing after April 2021, including their target antigen*.

Target antigen
CD3-FITC/CD4-PE/CD8-APC
CD5-FITC/CD21-PE/CD45-APC
MHCII-FITC/CD34-PE/CD80-APC
CD5-FITC/CD22-PE/CD25-A660

Before 2021, the same antibodies were used as single labels with the same or different fluorophores, with limited double labeling (MHCII and CD34 in some cases, CD4 and CD8). *The same antibodies listed in Table 1 were used in this panel. Resource registry number CD25: Thermofisher Scientific Cat#50–0250-42, RRID:AB_10609350. A660, Alexa Fluor™ 660; APC, Allophycocyanin, FITC, Fluorescein isothiocyanate, PE, Phycoerythrin.

antibody ($CD80^+$) and their CD80 median fluorescent intensity (MFI) was recorded for each gate. For the triple labels of CD80 vs. CD21 and CD5, all cells were examined for dual expression of CD80 and each lymphocyte antigen. The analysis was repeated on samples from 3 to 4 different dogs.

2.2.2 Single-labeled flow cytometric analysis of canine bone marrow mononuclear cells

Bone marrow was aspirated into a syringe containing 1.5 mL 3.8% sodium citrate, filtered (70 µm, BD Biosciences), layered on a double-density gradient with 1.119 Histopaque and 1.077 Ficoll paque plus (Cytiva, Marlborough, MA, United States), and then centrifuged (400 x *g*, 30 min, 10°C), as we have previously described for harvesting PBMCs (30). The BMMC at the interface of the plasma and 1.077 density media was harvested, washed 4 times in PBS, and resuspended in PBSA. Then, 1×10^6 cells were incubated with the anti-CD80 antibody for 30 min in PBSA, with unlabeled, isotype, and 7-aminoactinomycin D (7-AAD, for excluding dead cells) controls. The cells were washed in PBS for acquisition with an Accuri C6 BD Biosciences (the BD FACSCalibur™ was no longer available for use), then analyzed for labeling with the anti-CD80 antibody using a FSC vs. SSC plot on FloJo™ software.

2.2.3 Flow cytometric-based sorting of cells labeled with the anti-CD80-antibody in blood and bone marrow

For blood and BMMC, 1×10^7 cells were resuspended in PBS and incubated with the anti-CD80 and anti-CD14 antibodies (blood) or anti-CD80 antibody alone (BMMC) for 30 min on ice. The cells were resuspended in PBS with 1% BSA after a PBS wash and sorted into PBS with 10% BSA, using a MA900 (Sony Biotechnology, San Jose, CA, United States) or FACSAria™ III (BD Biosciences) flow cytometer (different sorters were used based on instrument availability) in the Cornell University BRC flow cytometry core facility (RRID:SCR_021740). Either 7-AAD or 4′,6-diamidino-2-phenylindole were used to exclude dead cells and single-labeled cells with isotype controls were used to define positive staining reactions during acquisition. For blood samples, double positive ($CD80^+$/$CD14^+$), single positive ($CD80^+$ or $CD14^+$), and double negative ($CD80^-$/$CD14^-$) cells were sorted. For BMMC, $CD80^+$, $CD80^-$ cells with high SSC ($CD80^-$/high SSC), and $CD80^-$ cells with low SSC ($CD80^-$/low SSC) were sorted. Cytospin smears were prepared from the sorted cells after a 500 x *g* centrifugation step (with resuspension in PBS) and stained with modified Wright's stain (Hematek 1,000, Siemens Healthcare Diagnostics Inc., Tarrytown, NJ, United States). A 100-cell differential cell count was done on each sorted population.

2.2.4 Leukocyte isolation from blood followed by labeling with the anti-CD80 antibody

Peripheral blood mononuclear cells were harvested from the plasma/1.077 interface after double-density centrifugation of blood, as described for BMMC. B cells, T cells, and monocytes were then individually isolated from PBMC using conjugated antibodies against CD21, CD5, and CD14, followed by anti-murine IgG magnetic microbeads for CD14 and CD21 (Miltenyi Biotec Cat# 130–048-402, RRID:AB_244361) and anti-rat IgG magnetic microbeads for CD5 (Miltenyi Biotec Cat# 130–048-502, RRID:AB_244364) and a magnetic column (LS column, Miltenyi Biotec, Gaithersburg, MD, United States) as we described previously for isolating $CD14^+$ monocytes (30). Isolated cells were then incubated with the anti-CD80 antibody, as described above for double- or triple-labeling, and flow cytometric analysis was performed to assess for dual expression of the markers. For neutrophil isolation, we harvested cells from the interface between the 1.077 and 1.119 gradients and lysed RBCs with 0.2% sodium chloride for 30 s, followed by quenching with 1.6% sodium chloride. This experiment was done on samples from 2 to 3 different dogs per cell type. We also performed differential cell counts on modified Wright's-stained smears of cytospin preparations of the isolated cells.

2.3 Testing for CD80 expression in hematopoietic neoplasms

Flow cytometric panels, including the anti-CD80 antibody, were performed on blood and lymph node, bone marrow, mass or body cavity fluid aspirates from dogs with hematopoietic neoplasia, including lymphoma and leukemia, using BD FACSCalibur™, Accuri C6 (BD Biosciences) or Novocyte (2000R, Agilent Technologies, Santa Clara, CA, United States) flow cytometers. Various software was used to analyze the data, including BD FACScan software, FloJo™ and FCS Express (*De Novo* Software, Dotmatics, Pasadena, CA). In samples collected after July 2019, 7-AAD was used to gate out dead cells, otherwise cell debris was excluded from analysis based on its location in a FSC vs. SSC dot plot. A tumor cell gate was created in the FSC vs. SSC dot plots, based on abundance of events and characteristic location (low to high FSC, low to medium SSC). When possible, residual normal leukocytes (neutrophils, monocytes, lymphocytes) were gated separately in the same plot. Antibody labeling of each gate was assessed in histogram, SSC vs. fluorescence, and quadrant fluorescence plots for triple labels or histograms and quadrant plots for single or double labels. Only data from the region containing the tumor cells was included in this study; however, antigen expression on residual normal leukocytes was assessed as internal positive and negative controls for antibody staining. For all markers other than CD34, expression on ≥20% of gated tumor cells was considered positive, in relation to an isotype control (31, 32); for CD34, ≥5% labeling of the tumor cells was considered positive (2, 3, 33). Since monocytes and lymphocytes can overlap or fall in the tumor cell gate, to avoid including these cells in the analysis of CD80 expression,

we compared the percentage of CD80$^+$ cells with the percentages of CD14$^+$ cells and monocytes in a differential cell count. We also assessed the location of CD80$^+$ and CD14$^+$ cells in FSC and SSC plots. When the percentage of CD80$^+$ and CD14$^+$ cells were similar (± 10%) and events overlapped in a typical location for monocytes in a FSC and SSC plot (medium to high FSC and medium SSC), they were considered residual monocytes. Similarly, when the tumor gate included residual normal lymphocytes (mostly in lymph node aspirates), we identified these normal cells based on their low FSC and SSC characteristics and flow cytometric results showing a mixed population of lymphocytes, i.e., CD21$^+$/CD22$^+$ B cells and CD3$^+$/CD4$^+$ and CD3$^+$/CD8$^+$ T cells.

Based on morphologic features and hematologic and flow cytometric results, the hematopoietic neoplasms in the dogs were classified as B or T lymphoma/leukemia, B or T chronic lymphocytic leukemia (CLL), acute myeloid leukemia (AML), or "mixed lineage" leukemia. Classification of lymphoid neoplasms as B or T was based on tumor cell expression of CD21$^+$ or CD22$^+$ or both and CD3$^+$ or CD5$^+$ or both, respectively. In select cases, immunocytochemical staining for CD3 was performed on blood or cytology smears to confirm a T cell origin or verify weak or negative flow cytometric reactions for CD3, with ≥20% CD3$^+$ tumor cells being defined as a positive reaction. B or T cell lymphoma/leukemias consisted of intermediate to large cells ("blasts") and were grouped as a single entity, regardless of the blast percentage in blood or bone marrow. Chronic lymphocytic leukemia was characterized by a mature lymphocytosis, with negative test results for tick-borne diseases. For B-CLL, we used previously defined criteria of > 5.0×10^9 small lymphocytes/L with > 60% CD21$^+$ cells (34). Similar criteria are lacking for T-CLL in dogs, so we used a cut-off of > 20.0×10^9 lymphocytes/uL with > 60% CD3 or CD5 expression. An acute leukemia was classified as AML on flow cytometric analysis if there were ≥ 20% blasts in blood or bone marrow, lymph node, tissue, or body cavity fluid aspirates and blasts were positive for myeloid-associated antigens CD4, CD11b, CD11c, CD14, and CD18, alone or in combination and negative for B and T cell markers (3). Because myeloid cells (monocytes, neutrophils, and eosinophils) typically comprise <5% of cells in normal lymph node aspirates (33, 35), we defined an extramedullary AML in lymph node aspirates as ≥20% blasts in cytologic smears combined with ≥5% positive reactions for myeloid-associated antigens on flow cytometric analysis. In cases in which we performed triple labeling with CD34/CD80/MHCII, CD34/CD11b/CD11c or CD34/CD11b/CD18, a leukemia was also classified as AML if there were ≥ 5% CD34$^+$/CD11b$^+$, CD34$^+$/CD11c$^+$, or CD34$^+$/CD18$^+$ cells. In acute leukemias that could not be phenotyped by flow cytometry, cytochemical staining was done to distinguish between AML and ALL, as described (2, 3, 36). Expression of alkaline phosphatase (ALP), alpha-naphthyl butyrate esterase (ANBE), chloroacetate esterase (CAE), myeloperoxidase (MPx), and Sudan Black B (SBB) in ≥3% of the cells, alone or in combination, was consistent with a myeloid lineage for an acute leukemia (Supplementary Table S1) (2, 3). AML was further classified into "not otherwise-specified" categories of unclassified, myelomonocytic, monocytic/monoblastic, and megakaryoblastic leukemia (Supplementary Table S2) (14, 15). A "mixed lineage" leukemia was diagnosed if blasts were positive for myeloid- and lymphoid-associated antigens on flow cytometric analysis or expressed lymphoid antigens on flow cytometric analysis but had cytochemical staining reactions typical of AML.

2.4 Statistical analysis

Normality was assessed with a Shapiro–Wilk test when there was more than 3 data points per group. Non-Gaussian data was described as median and range, whereas 3 data points per group were described as mean and range. Medians of two groups were compared with a Wilcoxon signed-rank test (e.g., median percentage of anti-CD80-labeled monocytes vs. neutrophils). Proportions were compared with a Fisher's exact test with a Bonferroni correction for the number of pairwise comparisons. Significance was set at $p < 0.05$.

3 Results

3.1 Binding of the anti-CD80 antibody to peripheral blood leukocytes from normal dogs

CD80, as detected with the clone in this study, was consistently expressed on >95% of cells gated as monocytes (CD14$^+$) and neutrophils (CD14$^-$) in blood samples taken from 4 different healthy dogs. The intensity of CD80 expression (MFI) in CD14$^+$ monocytes and CD14$^-$ neutrophils was similar (Table 3). In contrast, cells gated as lymphocytes in the CD80 vs. CD14 experiments or triple-labeled with CD80 and B and T cell markers, CD21 and CD5, respectively, were negative for CD80 (Figure 1, representative images from one dog for CD80 vs. CD14 and a different dog for CD80 vs. CD21 or CD5). Events gated as lymphocytes in the CD80 vs. CD14 experiments had a median CD80 MFI of 6 units (range, 1–9 units), which was not significantly different from the median CD80 MFI of 5 units (range, 4–7 units) for the isotype control in that gate ($p = 0.750$).

On flow cytometric sorting with CD80- and CD14-labeled cells, only three populations were evident: CD80$^+$/CD14$^+$, CD80$^+$/CD14$^-$, and CD80$^-$/CD14$^-$ cells. No cells were CD80$^-$/CD14$^+$, suggesting that all CD14$^+$ monocytes in blood from healthy dogs are CD80$^+$. Differential cell counts on modified Wright's-stained smears showed that monocytes, neutrophils, and lymphocytes dominated in the CD80$^+$/CD14$^+$, CD80$^+$/CD14$^-$ and CD80$^-$/CD14$^-$ populations, respectively (Figure 2, Table 4). Eosinophils were identified in the CD80$^-$/CD14$^-$ cells, indicating they are negative for CD80, when using the anti-hamster antibody (Table 4). Since eosinophils are found

TABLE 3 Labeling of leukocytes in the blood of healthy dogs with the anti-CD80 antibody, expressed as a percentage and median fluorescent intensity (MFI) of CD14$^+$ monocytes and CD14$^-$ neutrophils in regions gated as monocytes and neutrophils, respectively, in a forward and side scatter dot plot (see Figure 1) ($n = 4$).

	CD80$^+$ percentage*		CD80$^+$ MFI (units)*	
Gated cells	Median	Range	Median	Range
CD14$^+$ monocytes	100	97.9–100	153	93–204
CD14$^-$ neutrophils	98.6	96.3–99.9	132	99–208

Cells gated as lymphocytes did not label with the anti-CD80 antibody; their MFI (median, 6 units) was similar to the isotype control (median, 5 units) ($p = 0.750$). *The median percentage of CD80$^+$ cells and CD80 MFI in CD14$^+$ monocytes and CD14$^-$ neutrophils was not significantly different ($p > 0.05$).

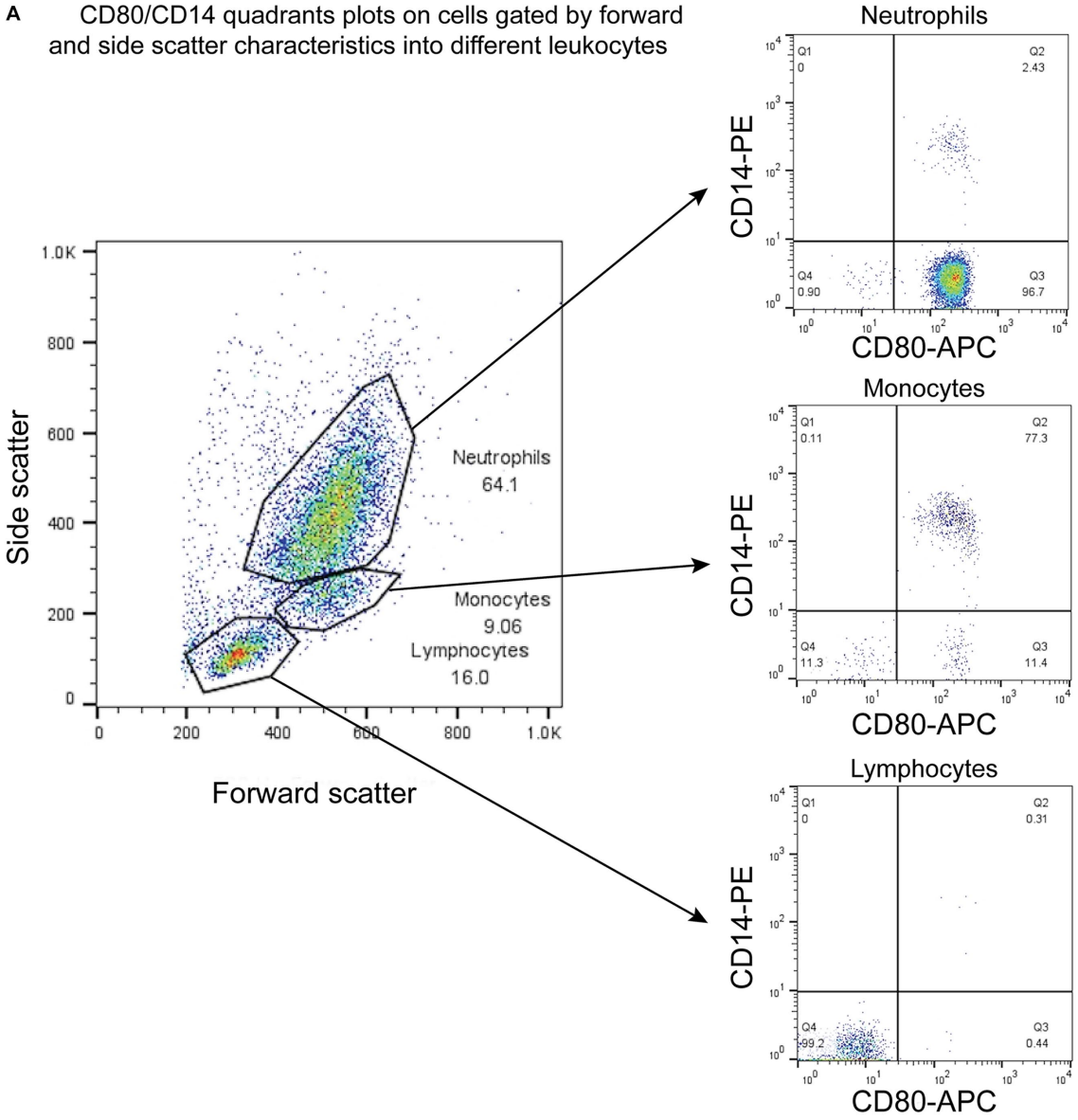

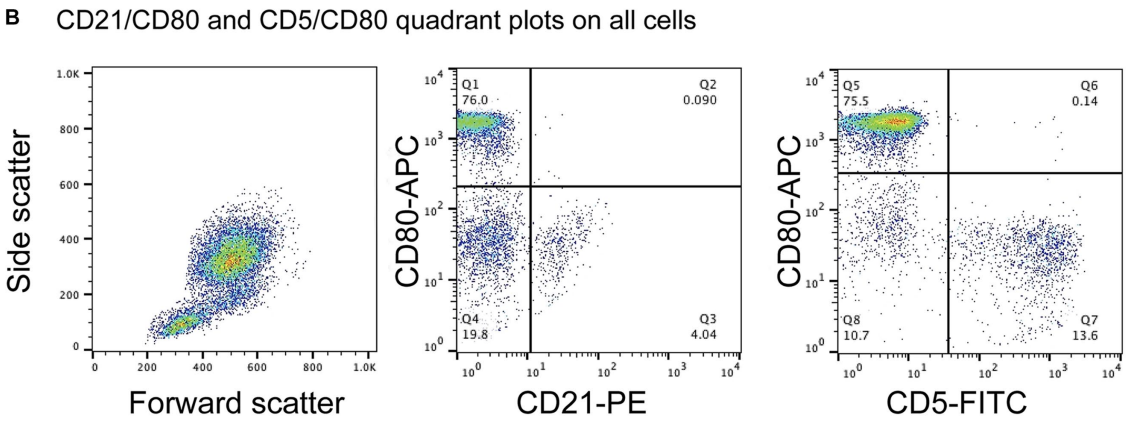

FIGURE 1
Flow cytometric dot plots of anti-CD80 antibody labeling of leukocytes in blood from healthy dogs. **(A)** Three different cell populations were identified on a forward and side scatter plot, corresponding to neutrophils, monocytes, and lymphocytes. The cells were double-labeled with anti-CD80-APC and -CD14-PE antibodies, with CD14 being used as a monocyte marker. CD80 was only expressed on $CD14^+$ monocytes and $CD14^-$ neutrophils but

(Continued)

FIGURE 1 (Continued)

not lymphocytes ($CD80^-/CD14^-$). The few $CD14^+$ and $CD14^-$ cells in the neutrophil and monocyte gates likely represent low numbers of monocytes and neutrophils in the respective gates. The $CD80^-/CD14^-$ cells in neutrophil and monocyte gates could be large lymphocytes (representative result from 1 of 4 dogs). **(B)** Triple-labeling of dog leukocytes with CD80-APC, CD21-PE and CD5-FITC shows that $CD21^+$ B cells and $CD5^+$ T cells are $CD80^-$ (representative result from 1 of 3 dogs). All leukocyte events were combined for analysis vs. splitting the events into different gates based on forward and side scatter.

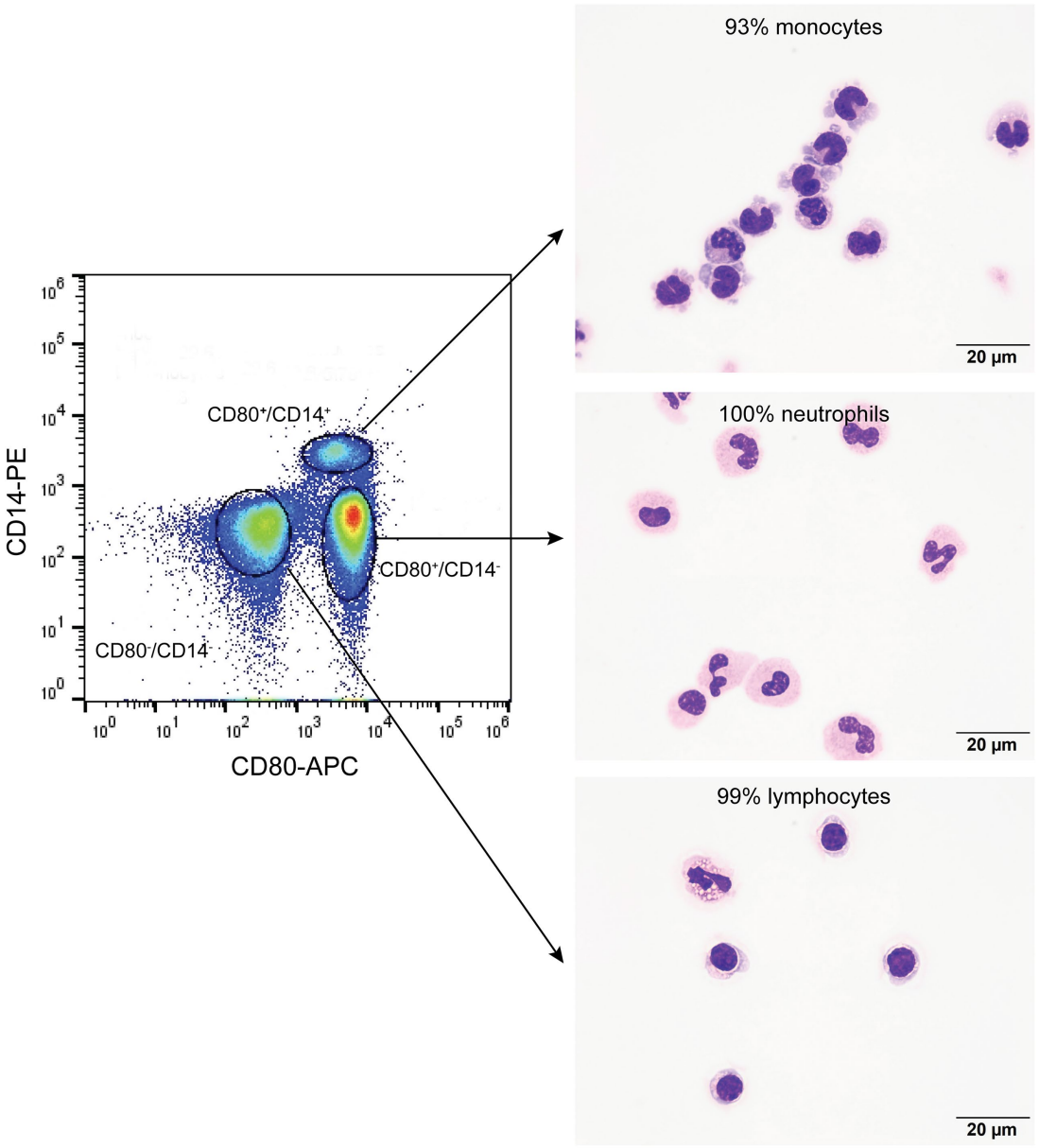

FIGURE 2
Flow cytometric sorting of peripheral blood leukocytes double-labeled with the anti-CD80 antibody and an anti-CD14 antibody into $CD80^+/CD14^+$, $CD80^+/CD14^-$, and $CD80^-/CD14^-$ populations (left panel) with corresponding images of modified Wright's-stained smears and percentages of the predominant cell from differential cell counts of cytospin smears of the sorted populations (right panel, scale bar = 20 µm). $CD80^-/CD14^+$ cells were not identified or sorted. The black circles indicate sorted events (a tight gate was chosen to minimize contamination from other populations; representative image from 1 of 3 dogs). $CD80^+/CD14^+$ sorted cells were mostly monocytes, a few of which contained low numbers of cytoplasmic vacuoles. The $CD80^+/CD14^-$ sorted cells were mostly neutrophils, many of which lacked nuclear segmentation or were undergoing pyknosis, which we attributed to the sorting procedure. The $CD80^-/CD14^-$ sorted cells were mostly lymphocytes, with a few eosinophils.

TABLE 4 Percentage differential cell counts (mean and range) from modified Wright's-stained cytospin smears of three cell populations sorted by flow cytometry using anti-CD80 and -CD14 antibodies in the blood of healthy dogs ($n = 3$): $CD80^+/CD14^+$, $CD80^+/CD14^-$ and $CD80^-/CD14^-$.

Sorted cells			
Leukocyte	$CD80^+/CD14^+$	$CD80^+/CD14^-$	$CD80^-/CD14^-$
Neutrophil %	2 (1–4)	97 (93–100)	1 (0–1)
Lymphocyte %	2 (0–5)	2 (0–5)	80 (63–99)
Monocyte %	96 (93–97)	1 (0–1)	1 (0–2)
Eosinophil %	0 (0–0)	0 (0–0)	18 (1–35)
Basophil %	0 (0–0)	0 (0–1)	0 (0–0)

A $CD80^-/CD14^+$ population was not identified (see Figure 2).

in low concentrations in blood and cannot be distinguished from neutrophils based on scatter characteristics or antibodies used in flow cytometric panels, their lack of binding of the anti-CD80 antibody was only uncovered by cell sorting.

When monocytes, B cells, and T cells were isolated via magnetic bead labeling with the anti-CD14, -CD21 and -CD5 antibodies then labeled with the anti-CD80 antibody, only $CD14^+$ monocytes were $CD80^+$, corroborating the results of the multiple labeling and cell sorter experiments. The purity of the isolated cells was generally >80% (Figures 3A–C, Table 5). Contaminating neutrophils in the CD14-magnetic bead isolated cells were weakly $CD14^+$, suggesting that neutrophils were activated by the procedure and either expressed CD14 or had bound $CD14^+$-microparticles shed from activated monocytes (Figure 3A). Similar to monocytes, neutrophils isolated from the double-density gradient were $CD80^+$ (Figure 3D) with a purity of 78% or higher (Table 5).

3.2 Binding of the anti-CD80 antibody to bone marrow mononuclear cells from normal dogs

When BMMC were incubated with the anti-CD80 antibody, a single $CD80^+$ population with high SSC was identified (Figure 4) and comprised a median of 66% (range, 61–71%) of the living cells ($n = 4$). Typically, neutrophils and monocytes have higher SSC than lymphocytes. There were two populations of $CD80^-$ cells; (1) One had similar high SSC to the $CD80^+$ cells and comprised a median of 16% (range 16–23%) of living cells, and (2) Another population with low side SSC, corresponding to cells with less complexity, such as lymphocytes (Figure 4), comprising a median of 13% (range 11–21%) of living cells. When differential cell counts were done on modified Wright's-stained cytospin smears of these 3 flow cytometric-sorted populations, the $CD80^+$ cells consisted of neutrophil precursors (bands to myelocytes, with rare progranulocytes) and monocytes (Figure 4C). In contrast, the $CD80^-$/high SSC cells were mostly mature and immature eosinophils with fewer monocytes, large reactive lymphocytes, and plasma cells (Figure 4C). Rare progranulocytes and basophils were seen. Lymphocytes comprised the majority of the $CD80^-$/low SSC cells, with fewer monocytes, and there were reactive lymphocytes in this population (Figure 4C). Segmented neutrophils were not seen in any fraction because these cells settle at the interface between the 1.077 and 1.119 density gradients. The BMMC sorting showed that the anti-CD80 antibody binds to mature and immature neutrophils and affirms that it does not bind to mature and immature eosinophils. In addition, the antibody may not detect plasma cells. It is difficult to determine whether the antibody labels progranulocytes and basophils, given that these cells were only seen in low numbers in the cytospin smears and progranulocytes were identified in both $CD80^+$ and $CD80^-$ high scatter fractions.

3.3 Binding of the anti-CD80 antibody to tumor cells in dogs with hematopoietic neoplasms

B cell neoplasms were identified in 37 dogs from blood ($n = 7$) or lymph node ($n = 27$), bone marrow ($n = 2$), or pleural fluid ($n = 1$) aspirates. The dogs were a median of 8 years old (range, 2–13 years) with 20 female (2 intact) and 17 male (2 intact) dogs. Breeds consisted of 17 mixed breed dogs, 5 German Shepherds, 3 Golden Retrievers, 2 Australian Shepherds, 2 Rottweilers, and one each of the following: Belgian Tervuren Shepherd, Bernese Mountain Dog, Bichon Frise, English Springer Spaniel, Jack Russell Terrier, Shih Tzu, Vizsla, and Yorkshire Terrier. Five dogs with a moderate to marked lymphocytosis (median, 60.4×10^6/mL, range, $18.1–146.8 \times 10^9$/L), consisting of small to intermediate lymphocytes, were diagnosed with B-CLL. The remaining 32 dogs were diagnosed with B cell lymphoma/leukemia from lymph node or bone marrow aspirates or blood samples, with 1 concurring histologic diagnosis on a lymph node biopsy. None of the tumor cells were labeled with the anti-CD80 antibody (Figure 5, Table 6, Supplementary Figure S1, Supplementary Table S3). Of the other myeloid antigens used in this study, tumor cells were $CD11c^+$ in 1/13 dogs (8%). A few dogs had aberrant $CD3^+$ (7/37, 19%) or $CD5^+$ (2/37, 5%) tumor cells; however, in all of these cases, tumor cells were $CD21^+$ and $CD22^+$, supporting a B cell neoplasm. In 3 dogs, there were discordant CD21 and CD22 reactions, with $CD21^-/CD22^+$ (n = 2) or $CD21^+/CD22^-$ ($n = 1$) cells (Supplementary Table S3). A B cell lineage was confirmed for 1 dog with a $CD21^-/CD22^+$ lymphoma/leukemia in the bone marrow on the basis of a clonal B cell population on polymerase testing for antigen receptor rearrangements (PARR) and $CD20^+/CD3^-$ cells on immunocytochemical staining of bone marrow smears (Supplementary Table S3).

T cell neoplasms were identified in *35* dogs from blood ($n = 17$) or aspirates from lymph node ($n = 11$), bone marrow ($n = 2$), mediastinal or lung masses ($n = 2$), or pleural ($n = 2$) or peritoneal ($n = 1$) fluid. The dogs were a median of 6 years old (range, 8 months to 14 years) with 12 female (1 intact) and 23 male (5 intact) dogs. Breeds consisted of 9 mixed breed dogs, 6 Golden Retrievers, 3 Labrador Retrievers, 2 German Shepherds, 2 Shih Tzus, and one each of the following: Australian Shepherd, American Bulldog, Bassett Hound, Bernese Mountain Dog, Bloodhound, Boxer, Bull Mastiff, Doberman, English Bulldog, Giant Schnauzer, Mi-Ki, Pug, and Staffordshire Bull Terrier. Two dogs with a lymphocytosis of granular lymphocytes (85.3 and 89.7×10^9/L) were diagnosed with $CD8^+$ T-CLL. Another dog had a mild lymphocytosis of granular lymphocytes (5.5×10^9/L), with an average of 39% granular lymphocytes in bone marrow. The dog (a Golden Retriever) also had a lymphocytosis (8.7×10^9/L) of T cells that lacked cytoplasmic granules and were $CD45^-$ on phenotyping, supporting a concurrent indolent T zone lymphocytosis. Given the bone marrow infiltrates of granular lymphocytes, this dog was placed in the $CD8^+$ T cell lymphoma/leukemia category

10.3389/fvets.2024.1405297

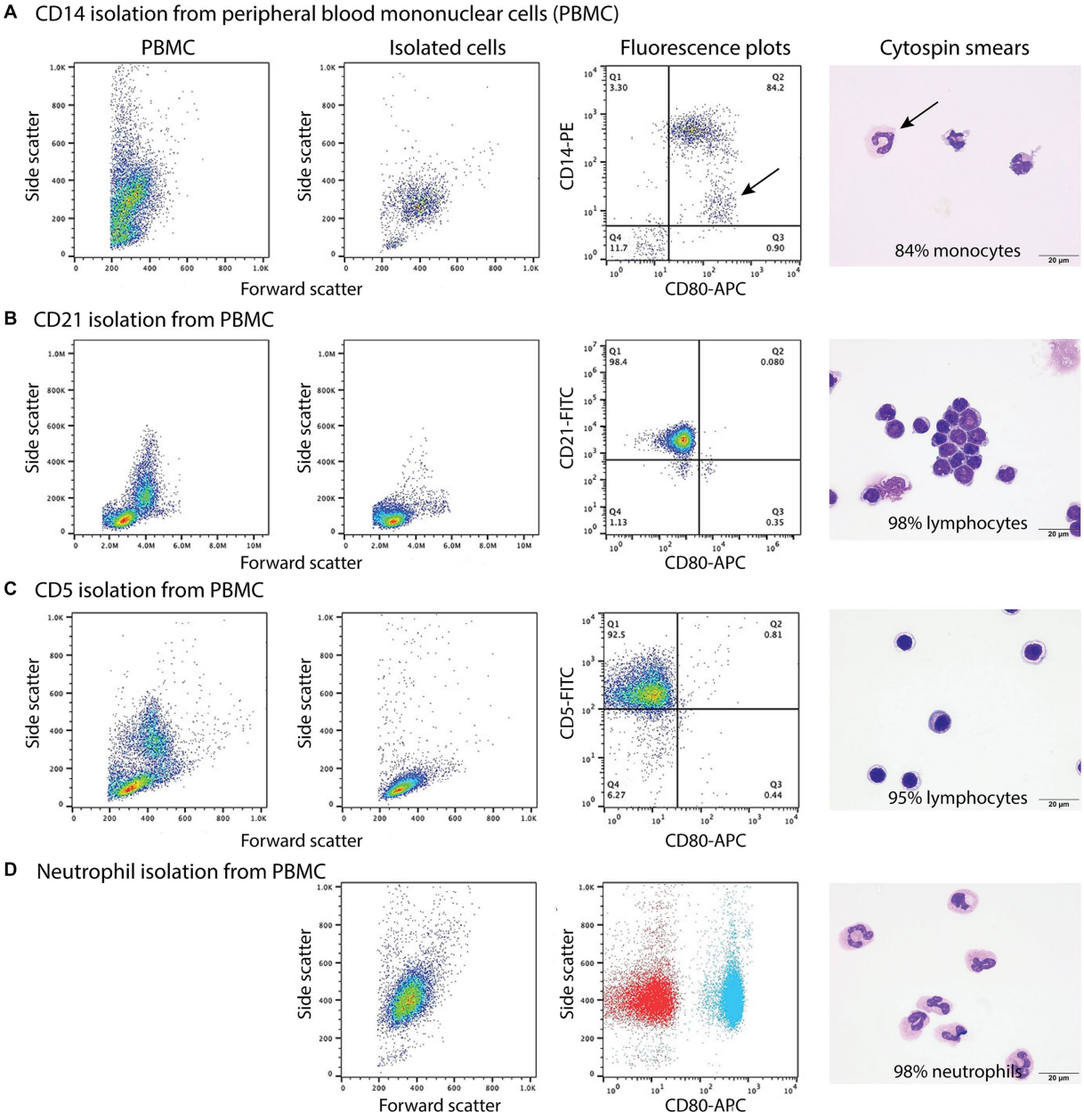

FIGURE 3
Labeling of monocytes, B cells, T cells, and neutrophils isolated from the blood of healthy dogs (representative results from 1 of 2–3 dogs for each cell type) with the anti-CD80 antibody. **(A-C)** Monocytes, B cells, and T cells were isolated from peripheral blood mononuclear cells (PBMCs) using immunomagnetic beads and anti-CD14-PE, -CD21-FITC, and -CD5-FITC antibodies, respectively. The first panel shows the forward and side scatter events in PBMCs while the second panel shows the forward and side scatter events of isolated cells. The third panel is a fluorescent quadrant plot of double-labeled cells after adding the anti-CD80-APC antibody. The fourth panel shows a representative modified Wright's-stained image of a cytospin smear of the isolated cells on which 100-cell differential cell counts were done (scale bar = 20 μm). **(A)** CD14-PE-isolated cells were mostly $CD80^+$ monocytes (84% of a differential cell count), with a few contaminating neutrophils (10%) that were weakly $CD14^+$ (arrows, third and fourth panels). A few monocytes had cytoplasmic vacuoles (fourth panel). Lymphocytes were negative for $CD80^-/CD14^-$ (lower left quadrant, third panel, 6%). **(B)** CD21-FITC-isolated cells were mostly lymphocytes, which were $CD80^-$ (third panel). Lymphocytes were primarily small cells, some of which had clefted or convoluted nuclei (variants of normal), with a few small or large reactive forms (fourth panel). **(C)** CD5-FITC-isolated cells were mostly lymphocytes, which were $CD80^-$ (third panel). Lymphocytes were small cells with a few large or reactive forms. Several lymphocytes had a few clear cytoplasmic vacuoles, which could be due to the isolation procedure (fourth panel). **(D)** Neutrophils were isolated from the 1.077/1.119 interface of the double-density gradient used to obtain PBMCs and were single-labeled with the anti-CD80-APC antibody. The first panel shows a forward vs. side scatter plot of the isolated neutrophils and the second panel is a CD80 fluorescence vs. side scatter dot plot (blue) with overlaid hamster-APC isotype (red), showing neutrophils are $CD80^+$. The third panel shows a representative modified Wright's-stained image of a cytospin smear of the isolated cells, which were primarily segmented neutrophils. The vacuolated cytoplasm in one neutrophil is likely an artifact of the isolation procedure (scale bar = 20 μm).

TABLE 5 Percentage differential cell counts (mean and range) from modified Wright's-stained cytospin smears of isolated monocytes, B cells, T cells, and neutrophils.

Leukocyte	Isolated cells			
	CD14⁺ monocytes	CD21⁺ B cells	CD5⁺ T cells	Neutrophils
Neutrophil %	5 (1–10)	11 (0–33)	5 (1–11)	88 (78–98)
Lymphocyte %	5 (4–6)	80 (42–100)	93 (88–97)	9 (0–16)
Monocyte %	90 (84–95)	4 (0–12)	1 (0–2)	0 (0–1)
Eosinophil %	0 (0–0)	5 (0–13)	1 (0–2)	2 (1–4)
Basophil %	0 (0–0)	0 (0–0)	0 (0–0)	0 (0–1)

Monocytes, B cells, and T cells were isolated by magnetic bead labeling using antibodies against CD14, CD21, and CD5, respectively ($n = 3$ for CD14 and CD5 and $n = 2$ for CD21). Neutrophils were isolated from the lower interface of the double-density gradient ($n = 3$).

(Supplementary Table S4). Another 33 dogs were diagnosed with T lymphoma/leukemia from blood or aspirates of lymph node, bone marrow, mediastinal or lung masses, or body cavity fluid, with 2 corroborating histologic diagnosis. One dog had a clonal T cell population with PARR in a lymph node aspirate. In 2 dogs (a Bull Mastiff and a Shih Tzu), the cells were CD45⁻ and had cytologic features of an indolent T zone lymphoma (6). None of the tumor cells in dogs with T cell neoplasms were labeled with the anti-CD80 antibody (Figure 4, Table 6, Supplementary Table S4); however, the cells were CD11b⁺ (2/22, 9%) or CD11c⁺ (6/19, 32%) in low numbers of dogs. There was discordant CD3 or CD5 expression in a few cases, with CD3⁻/CD5⁺ ($n = 4$) or CD3⁺/CD5⁻ ($n = 5$) cells. Tumor cells in 2 dogs were CD3⁻/CD5⁻ but were CD8⁺/ TCRαβ⁺ on flow cytometric analysis in one dog or strongly CD3⁺ on immunocytochemical staining in the other dog (Supplementary Table S4), supporting a T cell origin.

Thirty nine dogs were diagnosed with AML based on flow cytometric expression of myeloid-associated antigens ($n = 33$) or positive cytochemical staining reactions combined with negative staining for T (CD3/CD5) or B (CD21/CD22) lymphoid-associated antigens on flow cytometric analysis ($n = 6$) (Table 6, Supplementary Table S5). The phenotyping was done on blood ($n = 23$) or aspirates of bone marrow ($n = 10$), lymph node ($n = 5$), or pleural fluid ($n = 1$). In venous blood samples, blasts constituted ≥20% of a differential count in 22 dogs (22/23, 96%). The single dog with 10% blasts in blood had ≥20% blasts on cytologic examination of a lymph node aspirate (flow cytometric analysis was not done on the lymph node). The dogs were a median of 7.5 years old (range, 2–14 years) with 11 neutered female and 28 male (5 intact) dogs. Breeds consisted of 14 Golden Retrievers, 6 mixed breed dogs, 5 Labrador Retrievers, 4 German Shepherds, 2 Pembroke Welsh Corgis, and one each of the following: Anatolian Shepherd, Bernadoodle, Bernese Mountain Dog, Bulldog, Cockapoo, Maltese, Rhodesian Ridgeback, and Soft-coated Wheaten Terrier. Tumor cells were labeled with the anti-CD80 antibody in 28 cases (72%), mostly myelomonocytic and monocytic/monoblastic variants (Figure 4, Table 6, Supplementary Figure S1, Supplementary Table S5). However, 2 acute megakaryoblastic leukemias had CD80⁺ cells (Supplementary Table S5). A higher proportion of dogs had CD80⁺ cells compared to CD4⁺ (36%, 14/39), CD11b⁺ (44%, 17/39), CD11c⁺ (46%, 16/35), CD14⁺ (38%, 15/39), or CD18⁺ (56%, 10/17) cells; however, the difference was only significant for CD80⁺ vs. CD4⁺ ($p = 0.003$) or CD14⁺ ($p = 0.006$) (Supplementary Table S5). A few individual dogs with AML expressed only one myeloid antigen (CD11b in one dog, CD11c in one dog, CD80 in 4 dogs), however most dogs expressed different combinations of more than one myeloid antigen (Supplemental Table S5).

Eleven dogs were diagnosed with "mixed lineage" leukemia based on flow cytometric expression of myeloid-associated markers ($n = 5$) or positive cytochemical staining reactions combined with positive staining for B (CD21 or CD22) or T (CD3 or 5) lymphoid-associated antigens on flow cytometric analysis ($n = 6$) (Table 6, Supplementary Table S6). The phenotyping was done on blood ($n = 8$) or aspirates of bone marrow ($n = 1$) or lymph node ($n = 2$). Venous blood in 10 dogs contained ≥20% blasts and 1 dog had ≥20% blasts in a lymph node aspirate (Supplementary Table S6). The dogs were a median of 8 years old (range, 3–10 years) with 6 female (1 intact) and 5 male (2 intact) dogs. Breeds consisted of 3 Labrador Retrievers and one each of the following: Bernese Mountain Dog, Cavalier King Charles Spaniel, Golden Retriever, Labradoodle, mixed breed, Rottweiler, Swiss Mountain Dog, and Yorkshire Terrier. The neoplastic cells were weakly CD5⁺ or CD3⁺ ($n = 9$) or CD22⁺ ($n = 3$); no cases were CD21⁺ and 1 case was weakly CD3⁺/CD5⁺/CD22⁺. In two cases with weak CD3⁺ tumor cells on flow cytometric analysis, the tumor cells were negative for CD3 on immunocytochemical staining of smears, suggesting a false positive reaction. Tumor cells were labeled with the anti-CD80 antibody in 4 cases (36%), including 1 case that lacked other myeloid-associated antigens on flow cytometric analysis (Table 6, Supplementary Table S6). CD80⁺ cells were present in similar percentages to CD4⁺ (27%, 3/11), CD11b⁺ (45%, 5/11), CD11c⁺ (33%, 3/9), CD14⁺ (27%, 3/11), and CD18 (50%, 1/2) (Supplementary Table S6).

4 Discussion

We found that CD80, as detected with the antibody clone in this study, is a useful flow cytometric marker for AML, particularly myelomonocytic and monocytic/monoblastic variants. This finding is in concert with the antibody labeling neutrophils, neutrophil precursors (band neutrophils to myelocytes) and monocytes in peripheral blood and bone marrow from healthy dogs. Compared to the other myeloid-associated antigens used in this study, tumor cells were CD80⁺ in a higher proportion of dogs with AML. In addition, CD80 was the only myeloid antigen expressed in some dogs categorized as AML based on cytochemical staining reactions. These leukemias would not have been diagnosed as an AML with flow cytometric analysis, since cytochemical staining is not a routinely performed phenotyping test. Similarly, in acute leukemias expressing myeloid and lymphoid-associated antigens, the presence of CD80⁺ tumor cells would support an AML. Indeed, tumor cells in 3 of 4 dogs with "mixed lineage" leukemias were positive for multiple myeloid-associated antigens, including CD80, favoring an AML with aberrant, typically weak, lymphoid antigen expression. Given that a few dogs with AML only had positive results with single myeloid antigens, our results show that antibodies against multiple myeloid antigens should be applied when immunophenotyping an acute leukemia, including CD80. Our data for CD80 in dogs

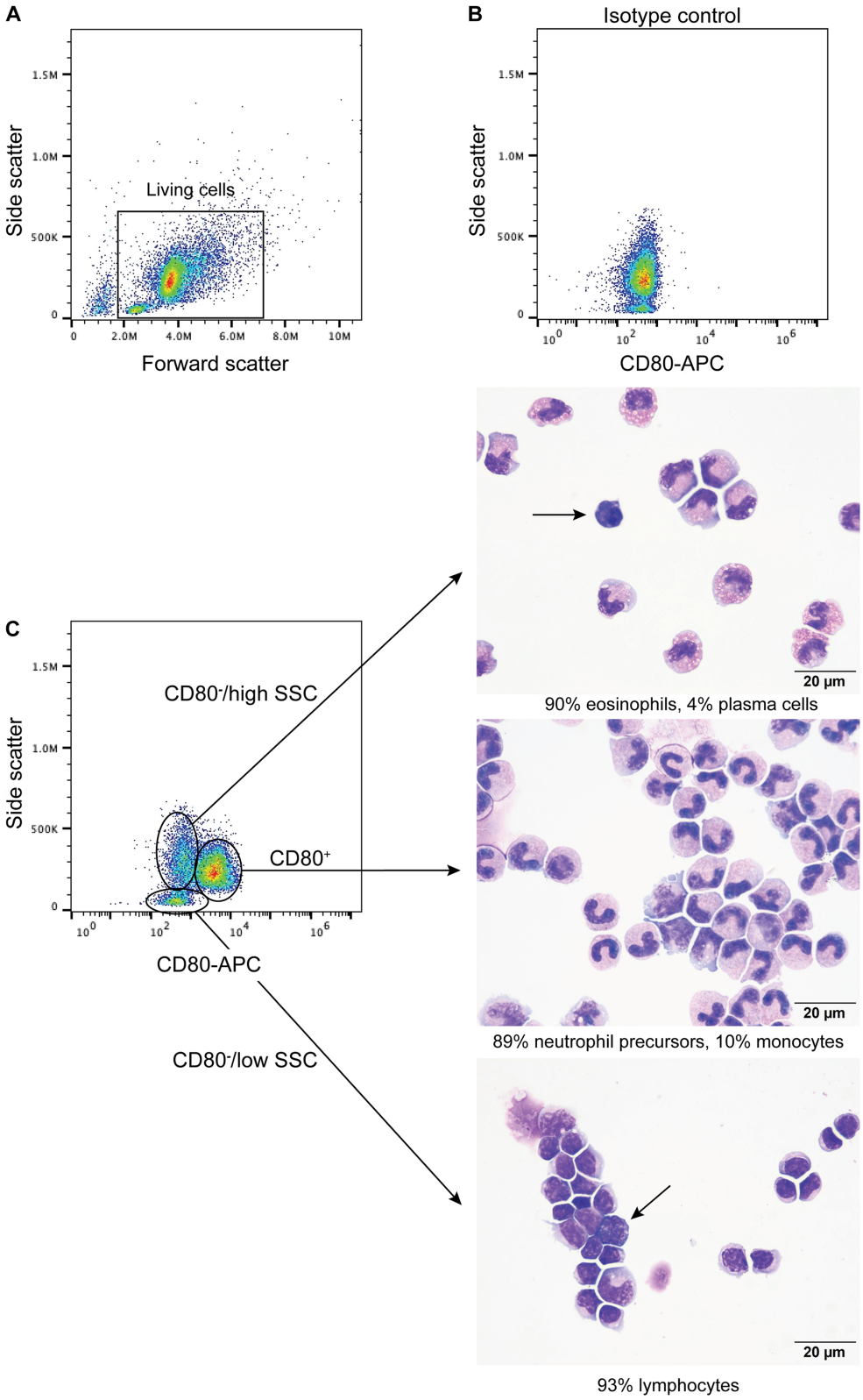

FIGURE 4
Labeling of bone marrow mononuclear cells from healthy dogs with the anti-CD80 antibody. Mononuclear cells were isolated from the plasma/1.077 interface of a double-density gradient after centrifugation of bone marrow aspirates from healthy dogs and labeled with the anti-CD80 antibody. After excluding dead cells (based on 7-AAD expression), lysed red blood cells and debris **(A)**, the living cells were evaluated for anti-CD80 antibody binding, using an isotype control **(B)** to determine positive labeling. A single population of $CD80^+$ cells with high side scatter (SSC) was identified in a CD80 fluorescence vs. SSC plot, with two $CD80^-$ populations, of high and low SSC (**C**, representative results from 4 experiments from 2 different dogs). The three different populations were then sorted from BMMC of one dog and differential cell counts were performed on modified Wright's-stained

(Continued)

FIGURE 4 (Continued)

cytospin smears of the sorted cells **(C)**. The CD80$^+$ cells were mostly neutrophil precursors and monocytes (differential cell count: 83% band neutrophils, 4% metamyelocytes, 2% myelocytes, 10% monocytes, and 1% lymphocytes). The CD80$^-$/high SSC fraction were mostly mature and immature eosinophils. Plasma cells were only seen in this fraction (arrow) (differential cell count: 90% eosinophils, including bands, metamyelocytes and myelocytes, 2% lymphocytes, 4% monocytes, and 4% plasma cells). The CD80$^-$/low SSC fraction were mostly lymphocytes with fewer monocytes (differential cell count: 93% lymphocytes and 7% monocytes). Lymphocytes included small and large reactive forms, with deep blue cytoplasm and convoluted nuclei (arrow).

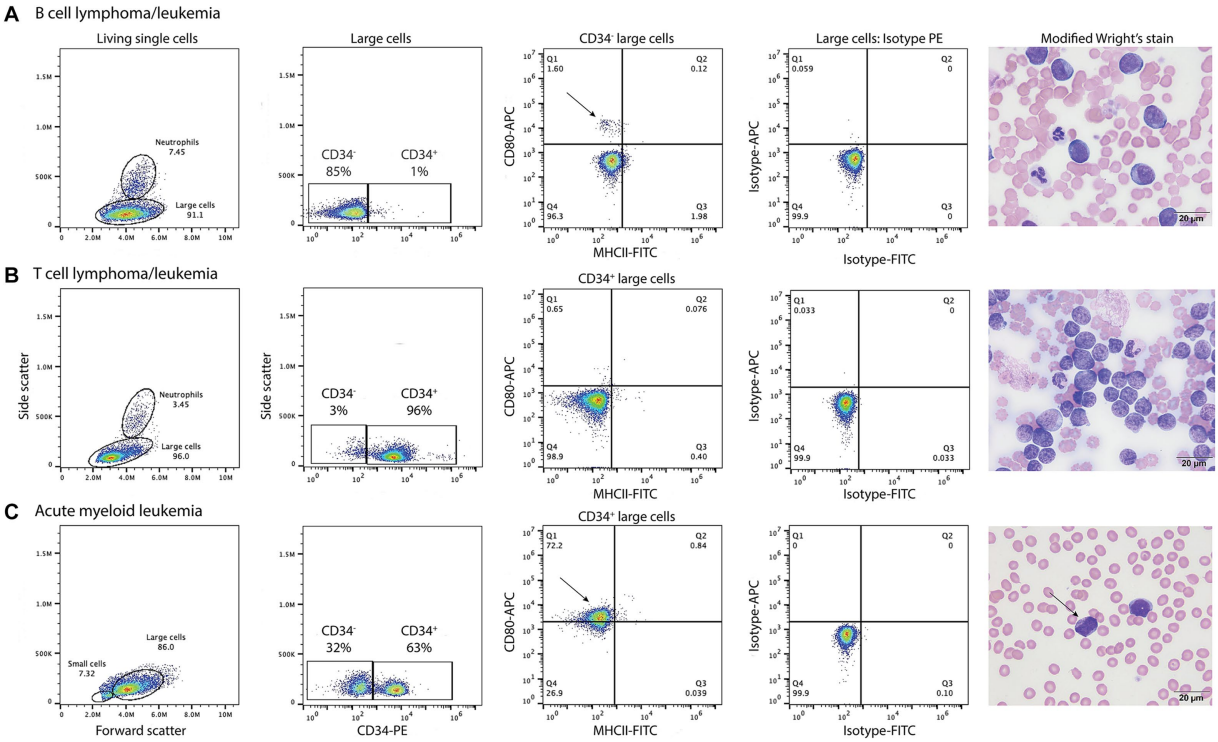

FIGURE 5

Labeling of tumor cells with the anti-CD80 antibody in dogs with hematopoietic neoplasia. Representative flow cytometric (first four panels) and modified Wright's-stained images (fifth panel, scale bar = 20 µm) of venous blood in one case each of B cell lymphoma/leukemia **(A)**, T cell lymphoma/leukemia **(B)**, and acute myeloid leukemia (AML, **C**). Gated tumor events were intermediate to large (large cells) in forward vs. side scatter plots (first panel) and were assessed for positive labeling with anti-CD34-phycoerythrin (PE), CD80-allophycocyanin (APC), and major histocompatibility II-fluorescein isothiocyanate (MHCII-FITC) antibodies. The large cell gate was separated into CD34$^+$ and CD34$^-$ events using a CD34-PE vs. side scatter plot (second panel). Quadrant plots of MHCII-FITC vs. CD80-APC were then used to further define the CD34$^-$ **(A)** and CD34$^+$ **(B,C)** cells (third panel). Isotype controls were used to set the quadrant regions (fourth panel). **(A)** The tumor cells in venous blood (large cell gate) from a dog with B cell lymphoma/leukemia were negative for CD34$^-$, CD80$^-$ and MHCII$^-$. The dog had 87% blasts in blood, which were large cells (11–14 µm) with round nuclei containing lightly stippled chromatin and up to 5 prominent nucleoli. The cells had a small amount of deep blue cytoplasm with a perinuclear clear zone. A small population of CD80$^+$/MHCII$^-$ cells (arrow, third panel) likely represent neutrophils inadvertently included in the large cell gate. **(B)** The tumor cells in venous blood from a dog with T cell lymphoma/leukemia were CD34$^+$ but CD80$^-$/MHCII$^-$. The tumor cells comprised 89% of the cells in blood and were intermediate to large (9–14 µm) with round to deeply convoluted nuclei containing lightly clumped chromatin and 1–2 indistinct nucleoli. They had a scant to small amount of medium blue cytoplasm. **(C)** In venous blood from a dog with AML, 63% of the tumor cells (large cells) were CD34$^+$. Of the CD34$^+$ cells, 72% were CD80$^+$/MHCII$^-$ (arrow, third panel). The dog had 79% blasts in blood, which were mostly intermediate to large cells (10–14 µm) with round to oval nuclei containing lightly stippled chromatin and 1–2 nucleoli. They had a small amount of light to medium blue cytoplasm and 5% of blasts contained purple or red cytoplasmic granules (arrow, fourth panel). See Supplementary Figure S1 for results from the neutrophil gated region in the dog with B lymphoma/leukemia and the small cell region in the dog with AML.

contrasts with that in human patients, where CD80 is an insensitive marker of AML, being positive in <20% of cases (31, 32, 37–40). Only one study of 105 AML human patients had a higher percentage of CD80$^+$ cases (33–100%) (41). However, the clone used in the studies was not always stated, making it difficult to explain discrepant results. In contrast, CD86, another member of the B7 family, is expressed on 23–90% of AML in studies of 20–110 human patients (31, 32, 37–41). CD80 can be upregulated in cultured AML cells after exposure to inflammatory cytokines (37, 42) and chemotherapeutic drugs, such as cytosine arabinoside (43). Upregulation of CD80 is speculated to promote a cytotoxic anti-tumor cell response (43).

TABLE 6 Positive labeling with the anti-CD80 antibody in tumor cells in dogs with hematopoietic neoplasms.

Neoplasm	Number	CD80 (*n*, %)
B cell	**37**	**0 (0%)**
Chronic lymphocytic leukemia	5	0 (0%)
Lymphoma/leukemia	32	0 (0%)
T cell	**35**	**0 (0%)**
Chronic lymphocytic leukemia: $CD8^+$	2	0 (0%)
Lymphoma/leukemia	33	
$CD4^+$	10	0 (0%)
$CD8^+$	8*	0 (0%)
$CD4^+/CD8^+$	2	0 (0%)
$CD4^-/CD8^-$	13	0 (0%)
Acute myeloid leukemia	**39**	**28 (72%)**
Unclassified	1	0 (0%)
Myelomonocytic	9	6 (67%)
Myelomonocytic (cytochemistry)	1	1 (100%)
Monocytic/monoblastic	20	18 (90%)
Monocytic/monoblastic (cytochemistry)	5	1 (20%)
Megakaryoblastic	3	2 (66%)
"Mixed lineage" leukemia	**11**	**4 (36%)**
Myeloid antigens/$CD3^+$	2	2 (100%)
Myeloid antigens/$CD5^+$	1	0 (0%)
Myeloid antigens/$CD22^+$	1	0 (0%)
Myeloid antigens/$CD3^+$/$CD5^+$/$CD22^+$	1	1 (100%)
Cytochemistry/$CD3^+$	1	0 (0%)
Cytochemistry/$CD5^+$	3	0 (0%)
Cytochemistry/$CD3^+/CD5^+$	1	0 (0%)
Cytochemistry/$CD22^+$	1	1 (100%)

*Includes a Golden Retriever with a granular lymphocytosis in blood and bone marrow and a concurrent lymphocytosis of $CD45^-$ cells (T zone).

Based on our results using the hamster anti-CD80 antibody, CD80 appears to be a specific marker for AML, whereas the other myeloid-associated antigens can be expressed in dogs with lymphoid neoplasms, as seen in this and other studies (2, 16, 33). However, continued testing of more dogs with hematopoietic neoplasia is warranted, as it is unlikely that any marker is 100% specific for AML. With a different CD80 clone (CA24.5D4), histiocytic tumors in 2 dogs (multiple cutaneous histiocytic sarcoma and dendritic cell leukemia) had positive reactions for CD80 on immunohistochemical staining (44, 45). These two reports suggest that CD80 could also be a marker of histiocytic neoplasms. In contrast to our results in dogs, in one study of 241 human patients, CD80 was expressed in 43 to 97% on B cell tumors, including diffuse large cell and marginal zone lymphoma (46), which are common subtypes of B cell tumors in dogs (47). Other studies have also shown CD80 expression on B cell tumors in humans (48–50). Unlike dogs, CD80 is expressed on human peripheral blood B cells and memory and germinal center B cells (39, 51), which would explain the positive reactions in B cell neoplasms. On the other hand, peripheral blood T cells in healthy human donors do not express CD80 (39), but positive reactions are seen in tumor cells of human patients with adult T cell leukemia/lymphoma and cutaneous lymphoma (52, 53).

Given the discrepant results in our study and reported findings in humans, it is possible that the hamster anti-CD80 antibody is cross-reacting with another member of the B7 family of molecules, such as CD74 or CD86, as found for other anti-CD80 antibodies (54). Regardless, the antibody is still detecting an antigen on neutrophils and monocytes in the blood and bone marrow of healthy dogs and on tumor cells in dogs with AML with flow cytometric analysis, which is the intended application of the antibody. Further studies, such as immunoblotting or immunoprecipitation followed by protein sequencing, would be required to determine the exact antigen detected by the hamster anti-CD80 antibody. However, these procedures are not listed in the application sheet for the antibody and the antibody may not work in denatured samples. Our results showing that the 16-10A1 clone binds to neutrophils and monocytes in healthy dog blood contrasts with previous studies. With the same clone, CD80 was not expressed in peripheral blood mononuclear cells (55), which contains monocytes (26, 27, 30), and there was no-to-weak expression in adherent monocytes in culture (27, 55). The reason for this discrepancy is unclear but may be related to technique (e.g., antibody dilution) or testing of cultured cells. We did not test other anti-CD80 antibody clones, including 1G10 and CA24.5D4. With flow cytometry, clone 1G10 labels 80% of peripheral blood monocytes and CD14-isolated monocytes after 12 days in culture, with cytokine stimulation upregulating expression intensity (26). Clone CA24.5D4 only bound to 10–20% of monocytes in canine PBMCs with flow cytometric analysis, but binding increased to more than 50% after distemper virus infection (28). These reports suggest that the 1G10, but not CA24.5D4, clone could be used to detect CD80 with flow cytometry in dogs with AML; however, this remains to be tested in future studies. Discrepant results between studies also reiterate the importance of the clone used for antigen detection and the need to provide this information in published studies. It would be worthwhile also testing an antibody against CD86 (e.g., clones CA24.3E4 or FUN-1) (26, 27, 56) in dogs with hematopoietic neoplasia as another potential flow cytometric myeloid marker. CD86 is weakly expressed on CD14-isolated canine monocytes after 7 days in culture, and higher proportions of monocytes expressed CD86 (clone CA24.3E4) vs. CD80 (clone CA24.5D4) after 1 day in culture (27), as assessed by flow cytometric analysis. Flow cytometric analysis of CD86 expression on canine hematopoietic neoplasms has not been performed to our knowledge but immunohistochemical staining with CD86 (clone CA24.3E4) yielded discrepant results (positive and negative) of histiocytic tumors in 2 dogs, both of which were also positive for CD80 (44, 45). Neither of the CA antibody clones for CD80 or CD86 are conjugated or commercially available, making it difficult to use them routinely for diagnostic purposes.

We only had low numbers of certain types of lymphoid tumors in this study, such as CLL, and continued testing of the anti-CD80 antibody for specificity in AML would be worthwhile. Several dogs

with lymphoid neoplasms had ≥25% blasts in blood or bone marrow and could have been an ALL, as defined per WHO guidelines (15), vs. lymphoma. However, it is difficult to accurately distinguish between lymphoma and leukemia (being two ends of a spectrum of lymphoid neoplasia), thus we grouped the dogs with lymphoid neoplasms other than CLL as lymphoma/leukemia. It is possible that some of the dogs classified as an AML based on cytochemical staining were T-ALL. Tumor cells in T cell neoplasms can have positive staining reactions for ALP, ANBE and CAE (2, 57), reinforcing that these stains are lineage-associated and not lineage-specific. Similarly, "mixed lineage" leukemias may reflect aberrant expression of markers vs. a true mixed lineage or mixed phenotype leukemia. Aberrant marker expression, including cross-lineage antigen expression and lack of lineage-associated antigens, has been reported in AML and lymphoid neoplasms in dogs (2, 3, 16, 33). False positive reactions may also explain the weak expression of lymphoid antigens in AML cases. For instance, weak positive flow cytometric reactions for CD3 were not always corroborated by immunocytochemical staining, suggesting a false positive reaction in certain cases. We only applied the anti-human CD18 antibody (clone YFC118.3) to low numbers of cases. We had previously used another anti-canine CD18 antibody (clone CA1.4E9; Bio-Rad Cat# MCA1780A647, RRID:AB_2020973) in flow cytometric panels, but the antibody stains all blood leukocytes (29). This staining pattern contrasts with the anti-human CD18 antibody, which only stains neutrophils and monocytes in canine blood and was used in a recently proposed scheme for classification of $CD34^+$ acute leukemia (16). We found the anti-human CD18 antibody was less sensitive than anti-CD80 antibody, even when these antibodies were combined with CD34 for dual labeling. However, additional comparative testing is needed. It is also possible that CD80 and other myeloid-associated antigen expression on residual normal monocytes or neutrophils contributed to the percentage of positive cells in the tumor cell gate. It is impossible to always distinguish normal leukocytes from neoplastic cells on dot plots; however, we attempted to separate out residual normal cells by comparing flow cytometric cell percentages to those in differential cell counts in modified Wright's-stained blood or cytology smears and looking for overlap with CD14 in expected regions in FSC and SSC plots to reduce the likelihood of false positive reactions from normal cells.

Data availability statement

The raw data supporting the conclusions of this article will be made available by the authors, without undue reservation.

Ethics statement

The animal studies were approved by Institutional Animal Care and Use Committee. The studies were conducted in accordance with the local legislation and institutional requirements. Written informed consent was obtained from the owners for the participation of their animals in this study.

Author contributions

TS: Conceptualization, Data curation, Formal analysis, Funding acquisition, Investigation, Methodology, Project administration, Supervision, Writing – original draft. ST: Formal analysis, Investigation, Writing – review & editing. MH: Methodology, Writing – review & editing. SZ: Data curation, Writing – review & editing.

Funding

The author(s) declare that financial support was received for the research, authorship, and/or publication of this article. This study was funded by a Riney Canine Health Center/Animal Health Foundation grant from Cornell University and a Canine Health Foundation grant from the American Kennel Club (#02987).

Acknowledgments

The authors acknowledge Nicole Belcher, who performed flow cytometric analysis on clinical cases as part of routine diagnostic service, Drs. Voight and Kim and the Center for Animal Resources and Education staff for co-ordinating and performing bone marrow aspirates on the healthy dogs, and Dr. Lydia Tesfa (director) and staff of the BRC flow core facility for performing the CD80 sorting in bone marrow as a fee-for-service. We also thank the owners of the healthy dogs and dogs with acute leukemia that consented to participate in this study.

Conflict of interest

The authors declare that the research was conducted in the absence of any commercial or financial relationships that could be construed as a potential conflict of interest.

Publisher's note

Supplementary material

The Supplementary material for this article can be found online at: https://www.frontiersin.org/articles/10.3389/fvets.2024.1405297/full#supplementary-material

References

1. Faldyna M, Samankova P, Leva L, Cerny J, Oujezdska J, Rehakova Z, et al. Cross-reactive anti-human monoclonal antibodies as a tool for B-cell identification in dogs and pigs. *Vet Immunol Immunopathol*. (2007) 119:56–62. doi: 10.1016/j.vetimm.2007.06.022

2. Stokol T, Schaefer DM, Shuman M, Belcher N, Dong L. Alkaline phosphatase is a useful cytochemical marker for the diagnosis of acute myelomonocytic and monocytic leukemia in the dog. *Vet Clin Pathol*. (2015) 44:79–93. doi: 10.1111/vcp.12227

3. Stokol T, Nickerson GA, Shuman M, Belcher N. Dogs with acute myeloid leukemia have clonal rearrangements in T and B cell receptors. *Front Vet Sci*. (2017) 4:76. doi: 10.3389/fvets.2017.00076

4. Wu Y, Chang Y-M, Stell AJ, Priestnall SL, Sharma E, Goulart MR, et al. Phenotypic characterisation of regulatory T cells in dogs reveals signature transcripts conserved in humans and mice. *Sci Rep*. (2019) 9:13478. doi: 10.1038/s41598-019-50065-8

5. Sheng R, Clarke D, Laver T, Meichner K, Northrup N, Tarigo J. Prognostic significance of CD25 expression in dogs with a noninvasive diagnosis of B-cell lymphoma treated with CHOP chemotherapy. *Vet Comp Oncol*. (2023) 21:28–35. doi: 10.1111/vco.12857

6. Seelig DM, Avery P, Webb T, Yoshimoto J, Bromberek J, Ehrhart EJ, et al. Canine T-zone lymphoma: unique immunophenotypic features, outcome, and population characteristics. *J Vet Intern Med*. (2014) 28:878–86. doi: 10.1111/jvim.12343

7. Wolf-Ringwall A, Lopez L, Elmslie R, Fowler B, Lori J, Sfiligoi G, et al. Prospective evaluation of flow cytometric characteristics, histopathologic diagnosis and clinical outcome in dogs with naïve B-cell lymphoma treated with a 19-week CHOP protocol. *Vet Comp Oncol*. (2020) 18:342–52. doi: 10.1111/vco.12553

8. Rout ED, Labadie JD, Yoshimoto JA, Avery PR, Curran KM, Avery AC. Clinical outcome and prognostic factors in dogs with B-cell chronic lymphocytic leukemia: a retrospective study. *J Vet Intern Med*. (2021) 35:1918–28. doi: 10.1111/jvim.16160

9. Villiers E, Baines S, Law AM, Mallows V. Identification of acute myeloid leukemia in dogs using flow cytometry with myeloperoxidase, MAC387, and a canine neutrophil-specific antibody. *Vet Clin Pathol*. (2006) 35:55–71. doi: 10.1111/j.1939-165X.2006.tb00089.x

10. Vernau W, Moore PF. An immunophenotypic study of canine leukemias and preliminary assessment of clonality by polymerase chain reaction. *Vet Immunol Immunopathol*. (1999) 69:145–64. doi: 10.1016/S0165-2427(99)00051-3

11. Novacco M, Comazzi S, Marconato L, Cozzi M, Stefanello D, Aresu L, et al. Prognostic factors in canine acute leukaemias: a retrospective study. *Vet Comp Oncol*. (2015) 14:409–16. doi: 10.1111/vco.12136

12. Dappiano E, Cagnotti G, Corona C, Riondato F, Iulini B, Pintore D, et al. Acute myelomonocytic leukemia with multifocal manifestation and spinal cord infiltration in a dog. *Schweiz Arch Tierheilkd*. (2022) 164:350–6. doi: 10.17236/sat00353

13. Tasca S, Carli E, Caldin M, Menegazzo L, Furlanello T, Gallego LS. Hematologic abnormalities and flow cytometric immunophenotyping results in dogs with hematopoietic neoplasia: 210 cases (2002-2006). *Veterin Clin Pathol*. (2009) 38:2–12. doi: 10.1111/j.1939-165X.2008.00099.x

14. Arber DA, Orazi A, Hasserjian R, Thiele J, Borowitz MJ, Le Beau MM, et al. The 2016 revision to the World Health Organization classification of myeloid neoplasms and acute leukemia. *Blood*. (2016) 127:2391–405. doi: 10.1182/blood-2016-03-643544

15. Swerdlow SH, Campo E, Harris NL, Jaffe ES, Stein H, Thiele J, et al. WHO classification of tumours of haematopoietic and lymphoid tissues. *4th* ed. Lyon, France: International Agency for Research on Cancer (2008).

16. Harris RA, Rout ED, Yoshimoto JA, Avery PR, Avery AC. Using digital RNA counting to establish flow cytometry diagnostic criteria for subtypes of CD34+ canine acute leukaemia. *Vet Comp Oncol*. (2022) 20:710–9. doi: 10.1111/vco.12825

17. Chabanne L, Marchal T, Kaplanski C, Fournel C, Magnol JP, Monier JC, et al. Screening of 78 monoclonal antibodies directed against human leukocyte antigens for cross-reactivity with surface markers on canine lymphocytes. *Tissue Antigens*. (1994) 43:202–5. doi: 10.1111/j.1399-0039.1994.tb02324.x

18. Bennett AL, Williams LE, Ferguson MW, Hauck ML, Suter SE, Lanier CB, et al. Canine acute leukaemia: 50 cases (1989-2014). *Vet Comp Oncol*. (2016) 15:1101–14. doi: 10.1111/vco.12251

19. McDonough SP, Moore PF. Clinical, hematologic and immunophenotypic characterization of canine large granular lymphocytosis. *Vet Pathol*. (2000) 37:637–46. doi: 10.1354/vp.37-6-637

20. Matsuyama A, Beeler-Marfisi J, Wood RD, Richardson D, Calvalido J, Mutsaers AJ, et al. Treatment of myeloid neoplasia with doxorubicin and cytarabine in 11 dogs. *Vet Comp Oncol*. (2023) 21:54–61. doi: 10.1111/vco.12860

21. Davis LL, Hume KR, Stokol T. A retrospective review of acute myeloid leukaemia in 35 dogs diagnosed by a combination of morphologic findings, flow cytometric immunophenotyping and cytochemical staining results (2007-2015). *Vet Comp Oncol*. (2018) 16:268–75. doi: 10.1111/vco.12377

22. Lanier LL, O'Fallon S, Somoza C, Phillips JH, Linsley PS, Okumura K, et al. CD80 (B7) and CD86 (B70) provide similar costimulatory signals for T cell proliferation, cytokine production, and generation of CTL. *J Immunol*. (1995) 154:97–105. doi: 10.4049/jimmunol.154.1.97

23. Powers GD, Faherty DA, Connaughton SE, Biondi DA, Godfrey DI, Gault A, et al. Expression and functional analysis of murine B7 delineated by a novel monoclonal antibody. *Cell Immunol*. (1994) 153:298–311. doi: 10.1006/cimm.1994.1030

24. Junginger J, Lemensieck F, Moore PF, Schwittlick U, Nolte I, Hewicker-Trautwein M. Canine gut dendritic cells in the steady state and in inflammatory bowel disease. *Innate Immun*. (2014) 20:145–60. doi: 10.1177/1753425913485475

25. Ricklin ME, Roosje P, Summerfield A. Characterization of canine dendritic cells in healthy, atopic, and non-allergic inflamed skin. *J Clin Immunol*. (2010) 30:845–54. doi: 10.1007/s10875-010-9447-9

26. Sugiura K, Wijewardana V, Fujimoto M, Akazawa T, Yahata M, Mito K, et al. Effect of IL-12 on canine dendritic cell maturation following differentiation induced by granulocyte-macrophage CSF and IL-4. *Vet Immunol Immunopathol*. (2010) 137:322–6. doi: 10.1016/j.vetimm.2010.06.006

27. Lyu Q, Veldhuizen EJA, Ludwig IS, Rutten VPMG, van Eden W, Sijts AJAM, et al. Characterization of polarization states of canine monocyte derived macrophages. *PLoS One*. (2023) 18:e0292757. doi: 10.1371/journal.pone.0292757

28. Stein VM, Schreiner NMS, Moore PF, Vandevelde M, Zurbriggen A, Tipold A. Immunophenotypical characterization of monocytes in canine distemper virus infection. *Vet Microbiol*. (2008) 131:237–46. doi: 10.1016/j.vetmic.2008.03.009

29. Moore PF, Rossitto PV, Danilenko DM. Canine leukocyte integrins: characterization of a CD18 homologue. *Tissue Antigens*. (1990) 36:211–20. doi: 10.1111/j.1399-0039.1990.tb01831.x

30. Ogasawara S, Daddona J, Trimpert J, Stokol T. The effect of recombinant canine interleukin-6 and interleukin-8 on tissue factor procoagulant activity on canine peripheral blood mononuclear cells and purified canine monocytes. *Vet Clin Pathol*. (2012) 41:325–35. doi: 10.1111/j.1939-165X.2012.00437.x

31. Re F, Arpinati M, Testoni N, Ricci P, Terragna C, Preda P, et al. Expression of CD86 in acute myelogenous leukemia is a marker of dendritic/monocytic lineage. *Exp Hematol*. (2002) 30:126–34. doi: 10.1016/s0301-472x(01)00768-8

32. Brouwer RE, Hoefnagel J, Borger van Der Burg B, Jedema I, Zwinderman KH, Starrenburg IC, et al. Expression of co-stimulatory and adhesion molecules and chemokine or apoptosis receptors on acute myeloid leukaemia: high CD40 and CD11a expression correlates with poor prognosis. *Br J Haematol*. (2001) 115:298–308. doi: 10.1046/j.1365-2141.2001.03085.x

33. Wilkerson MJ, Dolce K, Koopman T, Shuman W, Chun R, Garrett L, et al. Lineage differentiation of canine lymphoma/leukemias and aberrant expression of CD molecules. *Vet Immunol Immunopathol*. (2005) 106:179–96. doi: 10.1016/j.vetimm.2005.02.020

34. Bromberek JL, Rout ED, Agnew MR, Yoshimoto J, Morley PS, Avery AC. Breed distribution and clinical characteristics of B cell chronic lymphocytic leukemia in dogs. *J Vet Intern Med*. (2016) 30:215–22. doi: 10.1111/jvim.13814

35. Rütgen BC, König R, Hammer SE, Groiss S, Saalmüller A, Schwendenwein I. Composition of lymphocyte subpopulations in normal canine lymph nodes. *Vet Clin Pathol*. (2015) 44:58–69. doi: 10.1111/vcp.12221

36. Cagle LA, Stacy NI, Harvey JW, de Wit M, Adler L, Walsh M, et al. Cytochemical staining of leukocytes and platelets in the Florida manatee (*Trichechus manatus latirostris*): identification of a bilobed monocyte similar to other members of the Paenungulata. *Front Vet Sci*. (2023) 10:1149000. doi: 10.3389/fvets.2023.1149000

37. Costello RT, Mallet F, Sainty D, Maraninchi D, Gastaut JA, Olive D. Regulation of CD80/B7-1 and CD86/B7-2 molecule expression in human primary acute myeloid leukemia and their role in allogenic immune recognition. *Eur J Immunol*. (1998) 28:90–103. doi: 10.1002/(SICI)1521-4141(199801)28:01<90::AID-IMMU90>3.0.CO;2-5

38. Vollmer M, Li L, Schmitt A, Greiner J, Reinhardt P, Ringhoffer M, et al. Expression of human leucocyte antigens and co-stimulatory molecules on blasts of patients with acute myeloid leukaemia. *Br J Haematol*. (2003) 120:1000–8. doi: 10.1046/j.1365-2141.2003.04212.x

39. Whiteway A, Corbett T, Anderson R, Macdonald I, Prentice HG. Expression of co-stimulatory molecules on acute myeloid leukaemia blasts may effect duration of first remission. *Br J Haematol*. (2003) 120:442–51. doi: 10.1046/j.1365-2141.2003.04085.x

40. Maeda A, Yamamoto K, Yamashita K, Asagoe K, Nohgawa M, Kita K, et al. The expression of co-stimulatory molecules and their relationship to the prognosis of human acute myeloid leukaemia: poor prognosis of B7-2-positive leukaemia. *Br J Haematol*. (1998) 102:1257–62. doi: 10.1046/j.1365-2141.1998.00901.x

41. Graf M, Reif S, Hecht K, Pelka-Fleischer R, Kroell T, Pfister K, et al. High expression of costimulatory molecules correlates with low relapse-free survival probability in acute myeloid leukemia (AML). *Ann Hematol*. (2005) 84:287–97. doi: 10.1007/s00277-004-0978-0

42. Boyer MW, Waller EK, Bray RA, Unangst T, Johnson TS, Phillips C, et al. Cytokine upregulation of the antigen presenting function of acute myeloid leukemia cells. *Leukemia*. (2000) 14:412–8. doi: 10.1038/sj.leu.2401685

43. Vereecque R, Saudemont A, Quesnel B. Cytosine arabinoside induces costimulatory molecule expression in acute myeloid leukemia cells. *Leukemia*. (2004) 18:1223–30. doi: 10.1038/sj.leu.2403391

44. Mastrorilli C, Spangler EA, Christopherson PW, Aubry OA, Newton JC, Smith AN, et al. Multifocal cutaneous histiocytic sarcoma in a young dog and review of

histiocytic cell immunophenotyping. *Vet Clin Pathol*. (2012) 41:412–8. doi: 10.1111/j.1939-165X.2012.00449.x

45. Allison RW, Brunker JD, Breshears MA, Avery AC, Moore PF, Affolter VK, et al. Dendritic cell leukemia in a Golden retriever. *Veterin Clin Pathol*. (2008) 37:190–7. doi: 10.1111/j.1939-165X.2008.00042.x

46. Dakappagari N, Ho SN, Gascoyne RD, Ranuio J, Weng AP, Tangri S. CD80 (B7.1) is expressed on both malignant B cells and nonmalignant stromal cells in non-Hodgkin lymphoma. *Cytometry B Clin Cytom*. (2012) 82:112–9. doi: 10.1002/cyto.b.20631

47. Valli VE, Kass PH, San Myint M, Scott F. Canine lymphomas: association of classification type, disease stage, tumor subtype, mitotic rate, and treatment with survival. *Vet Pathol*. (2013) 50:738–48. doi: 10.1177/0300985813478210

48. Dorfman DM, Schultze JL, Shahsafaei A, Michalak S, Gribben JG, Freeman GJ, et al. In vivo expression of B7-1 and B7-2 by follicular lymphoma cells can prevent induction of T-cell anergy but is insufficient to induce significant T-cell proliferation. *Blood*. (1997) 90:4297–306. doi: 10.1182/blood.V90.11.4297

49. Chaperot L, Plumas J, Jacob MC, Bost F, Molens JP, Sotto JJ, et al. Functional expression of CD80 and CD86 allows immunogenicity of malignant B cells from non-Hodgkin's lymphomas. *Exp Hematol*. (1999) 27:479–88. doi: 10.1016/s0301-472x(98)00059-9

50. Nozawa Y, Wakasa H, Abe M. Costimulatory molecules (CD80 and CD86) on reed-Sternberg cells are associated with the proliferation of background T cells in Hodgkin's disease. *Pathol Int*. (1998) 48:10–4. doi: 10.1111/j.1440-1827.1998.tb03821.x

51. Liu YJ, Barthélémy C, de Bouteiller O, Arpin C, Durand I, Banchereau J. Memory B cells from human tonsils colonize mucosal epithelium and directly present antigen to T cells by rapid up-regulation of B7-1 and B7-2. *Immunity*. (1995) 2:239–48. doi: 10.1016/1074-7613(95)90048-9

52. Zhang Q, Wang HY, Wei F, Liu X, Paterson JC, Roy D, et al. Cutaneous T cell lymphoma expresses immunosuppressive CD80 (B7-1) cell surface protein in a STAT5-dependent manner. *J Immunol*. (2014) 192:2913–9. doi: 10.4049/jimmunol.1302951

53. Sakamoto Y, Ishida T, Masaki A, Takeshita M, Iwasaki H, Yonekura K, et al. Clinicopathological significance of CD28 overexpression in adult T-cell leukemia/lymphoma. *Cancer Sci*. (2022) 113:349–61. doi: 10.1111/cas.15191

54. Freeman GJ, Cardoso AA, Boussiotis VA, Anumanthan A, Groves RW, Kupper TS, et al. The BB1 monoclonal antibody recognizes both cell surface CD74 (MHC class II-associated invariant chain) as well as B7-1 (CD80), resolving the question regarding a third CD28/CTLA-4 counterreceptor. *J Immunol*. (1998) 161:2708–15. doi: 10.4049/jimmunol.161.6.2708

55. Wang YS, Chi KH, Liao KW, Liu CC, Cheng CL, Lin YC, et al. Characterization of canine monocyte-derived dendritic cells with phenotypic and functional differentiation. *Can J Vet Res*. (2007) 71:165–74.

56. Qeska V, Barthel Y, Herder V, Stein VM, Tipold A, Urhausen C, et al. Canine distemper virus infection leads to an inhibitory phenotype of monocyte-derived dendritic cells in vitro with reduced expression of co-stimulatory molecules and increased interleukin-10 transcription. *PLoS One*. (2014) 9:e96121. doi: 10.1371/journal.pone.0096121

57. Wellman ML, Couto CG, Starkey RJ, Rojko JL. Lymphocytosis of large granular lymphocytes in three dogs. *Vet Pathol*. (1989) 26:158–63. doi: 10.1177/030098588902600209

frontiers | Frontiers in Veterinary Science

TYPE Original Research
PUBLISHED 24 September 2024
DOI 10.3389/fvets.2024.1414271

OPEN ACCESS

EDITED BY
Maria Elena Gelain,
University of Padua, Italy

REVIEWED BY
Ricardo Marcos,
University of Porto, Portugal
Filippo Torrigiani,
Merck KgaA, Italy

*CORRESPONDENCE
Fulvio Riondato
✉ fulvio.riondato@unito.it

†These authors share first authorship

RECEIVED 08 April 2024
ACCEPTED 22 August 2024
PUBLISHED 24 September 2024

CITATION
Sini F, Melega M, Cannizzo FT, Miniscalco B, Valenti P and Riondato F (2024) Flow cytometry of non-hematopoietic cells in canine effusions. *Front. Vet. Sci.* 11:1414271. doi: 10.3389/fvets.2024.1414271

Flow cytometry of non-hematopoietic cells in canine effusions

Federica Sini[1†], Maverick Melega[1†], Francesca Tiziana Cannizzo[1], Barbara Miniscalco[1], Paola Valenti[2] and Fulvio Riondato[1*]

[1]Department of Veterinary Sciences, School of Agriculture and Veterinary Medicine, University of Turin, Grugliasco, TO, Italy, [2]Clinica Veterinaria Malpensa AniCura, Samarate, VA, Italy

The identification of non-hematopoietic cells in effusions is a diagnostic challenge in cytology. Biopsies from mesothelium or primary lesions are infrequently performed in clinical settings and immunochemistry on smears or immunohistochemistry on cell blocks are the most common ancillary test to refine the cytological diagnosis. Cavitary effusions are an ideal matrix for flow cytometry and the availability of a cytometric panel to describe non-hematopoietic cells would represent a useful tool. Here we present the results of the flow cytometric and immunohistochemical determination of cytokeratin (CK), vimentin (VIM) and desmin (DES) in 36 canine effusions. The concordance between the two methods was perfect for CK (100%), substantial for VIM (77.8%), and almost perfect for DES (97.2%). The panel was interpreted to define the epithelial (CK+VIM-DES-), mesothelial (CK+VIM+DES+), or mesenchymal (CK-VIM+DES-) origin of the cells. Unexpected profiles were considered doubtful and observed patterns were individually discussed. The concordance of the panel interpretation between two methods was 75%. The evaluation of discordant and doubtful cases suggests a lower sensitivity of flow cytometry in detecting VIM expression and revealed a high frequency of VIM+ epithelial cells, variable expression of VIM in mesothelial cells, and an important role of DES in excluding an epithelial origin when positive. Multicentric studies based on histopathological diagnoses are necessary to confirm these findings and evaluate the diagnostic utility of the panel to refine cytological diagnosis. Our results show that flow cytometry can be a timesaving alternative to IHC on cell blocks in clinical settings to detect CK, VIM and DES expression. The interpretation of the panel is similar in most cases; however, occasional discordant results, particularly for VIM, may occur.

KEYWORDS

effusion, cell block, flow cytometry, vimentin, cytokeratin, desmin, carcinoma, mesothelioma

1 Introduction

Effusion cytology is complex as multiple inflammatory, reactive, and possibly neoplastic cells may be present in the same sample. Main challenges include the identification of cells based on the shape (cells in fluid appear round regardless of their origin), the presence of mesothelial cells that readily exfoliate regardless the underlying cause, and the overlapping morphology of reactive mesothelial cells, neoplastic mesothelial cells and other exfoliative malignant cells (e.g., neoplastic epithelial cells). The presence of cohesive clusters can suggest an epithelial origin; however, both reactive and neoplastic

mesothelial cells can exfoliate in variably cohesive aggregates. Also, poorly differentiated carcinomas can be less cohesive with individualized cells predominating (1).

Whilst cytology can be useful to classify transudate and inflammatory effusions, its sensitivity for the diagnosis of malignancy is limited, particularly in case of non-hematopoietic (NH) cells (2–4). In these cases, a final diagnosis can be achieved with histopathology and possibly immunohistochemistry (IHC) of the primary lesions. However, fluid collection and cytology are often not followed by more invasive diagnostic procedures; the collection of intrathoracic or abdominal tissue biopsies is often declined by pet owners or is clinically not recommended given the unstable condition of some of these patients. Ancillary techniques can be used to refine the cytological diagnosis by defining the immunophenotype, and therefore the origin, of NH cell in cavitary effusions. In veterinary medicine, immunochemistry on cytological preparations (5) and IHC on cell blocks have been described and successfully applied on effusions for immunochemical characterization (4, 6–9).

Currently, the minimum panel to differentiate epithelial and mesothelial cells should include cytokeratin (CK) and vimentin (VIM) (10). Co-expression of CK and VIM is considered the main feature of mesothelial cells, while expression of CK or VIM only, is expected in epithelial and mesenchymal cells, respectively (11). However, several reports revealed variable VIM expression in epithelial and mesothelial cells (4, 7). To overcome this limitation, a wider panel including expected positive and negative markers has been recommended for the diagnosis of malignant mesothelioma in human medicine (12). Desmin (DES) is used to distinguish reactive mesothelial (DES+) from neoplastic mesothelial and epithelial cells (DES-) in people (13, 14). In veterinary medicine, DES does not appear to be an exclusive marker to distinguish reactive from neoplastic mesothelial cells, but it has been proven useful in differentiating mesothelial and epithelial cells (4, 5, 15). A combination of CK, VIM and DES can represent a starting panel to differentiate cell lineage in effusions. Immunochemical techniques and cell block production have limitations, such as the need for additional training and significant amount of hand-on technician time, long turnaround time, and limited possibility of multi-marker analysis (6, 16, 17). Conversely, flow cytometry (FC) is a sensitive, fast, and affordable method to study fluid matrices. It allows the simultaneous analysis of multiple antigens on a high number of cells if compared with IHC and allows the characterization of subsets of cells in a mixed population. However, it does not allow for retrospective studies as the analysis is limited to fresh samples and cell viability. In human medicine, several studies demonstrated that FC can contribute to refine the cytological diagnosis of non-hematopoietic disorders in effusions (17–19). While FC is routinely used in veterinary medicine for immunophenotyping of hematological disorders in peripheral blood, bone marrow, lymph nodes, peripheral tissues, and body fluids (20–23), no data are available about the use of this technique to characterize NH cells in cavitary effusions.

The aim of this study is to compare FC determination of CK, VIM and DES in NH cells in canine effusions with paired IHC results on cell blocks. The final goal is to provide an additional tool to characterize NH cells in effusions.

2 Materials and methods

Canine pleural, pericardial and peritoneal cavitary effusions received at the Laboratory for Clinical Analyses of the Veterinary Teaching Hospital of the University of Turin (Grugliasco, IT) were considered for the study. Dogs were privately owned and underwent sampling for diagnostic purposes with signed informed consent from the owners. Thus, specific formal approval by the authors' Institution Committee for Animal Care was not required (protocol 1965–2017, Ethical Committee, University of Turin). Samples were collected in EDTA tubes and routinely processed. Samples with cytological evidence of cells of suspected NH origin and samples with abundant reactive mesothelial cells were included in the study if at least 2 ml of fluid were available after routine analysis. Samples were processed for FC and cell blocks were prepared within 24 h from collection. Cases with inadequate cell blocks for IHC and samples with <1% of CD45-negative or large CD11b-negative population in FC were excluded.

2.1 Flow cytometry

FC analysis was performed with a BD Accuri C6 (Becton Dickinson, San Josè, CA) and a Cytoflex (Beckman Coulter, Brea, USA) flow cytometer.

NH cells were detected as CD45-negative (13 cases) or large CD11b-negative events (23 cases). We previously assessed the co-expression of the two markers on eight cases showing that the two labeling allow the detection of the same population (Supplementary Figure 1).

The cellularity of the sample was assessed by flow cytometry after removal of erythrocytes with an ammonium chloride-base buffer (1:10 dilution, 10 min incubation). The quality of the sample was assessed by further addition of 10 uL of propidium iodide. A tube with $\sim 60 \times 10^5$ cells was incubated 20 min at 4°C in the dark with previously titrated anti-CD11b or anti-CD45 monoclonal antibody. Erythrocytes were lysed as described above and cells were washed with PBS by centrifuging at 1,200 rpm for 5 min. The cell pellet was processed for cytoplasmic staining using a commercial kit (eBioscienceTM Intracellular Fixation & Permeabilization Buffer Set, ThermoFisher). Briefly, it was then incubated for 10 min at 4°C with fixation buffer, washed once with PBS and twice with permeabilization buffer, resuspended in 240 uL of permeabilization buffer and the obtained volume split in six tubes. Four tubes were used for direct staining: negative control (added with 10 uL of PBS) to set the autofluorescence, isotype control, CK and VIM according to previous titration. Two tubes were used for indirect staining adding 10 ul of PBS and anti-DES monoclonal antibody, respectively. Samples were incubated for 30 min at 4°C and washed twice with permeabilization solution. Tubes for direct staining were resuspended in PBS and immediately acquired at the cytometer. Tubes for indirect staining were incubated for an additional 20 min at 4°C with AlexaFluor488-conjugated secondary antibody, washed with permeabilization buffer, resuspended in PBS, and acquired. Information about the used antibodies is reported in Table 1.

TABLE 1 List of primary and secondary antibodies used in flow cytometry and immunohistochemistry.

Antibody	Clone	Source	Conjugation	Method
CD45	YKIX716.13	BioRad	AlexaFluor647	FC
CD11b	M1/70	Abcam	PE-Cy5	FC
CK	CK AE1 AE3	NovusBiologicals	AlexaFluor488/Unconjugated	FC/IHC
VIM	V9	NovusBiologicals	AlexaFluor488/Unconjugated	FC/IHC
Isotypic control (Anti-IgG1K)	—	R&D Systems	AlexaFluor488	FC
DES	DER-II	Novocastra	Unconjugated	FC/IHC
Secondary antibody	—	Invitrogen	AlexaFluor488	FC

CK, cytokeratin; VIM, vimentin; DES, desmin; FC, flow cytometry; IHC, immunohistochemistry on cell block.

A minimum of 1,000 large CD11b-negative or CD45-negative events were acquired for each tube. A first gate was set in an FSC-H vs. FSC-A scattergram to exclude doublets and a second morphological gate (FSC-A vs. SSC-A) to exclude events smaller than small lymphocytes. NH cells were gated as large CD11b-negative or CD45-negative events and the positive gate was depicted to include <1% of the events in negative controls (Supplementary Figure 2). Immunoreaction to cytoplasmic markers (CK, VIM, DES) was defined positive when at least 20% of the population fell in the positive gate. All cases were analyzed by the same pathologist (FR), who was blind to IHC results.

2.2 Cell blocks and immunohistochemistry

Cell tube blocks were prepared as previously described (6). H&E-stained sections were assessed for presence of target cells with adequate morphology and cellularity. Cell blocks deemed adequate for IHC were further processed and stained for CK, VIM and DES. Briefly, four micrometer sections were cut, placed on Tomo® IHC adhesive glass slides (Matsunami glass Ltd.) and dried in convection oven at 50°C for 30 min. IHC were performed in one session with an automated immunostainer (BenchMark XT processor, Ventana Medical Systems, Tucson, AZ). Sections were deparaffinized with xylene and rehydrated with decreasing concentrations of ethanol. Endogenous peroxidase activity was inhibited with a peroxide hydrogen 3% solution and heat induced antigen retrieval was performed with CC1 solution (EDTA) for 24 min at 100°C. Incubation was performed at 37°C for 30 min for all antibodies. Antibodies' clones were the same used in FC analysis (Table 1). The Ventana ultraView Universal DAB Detection kit was used for all samples. Histological section of canine intestine, liver, pancreas, spleen, and lymph node were used as controls.

IHC interpretation was performed reviewing May-Grunwald Giemsa cytological preparation and H&E-stained cell blocks to ensure a proper identification of NH-cells and assess the immunoreaction. Sections were assessed for proportion of NH positive cells providing a percentage from 0 to 100. The NH population was defined positive when more than 20% of the cells were positive. All samples were evaluated by the same pathologist (FTC).

2.3 Panel interpretation

Panels were interpreted for both methods based on the expected staining patterns for epithelial cells (CK+VIM-DES-), mesothelial cells (CK+VIM+DES+) and mesenchymal cells (CK-VIM+DES-), according to the most frequent presentation (4, 5, 10, 24). Patterns deviating from what expected were interpreted as "doubtful".

2.4 Statistical analysis

FC results for each parameter (CK, VIM, DES) are reported in the text as median percentage and range (minimum–maximum). Agreement between FC and IHC results was calculated for the expression (positive or negative) of the individual markers and for the panel interpretation. The degree of agreement was defined according to the kappa value as previously reported (25): poor (0–0.20), fair (0.21–0.40), moderate (0.41–0.60), substantial (0.61–0.80), or almost perfect (0.81–1.00).

3 Results

Thirty-six samples from the pleural (N = 19), peritoneal (N = 11) and pericardial (N = 6) cavities from 36 dogs were included. Patients were 17 females (9 neutered) and 19 males (3 neutered), the mean age was 9.7 years (range 4–15 years).

Results from routine fluid analysis including cytology, total nucleated cell count, total solids and final diagnostic interpretation based on clinical and clinical-pathological data are reported in Supplementary Table 1.

3.1 Flow cytometry

Details of the individual cases are shown in Table 2, Supplementary Table 1. The median proportion of NH cells was 13.1% (range 1.1%−65.3%). Thirty-five out of 36 samples were CK positive. The median proportion of positive target cells was 93.2% (range 45.3%−99.5%). One sample was CK negative (0.3% of the target population). Eighteen out of 36 samples were VIM positive (median 66.3%; range 21.4%−98.9%). Eighteen out of 36 samples

10.3389/fvets.2024.1414271

TABLE 2 Cytokeratin, vimentin, and desmin results reported by flow cytometry and immunohistochemistry on cell blocks and interpretation of the panel.

	CK		VIM		DES		Panel interpretation	
CASE	FC	IHC	FC	IHC	FC	IHC	FC	IHC
1	Pos	Pos	Neg	Pos	Pos	Pos	D	M
2	Pos	Pos	Neg	Pos	Pos	Pos	D	M
3	Pos	Pos	Pos	Pos	Pos	Pos	M	M
4	Pos	Pos	Pos	Pos	Neg	Neg	D	D
5	Pos	Pos	Neg	Pos	Neg	Neg	E	D
6	Neg	Neg	Pos	Pos	Neg	Neg	S	S
7	Pos	Pos	Neg	Pos	Pos	Pos	D	M
8	Pos	Pos	Neg	Neg	Neg	Neg	E	E
9	Pos	Pos	Pos	Pos	Neg	Neg	D	D
10	Pos	Pos	Pos	Pos	Neg	Neg	D	D
11	Pos	Pos	Pos	Pos	Pos	Pos	M	M
12	Pos	Pos	Pos	Pos	Pos	Pos	M	M
13	Pos	Pos	Pos	Pos	Pos	Pos	M	M
14	Pos	Pos	Neg	Neg	Neg	Neg	E	E
15	Pos	Pos	Pos	Pos	Pos	Pos	M	M
16	Pos	Pos	Pos	Pos	Neg	Neg	D	D
17	Pos	Pos	Pos	Pos	Pos	Pos	M	M
18	Pos	Pos	Neg	Neg	Neg	Neg	E	E
19	Pos	Pos	Neg	Pos	Neg	Neg	E	D
20	Pos	Pos	Pos	Pos	Neg	Neg	D	D
21	Pos	Pos	Pos	Pos	Neg	Neg	D	D
22	Pos	Pos	Pos	Pos	Pos	Pos	M	M
23	Pos	Pos	Neg	Pos	Neg	Neg	E	D
24	Pos	Pos	Pos	Pos	Pos	Pos	M	M
25	Pos	Pos	Neg	Neg	Neg	Neg	E	E
26	Pos	Pos	Neg	Neg	Pos	Neg	D	E
27	Pos	Pos	Neg	Neg	Neg	Neg	E	E
28	Pos	Pos	Neg	Pos	Pos	Pos	D	M
29	Pos	Pos	Pos	Pos	Pos	Pos	M	M
30	Pos	Pos	Neg	Neg	Neg	Neg	E	E
31	Pos	Pos	Pos	Pos	Pos	Pos	M	M
32	Pos	Pos	Neg	Neg	Neg	Neg	E	E
33	Pos	Pos	Neg	Pos	Neg	Neg	E	D
34	Pos	Pos	Pos	Pos	Pos	Pos	M	M
35	Pos	Pos	Neg	Neg	Neg	Neg	E	E
36	Pos	Pos	Neg	Neg	Neg	Neg	E	E

CK, cytokeratin; VIM, vimentin; DES, desmin; FC, flow cytometry; IHC, immunohistochemistry; Pos, positive; Neg, negative; E, epithelial; M, mesothelial; D, doubtful. Discordant results between FC and IHC are underlined.

were VIM negative (median 7.8%; range 0.4%−18.2%). Sixteen out of 36 samples were DES positive (median 76%; range 34%−96.2%). Twenty out of 36 samples were DES negative (median 4.3%; range 0.1%−18.2%).

According to the panel interpretation, NH cells were mesothelial in 11 cases (CK+VIM+DES+), epithelial in 13 cases (CK+VIM-DES-), mesenchymal in 1 case (CK-VIM+DES-) and doubtful in 11 cases (6 CK+VIM+DES- and 5 CK+VIM-DES+).

3.2 Immunohistochemistry

Details of the individual cases are shown in Table 2, Supplementary Table 1. Thirty-five out of 36 samples were CK positive. The median proportion of positive target cells was 91% (range 72%−100%). In one sample no CK positive cells were present. Twenty-six out of 36 samples were VIM positive (median 87%; range 21%−100%) while 10 samples were VIM negative (median 2.5%; range 0%−15%). Fifteen out of 36 samples were DES positive (median 78%; range 25%−92%) and 21 were DES negative (median 3%; range 0%−15%).

According to the panel interpretation, NH cells were mesothelial in 15 cases (CK+VIM+DES+), epithelial in 10 cases (CK+VIM-DES-), mesenchymal in 1 case (CK-VIM+DES-), and doubtful in 10 cases (CK+VIM+DES-).

3.3 Agreement between FC and IHC results

FC and IHC reported 36 CK concordant results (35 CK+ and 1 CK-) with 100% agreement.

The two methods reported 28 concordant (18 positive and 10 negative) and 8 discordant VIM results with a 77.8% agreement. All discordant cases were VIM- in FC and VIM+ in IHC on cell block. The percentage of positive events in FC was <10% in six cases, 17.4% and 18.2% in the remaining two. The percentage of positive cells in IHC was >70% in all but two cases (21% and 32%). FC and IHC reported 35 concordant (15 DES+ and 20 DES-) and one DES discordant results with a 97.2% agreement. The discordant case was DES+ in FC (34% of positive events) and DES- in IHC (15% of positive cells). Representative IHC pictures and FC scatterplots are shown in Figure 1.

The panel interpretation was concordant in 27/36 cases (11 mesothelial; 9 epithelial; 1 mesenchymal; 6 doubtful) with a 75% agreement. Among nine discordant cases, five were interpreted as doubtful in FC and mesothelial (4) or epithelial (1) in IHC on cell blocks. While four cases were epithelial in FC and doubtful in IHC. In 8/9 cases the discrepancy was due to VIM+ in IHC and VIM- in FC, in one case the discrepancy was due to DES- in IHC and DES+ in FC.

4 Discussion

Ancillary techniques such as immunocytochemistry and IHC on cell blocks are useful to refine the cytological diagnosis of effusions (10). Despite being routinely used for hematological malignancies in dogs and cats (26), the applications of FC in immunophenotyping NH cells in effusions has not been investigated in veterinary medicine. Here we describe for the first time a flow cytometric approach to immunophenotype NH cells in canine cavitary effusions.

FC requires cells to be in a suspension to be analyzed and body fluids are a "ready-to-use" matrix for this technique, making it a fast and cost-effective method to study effusions and a potential alternative to immunocytochemistry on smears and IHC on cell blocks. In human pathology, FC is being increasingly used to immunophenotype NH cells in effusions with promising results (17–19). FC allows the identification of subpopulations of cells based on morphological properties (i.e., size and complexity) and the use of combination of markers. Here, CD45 or CD11b where used to exclude hematopoietic cells from the analysis and to identify NH cells. Their phenotype was then described based on the immunoreaction to antibodies against three intermediate filaments (CK, VIM and DES). This approach allowed the analysis of samples even in the presence of low percentages of NH cells.

The agreement between FC and IHC in the interpretation of the individual markers was perfect for CK, almost perfect for DES, and substantial for VIM leading to substantial agreement in the final interpretation of the panel. The one case with discordant panel interpretation due to DES led to an epithelial classification in IHC (CK+VIM-DES-) and doubtful in FC (CK+VIM-DES+). This case was a pleural effusion suspected to be mesothelial-neoplastic in cytology; unfortunately, a definitive diagnosis was not available. All the other discordant results were due to a positive VIM reaction in IHC and negative in FC. Half of these cases were CK+VIM+DES- in IHC, interpreted as doubtful, and CK+VIM-DES- in FC, interpreted as epithelial. In this study the profile CK+VIM+DES- was considered doubtful, as possible interpretation include DES- mesothelial cells or VIM+ epithelial cells. DES- mesothelial cells have been previously reported (4, 15); however, this was considered unlikely in these cases. The epithelial origin was further supported by clinical, cytological and/or histopathological diagnosis of carcinoma (2 mammary carcinomas with multiorgan dissemination, 1 lung carcinoma, 1 gastric carcinoma). In these cases, although FC provided the expected phenotype for epithelial cells, a genuine expression of VIM was considered most likely given the strong and specific stain in IHC. VIM+ epithelial cells have been previously reported in effusions (4, 5, 7) and in some carcinomas (27). Variable VIM expression in neoplastic epithelial cells may results from type three epithelial-mesenchymal transition (EMT), where cells lose polarization and stability, gain migratory traits, and increase VIM while decreasing epithelial adhesion proteins like cadherins (28). The reason for the non-recognition of VIM in FC remains to be established and multiple factors may be contributing. NH cells aggregation may have affected permeabilization and prevented antigen-antibody binding. VIM expression may have been too low for detection by FC, where signal brightness correlates with the total amount of antigen in each cell, unlike in IHC, where staining intensity and cytoplasmatic pattern are independent parameters. All these cases were DES-, reinforcing the hypothesis that DES is negative in epithelial cells and suggesting that DES positivity could help to exclude an epithelial origin. In the remaining half of

10.3389/fvets.2024.1414271

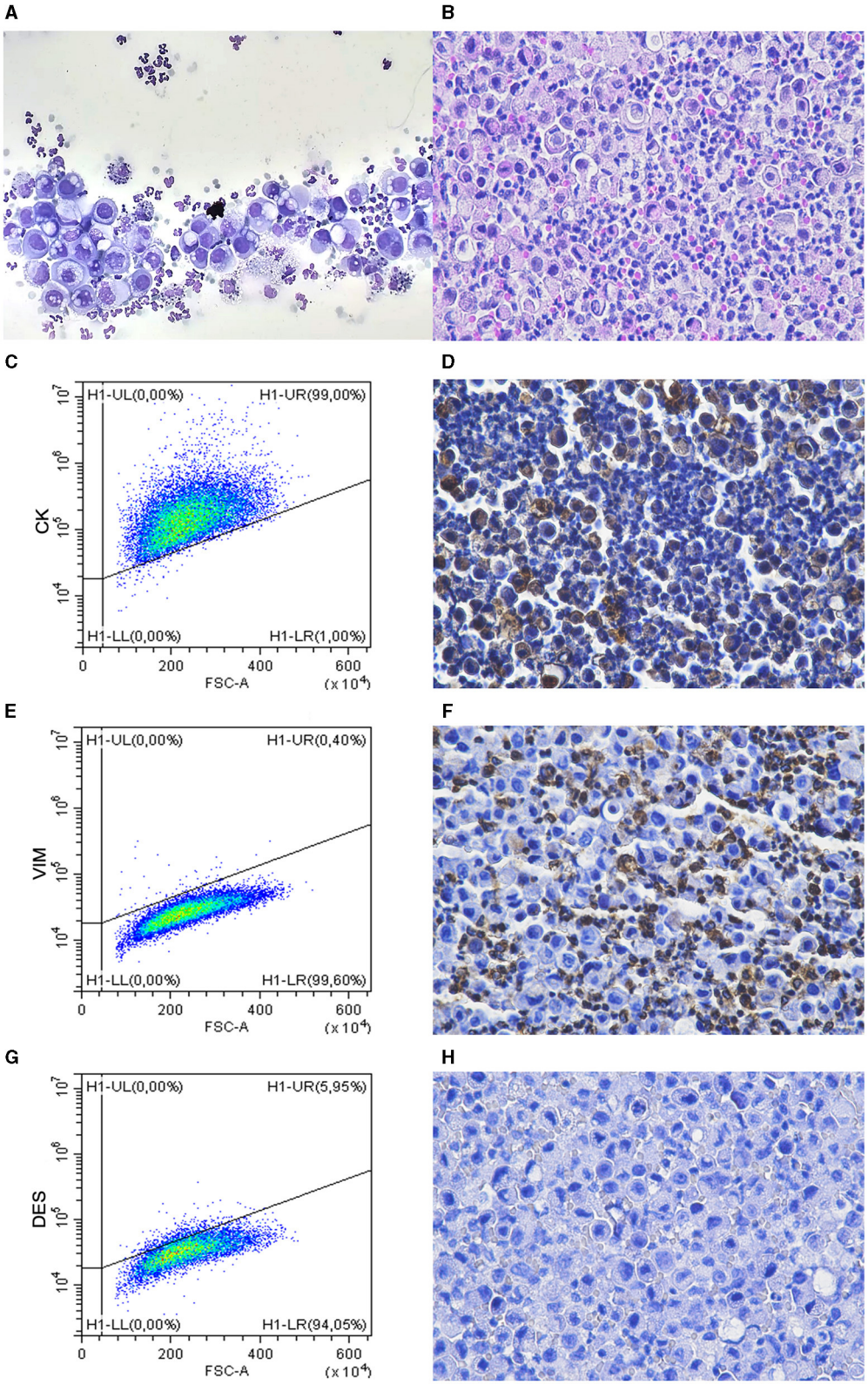

FIGURE 1
Cytology and FC results compared with H&E and IHC on cell blocks. Case 25. **(A)** Cytology. A population of large often vacuolated cells is present along with neutrophils and occasional macrophages. MGG stain. **(B)** Cell tube block. The two main population detected at cytology are recognized. H&E stain. **(C–H)** Flow cytometry **(C, E, G)** and IHC **(D, F, H)** showing NH are cells positive for CK **(C, D)** and negative for VIM **(E, F)** and DES **(G, H)**. Only CD45-negative cells are gated in flow cytometric analysis. Positive cells in **(F)** are neutrophils [negative in **(D, H)**].

the cases NH cells were CK+VIM+DES+ in IHC, interpreted as mesothelial, and CK+VIM-DES+ in FC, interpreted as doubtful. The profile CK+VIM-DES+ was considered doubtful, as possible interpretation include VIM- mesothelial cells or DES+ epithelial cells. The presence of DES+ epithelial cells has been reported in a small proportion of cells (1–25%) in the effusion of a dog with carcinoma (4). This possibility was considered less likely here as cytology, clinical, imaging, follow-up data were strongly supportive of reactive mesothelial origin of these cells in 3 out of 4 cases; a final clinical diagnosis of ascites due to congestive heart failure, idiopathic pericarditis (alive after 2 years, no relapse) and hemorrhagic pericardial effusion due ruptured right atrial mass consistent with hemangiosarcoma. Unfortunately, insufficient evidence for a definitive diagnosis was available in one case; this was a suspected mesothelioma based on cytology alone; the patients had recurrent pleural effusion with no evidence of a primary lesion on imaging and was euthanized 3 months after presentation, necropsy was declined. These findings support the current evidence that mesothelial cells variably express VIM, ranging from negative to strongly positive (4, 7, 15) and consolidate the hypothesis that lack of VIM does not exclude a mesothelial origin.

Overall, these findings confirm that the co-expression of CK and VIM alone is not reliable in distinguishing between epithelial and mesothelial cells in effusions as previously reported (4) and that a wider panel of markers is necessary. For instance, WT-1 (4, 7) and DES appear to be good candidates for this purpose. Looking at IHC as the reference method, the discrepancies between the two techniques suggest a lower reliability of FC in detecting VIM expression but the addition of DES is useful to rule out an epithelial origin. Further studies investigating different clones to detect VIM expression in FC may be indicated.

Whilst the presence itself of epithelial or mesenchymal cells in the effusion is a strong indicator of neoplasia, further characterization is needed to distinguish between reactive and neoplastic mesothelial cells. Based on the data available in this series, VIM was variably expressed in both suspected reactive and neoplastic mesothelial cells and a possible role of VIM expression in the differentiation between these two is unlikely. In people, DES is mainly used as to distinguish reactive (DES+) from neoplastic (DES-) mesothelial cell (13, 14), while in dogs it appears to be limited to distinguish between mesothelial and epithelial cells (4, 5, 15). In this cohort, six cases showed a doubtful DES- profile both by FC and IHC. Final clinical-pathological interpretation was indicative of neoplastic effusion in five of these cases; however, the limited number of cases and lack of a definitive diagnosis hamper any solid association between the lack of DES and neoplasia. A previously reported, it is likely that DES has lower sensitivity and specificity in dogs than in people to distinguish between reactive and neoplastic mesothelial cells (4, 5, 15); this also suggests that its utility in dogs is most likely limited to distinguish mesothelial and epithelial cells. To accurately differentiate between reactive and neoplastic mesothelial cells, additional markers for cell lineages are necessary. In humans, guidelines recommended using an IHC panel including at least two mesothelial and two epithelial markers, along with epithelial membrane antigen (EMA), glucose transporter 1 (GLUT1) and insulin-like growth factor II mRNA-binding protein 3 (IMP3) to distinguish between mesothelioma and reactive hyperplasia (12). Few of these markers have been tested in dogs for similar diagnostic purposes, such as EMA (29, 30), Calretinin (29, 31–36), HBME-1 (37, 38), WT1 (4, 7, 9, 29, 33, 39), GLUT1 and IMP3 (4, 15). Adding one or more of them to the panel may improve specificity and lineage cell classification accuracy.

Although not a restriction for the principal aim of the study (comparison of the results between FC and IHC), the lack of a definitive histopathologic diagnosis represents a main limitation of our study, hampering the assessment of the diagnostic value of the panel. However, by integrating the results of this study with the current available literature, a possible diagnostic algorithm to interpret a panel including CK, VIM and DES in FC is described in Supplementary Figure 3. Prospective studies based on histopathologic diagnoses on a larger cohort of cases are needed to investigate its application and revisions based on future investigation of markers of reactive and neoplastic mesothelial cells are warranted.

In conclusion, our results show that FC can be a timesaving and multiparametric alternative to IHC on cell blocks in clinical settings. Histopathology of the primary lesion and immunohistochemistry should still be considered the main tools for a definitive diagnosis. However, the described method is an effective and non-invasive technique to refine the cytological diagnosis and can be easily integrated into routine panels to diagnose and characterize hematopoietic disorders. The FC and IHC interpretation of the panel is similar in most cases; however, occasional discordant results, particularly for VIM, may occur. A larger cohort of cases with histologic diagnosis is needed to evaluate the diagnostic accuracy of this technique and of the proposed algorithm. Being FC a flexible method that guarantees multiparameter analysis, the development of a multicolor approach and the inclusion of additional markers can improve and consolidate the panel.

Data availability statement

The raw data supporting the conclusions of this article will be made available by the authors, without undue reservation.

Ethics statement

The requirement of ethical approval was waived by Ethical Committee, University of Turin for the studies involving animals because dogs were privately owned, affected by spontaneous diseases and underwent sampling for diagnostic purposes. The studies were conducted in accordance with the local legislation and institutional requirements. Written informed consent was obtained from the owners for the participation of their animals in this study.

Author contributions

FS: Data curation, Formal analysis, Investigation, Visualization, Writing – review & editing. MM: Conceptualization, Formal analysis, Investigation, Methodology, Writing – original draft,

Writing – review & editing. FC: Investigation, Writing – review & editing, Funding acquisition. BM: Investigation, Writing – review & editing. PV: Resources, Writing – review & editing. FR: Conceptualization, Data curation, Formal analysis, Funding acquisition, Investigation, Methodology, Project administration, Supervision, Visualization, Writing – original draft, Writing – review & editing.

Funding

The author(s) declare that no financial support was received for the research, authorship, and/or publication of this article.

Conflict of interest

The authors declare that the research was conducted in the absence of any commercial or financial relationships that could be construed as a potential conflict of interest.

The author(s) declared that they were an editorial board member of Frontiers, at the time of submission. This had no impact on the peer review process and the final decision.

Publisher's note

Supplementary material

The Supplementary Material for this article can be found online at: https://www.frontiersin.org/articles/10.3389/fvets.2024.1414271/full#supplementary-material

References

1. Valenciano AC, Rizzi TE. Abdominal, thoracic, and pericardial effusions. In: Valenciano AC, Cowell RL, editors. *Cowell and Tyler's Diagnostic Cytology and Hematology of the Dog and Cat*. St. Louis, Missouri: Elsevier (2020). p. 229–246.

2. Hirschberger J, DeNicola DB, Hermanns W, Kraft W. Sensitivity and specificity of cytologic evaluation in the diagnosis of neoplasia in body fluids from dogs and cats. *Vet Clin Pathol.* (1999) 28:142–6. doi: 10.1111/j.1939-165x.1999.tb01065.x

3. Cagle LA, Epstein SE, Owens SD, Mellema MS, Hopper K, Burton AG. Diagnostic yield of cytologic analysis of pericardial effusion in dogs. *J Vet Intern Med.* (2014) 28:66–71. doi: 10.1111/jvim.12253

4. Milne EM, Piviani M, Hodgkiss-Geere HM, Piccinelli C, Cheeseman M, Cazzini P, et al. Comparison of effusion cell block and biopsy immunohistochemistry in mesothelial hyperplasia, mesothelioma, and carcinoma in dogs. *Vet Clin Pathol.* (2021) 50:555–67. doi: 10.1111/vcp.13002

5. Przezdziecki R, Sapierzyński R. Using of immunocytochemistry in differential diagnosis of neoplasms of serosal cavities in dogs. *Pol J Vet Sci.* (2014) 17:149–59. doi: 10.2478/pjvs-2014-0020

6. Melega M, Santos M, Caniatti M, Valenti P, Miniscalco B, Sulce M, et al. Cell blocks in veterinary medicine: a comparison of two methods (cell tube and agar) in 52 effusions from dogs and cats. *Vet Clin Pathol.* (2020) 49:632–9. doi: 10.1111/vcp.12922

7. Marcos R, Marrinhas C, Malhão F, Canadas A, Santos M, Caniatti M. The cell tube block technique and an immunohistochemistry panel including Wilms tumor 1 to assist in diagnosing cavitary effusions in dogs and cats. *Vet Clin Pathol.* (2019) 48:50–60. doi: 10.1111/vcp.12709

8. Sampaio F, Marrinhas C, Fonte Oliveira L, Malhão F, Lopes C, Gregório H, et al. Detection of lymphoid markers (CD3 and PAX5) for immunophenotyping in dogs and cats: comparison of stained cytology slides and matched cell blocks. *Vet Sci.* (2023) 10:157. doi: 10.3390/vetsci10020157

9. Kita C, Chambers JK, Tanabe M, Irie M, Yamasaki H, Uchida K. Immunohistochemical features of canine ovarian papillary adenocarcinoma and utility of cell block technique for detecting neoplastic cells in body cavity effusions. *J Vet Med Sci.* (2022) 84:406–13. doi: 10.1292/jvms.21-0633

10. Camus S, Kelly LA, Barger AB. Immunocytochemistry. In Valenciano AC and Cowell RL, editors. *Cowell and Tyler's Diagnostic Cytology and Hematology of the Dog and Cat*. St. Louis, Missouri: Elsevier (2020). p. 512–520.

11. Sawa M, Yabuki A, Kohyama M, Miyoshi N, Yamato O. Rapid multiple immunofluorescent staining for the simultaneous detection of cytokeratin and vimentin in the cytology of canine tumors. *Vet Clin Pathol.* (2018) 47:326–32. doi: 10.1111/vcp.12598

12. Husain AN, Chapel DB, Attanoos R, et al. Guidelines for pathologic diagnosis of mesothelioma. *Arch Pathol Lab Med.* (2024). doi: 10.5858/arpa.2023-0304-RA. [Epub ahead of print].

13. Elmahdy M, Gouda MH, Eloseily GM. Immunohistochemical differentiation between reactive and malignant mesothelial proliferations in pleural effusion. *Med J Cairo Univ.* (2019) 87:4345–53. doi: 10.21608/mjcu.2019.78251

14. Attanoos RL, Griffin A, Gibbs AR. The use of immunohistochemistry in distinguishing reactive from neoplastic mesothelium. A novel use for desmin and comparative evaluation with epithelial membrane antigen, p53, platelet-derived growth factor-receptor, P-glycoprotein and Bcl-2. *Histopathology.* (2003) 43:231–8. doi: 10.1046/j.1365-2559.2003.01686.x

15. Milne E, Martinez Pereira Y, Muir C, Scase T, Shaw DJ, McGregor G, et al. Immunohistochemical differentiation of reactive from malignant mesothelium as a diagnostic aid in canine pericardial disease. *J Small Anim Pract.* (2018) 59:261–71. doi: 10.1111/jsap.12830

16. Priest HL, Hume KR, Killick D, Kozicki A, Rizzo VL, Seelig D, et al. The use, publication and future directions of immunocytochemistry in veterinary medicine: a consensus of the Oncology-Pathology Working Group. *Vet Comp Oncol.* (2017) 15:868–80. doi: 10.1111/vco.12228

17. Gaur G, Awasthi NP, Gupta A, Agarwal A, Sachan R, Malhotra KP, et al. Diagnostic accuracy of flow cytometry in detecting malignant epithelial cells in serous effusions. *J Am Soc Cytopathol.* (2023) 12:423–35. doi: 10.1016/j.jasc.2023.09.003

18. Gostomczyk K, Łukaszewska E, Borowczak J, Bator A, Zdrenka M, Bodnar M, et al. Flow cytometry in the detection of circulating tumor cells in neoplastic effusions. *Clin Chim Acta.* (2024) 552:117651. doi: 10.1016/j.cca.2023.117651

19. Wong-Arteta J, Rey M, Aragón L, Gil-Rodríguez E, Bujanda L. The utility of flow cytometry in the diagnostic work up of malignant effusions due to nonhematopoietic neoplasms. *Cytom Part B - Clin Cytom.* (2020) 98:504–15. doi: 10.1002/cyto.b.21886

20. Parys M, Bavcar S, Mellanby RJ, Argyle D, Kitamura T. Use of multi-color flow cytometry for canine immune cell characterization in cancer. *PLoS ONE.* (2023) 18:e0279057. doi: 10.1371/journal.pone.0279057

21. Sulce M, Marconato L, Martano M, Iussich S, Dentini A, Melega M, et al. Utility of flow cytometry in canine primary cutaneous and matched nodal mast cell tumor. *Vet J.* (2018) 242:15–23. doi: 10.1016/j.tvjl.2018.10.004

22. Comazzi S, Riondato F. Flow cytometry in the diagnosis of canine T-cell lymphoma. *Front Vet Sci.* (2021) 8:600963. doi: 10.3389/fvets.2021.600963

23. Riondato F, Comazzi S. Flow cytometry in the diagnosis of canine B-cell lymphoma. *Front Vet Sci.* (2021) 8:600986. doi: 10.3389/fvets.2021.600986

24. Wallace KA, Goldschmidt MH, Patel RT. Converting fluid-based cytologic specimens to histologic specimens for immunohistochemistry. *Vet Clin Pathol.* (2015) 44:303–9. doi: 10.1111/vcp.12239

25. Landis JR, Koch GG. The measurement of observer agreement for categorical data. *Biometrics.* (1977) 33:159–74. doi: 10.2307/2529310

26. Evans SJM. Flow cytometry in veterinary practice. *Vet Clin North Am - Small Anim Pract.* (2023) 53:89–100. doi: 10.1016/j.cvsm.2022.07.008

27. Burgess HJ, Kerr ME. Cytokeratin and vimentin co-expression in 21 canine primary pulmonary epithelial neoplasms. *J Vet Diagnostic Investig.* (2009) 21:815–20. doi: 10.1177/104063870902100607

28. Dongre A, Weinberg RA. New insights into the mechanisms of epithelial-mesenchymal transition and implications for cancer. *Nat Rev Mol Cell Biol.* (2019) 20:69–84. doi: 10.1038/s41580-018-0080-4

29. Sato T, Miyoshi T, Shibuya H, Fujikura J, Koie H, Miyazaki Y. Peritoneal biphasic mesothelioma in a dog. *J Vet Med A Physiol Pathol Clin Med.* (2005) 52:22–5. doi: 10.1111/j.1439-0442.2004.00680.x

30. Hu C, Zhao M, Wei Q, Chen Z, Zhao B. Sarcomatoid hepatocellular carcinoma: a case report and review of the literature. *Medicine*. (2024) 103:e37641. doi: 10.1097/MD.0000000000037641

31. Geninet C, Bernex F, Rakotovao F, Crespeau FL, Parodi AL, Fontaine JJ. Sclerosing peritoneal mesothelioma in a dog - a case report. *J Vet Med A Physiol Pathol Clin Med.* (2003) 50:402–5. doi: 10.1046/j.0931-184x.2003.00566.x

32. Morini M, Bettini G, Morandi F, Burdisso R, Marcato PS. Deciduoid peritoneal mesothelioma in a dog. *Vet Pathol.* (2006) 43:198–201. doi: 10.1354/vp.43-2-198

33. D'Angelo AR, Di Francesco G. Sclerosing peritoneal mesothelioma in a dog: histopathological, histochemical and immunohistochemical investigations. *Vet Ital.* (2014) 50:301–5. doi: 10.12834/VetIt.20.1309.130

34. Choi EW. Pericardial malignant mesothelioma diagnosed in a dog by immunocytochemistry of the pericardial fluid: a case report. *BMC Vet Res.* (2023) 19:89. doi: 10.1186/s12917-023-03655-8

35. Inanaga M, Yoneji W, Ozaki K. Localized pleural mesothelioma in a dog. *J Comp Pathol.* (2023) 207:25–9. doi: 10.1016/j.jcpa.2023.09.006

36. Osaki T, Amaha T, Murahata Y, et al. Utility of 5-aminolaevulinic acid fluorescence-guided endoscopic biopsy for malignant mesothelioma in a cat and dog. *Aust Vet J.* (2023) 101:99–105. doi: 10.1111/avj.13224

37. Machida N, Tanaka R, Takemura N, Fujii Y, Ueno A, Mitsumori K. Development of pericardial mesothelioma in golden retrievers with a long-term history of idiopathic haemorrhagic pericardial effusion. *J Comp Pathol.* (2004) 131:166–75. doi: 10.1016/j.jcpa.2004.03.002

38. Banco B, Antuofermo E, Borzacchiello G, Cossu-Rocca P, Grieco V. Canine ovarian tumors: an immunohistochemical study with HBME-1 antibody. *J Vet Diagn Invest.* (2011) 23:977–81. doi: 10.1177/1040638711416848

39. Vascellari M, Carminato A, Camali G, Melchiotti E, Mutinelli F. Malignant mesothelioma of the tunica vaginalis testis in a dog: histological and immunohistochemical characterization. *J Vet Diagn Invest.* (2011) 23:135–9. doi: 10.1177/104063871102300125

Frontiers in Veterinary Science

Transforms how we investigate and improve animal health

The third most-cited veterinary science journal, bridging animal and human health with a comparative approach to medical challenges. It explores innovative biotechnology and therapy for improved health outcomes.

Discover the latest Research Topics

See more →

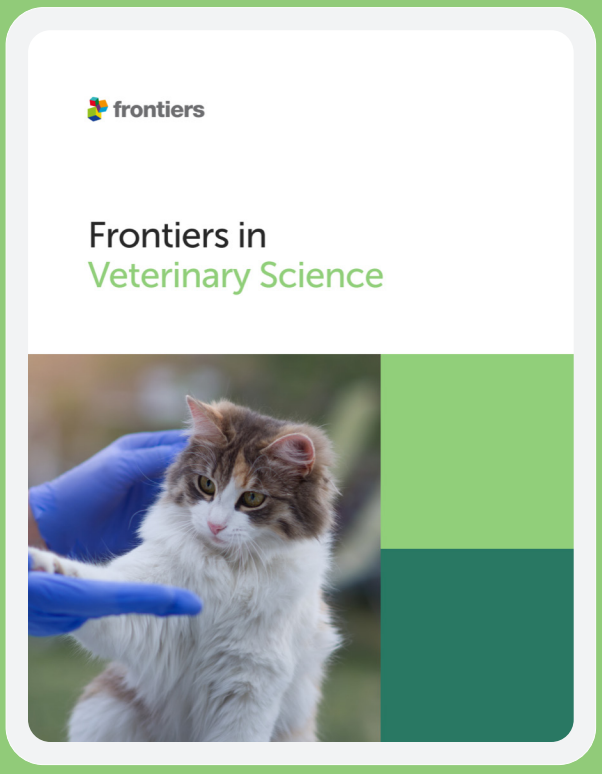

Frontiers

Avenue du Tribunal-Fédéral 34
1005 Lausanne, Switzerland
frontiersin.org

Contact us

+41 (0)21 510 17 00
frontiersin.org/about/contact